UNIVERSITI SAINS MALAYSIA

BORANG PENYERAHAN ASET / INVENTORI

===

A. BUTIR PENYELIDIK

1. NAMA PENYELIDIK :...Lim Jit Kang...

2. NO STAF :...USM 0839/09...

3. PTJ :...P.P. Kejuruteraan Kimia...............................

4. KOD PROJEK :...305/PJKIMIA/6013412...............................

5. TARIKH TAMAT PENYELIDIKAN :.......May 31, 2016...............................

B. MAKLUMAT ASET / INVENTORI

BIL	KETERANGAN ASET	NO HARTA	NO. SIRI	HARGA (RM)
1	Cary 60 UV-Vis Spectrophotometer with optical fiber probe	3AK00007146PJKIMIA		44,980.00
2	End-to-end rotator mixer	3AK00007663PJKIMIA		3,680.00

C. PERAKUAN PENYERAHAN

Saya dengan ini menyerahkan aset/ inventori seperti butiran B di atas kepada pihak Universiti:

....
(Lim Jit Kang   )   Tarikh: Oct 17, 2016

D. PERAKUAN PENERIMAAN

Saya telah memeriksa dan menyemak setiap alatan dan didapati :

☑ Lengkap
☐ Rosak
☐ Hilang   : Nyatakan...
☐ Lain-lain : Nyatakan ....

Diperakukan Oleh :

....
Tandatangan
Pegawai Aset PTJ

19 / 10 / 2016

Tarikh:

MOHD YUSOF ISMAIL
Penolong Jurutera
Pusat Pengajian Kejuruteraan Kimia
Kampus Kejuruteraan
Universiti Sains Malaysia
Seri Ampangan

*Nota :
Satu salinan borang yang telah dilengkapkan perlulah dikemukakan kepada Unit Pengurusan Harta, Jabatan Bendari dan RCMO untuk rekod

A. Description of the Project

1. Project number : 04-01-05-SF0617

2. Project title : Low Gradient Magnetic Separation of Microalgae from Fish Farm Water

3. Project leader : Lim Jit Kang

4. Project Team (Please provide an assessment of how the project team performed and highlight any significant departures from plan in either structure or actual man-days utilised)

In this project we have successfully demonstrated the ability to harvest microalgae from local fish farm water by using low gradient magnetic separation (LGMS). There is no any significant departures from the original plan as all proposed milestones have been completed successfully.

5. Industrial Partnership : (Please describe the nature of collaborations with relevant industry)

In this project, all the sample water is obtained directly from Aik Lee Fishery. We have initiated an active partnership with the industry by not only getting samples from them but also engage them in the design of our system.

6. National/International Collaboration (please identify research organisations and describe the nature of collaboration)

The PI of this project, JitKang Lim, has initiated an active collaborationship with Prof. Chun Zhao Liu's group from Chinese Academy of Science (CAS) working on magnetic separation of motile microalgae. Besides, he was also been invited to visit Prof. Jiwon Yang's group of The Korean Advanced Institute of Science and Technology (KAIST) to collaborate on microalgae separation technology.

7. Project Duration : 30.0 months.

Start Date : June(month)2013(Year)

End Date : November(month)2015(Year)

8. Total Budget Approved : RM RM298,263.00

B. Objectives of the project

1. Socio-economic Objectives (SEO)

Which socio-economic objectives are addressed by the project? (Please identify the Research Priority Area, SEO Category and SEO Group under which the project falls. Refer to the Malaysian R&D Classification System, 4th Edition.)

Research Cluster	SEA TO SPACE
SEO Category	: Natural Sciences, Technologies and Engineering
SEO Group	: Engineering Sciences
SEO Area	: Engineering Sciences

2. Fields of Research (FOR)

Which are the two main FOR Categories, FOR Groups, and FOR Areas of your project? (Please refer to the Malaysian R&D Classification System, 4th Edition)

a. Primary Field of Research

• FOR Category	: Environmental Sciences
• FOR Group	: Environment Technology/ Industry
• FOR Area	: Water and wastewater treatment technology

b. Secondary Field of Research (if applicable)

• FOR Category	: Material Sciences
• FOR Group	: Functional Materials
• FOR Area	: Magnetic materials

C. Objectives achievement

* **Original project objectives** (Please state the specific project objectives as described in Section II of the Application Form)

1. To design and synthesis environmental friendly and magnetically responsive magnetic iron oxide nanoparticles (MIOPs) with good colloidal stability. 2. To tagged the as synthesized MIOPs onto microalgae cells via electrostatic interaction. 3. To study the transport behavior of the MIOPs tagged microalgae within low field gradient under various conditions. 4. To study the kinetic of magnetophoresis aided separation of microalgae under low field gradient from fish farm water.

* **Objectives Achieved** (Please state the extent to which the project objectives were achieved)

1. Successfully synthesized surface-functionalized MIONPs with saturation magnetization of 35 emu/g 2. Successfully tagged the microalgal cells with surface-functionalized MIONPs via "electrostatic" interaction. 3. Successfully characterized the transport behaviors of (1) interacting vs non interacting system and (2) shape anisotropy system, on MIOPs tagged microalgal cells under low fied gradient. 4. Successfully recorded the separation kinetic profile of low gradient magnetophoresis for cell separation and use this information for the design of separation strategy.

* **Objectives not achieved** (Please state the extent to which the project objectives were achieved)

All objectives have been achieved.

D. Technology Transfer / Commercialisation Approach, if any. (Please describe the approach planned to transfer / commercialise the results of the project)

Currently, the PI is undergoing the coaching partnership of Biotech Corp on commercialization of this LGMS technology. There are two possible way to bring this technology to the market: (1) on the design of magnetic separator, and/or, (2) on the design of magnetophoresis reader. The first product is based on the design of rotary drum magnetic separator and its commercialization is not only restricted for fish farm usages but also for any kind of microalgae separation (including harvesting biofuel). Whereas, the potential market for magnetophoresis reader is from industry and academy research lab, in which, the study of kinetic behavior of magnetic separation process is being conducted. The PI is currently working on a bridging fund to bring these two technologies to the market.

E. Assessment of Research Approach (Please highlight the main steps actually performed and indicate any major departure from the planned approach or any major difficulty encountered)

F. Assessment of the Project Schedule (Please make any relevant comment regarding the actual duration

of the project and highlight any significant variation from plan)

This project was extended for 6 months to finish an added task of using a commerciallized available LGMS system

sold by Sepmag, Spain. All the objectives listed in the original proposal and the listed tasks have been completed

successfully.

G. Assessment of Project Costs (Please comment on the appropriateness of the original budget and

highlight any major departure from the planned budget)

Since both the PhD and MSc students working on this project is sponsored by MyBrain Scholarship, certain portion

of allocation in Vot 11,000 has been used for chemical supply.

H. Additional Project Fundling Obtained (In case of involvement of other funding sources,please

indicate the source and total funding provided)

An international grant with total value of USD 9,500 was obtained based on the results of this project: TWAS-

COMTECH Grant 13-378 RG/ENG/AS_C: Magnetophoretic Separation of Microalgae from Fishfarm Water at Low

Field Gradient – Collision Frequency Contribution from Foreign Objects

I. Benefits of the Project (Please identify the actual benefits arising from the project as defined in Section III of

the Application Form. For examples research direct outputs, organisational outcomes and sectoral/national impacts,

please refer to Section III of the Guidelines for the Application of R&D Funding under ScienceFund)

1. Direct Outputs of the Project (please describe as specifically as possible the outputs achieved and provide an assessment of their significant to users)

    i.   **Technical contribution of the project**

            a. What was the achieved direct output of the project:

<u>**Basic Research**</u>   **Description:**
<u>**Project**</u>

☐ Algorithm

☐ Structure

☒ Data

☐ Other, please specify : A LGMS Process Design

<u>**Basic Research Project**</u>   **Description:**

☒ Method/technique

☐ Demonstrator/prototype

☐ Product/component

☒ Process

☐ Software

☐ Other, please specify :

   b. How would you characterise the quality of this output?

☒ Significant breakthrough

☐ Major improvement

☐ Minor improvement

---

ii.   **Contribution of the project to knowledge**

   a. How has the output of the project been documented?

☐ Detailed project report

☐ Product/process specification documents

☐ Other, please specify :   Journal papers

---

   b. Did the project create an intellectual property stock?

☐ Patent obtained

☐ Patent pending

☐ Patent application will be filed

☐ Copyright

c. What publications are available?

	National	International

☒ Articles (s) in scientific publications   How many : 6

☐ Paper(s) delivered at conferences/seminars How many :

☐ Book   How many :

☐ Other, please specify :

d. How significant are citations of the results?

☐ Citations in national publications   How many : 48

☒ Citations in international publications How many :

☐ Not yet

☐ Not known

2. Organisational Outcomes of the Project (Please describe as specifically as possible the organisational benefits arising from the project and provide an assessment of their significance)

   i. Contribution of the project to expertise development

   a. How did the project contribute to expertise?

   Area of Specialisation:

[X] PhD degrees   How many : 1

[X] MSc degrees   How many : 1

[ ] Research staff with new specialty   How many :

[ ] Other, please specify :

   b. How significant is this expertise?

[ ] One of the key areas of priority for Malaysia

[X] An important area, but not a priority one

---

ii. Economic contribution of the project?

   a. How has the economic contribution of the project materialised?

                                        Description (if applicable)

[ ] Sales of manufactured product/equipment

[ ] Royalties from licensing

[ ] Cost savings

[X] Time savings

[ ] Other, please specify :

b. How important is this economic contribution?

☐ High economic contribution   Value : RM 0.00

☐ Medium economic contribution   Value : RM 0.00

☒ Low economic contribution   Value : RM 0.00

c. When has this economic contribution materialised?

☐ Already materialised

☐ Within months of project completion

☐ Within three years of project completion

☒ Expected in three years or more

☐ Unknown :

iii. Infrastructural contribution of the project

a. What infrastructural contribution has the project had?

[X] New equipment   Type :   Value : RM 48660.00

[ ] New/improved facility   Investment :   Value : RM 0.00

[ ] New information networks

[ ] Other, please specify :

b. How significant is this infrastructural contribution for the organisation?

[ ] Not significant/does not leverage other projects

[ ] Moderately significant

[X] Very significant/significantly leverages other projects

iv. Contribution of the project to the organisationâ€™s reputation

a. How has the project contributed to increasing the reputation of the Organisation

[ ] Recognition as a Center of Excellence

[X] National award (Type and category)

[X] International award (Type and category)

[ ] Demand for advisory services

[ ] Invitations to give speeches on conferences

[ ] Visits from other organisations

[ ] Other, please specify :

b. How important is the projectâ€™s contribution to the organisationâ€™s reputation?

[ ] Not significant

[ ] Moderately significant

[X] Very significant

3. **National Impacts of the Project** (If known at this point in time, please describe as specifically as possible the potential sectoral/national benefits arising from the project and provide an assessment of their significance)

   i. Contribution of the project to organisational linkages

      a. Which kinds of linkages did the project create?

[X] Domestic industry linkages

[ ] International industry linkages

[ ] Linkages with domestic research institutions, universities

[X] Linkages with international research institutions, universities

      b. What is the nature of the linkages?

[X] Staff exchanges

[ ] Inter-organisational project team

[ ] Research contract with a commercial client

[ ] Informal consultation

[ ] Other, please specify :

   i. Social-economic contribution of the project

      a. Who are the direct customer/beneficiaries of the project output?

Customers/beneficiaries	Number

      b. How has/will the socio-economic contribution of the project materialised?

[ ] Improvements in health

[ ] Improvements in safety

[ ] Improvements in the environment

[X] Improvements in energy consumption/supply

[ ] Improvements in international relations

[ ] Other, please specify :

      c. How important is this socio-economic contribution?

[X] High social contribution

[ ] Medium social contribution

[ ] Low social contribution

      d. When has/will this social contribution materialised?

[ ] Already materialised

[ ] Within three years of project completion

[X] Expected in three years or more

[ ] Unknown

Date :	Signature :

Short Communication

Challenges associated to magnetic separation of nanomaterials at low field gradient

CrossMark

JitKang Lim [a,b,*], Swee Pin Yeap [a], Siew Chun Low [a]

[a] School of Chemical Engineering, Universiti Sains Malaysia, Nibong Tebal, Penang 14300, Malaysia
[b] Department of Physics, Carnegie Mellon University, Pittsburgh, PA 15213, USA

ARTICLE INFO

ABSTRACT

Magnetic nanoparticles (MNPs) have been proposed as one of the effective tools for pollutant removal from aqueous environment. In most of the new strategies investigated, which involved the use of MNPs, the ability to reharvest back this nanomaterial by an externally applied magnetic field is always being emphasized. In this short communication, we discuss the challenges associated to the magnetic separation of MNPs from its suspending media through magnetophoresis under low magnetic field gradient. We highlight the major constraints, such as thermal energy, Stokes drag and gravitational pulling, which influence the successful separation of MNPs from aqueous environment by low gradient magnetic separation (LGMS). Dimensionless numbers are introduced to provide a more quantitative comparison between the aforementioned constraints with magnetophoresis at low field gradient. Finally, we focus our discussion on the role of (1) guided/self-assembly approaches and (2) on-site LGMS strategy as the most practical routes of using MNP for water remediation.

© 2014 Elsevier B.V. All rights reserved.

1. Introduction

In last decade, we have observed a booming of research findings on the huge potential of magnetic nanoparticles (MNPs) in removing dangerous pollutants, such as arsenic [1], heavy metals [2], chlorinated compounds [3], and also organic dyes [4] from water resources. One of the great advantages of this MNP based water treatment technique is the recollection ability of MNPs, which can be easily achieved by using a hand held permanent magnet [1,4], after the hazardous compound was adsorbed onto the particle surfaces. The underlying principle behind this separation technique is remarkably straightforward. It relies on the simple fact that the magnetic materials experience magnetophoretic force in the presence of magnetic field gradients and thus these materials can be physically separated out from the surrounding fluids by a magnetic source. In addition, MNPs can also be employed to impart a magnetic dipole moment to biological cells, through immobilization on the cell surfaces, which subsequently leading to magnetophoretic separation of biological substances [5].

The rapid magnetophoretic separation of MNPs under low magnetic field gradient ($\nabla B < 100$ Tesla/m), as observed by others is very likely through field-induced reversible aggregation of particles [6]. Under this scenario, the particle clusters formed would migrate to the region where the magnetic field gradient is the highest. Along its migration pathway, the moving MNP clusters collide with each other and integrated into larger aggregates with higher magnetophoretic velocity [6,7]. This mechanism is the key factor for successful separation of MNPs in real time and revealed the opportunity for the implementation of low gradient magnetic separation (LGMS) for engineering applications.

In contrast to conventional industry practice in which high gradient magnetic separation (HGMS) is normally being employed, the design rules for LGMS is ill-defined and poorly understood. Moreover, the key parameters involved for implementation of LGMS in water treatment technology are also not being fully explored yet. Recently, Mandel and Hutter have briefly discussed the problems related to MNPs separation [8]. They raised an interesting point in which the use of ferrofluid as a nanoemulsion provides better alternative for water treatment purpose compared to easily agglomerated MNP suspension. However, the liquid–liquid interface between the nanoemulsion and the aqueous media can be the major barrier toward the full realization of this noble idea. Nevertheless, the key question here is how the nanosized magnetic particles can be used effectively for water treatment, and more importantly, the recollection of these particles from their suspension. It is the purpose of this paper to illustrate some general rule of thumbs related to the separation of MNPs under low field gradient.

* Corresponding author at: School of Chemical Engineering, Engineering Campus, Universiti Sains Malaysia, Seri Ampangan, Nibong Tebal, Penang 14300, Malaysia. Tel.: +60 4 599 6423; fax: +60 4 599 1013.
E-mail address: chjitkangl@eng.usm.my (J. Lim).

2. Underlying problems associated to LGMS

It is often being illustrated that by introduction of a magnetic field, the separation of MNPs from aqueous environment can be made possible in real time as shown in Fig. 1. Even though, the separation time involved is very feasible for practical usages at lab scale, the possibility for this kind of setup to be fully implemented for water treatment purposes is as good as none. By taking the example of a cylindrical NdFeB magnet, the magnetic field B_x along its symmetry axis as a function of the distance x away from the magnet pole face can be estimated quite accurately by following equation [9]:

$$B_x = \frac{B_r}{2}\left[\frac{x+L}{\sqrt{(L+x)^2+R^2}} - \frac{x}{\sqrt{x^2+R^2}}\right] \qquad (1)$$

where R is the radius of the cylinder, L is the length of the cylinder, B_r is the remanence or residual induction of the magnetic material. For a grade N50 NdFeB, B_r is about 1.45 Tesla. This calculated B_x has a very good match with experimentally measured results [10] and for the permanent magnet shown in Fig. 1, with a dimension of $R = 0.7$ cm and $L = 1.5$ cm, its magnetic field B_x decay rapidly from the magnet pole face (Fig. 2). Once, the MNPs has been released into environment for water treatment purposes, there is no such magnet or magnetic separation devices/strategies can be employed to cope with the length scale involved, up to kilometers, in re-harvesting them back. For an example, according to Eq. (1), in order to generate an appropriate field gradient to achieve LGMS at separation distance of 1 km ($x = 1000$ m) would require a cylindrical NdFeB magnet (at the same aspect ratio of the magnet shown in Fig. 1) with radius of 140 m and length of 300 m.

This analogy bring out an important message in which for any in situ water treatment technology that involved the usages of MNPs, it is misleading to emphasize on its magnetic separation. Once being released into the environment there is no way for MNPs to be re-harvested back, at least not by magnetic separation. Thus, it is more appropriate for the implementation of MNPs under the setting of a on-site treatment facility. Under this context, the application of LGMS as a downstream separation unit can be both economical and technological feasible [5]. For engineering application, the (a) inhomogeneous field gradient and (b) complex distribution of magnetic field lines in three dimensional space of a permanent magnet can be extremely challenging to be properly integrated into a LGMS system.

3. Transport behaviors of MNPs due to "nanosize effects"

By taking non-interacting particles assumption, at magnetic field B, the magnetophoretic force F_{mag} needed to induce separation of spherical MNPs is [11,12]:

$$F_{mag} = \frac{4}{3}\pi r_{pt}^3 (M \cdot \nabla)B \qquad (2)$$

where r_{pt} and M are the radius and the magnetization (per unit volume) of the MNP, respectively. By equating the F_{mag} with viscous
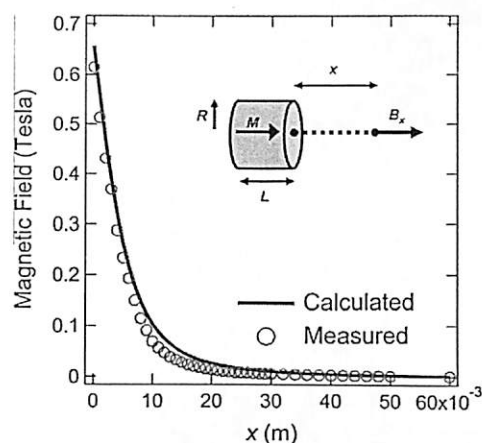

Fig. 2. Magnetic field B_x extended out from a cylindrical NdFeB magnet with radius of 0.07 m and length of 0.015 m. B_x is calculated by using Eq. (1).

drag force ($F_{drag} = 6\pi\eta r_{pt} \cdot u_{mag}$) experienced by a sphere [13], the magnetophoretic velocity u_{mag} can be calculated as

$$u_{mag} = \frac{2r_{pt}^2}{9\eta}(M \cdot \nabla)B \qquad (3)$$

where η is the viscosity of the suspending medium. For the case of very weak magnetic field, Eq. (2) can be further simplified to [14]:

$$F_{mag} = \frac{\Delta\chi V_p}{\mu_0}(\nabla B)B \qquad (4)$$

where μ_0 is the vacuum permeability, V_p is the particle volume ($V_p = 4\pi r_{pt}^3/3$) and $\Delta\chi$ is the different in magnetic susceptibility between the particle and the fluid. Eq. (4) raised an interesting observation, in which the F_{mag} experienced by a nanoparticle is not only dependent on the magnetic field and field gradient but the volume of the MNP involved is equally important. For any design purposes which involved transport behaviors of MNP, knowing the value of u_{mag} is vital as various transport phenomena analyses can be performed [15].

Since the particle size is in nanometer range, its motion is heavily influenced by thermal energy and viscous drag; hence, conventional dimensionless number analysis can be very helpful to characterize the flow behavior. Table 1 summarized some of the useful dimensionless numbers which are familiar to the chemical and mechanical engineers and can serve as an effective way to rationalize the transport behavior of MNPs under magnetophoresis. By using the value of B and ∇B as shown in Fig. 2 and hydrodynamic radius of the MNPs (Fig. 1) at 150 nm as determined by dynamic light scattering (DLS), the Reynolds (Re), Péclet (Pe) and Froude (Fr) numbers with respect to the separation distance x from the pole surface of NdFeB magnet can be calculated (see Fig. 3a). Here we used the mathematical equations presented in Table 1 for the calculation of each dimensionless number and according to Eq. (3) the MNPs would typically having a magnetophoretic velocity within the range of 0.5 μm/s to around 9000 μm/s. As
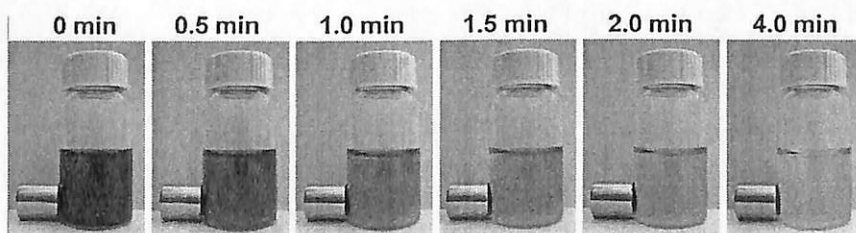

Fig. 1. Magnetophoretic collection of iron oxide MNPs with ~150 nm hydrodynamic radius in real time.

Table 1
Useful dimensionless number for characterization of MNP flow behaviors under magnetophoresis.

Dimensionless number	Equation[a]	Physical interpretation
Reynolds number, Re	$Re = \frac{\rho u_{mag} l}{\eta}$	Re defined the ratio of inertia to viscous force, as $Re \gg 1$, magnetophoresis dominated $Re \ll 1$, viscosity dominated
Péclet number, Pe	$Pe = \frac{u_{mag} l}{D}$	Pe defined the ratio of inertia to diffusion, as $Pe \gg 1$, magnetophoresis dominated $Pe \ll 1$, diffusion dominated
Froude number, Fr	$Fr = \frac{u_{mag}^2}{gl}$	Fr defined the ratio of inertia to gravitational pulling $Fr \gg 1$, magnetophoresis dominated $Fr \ll 1$, gravitational pulling dominated

[a] where l is the associated characteristic length scale, and for magnetophoresis study is concerned, it is typically taking as the diameter of MNP, ρ is the density of MNP and here we assumed it is purely magnetite with density of 5.2 g/cm³, D is the diffusivity of MNP and can be calculated by using Stokes–Einstein equation, and g is the acceleration due to gravity.

Fig. 3. Reynolds (Re), Péclet (Pe) and Froude (Fr) numbers calculated at (a) separation distance x from surface of a cylindrical NdFeB with varying B and ∇B values as shown in Fig. 2 and (b) different radius of MNPs at B = 0.049 Tesla and ∇B = 6.62 Tesla/m. Broken line indicate the dimensionless number at one, so, above this point the magnetophoretic flow of the MNP dominates viscous drag, thermal randomization and also gravitational pulling.

clearly depicted in Fig. 3a, under this setup there presents a critical distance at around x = 15 mm in which magnetophoresis of a spherical MNP dominates other disturbances, such as Brownian motion, viscous drag and gravitational pulling. Below this separation distance, all three calculated dimensionless numbers are greater than unity. The shaded area above the broken line in Fig. 3a defines the effective operation region where the magnetophoretic collection could occur deterministically. In fact, this is the same area in which magnetic field B decayed drastically with respect to the separation distance x as shown in Fig. 2. The averaged magnetic field gradient ∇B within this zone at around 54.67 Tesla/m certified the nature of this process as LGMS. Detailed spatial resolution revealed by this dimensionless number analysis provides useful information for the design of LGMS system.

In general, the migration of MNPs under LGMS as shown in Fig. 1 is a complex interplay between magnetophoresis, viscous drag and random Brownian motion in which all these phenomena scale differently with the particle size. By taking B = 0.049 Tesla and ∇B = 6.62 Tesla/m at critical separation distance of 15 mm, the Reynolds (Re), Péclet (Pe) and Froude (Fr) numbers can be calculated (see Fig. 3b) for MNPs with different radius. For magnetophoresis to play a dominant role, by having all three dimensionless numbers to be greater than one, MNP with radius between 140 nm and 180 nm is required. By taking the superparamagnetic size limit of magnetite (Fe₃O₄) particles at around r = 17.5 nm [16] gives dimensionless number of Re = 0.0013, Pe = 0.0002 and Fr = 0.0011, respectively. These very low values of Re, Pe and Fr numbers implied that the magnetophoretic motion of the MNP at this size would be overwhelmed by viscous drag, thermal energy and also

gravitational pulling. This examination is contradicting with the surprised results as observed by Yavuz and coworkers [1]. In directly, it has suggested the cooperative nature of the magnetophoresis and can also be generalized to our observation in Fig. 1.

At very high concentration in which the non-interacting particles assumption is not longer valid and magnetophoresis become concentration dependent [6], Eq. (3) alone is not suffice to estimate u_{mag} accurately. Under this scenario, a more sophisticated mathematic analysis such as the one suggested by Faraudo and Camacho is needed to estimate the separation time by taking into account the field induced aggregation of MNPs during the magnetophoresis [6,17]. For cooperative magnetophoresis, it is estimated that the recorded velocity can be 65 times higher than those predicted by conventional method [18]. Nevertheless, the dimensionless number analysis is still an easy route to provide quick feedback for checking the relation among important physical properties relevant to magnetophoresis of MNPs under LGMS as long as the u_{mag} can be estimated reasonably. More importantly, it also gives a useful approach to rationalize the complex interplay between the magnetophoresis with thermal energy, Stokes drag and gravitational pulling that eventually dictates the success or failure of LGMS in harvesting MNPs.

4. MNPs for engineering applications

For environmental engineering applications are concerned, MNP is typically being surface functionalized by macromolecules. This step is taken to mitigate the nanotoxicity associated to its small dimension [19], and to maintain its colloidal stability in

suspension [20]. However, just recently our group has revealed the conflicting role of colloidal stability in suppressing the magnetophoretic separation of MNPs [21,22]. After achieved good dispersibility, the polyelectrolyte coated iron oxide MNP become extremely difficult to be magnetophoretically separated out from its suspension even with the introduction of very high magnetic field gradient $\nabla B > 1000$ Tesla/m [22]. This in turn would suppress the cooperative effect as discussed in previous section and also prevent the chaining of MNPs that ultimately contribute to the rapid magnetophoresis [6]. The huge time lag and low efficiency observed might posed a serious challenge for the effective use of surface functionalized MNPs in any applications that required rapid separation.

It is obvious that MNPs cannot be a standalone nanoagent for most of the water treatment technology that required good colloidal stability and achieving rapid magnetophoretic separation while maintaining its other important properties, such as high specific surface area, catalytic activity, low nanotoxicity and etc. We anticipated that MNPs need to be combined with other components to fully realize its potential for water treatment applications. The integration of MNPs into polymeric microcapsule can be a feasible solution [23,24]. Other guided/self-assembly approaches, such as magnetoliposomes [25], pickering emulsion [26], templated-structure like silica-MNPs and activated carbon-MNPs [27,28], can also be a viable option. For the development of next generation MNP-enhanced nanomaterials for water treatment applications, the synthesis proceduce employed should be cost effective, environmental friendly and can produce large amount of nanomaterials within reasonable time frame. In addition, the magnetophoretic property should also be emphasized. This feature is necessary to ensure full recovery of the MNPs from treated water.

5. Conclusion

A more localized usages of MNP for water treatment purpose, such as in an on-site treatment facility, should be implemented in order to take full advantage of its magnetophoretic property. The idea of releasing enormous amount of MNPs into environment for water treatment purpose and magnetophoretically re-collecting this nanomaterial back is highly unrealistic. Cooperative phenomenon during the MNP magnetophoresis has greatly complicated the mathematical analysis on predicting the MNP velocity. In addition, the contribution of colloidal stability of MNPs toward LGMS is critical and should not be overlooked in any engineering applications. Dimensionless number calculation provides a fast and reliable analysis on the flow behavior of the MNPs under magnetophoresis. This analysis also related important physical properties associated to the magnetophoresis of MNPs under low field gradient. There are still many interesting opening questions related to magnetophoresis of MNPs [29]. More research efforts are needed in developing a practicable guided/self-assembly approach and efficient LGMS process for full utilization of MNPs in environmental engineering applications.

Acknowledgements

References

[1] C.T. Yavuz, J.T. Mayo, W.W. Yu, A. Prakash, J.C. Falkner, S. Yean, L. Cong, H.J. Shipley, A. Kan, M. Tomson, D. Natelson, V.L. Colvin, Low-field magnetic separation of monodisperse Fe₃O₄ nanocrystals, Science 314 (2006) 964–967.

[2] W. Yantasee, C.L. Warner, T. Sangvanich, R.S. Addleman, T.G. Carter, R.J. Wiacek, G.E. Fryxell, C. Timchalk, M.G. Warner, Removal of heavy metals from aqueous systems with thiol functionalized superparamagnetic nanoparticles, Environ. Sci. Technol. 41 (2007) 5114–5119.

[3] Y. Liu, T. Phenrat, G.V. Lowry, Effect of TCE concentration and dissolved groundwater solutes on NZVI-promoted TCE dechlorination and H₂ evolution, Environ. Sci. Technol. 41 (2007) 7881–7887.

[4] B. Saha, S. Das, J. Saikia, G. Das, Preferential and enhanced adsorption of different dyes on iron oxide nanoparticles: a comparative study, J. Phys. Chem. C. 115 (2001) 8024–8033.

[5] P.Y. Toh, S.P. Yeap, L.P. Kong, B.W. Ng, C.J.C. Derek, A.L. Ahmad, J.K. Lim, Magnetophoretic removal of microalgae from fishpond water: feasibility of high gradient and low gradient magnetic separation, Chem. Eng. J. 211–212 (2012) 22–30.

[6] G. Cuevas, J. Faraudo, J. Camacho, Low-gradient magnetophoresis through field-induced reversible aggregation, J. Phys. Chem. C. 112 (2008) 945–950.

[7] M. Benelmekki, C. Caparros, A. Montras, R. Goncalves, S. Lanceros-Mendez, LI.M. Martinez, Horizontal low gradient magnetophoresis behavior of iron oxide nanoclusters at the different steps of the synthesis route, J. Nanopart. Res. 13 (2011) 3199–3206.

[8] K. Mandel, F. Hutter, The magnetic nanoparticle separation problem, Nano Today 7 (2012) 485–487.

[9] V. Schaller, U. Kräling, C. Rusu, K. Petersson, J. Wipenmyr, A. Krozer, G. Wahnström, A. Sanz-Velasco, P. Enoksson, C. Johansson, Motion of nanometer sized magnetic particles in a magnetic field gradient, J. Appl. Phys. 104 (2008) 093918.

[10] J.K. Lim, C.J.C. Derek, S.A. Jalak, P.Y. Toh, N.H.M. Yasin, B.W. Ng, A.L. Ahmad, Rapid magnetophoretic separation of microalgae, Small 8 (2012) 1683–1692.

[11] G.D. Moeser, K.A. Roach, W.H. Green, T.A. Hatton, P.E. Laibinis, High-gradient magnetic separation of coated Magnetic nanoparticles, AIChE J. 50 (2004) 2835–2848.

[12] G.P. Hatch, R.E. Stelter, Magnetic design considerations for devices and particles used for biological high-gradient magnetic separation (HGMS) systems, J. Magn. Magn. Mater. 225 (2001) 262–276.

[13] M. Zborowski, L. Sun, L.R. Moore, P.S. Williams, J.J. Chalmers, Continuous cell separation using novel magnetic quadrupole flow sorter, J. Magn. Magn. Mater. 194 (1999) 224–230.

[14] N. Pamme, A. Manz, On-chip free-flow magnetophoresis: continuous-flow separation of magnetic particles and agglomerates, Anal. Chem. 76 (2004) 7250–7256.

[15] J.K. Lim, D.X. Tan, F. Lanni, R.D. Tilton, S.A. Majetich, Optical imaging and magnetophoresis of nanorods, J. Magn. Magn. Mater. 321 (2009) 1557–1562.

[16] D.J. Dunlop, Magnetite: behavior near the single-domain threshold, Science 176 (1972) 41–43.

[17] J. Faraudo, J. Camacho, Cooperative magnetophoresis of superparamagnetic colloids: theoretical aspects, Colloid Polym. Sci. 288 (2010) 207–215.

[18] J.S. Andreu, J. Camacho, J. Faraudo, M. Benelmekki, C. Rebollo, LI.M. Martinez, Simple analytical model for the magnetophoretic separation of superparamagnetic dispersions in a uniform magnetic gradient, Phys. Rev. E 84 (2011) 021402.

[19] A. Verma, F. Stellacci, Effect of surface properties of nanoparticle-cell interactions, Small 6 (2010) 12–21.

[20] P.L. Golas, S. Louie, G.V. Lowry, K. Matyjazsewski, R.D. Tilton, Comparative study of polymeric stabilizers for magnetite nanoparticles using ATRP, Langmuir 26 (2010) 16890–16900.

[21] S.P. Yeap, P.Y. Toh, A.L. Ahmad, S.C. Low, S.A. Majetich, J.K. Lim, Colloidal stability and magnetophoresis of gold-coated iron oxide nanorods in biological media, J. Phys. Chem. C. 116 (2012) 22561–22569.

[22] S.P. Yeap, A.L. Ahmad, B.S. Ooi, J.K. Lim, Electrosteric stabilization and its role in cooperative magnetophoresis of colloidal magnetic nanoparticles, Langmuir 28 (2012) 14878–14891.

[23] A.F. Ngomsik, A. Bee, J.M. Siaugue, V. Cabuil, G. Cote, Nickel adsorption by magnetic alginate microcapsules containing an extractant, Water Res. 40 (2006) 1848–1856.

[24] L.P. Kong, X.J. Gan, A.L. Ahmad, B.H. Hameed, E.R. Evarts, B.S. Ooi, J.K. Lim, Design and synthesis of magnetic nanoparticles augmented microcapsule with catalytic and magnetic bifunctionalities for dye removal, Chem. Eng. J. 197 (2012) 350–358.

[25] M. Gonzales, K.M. Krishnan, Synthesis of magnetoliposomes with monodisperse iron oxide nanocrystal cores for hyperthermia, J. Magn. Magn. Mater. 293 (2005) 265–270.

[26] A. Kaiser, T. Liu, W. Richtering, A.M. Schmidt, Magnetic capsules and pickering emulsions stabilized by core-shell particles, Langmuir 25 (2009) 7335–7341.

[27] W. Zhao, J. Gu, L. Zhang, H. Chen, J. Shi, Fabrication of uniform magnetic nanocomposite spheres with a magnetic core/mesoporous silica shell structure, J. Am. Chem. Soc. 127 (2005) 8916–8917.

[28] M. Schwickardi, S. Olejnik, E.L. Salabas, W. Schmidt, F. Schüth, Scalable synthesis of activated carbon with superparamagnetic properties, Chem. Commun. (2006) 3987–3989.

[29] J. Faraudo, J.S. Andreu, J. Camacho, Understanding diluted dispersion of superparamagnetic particles under strong magnetic fields: a review of concepts, theory and simulation, Soft Matter 9 (2013) 6654–6664.

Separation and Purification Technology

Short Communication

Challenges associated to magnetic separation of nanomaterials at low field gradient

CrossMark

JitKang Lim [a,b,*], Swee Pin Yeap [a], Siew Chun Low [a]

[a] School of Chemical Engineering, Universiti Sains Malaysia, Nibong Tebal, Penang 14300, Malaysia
[b] Department of Physics, Carnegie Mellon University, Pittsburgh, PA 15213, USA

ARTICLE INFO

ABSTRACT

Magnetic nanoparticles (MNPs) have been proposed as one of the effective tools for pollutant removal from aqueous environment. In most of the new strategies investigated, which involved the use of MNPs, the ability to reharvest back this nanomaterial by an externally applied magnetic field is always being emphasized. In this short communication, we discuss the challenges associated to the magnetic separation of MNPs from its suspending media through magnetophoresis under low magnetic field gradient. We highlight the major constraints, such as thermal energy, Stokes drag and gravitational pulling, which influence the successful separation of MNPs from aqueous environment by low gradient magnetic separation (LGMS). Dimensionless numbers are introduced to provide a more quantitative comparison between the aforementioned constraints with magnetophoresis at low field gradient. Finally, we focus our discussion on the role of (1) guided/self-assembly approaches and (2) on-site LGMS strategy as the most practical routes of using MNP for water remediation.

© 2014 Elsevier B.V. All rights reserved.

1. Introduction

In last decade, we have observed a booming of research findings on the huge potential of magnetic nanoparticles (MNPs) in removing dangerous pollutants, such as arsenic [1], heavy metals [2], chlorinated compounds [3], and also organic dyes [4] from water resources. One of the great advantages of this MNP based water treatment technique is the recollection ability of MNPs, which can be easily achieved by using a hand held permanent magnet [1,4], after the hazardous compound was adsorbed onto the particle surfaces. The underlying principle behind this separation technique is remarkably straightforward. It relies on the simple fact that the magnetic materials experience magnetophoretic force in the presence of magnetic field gradients and thus these materials can be physically separated out from the surrounding fluids by a magnetic source. In addition, MNPs can also be employed to impart a magnetic dipole moment to biological cells, through immobilization on the cell surfaces, which subsequently leading to magnetophoretic separation of biological substances [5].

The rapid magnetophoretic separation of MNPs under low magnetic field gradient ($\nabla B < 100$ Tesla/m), as observed by others is very likely through field-induced reversible aggregation of particles [6]. Under this scenario, the particle clusters formed would migrate to the region where the magnetic field gradient is the highest. Along its migration pathway, the moving MNP clusters collide with each other and integrated into larger aggregates with higher magnetophoretic velocity [6,7]. This mechanism is the key factor for successful separation of MNPs in real time and revealed the opportunity for the implementation of low gradient magnetic separation (LGMS) for engineering applications.

In contrast to conventional industry practice in which high gradient magnetic separation (HGMS) is normally being employed, the design rules for LGMS is ill-defined and poorly understood. Moreover, the key parameters involved for implementation of LGMS in water treatment technology are also not being fully explored yet. Recently, Mandel and Hutter have briefly discussed the problems related to MNPs separation [8]. They raised an interesting point in which the use of ferrofluid as a nanoemulsion provides better alternative for water treatment purpose compared to easily agglomerated MNP suspension. However, the liquid–liquid interface between the nanoemulsion and the aqueous media can be the major barrier toward the full realization of this noble idea. Nevertheless, the key question here is how the nanosized magnetic particles can be used effectively for water treatment, and more importantly, the recollection of these particles from their suspension. It is the purpose of this paper to illustrate some general rule of thumbs related to the separation of MNPs under low field gradient.

---

* Corresponding author at: School of Chemical Engineering, Engineering Campus, Universiti Sains Malaysia, Seri Ampangan, Nibong Tebal, Penang 14300, Malaysia. Tel.: +60 4 599 6423; fax: +60 4 599 1013.
 E-mail address: chjitkangl@eng.usm.my (J. Lim).

2. Underlying problems associated to LGMS

It is often being illustrated that by introduction of a magnetic field, the separation of MNPs from aqueous environment can be made possible in real time as shown in Fig. 1. Even though, the separation time involved is very feasible for practical usages at lab scale, the possibility for this kind of setup to be fully implemented for water treatment purposes is as good as none. By taking the example of a cylindrical NdFeB magnet, the magnetic field B_x along its symmetry axis as a function of the distance x away from the magnet pole face can be estimated quite accurately by following equation [9]:

$$B_x = \frac{B_r}{2} \left[\frac{x+L}{\sqrt{(L+x)^2 + R^2}} - \frac{x}{\sqrt{x^2 + R^2}} \right] \tag{1}$$

where R is the radius of the cylinder, L is the length of the cylinder, B_r is the remanence or residual induction of the magnetic material. For a grade N50 NdFeB, B_r is about 1.45 Tesla. This calculated B_x has a very good match with experimentally measured results [10] and for the permanent magnet shown in Fig. 1, with a dimension of $R = 0.7$ cm and $L = 1.5$ cm, its magnetic field B_x decay rapidly from the magnet pole face (Fig. 2). Once, the MNPs has been released into environment for water treatment purposes, there is no such magnet or magnetic separation devices/strategies can be employed to cope with the length scale involved, up to kilometers, in re-harvesting them back. For an example, according to Eq. (1), in order to generate an appropriate field gradient to achieve LGMS at separation distance of 1 km ($x = 1000$ m) would require a cylindrical NdFeB magnet (at the same aspect ratio of the magnet shown in Fig. 1) with radius of 140 m and length of 300 m.

This analogy bring out an important message in which for any in situ water treatment technology that involved the usages of MNPs, it is misleading to emphasize on its magnetic separation. Once being released into the environment there is no way for MNPs to be re-harvested back, at least not by magnetic separation. Thus, it is more appropriate for the implementation of MNPs under the setting of a on-site treatment facility. Under this context, the application of LGMS as a downstream separation unit can be both economical and technological feasible [5]. For engineering application, the (a) inhomogeneous field gradient and (b) complex distribution of magnetic field lines in three dimensional space of a permanent magnet can be extremely challenging to be properly integrated into a LGMS system.

3. Transport behaviors of MNPs due to "nanosize effects"

By taking non-interacting particles assumption, at magnetic field B, the magnetophoretic force F_{mag} needed to induce separation of spherical MNPs is [11,12]:

$$F_{mag} = \frac{4}{3}\pi r_{pt}^3 (M \cdot \nabla)B \tag{2}$$

where r_{pt} and M are the radius and the magnetization (per unit volume) of the MNP, respectively. By equating the F_{mag} with viscous
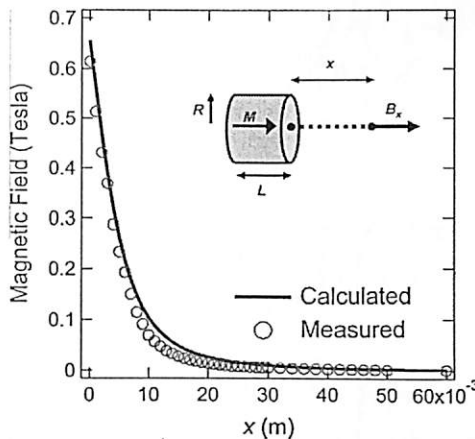

Fig. 2. Magnetic field B_x extended out from a cylindrical NdFeB magnet with radius of 0.07 m and length of 0.015 m. B_x is calculated by using Eq. (1).

drag force ($F_{drag} = 6\pi\eta r_{pt} \cdot u_{mag}$) experienced by a sphere [13], the magnetophoretic velocity u_{mag} can be calculated as

$$u_{mag} = \frac{2r_{pt}^2}{9\eta}(M \cdot \nabla)B \tag{3}$$

where η is the viscosity of the suspending medium. For the case of very weak magnetic field, Eq. (2) can be further simplified to [14]:

$$F_{mag} = \frac{\Delta\chi V_p}{\mu_0}(\nabla B)B \tag{4}$$

where μ_0 is the vacuum permeability, V_p is the particle volume ($V_p = 4\pi r_{pt}^3/3$) and $\Delta\chi$ is the different in magnetic susceptibility between the particle and the fluid. Eq. (4) raised an interesting observation, in which the F_{mag} experienced by a nanoparticle is not only dependent on the magnetic field and field gradient but the volume of the MNP involved is equally important. For any design purposes which involved transport behaviors of MNP, knowing the value of u_{mag} is vital as various transport phenomena analyses can be performed [15].

Since the particle size is in nanometer range, its motion is heavily influenced by thermal energy and viscous drag; hence, conventional dimensionless number analysis can be very helpful to characterize the flow behavior. Table 1 summarized some of the useful dimensionless numbers which are familiar to the chemical and mechanical engineers and can serve as an effective way to rationalize the transport behavior of MNPs under magnetophoresis. By using the value of B and ∇B as shown in Fig. 2 and hydrodynamic radius of the MNPs (Fig. 1) at 150 nm as determined by dynamic light scattering (DLS), the Reynolds (Re), Péclet (Pe) and Froude (Fr) numbers with respect to the separation distance x from the pole surface of NdFeB magnet can be calculated (see Fig. 3a). Here we used the mathematical equations presented in Table 1 for the calculation of each dimensionless number and according to Eq. (3) the MNPs would typically having a magnetophoretic velocity within the range of 0.5 μm/s to around 9000 μm/s. As
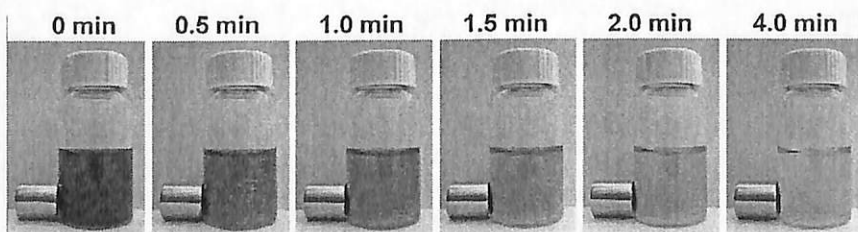

Fig. 1. Magnetophoretic collection of iron oxide MNPs with ~150 nm hydrodynamic radius in real time.

Table 1
Useful dimensionless number for characterization of MNP flow behaviors under magnetophoresis.

Dimensionless number	Equation[a]	Physical interpretation
Reynolds number, Re	$Re = \frac{\rho u_{mag} l}{\eta}$	Re defined the ratio of inertia to viscous force, as $Re \gg 1$, magnetophoresis dominated $Re \ll 1$, viscosity dominated
Péclet number, Pe	$Pe = \frac{u_{mag} l}{D}$	Pe defined the ratio of inertia to diffusion, as $Pe \gg 1$, magnetophoresis dominated $Pe \ll 1$, diffusion dominated
Froude number, Fr	$Fr = \frac{u_{mag}^2}{gl}$	Fr defined the ratio of inertia to gravitational pulling $Fr \gg 1$, magnetophoresis dominated $Fr \ll 1$, gravitational pulling dominated

[a] where l is the associated characteristic length scale, and for magnetophoresis study is concerned, it is typically taking as the diameter of MNP. ρ is the density of MNP and here we assumed it is purely magnetite with density of 5.2 g/cm³. D is the diffusivity of MNP and can be calculated by using Stokes–Einstein equation, and g is the acceleration due to gravity.

Fig. 3. Reynolds (Re), Péclet (Pe) and Froude (Fr) numbers calculated at (a) separation distance x from surface of a cylindrical NdFeB with varying B and ∇B values as shown in Fig. 2 and (b) different radius of MNPs at $B = 0.049$ Tesla and $\nabla B = 6.62$ Tesla/m. Broken line indicate the dimensionless number at one, so, above this point the magnetophoretic flow of the MNP dominates viscous drag, thermal randomization and also gravitational pulling.

clearly depicted in Fig. 3a, under this setup there presents a critical distance at around $x = 15$ mm in which magnetophoresis of a spherical MNP dominates other disturbances, such as Brownian motion, viscous drag and gravitational pulling. Below this separation distance, all three calculated dimensionless numbers are greater than unity. The shaded area above the broken line in Fig. 3a defines the effective operation region where the magnetophoretic collection could occur deterministically. In fact, this is the same area in which magnetic field B decayed drastically with respect to the separation distance x as shown in Fig. 2. The averaged magnetic field gradient ∇B within this zone at around 54.67 Tesla/m certified the nature of this process as LGMS. Detailed spatial resolution revealed by this dimensionless number analysis provides useful information for the design of LGMS system.

In general, the migration of MNPs under LGMS as shown in Fig. 1 is a complex interplay between magnetophoresis, viscous drag and random Brownian motion in which all these phenomena scale differently with the particle size. By taking $B = 0.049$ Tesla and $\nabla B = 6.62$ Tesla/m at critical separation distance of 15 mm, the Reynolds (Re), Péclet (Pe) and Froude (Fr) numbers can be calculated (see Fig. 3b) for MNPs with different radius. For magnetophoresis to play a dominant role, by having all three dimensionless numbers to be greater than one, MNP with radius between 140 nm and 180 nm is required. By taking the superparamagnetic size limit of magnetite (Fe_3O_4) particles at around $r = 17.5$ nm [16] gives dimensionless number of $Re = 0.0013$, $Pe = 0.0002$ and $Fr = 0.0011$, respectively. These very low values of Re, Pe and Fr numbers implied that the magnetophoretic motion of the MNP at this size would be overwhelmed by viscous drag, thermal energy and also

gravitational pulling. This examination is contradicting with the surprised results as observed by Yavuz and coworkers [1]. In directly, it has suggested the cooperative nature of the magnetophoresis and can also be generalized to our observation in Fig. 1.

At very high concentration in which the non-interacting particles assumption is not longer valid and magnetophoresis become concentration dependent [6], Eq. (3) alone is not suffice to estimate u_{mag} accurately. Under this scenario, a more sophisticated mathematic analysis such as the one suggested by Faraudo and Camacho is needed to estimate the separation time by taking into account the field induced aggregation of MNPs during the magnetophoresis [6,17]. For cooperative magnetophoresis, it is estimated that the recorded velocity can be 65 times higher than those predicted by conventional method [18]. Nevertheless, the dimensionless number analysis is still an easy route to provide quick feedback for checking the relation among important physical properties relevant to magnetophoresis of MNPs under LGMS as long as the u_{mag} can be estimated reasonably. More importantly, it also gives a useful approach to rationalize the complex interplay between the magnetophoresis with thermal energy, Stokes drag and gravitational pulling that eventually dictates the success or failure of LGMS in harvesting MNPs.

4. MNPs for engineering applications

For environmental engineering applications are concerned, MNP is typically being surface functionalized by macromolecules. This step is taken to mitigate the nanotoxicity associated to its small dimension [19], and to maintain its colloidal stability in

suspension [20]. However, just recently our group has revealed the conflicting role of colloidal stability in suppressing the magnetophoretic separation of MNPs [21,22]. After achieved good dispersibility, the polyelectrolyte coated iron oxide MNP become extremely difficult to be magnetophoretically separated out from its suspension even with the introduction of very high magnetic field gradient $\nabla B > 1000\,\text{Tesla/m}$ [22]. This in turn would suppress the cooperative effect as discussed in previous section and also prevent the chaining of MNPs that ultimately contribute to the rapid magnetophoresis [6]. The huge time lag and low efficiency observed might posed a serious challenge for the effective use of surface functionalized MNPs in any applications that required rapid separation.

It is obvious that MNPs cannot be a standalone nanoagent for most of the water treatment technology that required good colloidal stability and achieving rapid magnetophoretic separation while maintaining its other important properties, such as high specific surface area, catalytic activity, low nanotoxicity and etc. We anticipated that MNPs need to be combined with other components to fully realize its potential for water treatment applications. The integration of MNPs into polymeric microcapsule can be a feasible solution [23,24]. Other guided/self-assembly approaches, such as magnetoliposomes [25], pickering emulsion [26], templated-structure like silica-MNPs and activated carbon-MNPs [27,28], can also be a viable option. For the development of next generation MNP-enhanced nanomaterials for water treatment applications, the synthesis proceduce employed should be cost effective, environmental friendly and can produce large amount of nanomaterials within reasonable time frame. In addition, the magnetophoretic property should also be emphasized. This feature is necessary to ensure full recovery of the MNPs from treated water.

5. Conclusion

A more localized usages of MNP for water treatment purpose, such as in an on-site treatment facility, should be implemented in order to take full advantage of its magnetophoretic property. The idea of releasing enormous amount of MNPs into environment for water treatment purpose and magnetophoretically re-collecting this nanomaterial back is highly unrealistic. Cooperative phenomenon during the MNP magnetophoresis has greatly complicated the mathematical analysis on predicting the MNP velocity. In addition, the contribution of colloidal stability of MNPs toward LGMS is critical and should not be overlooked in any engineering applications. Dimensionless number calculation provides a fast and reliable analysis on the flow behavior of the MNPs under magnetophoresis. This analysis also related important physical properties associated to the magnetophoresis of MNPs under low field gradient. There are still many interesting opening questions related to magnetophoresis of MNPs [29]. More research efforts are needed in developing a practicable guided/self-assembly approach and efficient LGMS process for full utilization of MNPs in environmental engineering applications.

Acknowledgements

References

[1] C.T. Yavuz, J.T. Mayo, W.W. Yu, A. Prakash, J.C. Falkner, S. Yean, L. Cong, H.J. Shipley, A. Kan, M. Tomson, D. Natelson, V.L. Colvin, Low-field magnetic separation of monodisperse Fe₃O₄ nanocrystals, Science 314 (2006) 964–967.

[2] W. Yantasee, C.L. Warner, T. Sangvanich, R.S. Addleman, T.G. Carter, R.J. Wiacek, G.E. Fryxell, C. Timchalk, M.G. Warner, Removal of heavy metals from aqueous systems with thiol functionalized superparamagnetic nanoparticles, Environ. Sci. Technol. 41 (2007) 5114–5119.

[3] Y. Liu, T. Phenrat, G.V. Lowry, Effect of TCE concentration and dissolved groundwater solutes on NZVI-promoted TCE dechlorination and H₂ evolution, Environ. Sci. Technol. 41 (2007) 7881–7887.

[4] B. Saha, S. Das, J. Saikia, G. Das, Preferential and enhanced adsorption of different dyes on iron oxide nanoparticles: a comparative study, J. Phys. Chem. C. 115 (2001) 8024–8033.

[5] P.Y. Toh, S.P. Yeap, L.P. Kong, B.W. Ng, C.J.C. Derek, A.L. Ahmad, J.K. Lim, Magnetophoretic removal of microalgae from fishpond water: feasibility of high gradient and low gradient magnetic separation, Chem. Eng. J. 211–212 (2012) 22–30.

[6] G. Cuevas, J. Faraudo, J. Camacho, Low-gradient magnetophoresis through field-induced reversible aggregation, J. Phys. Chem. C. 112 (2008) 945–950.

[7] M. Benelmekki, C. Caparros, A. Montras, R. Goncalves, S. Lanceros-Mendez, LI.M. Martinez, Horizontal low gradient magnetophoresis behavior of iron oxide nanoclusters at the different steps of the synthesis route, J. Nanopart. Res. 13 (2011) 3199–3206.

[8] K. Mandel, F. Hutter, The magnetic nanoparticle separation problem, Nano Today 7 (2012) 485–487.

[9] V. Schaller, U. Kräling, C. Rusu, K. Petersson, J. Wipenmyr, A. Krozer, G. Wahnström, A. Sanz-Velasco, P. Enoksson, C. Johansson, Motion of nanometer sized magnetic particles in a magnetic field gradient, J. Appl. Phys. 104 (2008) 093918.

[10] J.K. Lim, C.J.C. Derek, S.A. Jalak, P.Y. Toh, N.H.M. Yasin, B.W. Ng, A.L. Ahmad, Rapid magnetophoretic separation of microalgae, Small 8 (2012) 1683–1692.

[11] G.D. Moeser, K.A. Roach, W.H. Green, T.A. Hatton, P.E. Laibinis, High-gradient magnetic separation of coated Magnetic nanoparticles, AIChE J. 50 (2004) 2835–2848.

[12] G.P. Hatch, R.E. Stelter, Magnetic design considerations for devices and particles used for biological high-gradient magnetic separation (HGMS) systems, J. Magn. Magn. Mater. 225 (2001) 262–276.

[13] M. Zborowski, L. Sun, L.R. Moore, P.S. Williams, J.J. Chalmers, Continuous cell separation using novel magnetic quadrupole flow sorter, J. Magn. Magn. Mater. 194 (1999) 224–230.

[14] N. Pamme, A. Manz, On-chip free-flow magnetophoresis: continuous-flow separation of magnetic particles and agglomerates, Anal. Chem. 76 (2004) 7250–7256.

[15] J.K. Lim, D.X. Tan, F. Lanni, R.D. Tilton, S.A. Majetich, Optical imaging and magnetophoresis of nanorods, J. Magn. Magn. Mater. 321 (2009) 1557–1562.

[16] D.J. Dunlop, Magnetite: behavior near the single-domain threshold, Science 176 (1972) 41–43.

[17] J. Faraudo, J. Camacho, Cooperative magnetophoresis of superparamagnetic colloids: theoretical aspects, Colloid Polym. Sci. 288 (2010) 207–215.

[18] J.S. Andreu, J. Camacho, J. Faraudo, M. Benelmekki, C. Rebollo, LI.M. Martinez, Simple analytical model for the magnetophoretic separation of superparamagnetic dispersions in a uniform magnetic gradient, Phys. Rev. E 84 (2011) 021402.

[19] A. Verma, F. Stellacci, Effect of surface properties of nanoparticle-cell interactions, Small 6 (2010) 12–21.

[20] P.L. Golas, S. Louie, G.V. Lowry, K. Matyjazsewski, R.D. Tilton, Comparative study of polymeric stabilizers for magnetite nanoparticles using ATRP, Langmuir 26 (2010) 16890–16900.

[21] S.P. Yeap, P.Y. Toh, A.L. Ahmad, S.C. Low, S.A. Majetich, J.K. Lim, Colloidal stability and magnetophoresis of gold-coated iron oxide nanorods in biological media, J. Phys. Chem. C. 116 (2012) 22561–22569.

[22] S.P. Yeap, A.L. Ahmad, B.S. Ooi, J.K. Lim, Electrosteric stabilization and its role in cooperative magnetophoresis of colloidal magnetic nanoparticles, Langmuir 28 (2012) 14878–14891.

[23] A.F. Ngomsik, A. Bee, J.M. Siaugue, V. Cabuil, G. Cote, Nickel adsorption by magnetic alginate microcapsules containing an extractant, Water Res. 40 (2006) 1848–1856.

[24] L.P. Kong, X.J. Gan, A.L. Ahmad, B.H. Hameed, E.R. Evarts, B.S. Ooi, J.K. Lim, Design and synthesis of magnetic nanoparticles augmented microcapsule with catalytic and magnetic bifunctionalities for dye removal, Chem. Eng. J. 197 (2012) 350–358.

[25] M. Gonzales, K.M. Krishnan, Synthesis of magnetoliposomes with monodisperse iron oxide nanocrystal cores for hyperthermia, J. Magn. Magn. Mater. 293 (2005) 265–270.

[26] A. Kaiser, T. Liu, W. Richtering, A.M. Schmidt, Magnetic capsules and pickering emulsions stabilized by core-shell particles, Langmuir 25 (2009) 7335–7341.

[27] W. Zhao, J. Gu, L. Zhang, H. Chen, J. Shi, Fabrication of uniform magnetic nanocomposite spheres with a magnetic core/mesoporous silica shell structure, J. Am. Chem. Soc. 127 (2005) 8916–8917.

[28] M. Schwickardi, S. Olejnik, E.L. Salabas, W. Schmidt, F. Schüth, Scalable synthesis of activated carbon with superparamagnetic properties, Chem. Commun. (2006) 3987–3989.

[29] J. Faraudo, J.S. Andreu, J. Camacho, Understanding diluted dispersion of superparamagnetic particles under strong magnetic fields: a review of concepts, theory and simulation, Soft Matter 9 (2013) 6654–6664.

CrossMark
← click for updates

The role of particle-to-cell interactions in dictating nanoparticle aided magnetophoretic separation of microalgal cells†

Pey Yi Toh,[a] Bee Wah Ng,[a,b] Abdul Latif Ahmad,[a] Derek Chan Juinn Chieh[a] and JitKang Lim*[a,c]

Successful application of a magnetophoretic separation technique for harvesting biological cells often relies on the need to tag the cells with magnetic nanoparticles. This study investigates the underlying principle behind the attachment of iron oxide nanoparticles (IONPs) onto microalgal cells, *Chlorella* sp. and *Nannochloropsis* sp., in both freshwater and seawater, by taking into account the contributions of various colloidal forces involved. The complex interplay between van der Waals (vdW), electrostatic (ES) and Lewis acid−base interactions (AB) in dictating IONP attachment was studied under the framework of extended Derjaguin−Landau−Verwey−Overbeek (XDLVO) analysis. Our results showed that ES interaction plays an important role in determining the net interaction between the *Chlorella* sp. cells and IONPs in freshwater, while the AB and vdW interactions play a more dominant role in dictating the net particle-to-cell interaction in high ionic strength media ($\geq$100 mM NaCl), such as seawater. XDLVO predicted effective attachment between cells and surface functionalized IONPs (SF-IONPs) with an estimated secondary minimum of −3.12 kT in freshwater. This prediction is in accordance with the experimental observation in which 98.89% of cells can be magnetophoretically separated from freshwater with SF-IONPs. We have observed successful magnetophoretic separation of microalgal cells from freshwater and/or seawater for all the cases as long as XDLVO analysis predicts particle attachment. For both the conditions, no pH adjustment is required for particle-to-cell attachment.

[a]School of Chemical Engineering, Universiti Sains Malaysia, Nibong Tebal, Penang 14300, Malaysia. E-mail: chjitkangl@usm.my
[b]School of Biological Sciences, Universiti Sains Malaysia, Minden, Penang 11800, Malaysia
[c]Department of Physics, Carnegie Mellon University, Pittsburgh, PA 15213, USA
†Electronic supplementary information (ESI) available: Table S1: Contact angle measurements. Table S2: Surface energy components of the liquids. Fig. S1: Microscopy images of *Chlorella* sp. cells trapped inside the bare-IONP flocculated matrix. Fig. S2–S3: TEM micrograph shows the relative size of IONPs to *Chlorella* sp. cells and the internalization of SF-IONPs into *Chlorella* sp. cells after effective attachment. Fig. S4: XDLVO diagram of the interaction between *Chlorella* sp. cells and SF-IONPs in freshwater and seawater. Fig. S5: Zeta potential of *Chlorella* sp. and SF-IONPs with respect to NaCl concentration. Fig. S6: Detachment efficiency of *Chlorella* sp. cells from SF-IONP-attached cell biomass in different concentrations of NaCl. Fig. S7: pH of the *Chlorella* sp. culture medium as a function of days. Fig. S8: Zeta potentials of *Chlorella* sp., bare-IONPs and SF-IONPs as a function of pH. Fig. S9: XDLVO diagram of *Chlorella* sp. interacting with SF-IONPs in pH 11 of 1 mM NaCl medium. Fig. S10: Microscopy images showed the attachment of particles to the marine species *Nannochloropsis* sp. Fig. S11: Cell separation efficiency of *Chlorella* sp. with different dosages of bare-IONPs. See DOI: 10.1039/c4nr03121k

1   Introduction

Given the current state of energy crisis, the recovery of microalgae biomass is crucial because it can serve as a sustainable alternative for the production of biofuel.[1,2] In this regard, magnetophoretic separation has been developed as an effective downstream separation technique to harvest microalgal biomass from aqueous environments.[3-7] The origin of this idea can be traced back to 1970s, when this method was applied for environmental engineering applications in removing microalgae that plagued fresh water lakes and caused eutrophication.[8,9] Compared to the more conventional separation technologies, magnetophoretic separation shows remarkable potential for the harvesting of microalgal cells because this technique has (1) high throughput, (2) low operational cost, (3) less energy intensive, (4) high separation efficiency, and (5) flexible for implementation and scalability.[3,10,11]

The underlying working principle for the magnetophoretic separation technique is straightforward. It centers on the need to tag non-magnetic microalgal cells with iron oxide nanoparticles (IONPs).[5,7,12,13] Later, the tagged biomass are exposed to an externally applied magnetic field to achieve its separation

from the surrounding media. Hence, the ability to predict the success or failure of magnetic nanomaterial attachment onto the microalgal cell surface is crucial for the implementation of this technology. From the seminal work of Xu and coworkers, adsorption isotherm analysis has been employed to make accurate yet simple estimation of the binding affinity and also the adsorption capacity of IONPs onto microalgae.[5] To verify the nature of interactions involved between the IONPs and microalgal cells, it is necessary to further identify the main driving factor behind this adsorption process.

So far, the attachment of IONPs onto microalgal cells can be promoted through the presence of macromolecules as a binding agent. Numerous macromolecules, such as chitosan, polyethylenimine, poly(diallyldimethylammonium chloride) etc.,[3,11,13,14] have been employed and shown remarkable capability to bind the IONPs onto the negatively charged microalgal cells. For freshwater species, the nature of interactions between the nanoparticles and microalgal cells is very likely dominated by electrostatic interaction.[13,14] With respect to marine species, the magnetophoretic technique works equally well with a separation efficiency of more than 90%.[4] Supposedly, the ionic stress induced by the high salt concentration in seawater would cause retardation and inhibit the electrostatic (ES) attraction between the cells and IONPs.[15] Under this circumstance, bridging flocculation can be important, but in the absence of extracellular polymeric substances on the microalgae surface, there exists some existing experimental evidence against this possibility.[16] By excluding both the ES and bridging effects, van der Waals (vdW) interaction should play a more pronounced role in promoting attachment of the IONPs onto marine microalgal cells. Moreover, since microalgae are considered hydrophilic bio-colloids due to their natural surface properties,[17] we may need to account for Lewis acid-based interactions in the entire adsorption mechanism.[11] It is the aim of this study to investigate the complex interplay of the aforementioned interactions in dictating the attachment of IONPs on microalgal cells.

The present study is dedicated to identifying the colloidal interactions involved in determining the successful attachment of IONPs onto microalgal cells. Experimentally we verified the attachment of IONPs by checking the magnetophoretic responsiveness of the tagged cells and direct visualization through optical microscopy. Electrophoretic mobility measurements were used to provide information on the surface charge of IONPs before and after their surface functionalization and also for microalgal cells. By employing Chlorella sp. as a model system, we investigated the attachment efficiency of IONPs onto this cell line within both freshwater and seawater. Extended Derjaguin–Landau–Verwey–Overbeek (XDLVO) theory, which takes into account the contribution of vdW, ES and the Lewis acid–base (AB) interaction, was employed to rationalize the colloidal interactions involved inparticle–microalgae interactions. Here, XDLVO analysis can be a clear-cut method to provide guidance in predicting the success or failure of IONP attachment onto microalgal cells, which further leads to the effective implementation of magne-

tophoretic separation. A marine species, Nannochloropsis sp., was employed to further confirm the reliability of the XDLVO prediction.

2 Experimental section

2.1 Materials

Bare iron oxide magnetic nanoparticles (bare-IONPs) with diameters at around 20–30 nm were obtained from Nanostructured & Amorphous Materials, Inc. The 35 wt% very low molecular weight poly(diallyldimethylammonium chloride) (PDDA) in water with molecular weight, $M_w < 100\,000$ g mol^{-1} was supplied by Sigma-Aldrich, Inc. Hydrochloric acid was purchased from PC Laboratory Reagents. The sodium hydroxide pellet and sodium chloride were supplied by MERCK & Co., Inc. Deionised water was obtained by reverse osmosis and further treated by the Milli-Q Plus system (Lillipore) to 18 MΩ cm resistivity.

2.2 Culture, preparation and characterization of Chlorella sp. and Nannochloropsis sp. cells

The Chlorella sp. and Nannochloropsis sp. strains were obtained from the School of Biological Sciences, Universiti Sains, Malaysia. The Chlorella sp. was cultivated in 250 ml Bold's Basal Medium (BBM), while the Nannochloropsis sp. was cultivated in 250 ml Conway medium. Both cultures were maintained under continuous illumination at 2000 lux and 25 °C. The media and flasks were autoclaved at temperature 121 °C for 15 minutes before cell cultivation. Continuous aeration was provided for the culture medium throughout the cultivation period. In this study, cell density of Chlorella sp. was maintained at around 3×10^7 cells ml^{-1} (after 10 culturing days) for all experiments. For subsequent experiments, the cells were collected through centrifugation and redispersed in deionized water multiple times to exclude the present of growth media. Later, the concentrated biomass was then redispersed into the desired medium (with different pH and ionic strength) as planned for experiments. For Nannochloropsis sp., the removal experiment was conducted right after 7 culture days to ensure the same cell density has been achieved similar to Chlorella sp. Cell numbers were determined by using a heamocytometer, while the size of cells was measured microscopically using Image Analysis Software. The average size of cells was calculated from 500 measurements.[18] The pH was measured by Eutech CyberScan pH 1500. The zeta potential of the microalgae was calculated based upon the Helmholtz–Smoluchowski limit using a Malvern Zetasizer.

2.3 Preparation and characterization of surface functionalized iron oxide nanoparticles (SF-IONPs)

The "attached-to" approach was employed to achieve attachment between the IONPs and cells.[14] The bare-IONPs were dispersed in deionized water and sonicated to achieve good dispersion at 1 g L^{-1}. PDDA was dispersed in deionized water (17 g L^{-1}) and stirred (500 rpm) for 1 day to achieve complete

dissolution. Then the bare-IONPs dispersion was added to the macromolecule solution, and the entire mixture was sonicated in a low power bath sonicator (40 kHz) to avoid degradation of the molecular structure.[19] This solution was then left on an end-to-end rotating mixer at 40 rpm overnight. After this surface modification step, a permanent magnet was used to collect the surface functionalized IONPs (SF-IONPs). The supernatant was discarded, while the SF-IONPs were again dispersed in deionized water. The electrophoretic mobility of bare-IONPs and SF-IONPs in different media of differing pH and ionic strength were measured using the Malvern Instruments Nanosizer. Unless otherwise stated, the zeta potentials of the bare-IONPs and SF-IONPs were then calculated based upon the Helmholtz–Smoluchowski limit.

2.4 Low gradient magnetic separation (LGMS)

For every separation study, 300 mg L^{-1} of bare-IONPs/SF-IONPs were added into cell medium to ensure an excess supply of particles. A total of 2 ml of 1.5 g L^{-1} particles, either bare-IONPs or SF-IONPs, was added to 8 ml cell medium followed with simple mixing for 30 seconds to ensure uniform mixing and dispersion. The mixture was left for another 30 seconds before use for the magnetophoretic separation study. Magnetophoretic separation of *Chlorella* sp. was carried under low gradient magnetic separation (LGMS) for 6 minutes. A N50-graded NdFeB permanent magnet was used to induce an inhomogeneous magnetic field with field gradient $\nabla B < 80$ T m^{-1}.[3] The absorbance of the cell was measured spectrophotometrically by a UVmini-1240 Shimadzu at the wavelength of 660 nm (measured by Agilent Technologies Carry 60 UV-Vis). The cell separation efficiency was determined as:

$$\text{Cell separation efficiency (\%)} = \frac{I_0 - I(t)}{I_0 - I_{\text{centrifuged}}} \times 100\% \quad (1)$$

where I_0 represents the initial absorbance intensity of the microalgae suspension after dilution with 2 ml deionized water, $I(t)$ represents the absorbance intensity of the micro-algae suspension during magnetophoretic separation at time t, and the $I_{\text{centrifuged}}$ represents the clear sample after centrifugation with the same dilution factor.

2.5 Contact angle measurement

The surface free energy of the microalgal cells and the bare-IONPs/SF-IONPs were determined by contact angle measurements. These contact angles were measured by using a contact angle goniometer (Rame-Hart Instrument Co.). Microalgal cells were pre-concentrated by centrifugation at 2500g for 4 minutes. A flat layer of cells was deposited on agar to stabilize the cell moisture content.[20] The flat surface of bare-IONPs was obtained by mechanically compressing the powder into pellets.[21] The concentrated solutions of SF-IONPs were deposited onto glass slides to form completely covered flat surfaces and dried at room temperature. Measurements were performed with two polar liquids (water and glycerol) and an apolar liquid (1-bromonaphthalene). The contact angle measurements were carried out by a sessile drop technique, and the readings were averaged from three replicate measurements.[18]

3   Results and discussion

3.1   Particle–microalgae interaction in freshwater and seawater

Magnetophoretic separation of microalgae from freshwater medium has proven to be feasible in previous studies.[3,14] We hypothesized that the effective attachment of iron oxide nanoparticles (IONPs) onto the surface of *Chlorella* sp. is mediated by electrostatic (ES) attraction.[12,13] A similar model system is employed in this study to further identify the actual contribution of the interactions involved. Fig. 1 shows that the bare iron oxide nanoparticles (bare-IONPs) do not adhere onto *Chlorella* sp. cells in freshwater. Only about 2.68% of cells were removed magnetophoretically with most of the cells entrapped
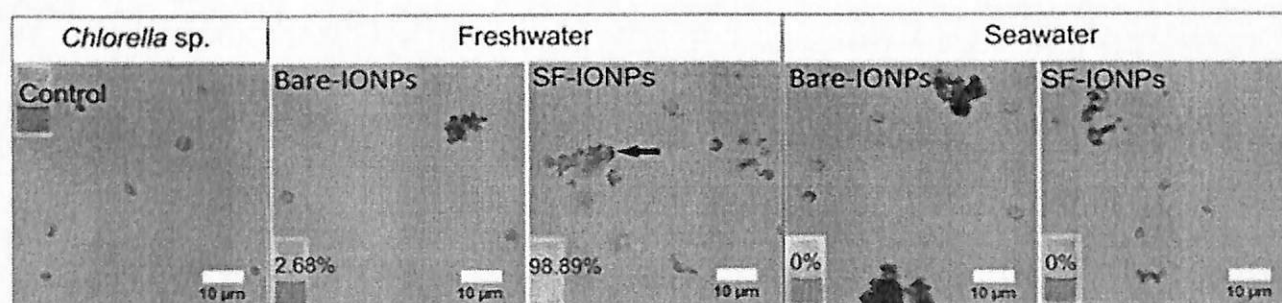

Fig. 1 Optical micrographs showing the degree of attachment for both bare- and SF-IONPs onto *Chlorella* sp. cells in freshwater and seawater. For bare-IONPs, under both aqueous environments, the particles aggregated extensively to form large clusters with no hint of attachment (dark ring around the cells) on the cell. Whereas for the case of SF-IONPs, the black arrow pointing toward the dark area indicates the presence of particles on the cell surface in freshwater. However, there is no clear indication showing the attachment of SF-IONPs onto microalgal cells in seawater. The bottom left corner of each micrograph shows a photo depicting the microalgae suspension after going through magnetophoretic separation. Use of bare-IONPs resulted in minimum magnetophoretic separation efficiencies of 2.68% and 0% for freshwater and seawater, respectively. There is also no clear cell separation for the case of SF-IONPs in seawater, but this particle is proven to be an effective tagging agent for promoting the magnetophoretic separation of microalgal cells in freshwater with a 98.89% separation efficiency.

Table 1 Details on the zeta-potential of each surface when dispersed in different media conditions together with pH

Conditions			
Fresh medium	pH	Surface	Zeta-potential (mV)
Freshwater	6.58	*Chlorella* sp.	−27.8 ± 5.5
		Bare-IONPs	−30.4 ± 4.9
		SF-IOPNs	25.2 ± 4.7
Seawater	6.32	*Chlorella* sp.	−9.1 ± 0.3
		Bare-IONPs	3.84 ± 1.0
		SF-IOPNs	4.95 ± 0.6

within the flocculated nanoparticle matrix (see ESI Fig. S1†). On the other hand, the surface functionalized iron oxide nanoparticles (SF-IONPs) are very likely to attach onto cell surfaces in freshwater condition, judging from the fact that a dark ring formed around most of the microalgal cells (arrow pointed area in Fig. 1). A cell separation efficiency as high as 98.89% was recorded with a particle dosage of 0.84 g per 1 g of dry biomass. This observation also serves as indirect confirmation of our speculation about the successful magnetic seeding of microalgal cells by SF-IONPs. By referring to Table 1, the surface charge of cells and bare-IONPs are similar, while the SF-IONPs have an opposite charge to the cells. These measurements have verified that the electrostatic (ES) interaction causes the cells and SF-IONPs to attract while it causes the cells and bare-IONPs to repel each other.

In seawater, both the bare-IONPs and SF-IONPs do not attach onto the cells (Fig. 1). As a consequence, there is no cell collection that can be detected optically. Table 1 shows that the surface charge of the cells and nanoparticles are suppressed to very low values compared to those in freshwater conditions. Typical seawater contains various types of dissolved salt, mainly Na^+ and Cl^- ions. The ionic strength of seawater is approximately 700 mM.[22] Hence, we hypothesized that the high ionic strength of seawater causes strong Deybe screening and weakens the electrostatic-repulsion between the particles. The particles aggregate extensively before their attachment onto the cells. Large aggregates found in seawater, as illustrated in Fig. 1, strongly support our hypothesis.

In classical DLVO analysis, the total interaction potential (U_{DLVO}) between two colloidal particles is described as a balance between the van der Waals (U_{vdW}) and ES (U_{ES}) interactions

$$U_{DLVO} = U_{vdW} + U_{ES} \qquad (2)$$

in which the extent of ES interaction depends on the surface charge/zeta potential of the interacting particles, and it can be attractive or repulsive.

In this study, due to the huge size mismatch between the IONPs and the microalgal cells (see ESI Fig. S2†), where the mean size of *Chlorella* sp. cells is 3.45 μm and is far larger than the IONPs with a diameter at around 25 nm, the surface of the cell is assumed to be flat with respect to the spherical IONPs. Under this scenario, the surface curvature of cell is
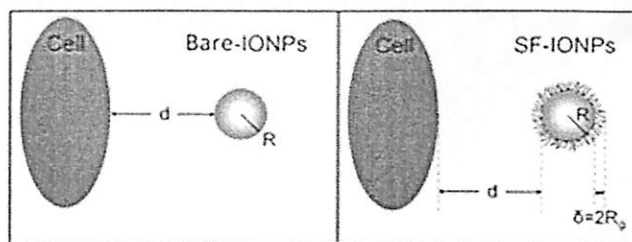

Fig. 2 Schematic illustration of a microalgal cell interacting with either a bare-IONPs (left) and SF-IONPs (right). Due to the large size mismatch between these two entities, we simplified our analysis to sphere–plane interaction. In this diagram, *d* represents the surface-to-surface separation distance between the cell and particle, *R* is the particle radius, δ is the thickness of the polymer adlayer coated on the IONP surface. All the symbols are in accordance to the parameters used in our analysis.

negligible with respect to the high curvature of nano-sized IONPs. The Lifshitz–van der Waals equation for sphere–plane configuration is applied[23] as a function of separation distance, *d*:

$$U_{vdw} = -\frac{A_{eff}R}{6}\left[\frac{1}{d} + \frac{1}{d+2R}\right] - \frac{A_{eff}}{6}\ln\left[\frac{d}{d+2R}\right] \qquad (3)$$

Here *d* is the surface-to-surface separation distance between the cell and the IONP (Fig. 2); A_{eff} represents the effective Hamaker constant; and *R* is the radius of the IONP. The Hamaker constant of each surface was estimated by contact angle measurement (see ESI Table S1†) with the use of at least three different liquids (polar or apolar), of which two must be polar liquids (see ESI Table S2†).[24,25] The Hamaker constant of material *i*, A_i is proportional to the vdW component of the material surface tension, γ_i^{LW}, and can be defined as follows:[24]

$$A_i = 24\pi d_0^2 \gamma_i^{LW} \qquad (4)$$

where d_0 is the minimum equilibrium distance between two condensed-phase surfaces (d_0 = 0.657 ± 0.01 nm).[26] The γ_i^{LW} can then be determined by using the Young's equation (Table 2):[27]

$$(1 + \cos\theta)\gamma_L = 2\left(\sqrt{\gamma_S^{LW}\gamma_L^{LW}} + \sqrt{\gamma_S^{\oplus}\gamma_L^{\ominus}} + \sqrt{\gamma_S^{\ominus}\gamma_L^{\oplus}}\right) \qquad (5)$$

where γ is surface tension, mJ m^{-2}; $\gamma^{\oplus}$ is the electron-acceptor parameter of the polar surface tension component, while $\gamma^{\ominus}$ is the electron-donor parameter of the polar surface tension component; and the subscripts S and L stand for the solid and liquid, respectively.

The effective Hamaker constant, A_{eff} is the combined relationship between different materials that contributes to the vdW body–body interaction. The A_{eff} of interaction between materials 1 and 3 separated by medium 2 can be defined as:[28]

$$A_{eff} = A_{123} = \left(\sqrt{A_{11}} - \sqrt{A_{22}}\right)\left(\sqrt{A_{33}} - \sqrt{A_{22}}\right) \qquad (6)$$

According to this definition, for two colloidal particles suspended in liquid, the vdW interaction can be either attractive

*Table 2 Surface energy and Interfacial energy involved for the calculation of Lewis acid—base interaction. Subscript *iw* implies the interfacial energy of surface *i* in water and *iwi* implies the interfacial energy of surface *i* to surface *i* in water

Surface, i	Surface energy (mJ m^{-2})					Interfacial energy (mJ m^{-2})	
	γ^{tot}	γ^{LW}	γ^{AB}	$\gamma^{\oplus}$	$\gamma^{\ominus}$	ΔG_{iw}	$\Delta G_{iwi}{}^{AB}$
Chlorella sp.	75.0	22.2	52.8	4.8	145.1	−188	80
Bare-IONPs	48.1	44.0	4.2	0.06	74.2	−151	69
SF-IONPs	45.31	43.5	1.81	0.01	74.4	−150	71
Nannochloropsis sp.	40.0	26.2	13.8	0.65	73.3	−142	60

or repulsive.[29] The calculated A_{eff} between the *Chlorella* sp. cells and the bare-IONPs and SF-IONPs are 2.86×10^{-21} J and 2.81×10^{-21} J respectively.

ES interaction between a charged plane and a charged sphere is modeled as:[23]

$$U_{ES} = \pi \varepsilon R' \left(\xi_1{}^2 + \xi_2{}^2\right) \left[\frac{2\xi_1\xi_2}{\xi_1{}^2 + \xi_2{}^2} \ln\frac{1 + e^{-\kappa d}}{1 - e^{-\kappa d}} + \ln\left(1 - e^{-\kappa d}\right) \right] \quad (7)$$

where ξ is the zeta potential; κ is the Debye–Hückel parameter; and the ε represents the permittivity of the medium, where $\varepsilon = \varepsilon_r\varepsilon_0$. The permittivity of free space, ε_0, is 8.854×10^{-12} F m^{-1}. In the case of SF-IONPs, $R' = R + \delta$ where δ is the adlayer thickness, which is determined at 4.85 nm.[15]

According to the classical DLVO analysis under freshwater conditions (Fig. 3a), the ES interaction between differently charged cells and SF-IONPs enables effective particle-to-cell linkage as evident from the net attractive interaction. Interestingly, we observed particle internalization into the cells for the case of SF-IONPs.[12] This process most likely happens through the membrane deformation caused by reorganization of the lipid bilayer when the nanoparticles successfully attach on the cell surface (see ESI Fig. S3†). This observation is in accordance with the optical micrograph shown in Fig. 1. However, for the bare-IONPs, the energy barrier with the *Chlorella* sp. cell is more than 10 kT and prohibits the attachment of particles. In seawater, the classical DLVO theory (Fig. 3b) predicts the bare-IONPs and SF-IONPs are always ready to attach on the cell
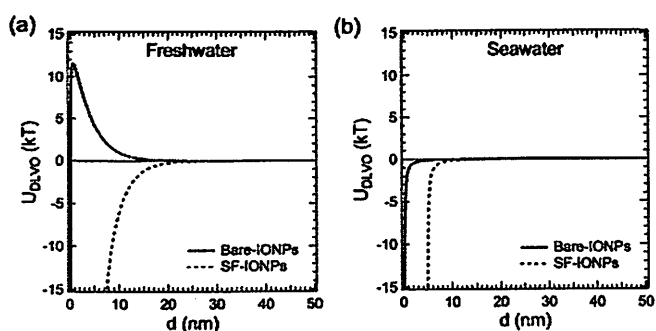

Fig. 3 Classical DLVO profiles for the interaction between *Chlorella* sp. cells and bare-IONPs/SF-IONPs in (a) freshwater and (b) seawater with the overall interacting potential U_{DLVO} plotted for both species of IONPs used.

surface promoted by the attractive vdW force. However, we observed no separation of microalgal cells for both species of nanoparticles (Fig. 1). Even though the rapid aggregation of particles might be the dominant factor causing poor separation efficiency, from the optical microscopy observation we have also failed to detect any hint of particle attachment. This in turn has indirectly suggested that the classical DLVO analysis is insufficient to provide useful prediction related to particle attachment within our experimental conditions.

3.2 XDLVO considerations

From the existing literature, there are a number of studies emphasizing the need to include polar interactions into the analysis involving biological cells.[11,18,23,27] Since microalgal cells are also a hydrophilic biocolloid due to their natural surface properties, where the outer cell membrane is made up of the hydrophilic end of the phospholipid layer,[17,27] the polar interaction based on electron acceptor–electron donor (Lewis acid–base, AB) interactions may be important. In this context, the AB interaction can be up to two orders of magnitude higher than those commonly encountered among the components of the traditional DLVO energy balance.[24] In addition complexity may arise as the changes in the ionic strength of culture media would suppress the electric double layer and therefore retard the ES interaction. This condition will become more pronounced in seawater culture with the complex ionic environment. As such, a more physically sound analysis taking into account the AB interaction might be necessary, and this new physicochemical approach, which takes into account contributions other than vdW and ES interactions, is known as the extended DLVO (XDLVO) analysis.

In this study, the van Oss–Chaudhury–Good (OCG) thermodynamic approach is used to determine the AB interaction.[24] Table 2 shows that the *Chlorella* sp., bare-IONPs and SF-IONPs are strongly hydrophilic since their $\gamma^{\ominus}$ values are larger than that of the water, while their $\gamma^{\oplus}$ values are far less than that of water, where $\gamma_w^{\oplus} = \gamma_w^{\ominus} = 25.5$ mJ m^{-2} for water. A larger $\gamma^{\ominus}$ surface exhibits strong affinity to water molecules *via* the formation of hydrogen bonds. The *Chlorella* sp., bare-IONPs and SF-IONPs tend to bind water strongly with free energies in the range of −140 to −190 mJ m^{-2}, which are stronger than the hydrogen-bonding energy of water (−102 mJ m^{-2}).[30] When these hydrophilic cells/particles disperse in water, they experience hydrophilic repulsion with an AB interfacial interaction

energy greater than zero ($\Delta G_{iwi}{}^{AB} > 0$). This interfacial interaction energy is defined as:

$$\Delta G_{iwi}{}^{AB} = 4\left(\sqrt{\gamma_i^{\oplus}\gamma_w^{\ominus}} + \sqrt{\gamma_w^{\oplus}\gamma_i^{\ominus}} - \sqrt{\gamma_i^{\oplus}\gamma_i^{\ominus}} - \sqrt{\gamma_w^{\oplus}\gamma_w^{\ominus}} \right) \quad (8)$$

$\Delta G_{iwi}{}^{AB}$ decreases in the order of *Chlorella* sp. > SF-IONPs > bare-IONPs, at 80, 71 and 69 mJ m^{-2} respectively.[25,27] After cells and bare-IONPs/SF-IONPs are mixed in water, both surfaces experience hydrophilic repulsion with respect to each other. The $\Delta G_{iwj}{}^{AB}$ for the configuration of *Chlorella* sp. cells and bare-IONPs is 87.7 mJ m^{-2}, and for cells interacting with SF-IONPs, it is 89.6 mJ m^{-2}.

$$\Delta G_{iwj}{}^{AB} = 2\left(\sqrt{\gamma_i^{\ominus}\gamma_j^{\ominus}} + \sqrt{\gamma_j^{\ominus}\gamma_w^{\ominus}} + \sqrt{\gamma_w^{\oplus}\gamma_i^{\ominus}} + \sqrt{\gamma_w^{\ominus}\gamma_j^{\ominus}} \right.$$
$$\left. - 2\sqrt{\gamma_w^{\oplus}\gamma_w^{\ominus}} - \sqrt{\gamma_i^{\ominus}\gamma_i^{\ominus}} - \sqrt{\gamma_j^{\oplus}\gamma_i^{\ominus}} \right) \quad (9)$$

From the above point of view, the AB interaction should be included in the XDLVO analysis:

$$U_{XDLVO} = U_{vdW} + U_{ES} + U_{AB} \quad (10)$$

The AB interaction between a plane and sphere, as a function of distance, can be predicted as:[23,31]

$$U_{AB} = 2\pi a \lambda \Delta G_{d_0}^{AB} \exp\left[\frac{d_0 - d}{\lambda} \right] \quad (11)$$

where λ is the correlation length of molecule in a liquid medium. For hydrophilic repulsion, $\lambda = 0.6$ nm; for hydrophobic attraction, $\lambda = 13$ nm.[30]

In freshwater, the XDLVO analysis shown in Fig. 4a predicts a high energy barrier between cells and bare-IONPs at around >1000 kT, which strongly prohibits the effective particle-to-cell attachment. For the case of SF-IONPs, a secondary minimum (−3.12 kT) is observed once the AB interaction is considered. At this point, the attachment of cells with SF-IONPs is effective.[32] The major difference between the DLVO and XDLVO analyses for interaction between *Chlorella* sp. and SF-IONPs is that the DLVO predicts net attraction, whereas the XDLVO predicts the present of a secondary minimum followed with strong hydrophilic repulsion (due to U_{AB}) as the particle–

cell separation distance approaches the layer thickness of the PDDA coating (see ESI Fig. S4a†). Nevertheless, both analyses predicted successful attachment of the SF-IONPs onto *Chlorella* sp.

In seawater, as shown in Fig. 4b, the XDLVO analysis predicts net repulsion between the cells and the bare-IONPs/SF-IONPs. The available repulsive AB interaction strongly prohibited the effective attachment for both cases in which the energy barrier is much higher than 100 kT (see ESI Fig. S4b†). This prediction is in accordance with the observation delineated in Fig. 1. Therefore, from a theoretical perspective, the AB interaction plays a crucial role in determining the net interaction between the nanoparticles and microalgal cells under seawater conditions.

3.3 Variation of ionic strength verified the important role of AB interactions

Our XDLVO analysis confirms that the ES and AB interactions are both important in governing the net interaction of cells and nanoparticles in different ionic strength conditions. An interacting system between the cells and SF-IONPs is monitored to investigate the inter-relationship of the ES and AB as ionic strength increases from 1 to 700 mM. Since the dissolved mineral substance of seawater is mainly made up of Na$^+$ and Cl$^-$ ions, about 30.6% and 55%, respectively, sodium chloride (NaCl) salt is used for adjusting the ionic strength.[33]

Fig. 5 shows the cell separation efficiency is the highest in 1 mM ionic strength medium using SF-IONPs. At this level of ionic strength, it is possible to achieve an overall cell separation efficiency at around 98.82 ± 0.31%; the left over crystal

Fig. 5 Separation efficiency of *Chlorella* sp. cell as a function of NaCl concentration up to 700 mM, which is equivalent to the ionic strength of seawater. Here, 300 mg L^{-1} of SF-IONPs is added to the cell suspension corresponding to 1.27 g nanoparticles per 1 g dry biomass. All separation processes were conducted at low field gradient for 6 minutes. Bottom images shows how the final suspensions look after the separation.
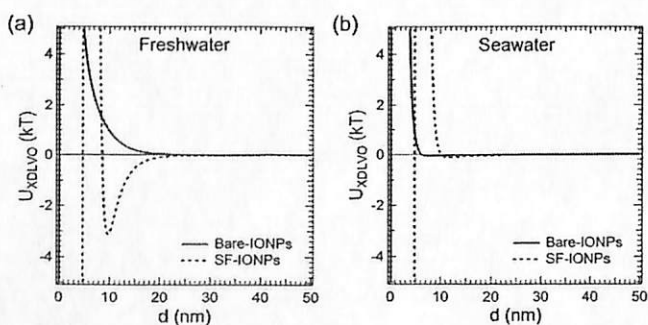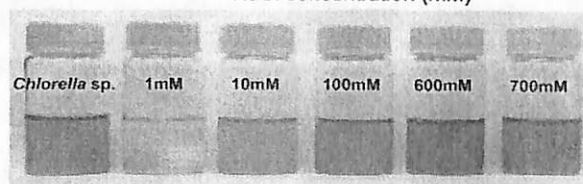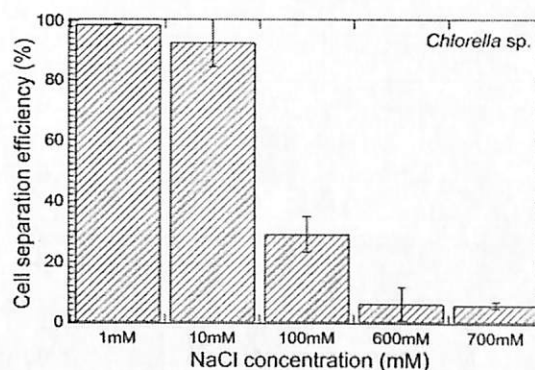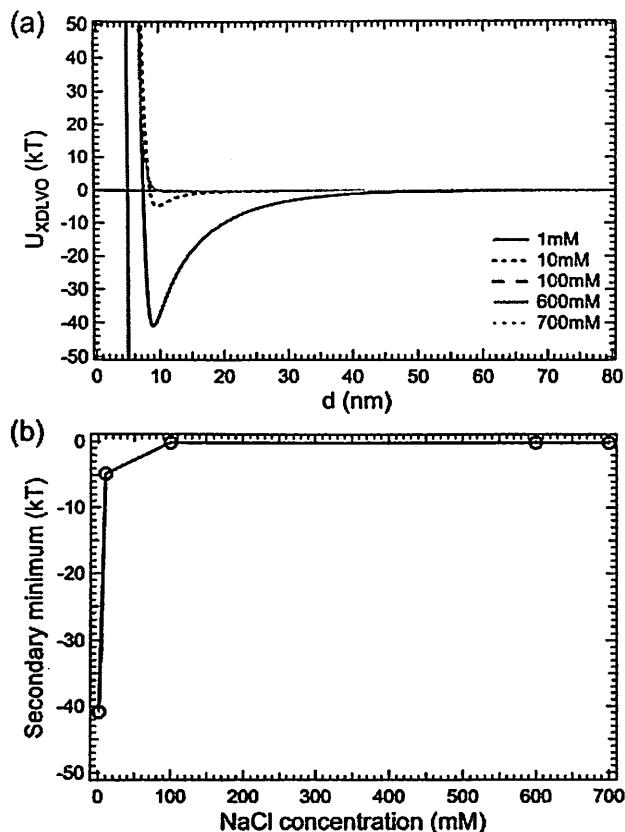
Fig. 4 XDLVO profiles for the interaction between *Chlorella* sp. cells and bare-IONPs/SF-IONPs in (a) freshwater and (b) seawater with the overall interacting potential U_{XDLVO} plotted for both species of IONPs used.

Fig. 6 (a) XDLVO profile showing the net interaction between the Chlorella sp. cells and SF-IONPs at different NaCl concentrations. (b) Well depth of the secondary minimum predicted by the XDLVO as a function of NaCl concentration from part (a).
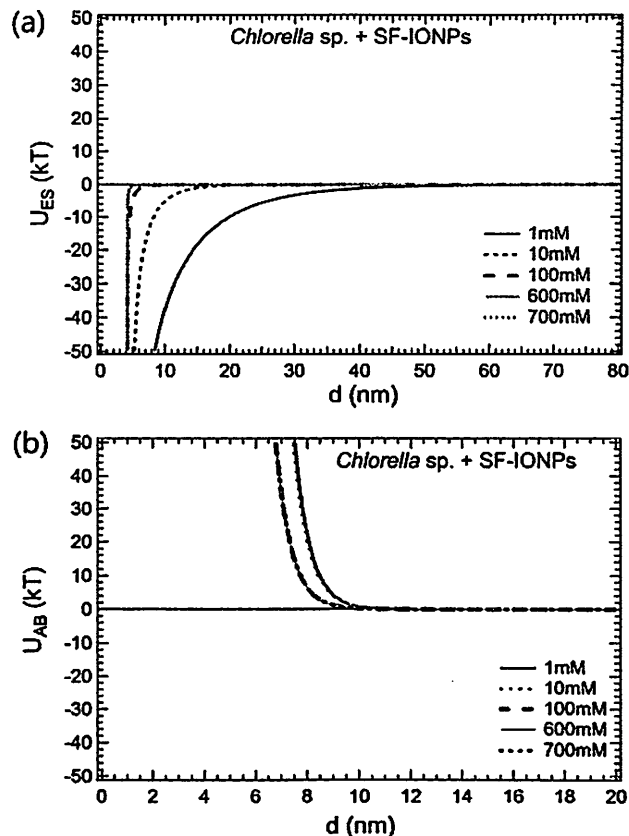

Fig. 7 Normalized interacting potential of (a) electrostatic and (b) Lewis acid–base interaction with respect to the separation distance, d between Chlorella sp. and SF-IONPs at different NaCl concentrations. Regardless of ionic strength, U_{ES} is always negative (attractive) and U_{AB} is always positive (repulsive) within the investigated concentration range of NaCl.

clear supernatant indicated that most cells have been successfully collected. Overall cell separation efficiency dropped to 92.84 ± 8.32% as we further increased the ionic strength of the suspension to 10 mM. When the ionic strength increased to more than 100 mM, cell separation efficiency becomes much lower, and only 5.75 ± 1.09% of cells are removed in 700 mM medium. This experimental observation is in accordance with the XDLVO model prediction as shown in Fig. 6. The well depth of the secondary minimum sharply decreases from −41 kT to −5 kT when ionic strength increases from 1 mM to 10 mM. The net repulsive interaction predicted from the XDLVO analysis above, without the presence of a secondary minimum at ionic strength of 100 mM, indicates that no effective attachment between the SF-IONPs and cells can occur. They tend to repel each other, and this is in good agreement with our previous observation in which no SF-IONP attachment is observed in seawater.

As shown in Fig. 7a and b, both the effective length scale for ES and AB interactions between SF-IONPs and Chlorella sp. decreased with the increase in ionic strength. For the former case, the reduction in terms of the effective interaction range is due to the Debye screening effect as discussed previously (see ESI Fig. S5†). Moreover, it should be noted that the extent of reduction in the effective interaction range is much more

pronounced for ES interaction compared to AB interaction. In fact, this slight reduction in the interaction range for the AB case is very likely due to the complex interplay of the salting out effect and conformational changes in the polyelectrolyte layer.[34,35] Suppression of the physical barrier formed due to polyelectrolyte layer adsorption, which subsequently reduces the absolute surface-to-surface separation distances, should be the main reason for the decreasing range of AB interaction.

This study shows the ES interaction is crucial to facilitate effective particle-to-cell attachment in freshwater, while the AB interaction is more dominant in high ionic strength condition (≥100 mM). Having this kind of information, especially by knowing the extent of interaction involved, has provided us a guideline to design an effective strategy to promote particle detachment. For example, since ES interaction is most influential on the particle-to-cell attachment in freshwater, suppression of this interaction by introducing an ionic stress could disrupt the entire interaction scheme, which subsequently could cause particle detachment (see ESI Fig. S6†). This investigation is important for the recovery of SF-IONPs by magnetophoresis without the need for pH adjustment for effective implementation of magnetophoretic separation of microalgae without taking the risk of causing cell lysis.[36,37]

3.4 Domination of ES interaction with respect to pH

Throughout the entire time course of the cultivation process, the pH of the culture media shifted to a more alkaline condition (see ESI Fig. S7†). In addition, the ES interaction is sensitive toward the pH change in the surrounding media through the influence on the surface charge. These two important phenomena motivated our work in this section, which focuses on the effect of pH on the interactions between microalgal cells and bare-IONPs/SF-IONPs.

In this study, the bare-IONPs have an isoelectric point at about pH 8, while both *Chlorella* sp. cells and SF-IONPs did not show any charge reversal behavior within the pH range of 3 to 11 (see ESI Fig. S8†: cells will always carry a net negative charge and the SF-IONPs will always in a positive charge). The results in Fig. 8 show that the U_{ES} in the case of cells with bare-IONPs changes from attraction (negative zone) to repulsion (positive zone) when the pH changes across the isoelectric point of bare-IONPs. Associated with this change is the obvious diminishing of the secondary minimum with a well depth of −7.68 kT at pH 3 to net repulsion at pH 11 (Fig. 9a). Our experimental results (Fig. 9b) have proven the reliability and versatility of the XDLVO analysis where the attractive interaction binds the cells and bare-IONPs together and forms cell-particle clusters at pH 3, as shown in Fig. 9c. For the case of SF-IONPs, the results in Fig. 8b illustrate that the U_{ES} always maintains attraction between the negative charged cells and positive charged SF-IONPs. The secondary minimum predicted by XDLVO theory (Fig. 9a) is nicely developed (>9 kT in magnitude) and promotes attachment of the SF-IONPs on the microalgal cell surface. This observation is consistent with the experimental results (Fig. 9b) with a cell separation efficiency of more than 90% in all pH values. It should be noted that in our case the ES interaction has a slightly longer range compared to the AB interaction (see ESI Fig. S9†), and thus, the ES dominates the net interaction energy, U_{XDLVO}, with respect to pH. Our optical microscopy observations (Fig. 9d) clearly show the effective attachment of particles to cells for the case of SF-IONPs. This study has confirmed the important role of ES and AB interactions under freshwater conditions. Therefore, these two interactions need to be considered in order to predict successful particle-to-cell attachment by XDLVO analysis.
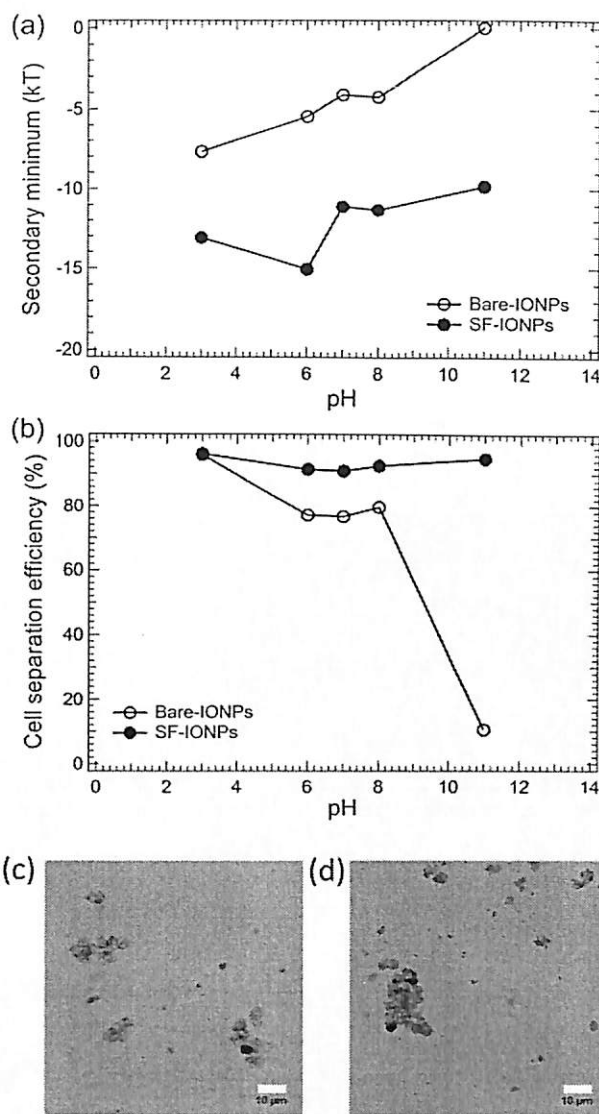

Fig. 9 Diagrams showing the (a) well depth of secondary minimum predicted by the XDLVO analysis and the (b) cell separation efficiency from experiment observations when the *Chlorella* sp. cells are interacting with the bare-IONPs and SF-IONPs at different pH. Cell separation is performed by a NdFeB cylindrical magnet with a total collection time of 6 minutes at a dosage of 1.27 g nanoparticles per 1 g dry biomass. Microscopy images showing the effective attachment between cells and (c) bare-IONPs in pH 3 and (d) SF-IONPs in pH 11. Dark rings and spots detected over most of the cell surface indicated the successful attachment of particles.
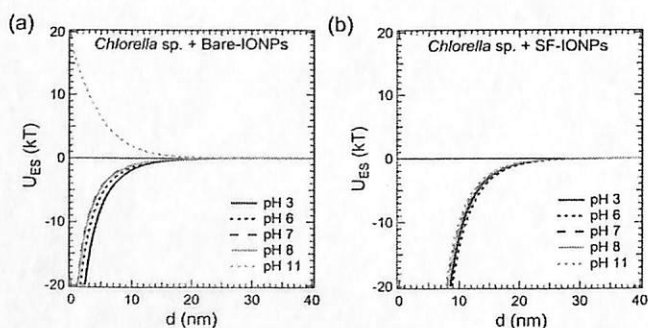
3.5 Attachment of nanoparticles on marine species

In order to further verify the feasibility of the XDLVO theory in predicting the particle-to-cell interaction in seawater, another marine species of microalgae, named *Nannochloropsis* sp., was employed for a particle-to-cell attachment study.

In general, *Nannochloropsis* sp. cells have a simple spherical structure with a diameter around 3–5 μm, resembling the size and shape of *Chlorella* sp. Table 2 shows that the AB interfacial interaction energy (per unit contact area) between the surfaces of *Nannochloropsis* sp. is weaker than the *Chlorella* sp.

Fig. 8 U_{ES} curve as a function of distance between *Chlorella* sp. and (a) bare-IONPs and (b) SF-IONPs at different pH.

The *Nannochloropsis* sp. experiences weaker AB repulsive interaction when in contact with the bare-IONPs and SF-IONPs, with its surface energy at 64.0 mJ m^{-2} and 65.1 mJ m^{-2} compared to that of the *Chlorella* sp., at 87.7 mJ m^{-2} and 89.6 mJ m^{-2}, respectively. Our XDLVO analysis predicts a secondary minimum well depth at −0.90 kT for cell/bare-IONP interaction and −1.94 kT for cell/SF-IONP interaction (see Fig. 10). With a low particle-to-cell ratio at 0.42 g g^{-1}, there is no obvious attachment of bare-IONPs onto cells and almost all of the particles have aggregated to form large clusters (see Fig. S10 in ESI†). However, for the case of SF-IONPs, we observed particle attachment even at a very low particle-to-cell ratio of 0.21 g g^{-1} (Fig. S10†). Together with the results presented in Fig. 10, our microscopy observations support our hypothesis that magnetic separation would definitely occur as long as there is particle attachment. Fig. 10b shows that the magnetophoretic separation efficiencies achieved are 97.90 ± 0.27% and 4.94 ± 0.50% for SF-IONPs and bare-IONPs, respectively, when in particle-to-cell ratio is 0.42 g g^{-1} (see ESI Fig. S10†). The recorded separation efficiency has indirectly confirmed that particle-to-cell aggregation is weak and insignificant for well depths less than ~1.5 kT.[38] In thermal equilibrium, according to the equipartition theorem, a particle has the same average energy associated with each independent degree of freedom of their motion. Hence, the translational kinetic energy possessed by a free particle is equivalent to 3/2 kT ($<E_{kinetic}>$ = 1.5 kT). The overall attractive interaction between the IONPs and microalgal cells need to overcome this energy for binding to happen. The results shown in Fig. 10a and b are nicely aligned with this classical prediction and provide a proper guideline for magnetic seeding of microalgal cells. Under this principle, particle attachment could only happen if the particle-to-cell interaction achieved a well-depth of secondary minimum beyond 1.5 kT under XDLVO analysis. Even though the magnitude of attractive interaction is weak for the case of bare-IONPs on *Nannochloropsis* sp., magnetophoretic separation of this species of microalgae can still be implemented by increasing the particle concentration. Since the electrostatic interaction within seawater is relatively weak, as suggested by our previous XDLVO analysis, we hypothesized that the vdW and AB interactions should play a major role here. Moreover, the high concentration of particles enables the cells and bare-IONPs to collide more frequently, hence increasing the probability of particle attachment. Fig. 10b shows that a separation efficiency of *Nannochloropsis* sp. up to 80.22 ± 10.57% can only be achieved with a particle-to-cell ratio of 2.11 g g^{-1} (see ESI Fig. S10†). By taking the density of iron oxide at 4.95 g cm^{-3} and the mean diameter of the particles as 25 nm, we estimated that there are around 1.74 × 10^{12} particles per cell.

By referring back to the case of *Chlorella* sp. with bare-IONPs, the net repulsive interaction predicted by the XDLVO theory has suggested that under all circumstances, even at high particle concentrations, there should be no particle attachment, and hence no microalgae separation. Our results confirmed this observation (ESI Fig. S11†) and verified the critical need to take into account AB interaction in predicting the particle-to-cell interaction. Moreover, the vdW and AB interactions should be taken into account to predict the effectiveness of particle-to-cell attachment in seawater without the need to consider the ES interaction due to the Debye screening effect.[15] From all the data presented, magnetophoretic separation can be implemented successfully as long as the particles attach. This finding makes the prediction of particle attachment, such as discussed in this work, crucial for the implementation of magnetophoretic separation of microalgal cells.
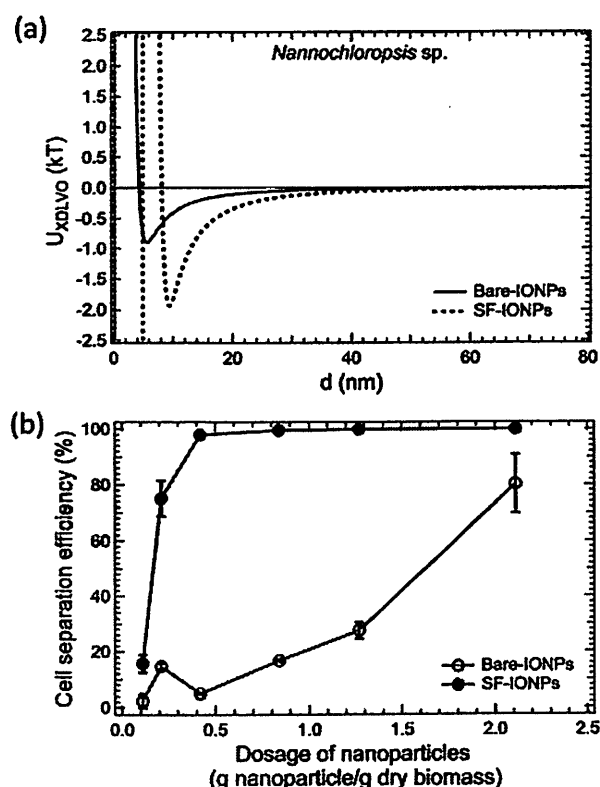

Fig. 10 (a) XDLVO analysis for the interaction between the marine species *Nannochloropsis* sp. with bare-IONPs and SF-IONPs. The well depth of secondary minimum predicted for each case is −0.90 kT (bare-IONPs) and −1.94 kT (SF-IONPs). (b) Separation efficiency of *Nannochloropsis* sp. under LGMS at different dosages.

4 Conclusions

XDLVO analysis can be employed as a very useful mathematical analysis to predict the successful IONP attachment onto the microalgal cells, either in freshwater or seawater. In freshwater, the effectiveness of the particle-to-cell attachment is always governed by ES interaction, in which this interaction is strongly affected by the surface zeta-potential. The AB interaction between *Chlorella* sp. and bare-IONPs/SF-IONPs has a shorter interaction distance than ES interaction. The XDLVO analysis has predicted a net repulsion between *Chlorella* sp. cells and bare-IONPs while predicting effective attachment of

SF-IONPs onto cell surface with a secondary minimum of −3.12 kT, which is in accordance with our experimental observation. In seawater, the AB interaction plays a pivotal role in determining the net interaction between the cells and IONPs. High ionic strength suppresses the Debye screening length of the charged particles and induces a relatively short length for ES interaction, between cells and IONPs. This observation is beneficial for the design of an effective protocol to promote particle detachment from cell surfaces, which would greatly improve the reusability of the IONPs for subsequent separation cycles. The XDLVO theory has predicted the presence of a secondary minimum with a well depth of −1.94 kT, which is mainly dominated by the vdW interaction, and followed by a strong hydrophilic repulsion (U_{AB}) for the case of marine species *Nannochloropsis* sp. cells interact with SF-IONPs in seawater. Under this scenario, 97.90 ± 0.27% of cells were magnetophoretically separated at a particle dosage of 0.42 g particles per 1 g dry biomass. This prediction is strongly related to the less hydrophilic surface of *Nannochloropsis* sp. We anticipate that the XDLVO analysis presented here can be employed to aid the process of (1) selecting an appropriate molecular binder for surface functionalization of IONPs, which subsequently promotes particle attachment onto microalgal cells, and more importantly, (2) predicting the successful implementation of magnetophoretic separation without the need to conduct tedious and lengthy experiments.

Acknowledgements

Notes and references

1 Demirbas, *Energy Convers. Manage.*, 2010, 51, 2738–2749.
2 A. L. Ahmad, N. H. M. Yasin, C. J. C. Derek and J. K. Lim, *Renewable Sustainable Energy Rev.*, 2011, 15, 584–593.
3 P. Y. Toh, S. P. Yeap, L. P. Kong, B. W. Ng, D. J. C. Chan, A. L. Ahmad and J. K. Lim, *Chem. Eng. J.*, 2012, 211–212, 22–30.
4 M. Cerff, M. Morweiser, R. Dillschneider, A. Michel, K. Menzel and C. Posten, *Bioresour. Technol.*, 2012, 118, 289–295.
5 L. Xu, C. Guo, F. Wang, S. Zheng and C. Z. Liu, *Bioresour. Technol.*, 2011, 102, 10047–10051.
6 Y. R. Hu, F. Wang, S. K. Wang, C. Z. Liu and C. Guo, *Bioresour. Technol.*, 2013, 138, 387–390.
7 G. Prochazkova, I. Safarik and T. Branyik, *Bioresour. Technol.*, 2013, 130, 472–477.
8 G. Bitton, J. L. Fox and H. G. Strickland, *Appl. Microbiol.*, 1975, 30, 905–908.
9 R. Yadida, A. Abeliovich and G. Belfort, *Environ. Sci. Technol.*, 1977, 11, 913–916.
10 M. Zborowski, L. R. Moore, S. William and J. J. Chalmers, *Sep. Sci. Technol.*, 2002, 37, 3611–3633.
11 G. Prochazkova, N. Podolova, I. Safarik, V. Zachleder and T. Branyik, *Colloids Surf., B*, 2013, 112, 213–218.
12 P. Y. Toh, B. W. Ng, C. H. Chong, A. L. Ahmad, J.-W. Yang, D. J. C. Chan and J. K. Lim, *RSC Adv.*, 2014, 4, 4114–4121.
13 P. Y. Toh, B. W. Ng, A. L. Ahmad, C. J. C. Derek and J. K. Lim, *Process Saf. Environ.*, 2014, DOI: 10.1016/j.psep.2014.03.010.
14 J. K. Lim, C. J. C. Derek, S. A. Jalak, P. Y. Toh, N. H. M. Yasin, B. W. Ng and A. L. Ahmad, *Small*, 2012, 8, 1683–1692.
15 S. P. Yeap, A. L. Ahmad, B. S. Ooi and J. K. Lim, *Langmuir*, 2012, 28, 14878–14891.
16 A. K. Lee, D. M. Lewis and P. J. Ashman, *J. Appl. Phycol.*, 2009, 21, 559–567.
17 M. W. Tenney, W. F. Echelberger, R. G. Schuessler Jr. and J. L. Pavoni, *Appl. Microbiol.*, 1969, 18, 965–971.
18 M. Sirmerova, G. Prochazkova, L. Siristova, Z. Kolska and T. Branyik, *J. Appl. Phycol.*, 2013, 25, 1687–1695.
19 C. Park, Z. Ounaies, K. A. Watson, R. E. Crooks, J. Smith Jr., S. E. Lowther, J. W. Connell, E. J. Siochi, J. S. Harrison and T. L. St. Clair, *Chem. Phys. Lett.*, 2002, 364, 303–308.
20 P. B. Dengis, L. R. Nelissen and P. G. Rouxhet, *Appl. Environ. Microbiol.*, 1995, 61, 718–728.
21 J. Norris, R. F. Giese, C. J. van Oss and P. M. Costanzo, *Clays Clay Miner.*, 1992, 40, 327–334.
22 Y. R. Hunter and J. S. Kuwabara, *Bull. Environ. Contam. Toxicol.*, 1994, 52, 311–318.
23 R. Bos, H. C. van der Mei and H. J. Busscher, *FEMS Microbiol. Rev.*, 1999, 23, 179–230.
24 C. J. Van Oss, M. K. Chaudhury and R. J. Good, *Chem. Rev.*, 1988, 88, 927–941.
25 C. J. Van Oss, *Mol. Immunol.*, 1995, 32, 199–211.
26 P. K. Sharma and K. H. Rao, *Colloids Surf., B*, 2003, 29, 21–38.
27 C. J. Van Oss, *Colloids Surf., B*, 1995, 5, 91–110.
28 P. C. Hiemenz and R. Rajagopalan, *Principles of colloid and surface chemistry*, Marcel Dekker, Inc., New York, 3rd edn, revised and expanded, 1997.
29 H. C. Hamaker, *Physica*, 1937, 4, 1058–1072.
30 C. J. Van Oss, Polar or Lewis acid–base interaction, in *Interfacial forces in aqueous media*, Marcel Dekker, Inc., New York, 1994, pp. 18–44.
31 C. J. Van Oss, *J. Mol. Recognit.*, 2003, 16, 177–190.
32 M. C. M. Van Loosdrecht, J. Lyklema, W. Norde and A. J. B. Zehnder, *Microb. Ecol.*, 1989, 17, 1–15.
33 M. E. Q. Pilson, *An introduction to the chemistry of the sea*, University of Rhade Island, Prentice Hall, Pearson Education Inc, UK, 1st edn, 1998, ch. 4.

34 I. F. Hakem and J. Lal, *Europhys. Lett.*, 2013, 64, 204–210.

35 Y. Zhang, M. Tirrell and J. W. Mays, *Macromolecules*, 1996, 29, 7299–7301.

36 D. Surendhiran and M. Vijay, *ISRN Chem. Eng.*, 2014, 1–9.

37 R. Udhaya, L. B. Bruno and S. Sandhya, *Int. J. Environ. Sci.*, 2014, 4, 899–905.

38 D. H. Napper, *Polymeric Stabilization of Colloidal Dispersions*, Academic Press, New York, 1983.

CrossMark
← click for updates

The role of particle-to-cell interactions in dictating nanoparticle aided magnetophoretic separation of microalgal cells†

Pey Yi Toh,[a] Bee Wah Ng,[a,b] Abdul Latif Ahmad,[a] Derek Chan Juinn Chieh[a] and JitKang Lim*[a,c]

Successful application of a magnetophoretic separation technique for harvesting biological cells often relies on the need to tag the cells with magnetic nanoparticles. This study investigates the underlying principle behind the attachment of iron oxide nanoparticles (IONPs) onto microalgal cells, Chlorella sp. and Nannochloropsis sp., in both freshwater and seawater, by taking into account the contributions of various colloidal forces involved. The complex interplay between van der Waals (vdW), electrostatic (ES) and Lewis acid−base interactions (AB) in dictating IONP attachment was studied under the framework of extended Derjaguin−Landau−Verwey−Overbeek (XDLVO) analysis. Our results showed that ES interaction plays an important role in determining the net interaction between the Chlorella sp. cells and IONPs in freshwater, while the AB and vdW interactions play a more dominant role in dictating the net particle-to-cell interaction in high ionic strength media (≥100 mM NaCl), such as seawater. XDLVO predicted effective attachment between cells and surface functionalized IONPs (SF-IONPs) with an estimated secondary minimum of −3.12 kT in freshwater. This prediction is in accordance with the experimental observation in which 98.89% of cells can be magnetophoretically separated from freshwater with SF-IONPs. We have observed successful magnetophoretic separation of microalgal cells from freshwater and/or seawater for all the cases as long as XDLVO analysis predicts particle attachment. For both the conditions, no pH adjustment is required for particle-to-cell attachment.

[a]School of Chemical Engineering, Universiti Sains Malaysia, Nibong Tebal, Penang 14300, Malaysia. E-mail: chjitkangl@usm.my
[b]School of Biological Sciences, Universiti Sains Malaysia, Minden, Penang 11800, Malaysia
[c]Department of Physics, Carnegie Mellon University, Pittsburgh, PA 15213, USA
†Electronic supplementary information (ESI) available: Table S1: Contact angle measurements. Table S2: Surface energy components of the liquids. Fig. S1: Microscopy images of Chlorella sp. cells trapped inside the bare-IONP flocculated matrix. Fig. S2–S3: TEM micrograph shows the relative size of IONPs to Chlorella sp. cells and the internalization of SF-IONPs into Chlorella sp. cells after effective attachment. Fig. S4: XDLVO diagram of the interaction between Chlorella sp. cells and SF-IONPs in freshwater and seawater. Fig. S5: Zeta potential of Chlorella sp. and SF-IONPs with respect to NaCl concentration. Fig. S6: Detachment efficiency of Chlorella sp. cells from SF-IONP-attached cell biomass in different concentrations of NaCl. Fig. S7: pH of the Chlorella sp. culture medium as a function of days. Fig. S8: Zeta potentials of Chlorella sp., bare-IONPs and SF-IONPs as a function of pH. Fig. S9: XDLVO diagram of Chlorella sp. interacting with SF-IONPs in pH 11 of 1 mM NaCl medium. Fig. S10: Microscopy images showed the attachment of particles to the marine species Nannochloropsis sp. Fig. S11: Cell separation efficiency of Chlorella sp. with different dosages of bare-IONPs. See DOI: 10.1039/c4nr03121k

1   Introduction

Given the current state of energy crisis, the recovery of microalgae biomass is crucial because it can serve as a sustainable alternative for the production of biofuel.[1,2] In this regard, magnetophoretic separation has been developed as an effective downstream separation technique to harvest microalgal biomass from aqueous environments.[3–7] The origin of this idea can be traced back to 1970s, when this method was applied for environmental engineering applications in removing microalgae that plagued fresh water lakes and caused eutrophication.[8,9] Compared to the more conventional separation technologies, magnetophoretic separation shows remarkable potential for the harvesting of microalgal cells because this technique has (1) high throughput, (2) low operational cost, (3) less energy intensive, (4) high separation efficiency, and (5) flexible for implementation and scalability.[3,10,11]

The underlying working principle for the magnetophoretic separation technique is straightforward. It centers on the need to tag non-magnetic microalgal cells with iron oxide nanoparticles (IONPs).[5,7,12,13] Later, the tagged biomass are exposed to an externally applied magnetic field to achieve its separation

from the surrounding media. Hence, the ability to predict the success or failure of magnetic nanomaterial attachment onto the microalgal cell surface is crucial for the implementation of this technology. From the seminal work of Xu and coworkers, adsorption isotherm analysis has been employed to make accurate yet simple estimation of the binding affinity and also the adsorption capacity of IONPs onto microalgae.[5] To verify the nature of interactions involved between the IONPs and microalgal cells, it is necessary to further identify the main driving factor behind this adsorption process.

So far, the attachment of IONPs onto microalgal cells can be promoted through the presence of macromolecules as a binding agent. Numerous macromolecules, such as chitosan, polyethylenimine, poly(diallyldimethylammonium chloride) etc.,[3,11,13,14] have been employed and shown remarkable capability to bind the IONPs onto the negatively charged microalgal cells. For freshwater species, the nature of interactions between the nanoparticles and microalgal cells is very likely dominated by electrostatic interaction.[13,14] With respect to marine species, the magnetophoretic technique works equally well with a separation efficiency of more than 90%.[4] Supposedly, the ionic stress induced by the high salt concentration in seawater would cause retardation and inhibit the electrostatic (ES) attraction between the cells and IONPs.[15] Under this circumstance, bridging flocculation can be important, but in the absence of extracellular polymeric substances on the microalgae surface, there exists some existing experimental evidence against this possibility.[16] By excluding both the ES and bridging effects, van der Waals (vdW) interaction should play a more pronounced role in promoting attachment of the IONPs onto marine microalgal cells. Moreover, since microalgae are considered hydrophilic bio-colloids due to their natural surface properties,[17] we may need to account for Lewis acid-based interactions in the entire adsorption mechanism.[11] It is the aim of this study to investigate the complex interplay of the aforementioned interactions in dictating the attachment of IONPs on microalgal cells.

The present study is dedicated to identifying the colloidal interactions involved in determining the successful attachment of IONPs onto microalgal cells. Experimentally we verified the attachment of IONPs by checking the magnetophoretic responsiveness of the tagged cells and direct visualization through optical microscopy. Electrophoretic mobility measurements were used to provide information on the surface charge of IONPs before and after their surface functionalization and also for microalgal cells. By employing Chlorella sp. as a model system, we investigated the attachment efficiency of IONPs onto this cell line within both freshwater and seawater. Extended Derjaguin–Landau–Verwey–Overbeek (XDLVO) theory, which takes into account the contribution of vdW, ES and the Lewis acid–base (AB) interaction, was employed to rationalize the colloidal interactions involved in particle–microalgae interactions. Here, XDLVO analysis can be a clear-cut method to provide guidance in predicting the success or failure of IONP attachment onto microalgal cells, which further leads to the effective implementation of magne-

tophoretic separation. A marine species, Nannochloropsis sp., was employed to further confirm the reliability of the XDLVO prediction.

2 Experimental section

2.1 Materials

Bare iron oxide magnetic nanoparticles (bare-IONPs) with diameters at around 20–30 nm were obtained from Nanostructured & Amorphous Materials, Inc. The 35 wt% very low molecular weight poly(diallyldimethylammonium chloride) (PDDA) in water with molecular weight, $M_w < 100\,000$ g mol^{-1} was supplied by Sigma-Aldrich, Inc. Hydrochloric acid was purchased from PC Laboratory Reagents. The sodium hydroxide pellet and sodium chloride were supplied by MERCK & Co., Inc. Deionised water was obtained by reverse osmosis and further treated by the Milli-Q Plus system (Lillipore) to 18 MΩ cm resistivity.

2.2 Culture, preparation and characterization of Chlorella sp. and Nannochloropsis sp. cells

The Chlorella sp. and Nannochloropsis sp. strains were obtained from the School of Biological Sciences, Universiti Sains, Malaysia. The Chlorella sp. was cultivated in 250 ml Bold's Basal Medium (BBM), while the Nannochloropsis sp. was cultivated in 250 ml Conway medium. Both cultures were maintained under continuous illumination at 2000 lux and 25 °C. The media and flasks were autoclaved at temperature 121 °C for 15 minutes before cell cultivation. Continuous aeration was provided for the culture medium throughout the cultivation period. In this study, cell density of Chlorella sp. was maintained at around 3×10^7 cells ml^{-1} (after 10 culturing days) for all experiments. For subsequent experiments, the cells were collected through centrifugation and redispersed in deionized water multiple times to exclude the present of growth media. Later, the concentrated biomass was then redispersed into the desired medium (with different pH and ionic strength) as planned for experiments. For Nannochloropsis sp., the removal experiment was conducted right after 7 culture days to ensure the same cell density has been achieved similar to Chlorella sp. Cell numbers were determined by using a heamocytometer, while the size of cells was measured microscopically using Image Analysis Software. The average size of cells was calculated from 500 measurements.[18] The pH was measured by Eutech CyberScan pH 1500. The zeta potential of the microalgae was calculated based upon the Helmholtz–Smoluchowski limit using a Malvern Zetasizer.

2.3 Preparation and characterization of surface functionalized iron oxide nanoparticles (SF-IONPs)

The "attached-to" approach was employed to achieve attachment between the IONPs and cells.[14] The bare-IONPs were dispersed in deionized water and sonicated to achieve good dispersion at 1 g L^{-1}. PDDA was dispersed in deionized water (17 g L^{-1}) and stirred (500 rpm) for 1 day to achieve complete

dissolution. Then the bare-IONPs dispersion was added to the macromolecule solution, and the entire mixture was sonicated in a low power bath sonicator (40 kHz) to avoid degradation of the molecular structure.[19] This solution was then left on an end-to-end rotating mixer at 40 rpm overnight. After this surface modification step, a permanent magnet was used to collect the surface functionalized IONPs (SF-IONPs). The supernatant was discarded, while the SF-IONPs were again dispersed in deionized water. The electrophoretic mobility of bare-IONPs and SF-IONPs in different media of differing pH and ionic strength were measured using the Malvern Instruments Nanosizer. Unless otherwise stated, the zeta potentials of the bare-IONPs and SF-IONPs were then calculated based upon the Helmholtz–Smoluchowski limit.

2.4 Low gradient magnetic separation (LGMS)

For every separation study, 300 mg L^{-1} of bare-IONPs/SF-IONPs were added into cell medium to ensure an excess supply of particles. A total of 2 ml of 1.5 g L^{-1} particles, either bare-IONPs or SF-IONPs, was added to 8 ml cell medium followed with simple mixing for 30 seconds to ensure uniform mixing and dispersion. The mixture was left for another 30 seconds before use for the magnetophoretic separation study. Magnetophoretic separation of *Chlorella* sp. was carried under low gradient magnetic separation (LGMS) for 6 minutes. A N50-graded NdFeB permanent magnet was used to induce an inhomogeneous magnetic field with field gradient $\nabla B < 80$ T m^{-1}.[3] The absorbance of the cell was measured spectrophotometrically by a UVmini-1240 Shimadzu at the wavelength of 660 nm (measured by Agilent Technologies Carry 60 UV-Vis). The cell separation efficiency was determined as:

$$\text{Cell separation efficiency (\%)} = \frac{I_0 - I(t)}{I_0 - I_{\text{centrifuged}}} \times 100\% \quad (1)$$

where I_0 represents the initial absorbance intensity of the microalgae suspension after dilution with 2 ml deionized water, $I(t)$ represents the absorbance intensity of the micro-

algae suspension during magnetophoretic separation at time t, and the $I_{\text{centrifuged}}$ represents the clear sample after centrifugation with the same dilution factor.

2.5 Contact angle measurement

The surface free energy of the microalgal cells and the bare-IONPs/SF-IONPs were determined by contact angle measurements. These contact angles were measured by using a contact angle goniometer (Rame-Hart Instrument Co.). Microalgal cells were pre-concentrated by centrifugation at 2500g for 4 minutes. A flat layer of cells was deposited on agar to stabilize the cell moisture content.[20] The flat surface of bare-IONPs was obtained by mechanically compressing the powder into pellets.[21] The concentrated solutions of SF-IONPs were deposited onto glass slides to form completely covered flat surfaces and dried at room temperature. Measurements were performed with two polar liquids (water and glycerol) and an apolar liquid (1-bromonaphthalene). The contact angle measurements were carried out by a sessile drop technique, and the readings were averaged from three replicate measurements.[18]

3 Results and discussion

3.1 Particle–microalgae interaction in freshwater and seawater

Magnetophoretic separation of microalgae from freshwater medium has proven to be feasible in previous studies.[3,14] We hypothesized that the effective attachment of iron oxide nanoparticles (IONPs) onto the surface of *Chlorella* sp. is mediated by electrostatic (ES) attraction.[12,13] A similar model system is employed in this study to further identify the actual contribution of the interactions involved. Fig. 1 shows that the bare iron oxide nanoparticles (bare-IONPs) do not adhere onto *Chlorella* sp. cells in freshwater. Only about 2.68% of cells were removed magnetophoretically with most of the cells entrapped
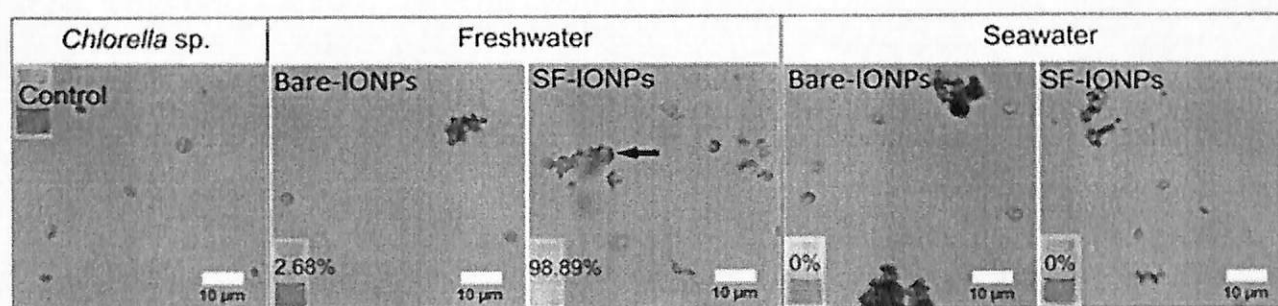

Fig. 1 Optical micrographs showing the degree of attachment for both bare- and SF-IONPs onto *Chlorella* sp. cells in freshwater and seawater. For bare-IONPs, under both aqueous environments, the particles aggregated extensively to form large clusters with no hint of attachment (dark ring around the cells) on the cell. Whereas for the case of SF-IONPs, the black arrow pointing toward the dark area indicates the presence of particles on the cell surface in freshwater. However, there is no clear indication showing the attachment of SF-IONPs onto microalgal cells in seawater. The bottom left corner of each micrograph shows a photo depicting the microalgae suspension after going through magnetophoretic separation. Use of bare-IONPs resulted in minimum magnetophoretic separation efficiencies of 2.68% and 0% for freshwater and seawater, respectively. There is also no clear cell separation for the case of SF-IONPs in seawater, but this particle is proven to be an effective tagging agent for promoting the magnetophoretic separation of microalgal cells in freshwater with a 98.89% separation efficiency.

Table 1 Details on the zeta-potential of each surface when dispersed in different media conditions together with pH

Conditions			
Fresh medium	pH	Surface	Zeta-potential (mV)
Freshwater	6.58	*Chlorella* sp.	−27.8 ± 5.5
		Bare-IONPs	−30.4 ± 4.9
		SF-IOPNs	25.2 ± 4.7
Seawater	6.32	*Chlorella* sp.	−9.1 ± 0.3
		Bare-IONPs	3.84 ± 1.0
		SF-IOPNs	4.95 ± 0.6

within the flocculated nanoparticle matrix (see ESI Fig. S1†). On the other hand, the surface functionalized iron oxide nanoparticles (SF-IONPs) are very likely to attach onto cell surfaces in freshwater condition, judging from the fact that a dark ring formed around most of the microalgal cells (arrow pointed area in Fig. 1). A cell separation efficiency as high as 98.89% was recorded with a particle dosage of 0.84 g per 1 g of dry biomass. This observation also serves as indirect confirmation of our speculation about the successful magnetic seeding of microalgal cells by SF-IONPs. By referring to Table 1, the surface charge of cells and bare-IONPs are similar, while the SF-IONPs have an opposite charge to the cells. These measurements have verified that the electrostatic (ES) interaction causes the cells and SF-IONPs to attract while it causes the cells and bare-IONPs to repel each other.

In seawater, both the bare-IONPs and SF-IONPs do not attach onto the cells (Fig. 1). As a consequence, there is no cell collection that can be detected optically. Table 1 shows that the surface charge of the cells and nanoparticles are suppressed to very low values compared to those in freshwater conditions. Typical seawater contains various types of dissolved salt, mainly Na^+ and Cl^- ions. The ionic strength of seawater is approximately 700 mM.[22] Hence, we hypothesized that the high ionic strength of seawater causes strong Deybe screening and weakens the electrostatic-repulsion between the particles. The particles aggregate extensively before their attachment onto the cells. Large aggregates found in seawater, as illustrated in Fig. 1, strongly support our hypothesis.

In classical DLVO analysis, the total interaction potential (U_{DLVO}) between two colloidal particles is described as a balance between the van der Waals (U_{vdW}) and ES (U_{ES}) interactions

$$U_{DLVO} = U_{vdW} + U_{ES} \qquad (2)$$

in which the extent of ES interaction depends on the surface charge/zeta potential of the interacting particles, and it can be attractive or repulsive.

In this study, due to the huge size mismatch between the IONPs and the microalgal cells (see ESI Fig. S2†), where the mean size of *Chlorella* sp. cells is 3.45 μm and is far larger than the IONPs with a diameter at around 25 nm, the surface of the cell is assumed to be flat with respect to the spherical IONPs. Under this scenario, the surface curvature of cell is
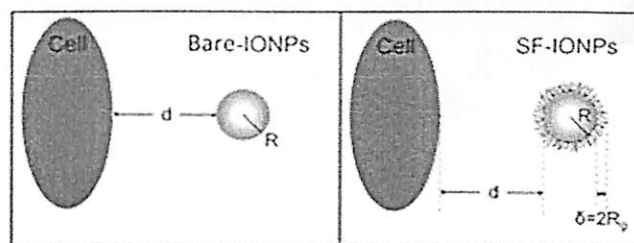

Fig. 2 Schematic illustration of a microalgal cell interacting with either a bare-IONPs (left) and SF-IONPs (right). Due to the large size mismatch between these two entities, we simplified our analysis to sphere–plane interaction. In this diagram, d represents the surface-to-surface separation distance between the cell and particle, R is the particle radius, δ is the thickness of the polymer adlayer coated on the IONP surface. All the symbols are in accordance to the parameters used in our analysis.

negligible with respect to the high curvature of nano-sized IONPs. The Lifshitz–van der Waals equation for sphere–plane configuration is applied[23] as a function of separation distance, d:

$$U_{vdw} = -\frac{A_{eff}R}{6}\left[\frac{1}{d} + \frac{1}{d+2R}\right] - \frac{A_{eff}}{6}\ln\left[\frac{d}{d+2R}\right] \qquad (3)$$

Here d is the surface-to-surface separation distance between the cell and the IONP (Fig. 2); A_{eff} represents the effective Hamaker constant; and R is the radius of the IONP. The Hamaker constant of each surface was estimated by contact angle measurement (see ESI Table S1†) with the use of at least three different liquids (polar or apolar), of which two must be polar liquids (see ESI Table S2†).[24,25] The Hamaker constant of material i, A_i is proportional to the vdW component of the material surface tension, γ_i^{LW}, and can be defined as follows:[24]

$$A_i = 24\pi d_0^2 \gamma_i^{LW} \qquad (4)$$

where d_0 is the minimum equilibrium distance between two condensed-phase surfaces ($d_0 = 0.657 \pm 0.01$ nm).[26] The γ_i^{LW} can then be determined by using the Young's equation (Table 2):[27]

$$(1 + \cos\theta)\gamma_L = 2\left(\sqrt{\gamma_S^{LW}\gamma_L^{LW}} + \sqrt{\gamma_S^{\oplus}\gamma_L^{\ominus}} + \sqrt{\gamma_S^{\ominus}\gamma_L^{\oplus}}\right) \qquad (5)$$

where γ is surface tension, mJ m^{-2}; $\gamma^{\oplus}$ is the electron-acceptor parameter of the polar surface tension component, while $\gamma^{\ominus}$ is the electron-donor parameter of the polar surface tension component; and the subscripts S and L stand for the solid and liquid, respectively.

The effective Hamaker constant, A_{eff} is the combined relationship between different materials that contributes to the vdW body–body interaction. The A_{eff} of interaction between materials 1 and 3 separated by medium 2 can be defined as:[28]

$$A_{eff} = A_{123} = \left(\sqrt{A_{11}} - \sqrt{A_{22}}\right)\left(\sqrt{A_{33}} - \sqrt{A_{22}}\right) \qquad (6)$$

According to this definition, for two colloidal particles suspended in liquid, the vdW interaction can be either attractive

Table 2 Surface energy and Interfacial energy involved for the calculation of Lewis acid–base interaction. Subscript *iw* implies the interfacial energy of surface *i* in water and *iwi* implies the interfacial energy of surface *i* to surface *i* in water

Surface, *i*	Surface energy (mJ m^{-2})					Interfacial energy (mJ m^{-2})	
	γ^{tot}	γ^{LW}	γ^{AB}	$\gamma^{\oplus}$	$\gamma^{\ominus}$	ΔG_{iw}	ΔG_{iwi}^{AB}
Chlorella sp.	75.0	22.2	52.8	4.8	145.1	−188	80
Bare-IONPs	48.1	44.0	4.2	0.06	74.2	−151	69
SF-IONPs	45.31	43.5	1.81	0.01	74.4	−150	71
Nannochloropsis sp.	40.0	26.2	13.8	0.65	73.3	−142	60

or repulsive.[29] The calculated A_{eff} between the *Chlorella* sp. cells and the bare-IONPs and SF-IONPs are 2.86×10^{-21} J and 2.81×10^{-21} J respectively.

ES interaction between a charged plane and a charged sphere is modeled as:[23]

$$U_{ES} = \pi \varepsilon R' \left(\xi_1^2 + \xi_2^2 \right) \left[\frac{2\xi_1 \xi_2}{\xi_1^2 + \xi_2^2} \ln \frac{1 + e^{-\kappa d}}{1 - e^{-\kappa d}} + \ln\left(1 - e^{-\kappa d}\right) \right] \quad (7)$$

where ξ is the zeta potential; κ is the Debye–Hückel parameter; and the ε represents the permittivity of the medium, where $\varepsilon = \varepsilon_r \varepsilon_0$. The permittivity of free space, ε_0, is 8.854×10^{-12} F m^{-1}. In the case of SF-IONPs, $R' = R + \delta$ where δ is the adlayer thickness, which is determined at 4.85 nm.[15]

According to the classical DLVO analysis under freshwater conditions (Fig. 3a), the ES interaction between differently charged cells and SF-IONPs enables effective particle-to-cell linkage as evident from the net attractive interaction. Interestingly, we observed particle internalization into the cells for the case of SF-IONPs.[12] This process most likely happens through the membrane deformation caused by reorganization of the lipid bilayer when the nanoparticles successfully attach on the cell surface (see ESI Fig. S3†). This observation is in accordance with the optical micrograph shown in Fig. 1. However, for the bare-IONPs, the energy barrier with the *Chlorella* sp. cell is more than 10 kT and prohibits the attachment of particles. In seawater, the classical DLVO theory (Fig. 3b) predicts the bare-IONPs and SF-IONPs are always ready to attach on the cell
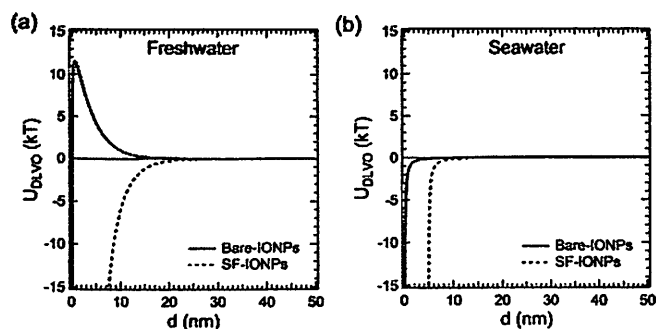

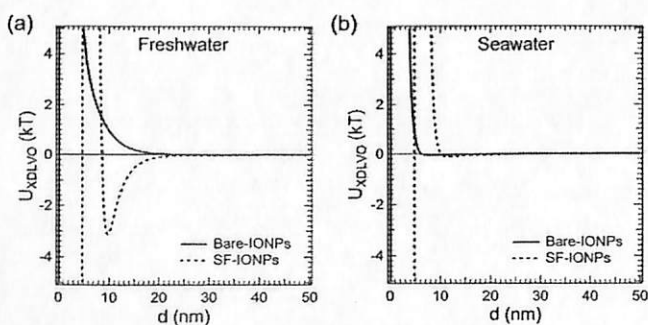Fig. 3 Classical DLVO profiles for the interaction between *Chlorella* sp. cells and bare-IONPs/SF-IONPs in (a) freshwater and (b) seawater with the overall interacting potential U_{DLVO} plotted for both species of IONPs used.

surface promoted by the attractive vdW force. However, we observed no separation of microalgal cells for both species of nanoparticles (Fig. 1). Even though the rapid aggregation of particles might be the dominant factor causing poor separation efficiency, from the optical microscopy observation we have also failed to detect any hint of particle attachment. This in turn has indirectly suggested that the classical DLVO analysis is insufficient to provide useful prediction related to particle attachment within our experimental conditions.

3.2 XDLVO considerations

From the existing literature, there are a number of studies emphasizing the need to include polar interactions into the analysis involving biological cells.[11,18,23,27] Since microalgal cells are also a hydrophilic biocolloid due to their natural surface properties, where the outer cell membrane is made up of the hydrophilic end of the phospholipid layer,[17,27] the polar interaction based on electron acceptor–electron donor (Lewis acid–base, AB) interactions may be important. In this context, the AB interaction can be up to two orders of magnitude higher than those commonly encountered among the components of the traditional DLVO energy balance.[24] In addition complexity may arise as the changes in the ionic strength of culture media would suppress the electric double layer and therefore retard the ES interaction. This condition will become more pronounced in seawater culture with the complex ionic environment. As such, a more physically sound analysis taking into account the AB interaction might be necessary, and this new physicochemical approach, which takes into account contributions other than vdW and ES interactions, is known as the extended DLVO (XDLVO) analysis.

In this study, the van Oss–Chaudhury–Good (OCG) thermodynamic approach is used to determine the AB interaction.[24] Table 2 shows that the *Chlorella* sp., bare-IONPs and SF-IONPs are strongly hydrophilic since their $\gamma^{\ominus}$ values are larger than that of the water, while their $\gamma^{\oplus}$ values are far less than that of water, where $\gamma_w^{\oplus} = \gamma_w^{\ominus} = 25.5$ mJ m^{-2} for water. A larger $\gamma^{\ominus}$ surface exhibits strong affinity to water molecules *via* the formation of hydrogen bonds. The *Chlorella* sp., bare-IONPs and SF-IONPs tend to bind water strongly with free energies in the range of −140 to −190 mJ m^{-2}, which are stronger than the hydrogen-bonding energy of water (−102 mJ m^{-2}).[30] When these hydrophilic cells/particles disperse in water, they experience hydrophilic repulsion with an AB interfacial interaction

energy greater than zero ($\Delta G_{iwi}{}^{AB} > 0$). This interfacial interaction energy is defined as:

$$\Delta G_{iwi}^{AB} = 4\left(\sqrt{\gamma_i^{+}\gamma_w^{-}} + \sqrt{\gamma_w^{+}\gamma_i^{-}} - \sqrt{\gamma_i^{+}\gamma_i^{-}} - \sqrt{\gamma_w^{+}\gamma_w^{-}} \right) \quad (8)$$

$\Delta G_{iwi}{}^{AB}$ decreases in the order of Chlorella sp. > SF-IONPs > bare-IONPs, at 80, 71 and 69 mJ m^{-2} respectively.[25,27] After cells and bare-IONPs/SF-IONPs are mixed in water, both surfaces experience hydrophilic repulsion with respect to each other. The $\Delta G_{iwj}{}^{AB}$ for the configuration of Chlorella sp. cells and bare-IONPs is 87.7 mJ m^{-2}, and for cells interacting with SF-IONPs, it is 89.6 mJ m^{-2}.

$$\Delta G_{iwj}^{AB} = 2\left(\sqrt{\gamma_i^{-}\gamma_w^{-}} + \sqrt{\gamma_j^{-}\gamma_w^{-}} + \sqrt{\gamma_w^{+}\gamma_i^{-}} + \sqrt{\gamma_w^{-}\gamma_j^{-}} \right.$$
$$\left. - 2\sqrt{\gamma_w^{+}\gamma_w^{-}} - \sqrt{\gamma_i^{+}\gamma_j^{-}} - \sqrt{\gamma_j^{+}\gamma_i^{-}} \right) \quad (9)$$

From the above point of view, the AB interaction should be included in the XDLVO analysis:

$$U_{XDLVO} = U_{vdw} + U_{ES} + U_{AB} \quad (10)$$

The AB interaction between a plane and sphere, as a function of distance, can be predicted as:[23,31]

$$U_{AB} = 2\pi a \lambda \Delta G_{d_0}^{AB} \exp\left[\frac{d_0 - d}{\lambda} \right] \quad (11)$$

where λ is the correlation length of molecule in a liquid medium. For hydrophilic repulsion, $\lambda = 0.6$ nm; for hydrophobic attraction, $\lambda = 13$ nm.[30]

In freshwater, the XDLVO analysis shown in Fig. 4a predicts a high energy barrier between cells and bare-IONPs at around >1000 kT, which strongly prohibits the effective particle-to-cell attachment. For the case of SF-IONPs, a secondary minimum (−3.12 kT) is observed once the AB interaction is considered. At this point, the attachment of cells with SF-IONPs is effective.[32] The major difference between the DLVO and XDLVO analyses for interaction between Chlorella sp. and SF-IONPs is that the DLVO predicts net attraction, whereas the XDLVO predicts the present of a secondary minimum followed with strong hydrophilic repulsion (due to U_{AB}) as the particle–

cell separation distance approaches the layer thickness of the PDDA coating (see ESI Fig. S4a†). Nevertheless, both analyses predicted successful attachment of the SF-IONPs onto Chlorella sp.

In seawater, as shown in Fig. 4b, the XDLVO analysis predicts net repulsion between the cells and the bare-IONPs/SF-IONPs. The available repulsive AB interaction strongly prohibited the effective attachment for both cases in which the energy barrier is much higher than 100 kT (see ESI Fig. S4b†). This prediction is in accordance with the observation delineated in Fig. 1. Therefore, from a theoretical perspective, the AB interaction plays a crucial role in determining the net interaction between the nanoparticles and microalgal cells under seawater conditions.

3.3 Variation of ionic strength verified the important role of AB interactions

Our XDLVO analysis confirms that the ES and AB interactions are both important in governing the net interaction of cells and nanoparticles in different ionic strength conditions. An interacting system between the cells and SF-IONPs is monitored to investigate the inter-relationship of the ES and AB as ionic strength increases from 1 to 700 mM. Since the dissolved mineral substance of seawater is mainly made up of Na$^+$ and Cl$^-$ ions, about 30.6% and 55%, respectively, sodium chloride (NaCl) salt is used for adjusting the ionic strength.[33]

Fig. 5 shows the cell separation efficiency is the highest in 1 mM ionic strength medium using SF-IONPs. At this level of ionic strength, it is possible to achieve an overall cell separation efficiency at around 98.82 ± 0.31%; the left over crystal

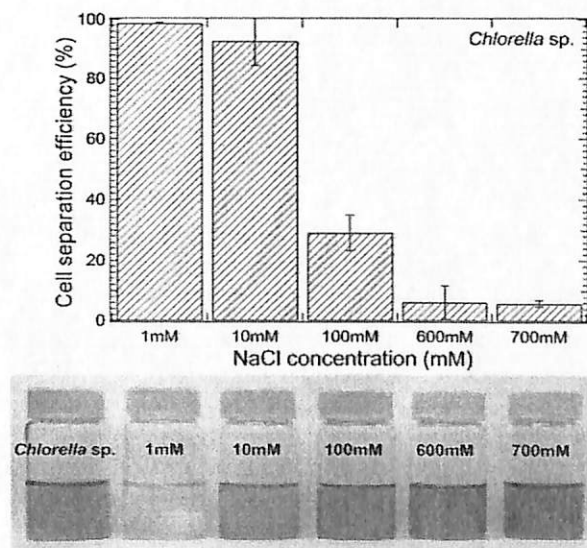Fig. 5 Separation efficiency of Chlorella sp. cell as a function of NaCl concentration up to 700 mM, which is equivalent to the ionic strength of seawater. Here, 300 mg L^{-1} of SF-IONPs is added to the cell suspension corresponding to 1.27 g nanoparticles per 1 g dry biomass. All separation processes were conducted at low field gradient for 6 minutes. Bottom images shows how the final suspensions look after the separation.

Fig. 4 XDLVO profiles for the interaction between Chlorella sp. cells and bare-IONPs/SF-IONPs in (a) freshwater and (b) seawater with the overall interacting potential U_{XDLVO} plotted for both species of IONPs used.
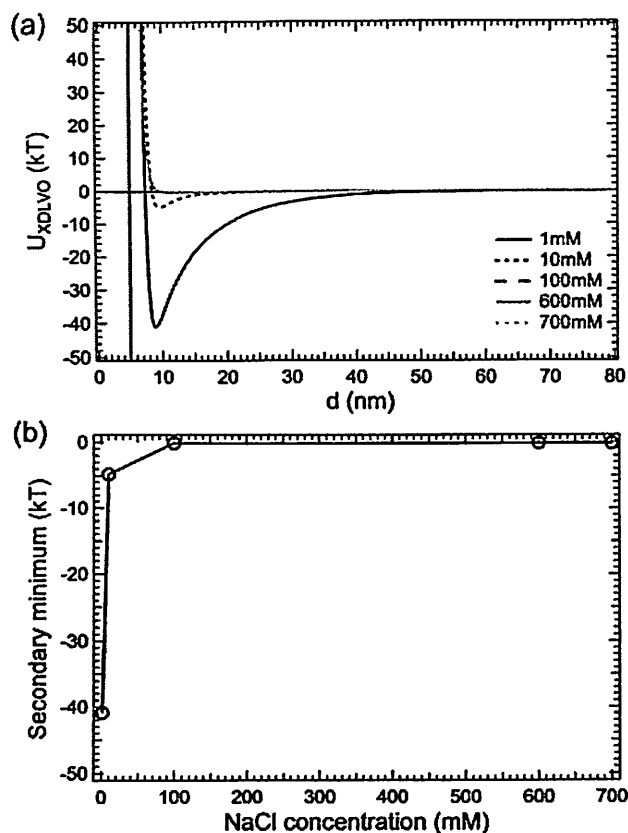
Fig. 6 (a) XDLVO profile showing the net interaction between the *Chlorella* sp. cells and SF-IONPs at different NaCl concentrations. (b) Well depth of the secondary minimum predicted by the XDLVO as a function of NaCl concentration from part (a).
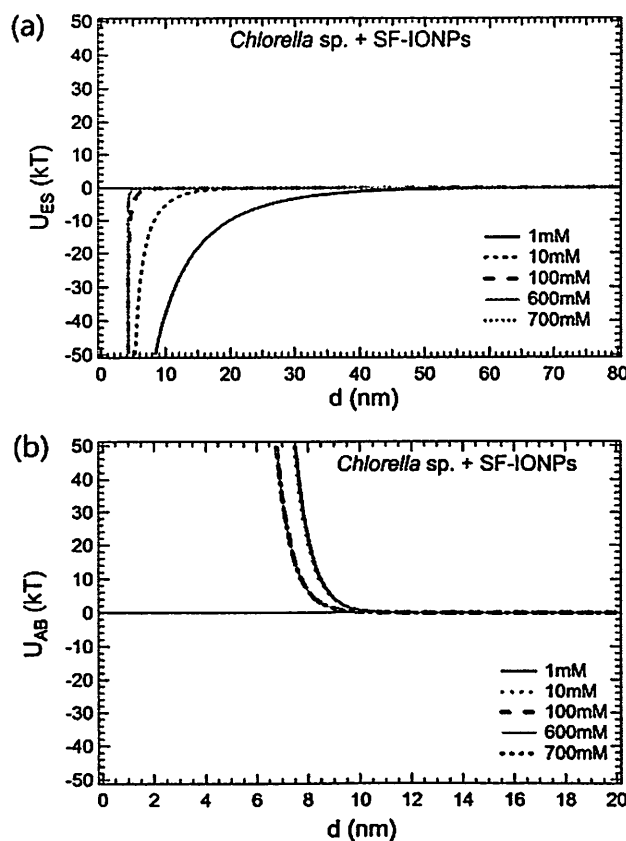

Fig. 7 Normalized interacting potential of (a) electrostatic and (b) Lewis acid–base interaction with respect to the separation distance, d between *Chlorella* sp. and SF-IONPs at different NaCl concentrations. Regardless of ionic strength, U_{ES} is always negative (attractive) and U_{AB} is always positive (repulsive) within the investigated concentration range of NaCl.

clear supernatant indicated that most cells have been successfully collected. Overall cell separation efficiency dropped to 92.84 ± 8.32% as we further increased the ionic strength of the suspension to 10 mM. When the ionic strength increased to more than 100 mM, cell separation efficiency becomes much lower, and only 5.75 ± 1.09% of cells are removed in 700 mM medium. This experimental observation is in accordance with the XDLVO model prediction as shown in Fig. 6. The well depth of the secondary minimum sharply decreases from −41 kT to −5 kT when ionic strength increases from 1 mM to 10 mM. The net repulsive interaction predicted from the XDLVO analysis above, without the presence of a secondary minimum at ionic strength of 100 mM, indicates that no effective attachment between the SF-IONPs and cells can occur. They tend to repel each other, and this is in good agreement with our previous observation in which no SF-IONP attachment is observed in seawater.

As shown in Fig. 7a and b, both the effective length scale for ES and AB interactions between SF-IONPs and *Chlorella* sp. decreased with the increase in ionic strength. For the former case, the reduction in terms of the effective interaction range is due to the Debye screening effect as discussed previously (see ESI Fig. S5†). Moreover, it should be noted that the extent of reduction in the effective interaction range is much more

pronounced for ES interaction compared to AB interaction. In fact, this slight reduction in the interaction range for the AB case is very likely due to the complex interplay of the salting out effect and conformational changes in the polyelectrolyte layer.[34,35] Suppression of the physical barrier formed due to polyelectrolyte layer adsorption, which subsequently reduces the absolute surface-to-surface separation distances, should be the main reason for the decreasing range of AB interaction.

This study shows the ES interaction is crucial to facilitate effective particle-to-cell attachment in freshwater, while the AB interaction is more dominant in high ionic strength condition (≥100 mM). Having this kind of information, especially by knowing the extent of interaction involved, has provided us a guideline to design an effective strategy to promote particle detachment. For example, since ES interaction is most influential on the particle-to-cell attachment in freshwater, suppression of this interaction by introducing an ionic stress could disrupt the entire interaction scheme, which subsequently could cause particle detachment (see ESI Fig. S6†). This investigation is important for the recovery of SF-IONPs by magnetophoresis without the need for pH adjustment for effective implementation of magnetophoretic separation of microalgae without taking the risk of causing cell lysis.[36,37]

3.4 Domination of ES interaction with respect to pH

Throughout the entire time course of the cultivation process, the pH of the culture media shifted to a more alkaline condition (see ESI Fig. S7†). In addition, the ES interaction is sensitive toward the pH change in the surrounding media through the influence on the surface charge. These two important phenomena motivated our work in this section, which focuses on the effect of pH on the interactions between microalgal cells and bare-IONPs/SF-IONPs.

In this study, the bare-IONPs have an isoelectric point at about pH 8, while both *Chlorella* sp. cells and SF-IONPs did not show any charge reversal behavior within the pH range of 3 to 11 (see ESI Fig. S8†: cells will always carry a net negative charge and the SF-IONPs will always in a positive charge). The results in Fig. 8 show that the U_{ES} in the case of cells with bare-IONPs changes from attraction (negative zone) to repulsion (positive zone) when the pH changes across the isoelectric point of bare-IONPs. Associated with this change is the obvious diminishing of the secondary minimum with a well depth of −7.68 kT at pH 3 to net repulsion at pH 11 (Fig. 9a). Our experimental results (Fig. 9b) have proven the reliability and versatility of the XDLVO analysis where the attractive interaction binds the cells and bare-IONPs together and forms cell-particle clusters at pH 3, as shown in Fig. 9c. For the case of SF-IONPs, the results in Fig. 8b illustrate that the U_{ES} always maintains attraction between the negative charged cells and positive charged SF-IONPs. The secondary minimum predicted by XDLVO theory (Fig. 9a) is nicely developed (>9 kT in magnitude) and promotes attachment of the SF-IONPs on the microalgal cell surface. This observation is consistent with the experimental results (Fig. 9b) with a cell separation efficiency of more than 90% in all pH values. It should be noted that in our case the ES interaction has a slightly longer range compared to the AB interaction (see ESI Fig. S9†), and thus, the ES dominates the net interaction energy, U_{XDLVO}, with respect to pH. Our optical microscopy observations (Fig. 9d) clearly show the effective attachment of particles to cells for the case of SF-IONPs. This study has confirmed the important role of ES and AB interactions under freshwater conditions. Therefore, these two interactions need to be considered in order to predict successful particle-to-cell attachment by XDLVO analysis.
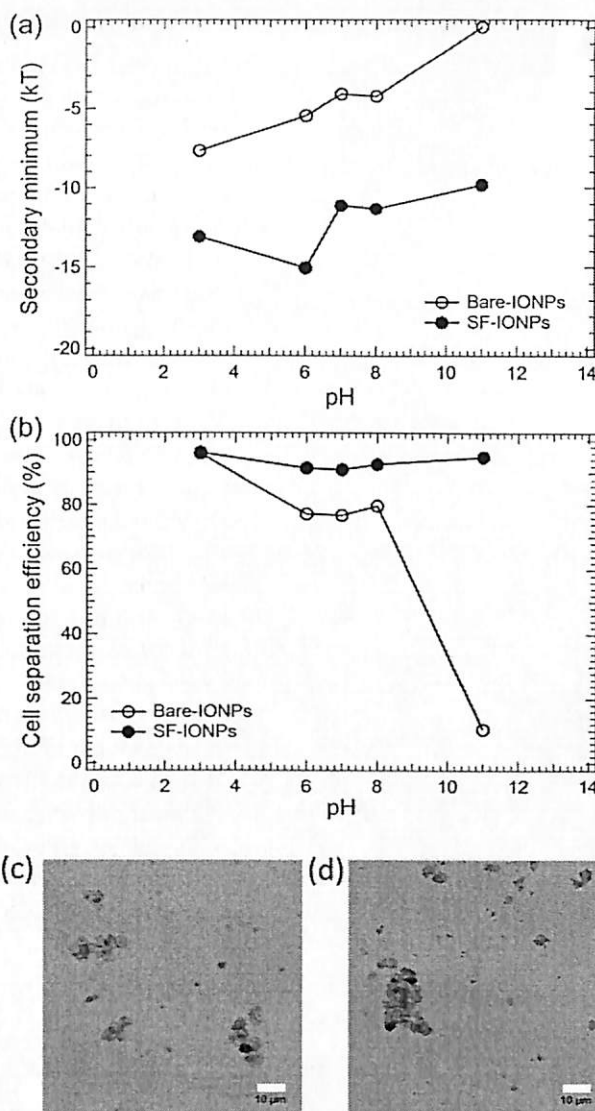

Fig. 9 Diagrams showing the (a) well depth of secondary minimum predicted by the XDLVO analysis and the (b) cell separation efficiency from experiment observations when the *Chlorella* sp. cells are interacting with the bare-IONPs and SF-IONPs at different pH. Cell separation is performed by a NdFeB cylindrical magnet with a total collection time of 6 minutes at a dosage of 1.27 g nanoparticles per 1 g dry biomass. Microscopy images showing the effective attachment between cells and (c) bare-IONPs in pH 3 and (d) SF-IONPs in pH 11. Dark rings and spots detected over most of the cell surface indicated the successful attachment of particles.
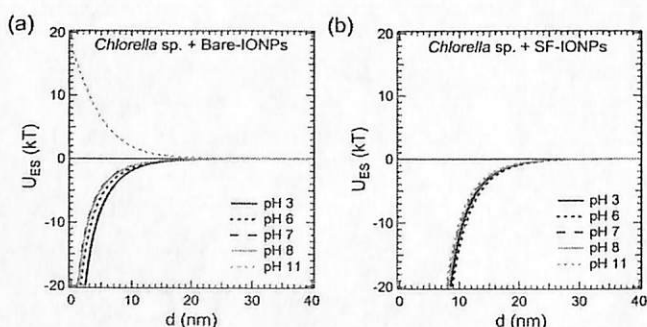
3.5 Attachment of nanoparticles on marine species

In order to further verify the feasibility of the XDLVO theory in predicting the particle-to-cell interaction in seawater, another marine species of microalgae, named *Nannochloropsis* sp., was employed for a particle-to-cell attachment study.

In general, *Nannochloropsis* sp. cells have a simple spherical structure with a diameter around 3–5 μm, resembling the size and shape of *Chlorella* sp. Table 2 shows that the AB interfacial interaction energy (per unit contact area) between the surfaces of *Nannochloropsis* sp. is weaker than the *Chlorella* sp.

Fig. 8 U_{ES} curve as a function of distance between *Chlorella* sp. and (a) bare-IONPs and (b) SF-IONPs at different pH.

◦ The *Nannochloropsis* sp. experiences weaker AB repulsive interaction when in contact with the bare-IONPs and SF-IONPs, with its surface energy at 64.0 mJ m^{-2} and 65.1 mJ m^{-2} compared to that of the *Chlorella* sp., at 87.7 mJ m^{-2} and 89.6 mJ m^{-2}, respectively. Our XDLVO analysis predicts a secondary minimum well depth at −0.90 kT for cell/bare-IONP interaction and −1.94 kT for cell/SF-IONP interaction (see Fig. 10). With a low particle-to-cell ratio at 0.42 g g^{-1}, there is no obvious attachment of bare-IONPs onto cells and almost all of the particles have aggregated to form large clusters (see Fig. S10 in ESI†). However, for the case of SF-IONPs, we observed particle attachment even at a very low particle-to-cell ratio of 0.21 g g^{-1} (Fig. S10†). Together with the results presented in Fig. 10, our microscopy observations support our hypothesis that magnetic separation would definitely occur as long as there is particle attachment. Fig. 10b shows that the magnetophoretic separation efficiencies achieved are 97.90 ± 0.27% and 4.94 ± 0.50% for SF-IONPs and bare-IONPs, respectively, when in particle-to-cell ratio is 0.42 g g^{-1} (see ESI Fig. S10†). The recorded separation efficiency has indirectly confirmed that particle-to-cell aggregation is weak and insignificant for well depths less than ~1.5 kT.[38] In thermal equilibrium, according to the equipartition theorem, a particle has the same average energy associated with each independent degree of freedom of their motion. Hence, the translational

kinetic energy possessed by a free particle is equivalent to 3/2 kT ($<E_{kinetic}>$ = 1.5 kT). The overall attractive interaction between the IONPs and microalgal cells need to overcome this energy for binding to happen. The results shown in Fig. 10a and b are nicely aligned with this classical prediction and provide a proper guideline for magnetic seeding of microalgal cells. Under this principle, particle attachment could only happen if the particle-to-cell interaction achieved a well-depth of secondary minimum beyond 1.5 kT under XDLVO analysis. Even though the magnitude of attractive interaction is weak for the case of bare-IONPs on *Nannochloropsis* sp., magnetophoretic separation of this species of microalgae can still be implemented by increasing the particle concentration. Since the electrostatic interaction within seawater is relatively weak, as suggested by our previous XDLVO analysis, we hypothesized that the vdW and AB interactions should play a major role here. Moreover, the high concentration of particles enables the cells and bare-IONPs to collide more frequently, hence increasing the probability of particle attachment. Fig. 10b shows that a separation efficiency of *Nannochloropsis* sp. up to 80.22 ± 10.57% can only be achieved with a particle-to-cell ratio of 2.11 g g^{-1} (see ESI Fig. S10†). By taking the density of iron oxide at 4.95 g cm^{-3} and the mean diameter of the particles as 25 nm, we estimated that there are around 1.74 × 10^{12} particles per cell.

By referring back to the case of *Chlorella* sp. with bare-IONPs, the net repulsive interaction predicted by the XDLVO theory has suggested that under all circumstances, even at high particle concentrations, there should be no particle attachment, and hence no microalgae separation. Our results confirmed this observation (ESI Fig. S11†) and verified the critical need to take into account AB interaction in predicting the particle-to-cell interaction. Moreover, the vdW and AB interactions should be taken into account to predict the effectiveness of particle-to-cell attachment in seawater without the need to consider the ES interaction due to the Debye screening effect.[15] From all the data presented, magnetophoretic separation can be implemented successfully as long as the particles attach. This finding makes the prediction of particle attachment, such as discussed in this work, crucial for the implementation of magnetophoretic separation of microalgal cells.
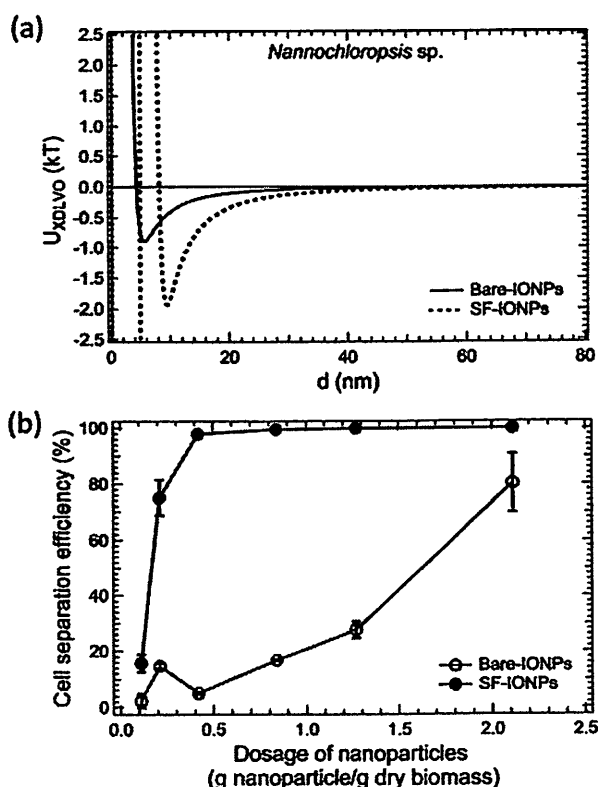

Fig. 10 (a) XDLVO analysis for the interaction between the marine species *Nannochloropsis* sp. with bare-IONPs and SF-IONPs. The well depth of secondary minimum predicted for each case is −0.90 kT (bare-IONPs) and −1.94 kT (SF-IONPs). (b) Separation efficiency of *Nannochloropsis* sp. under LGMS at different dosages.

4 Conclusions

XDLVO analysis can be employed as a very useful mathematical analysis to predict the successful IONP attachment onto the microalgal cells, either in freshwater or seawater. In freshwater, the effectiveness of the particle-to-cell attachment is always governed by ES interaction, in which this interaction is strongly affected by the surface zeta-potential. The AB interaction between *Chlorella* sp. and bare-IONPs/SF-IONPs has a shorter interaction distance than ES interaction. The XDLVO analysis has predicted a net repulsion between *Chlorella* sp. cells and bare-IONPs while predicting effective attachment of

SF-IONPs onto cell surface with a secondary minimum of −3.12 kT, which is in accordance with our experimental observation. In seawater, the AB interaction plays a pivotal role in determining the net interaction between the cells and IONPs. High ionic strength suppresses the Debye screening length of the charged particles and induces a relatively short length for ES interaction, between cells and IONPs. This observation is beneficial for the design of an effective protocol to promote particle detachment from cell surfaces, which would greatly improve the reusability of the IONPs for subsequent separation cycles. The XDLVO theory has predicted the presence of a secondary minimum with a well depth of −1.94 kT, which is mainly dominated by the vdW interaction, and followed by a strong hydrophilic repulsion (U_{AB}) for the case of marine species Nannochloropsis sp. cells interact with SF-IONPs in seawater. Under this scenario, 97.90 ± 0.27% of cells were magnetophoretically separated at a particle dosage of 0.42 g particles per 1 g dry biomass. This prediction is strongly related to the less hydrophilic surface of Nannochloropsis sp. We anticipate that the XDLVO analysis presented here can be employed to aid the process of (1) selecting an appropriate molecular binder for surface functionalization of IONPs, which subsequently promotes particle attachment onto microalgal cells, and more importantly, (2) predicting the successful implementation of magnetophoretic separation without the need to conduct tedious and lengthy experiments.

Acknowledgements

Notes and references

1 Demirbas, Energy Convers. Manage., 2010, 51, 2738–2749.
2 A. L. Ahmad, N. H. M. Yasin, C. J. C. Derek and J. K. Lim, Renewable Sustainable Energy Rev., 2011, 15, 584–593.
3 P. Y. Toh, S. P. Yeap, L. P. Kong, B. W. Ng, D. J. C. Chan, A. L. Ahmad and J. K. Lim, Chem. Eng. J., 2012, 211–212, 22–30.
4 M. Cerff, M. Morweiser, R. Dillschneider, A. Michel, K. Menzel and C. Posten, Bioresour. Technol., 2012, 118, 289–295.
5 L. Xu, C. Guo, F. Wang, S. Zheng and C. Z. Liu, Bioresour. Technol., 2011, 102, 10047–10051.
6 Y. R. Hu, F. Wang, S. K. Wang, C. Z. Liu and C. Guo, Bioresour. Technol., 2013, 138, 387–390.
7 G. Prochazkova, I. Safarik and T. Branyik, Bioresour. Technol., 2013, 130, 472–477.
8 G. Bitton, J. L. Fox and H. G. Strickland, Appl. Microbiol., 1975, 30, 905–908.
9 R. Yadida, A. Abeliovich and G. Belfort, Environ. Sci. Technol., 1977, 11, 913–916.
10 M. Zborowski, L. R. Moore, S. William and J. J. Chalmers, Sep. Sci. Technol., 2002, 37, 3611–3633.
11 G. Prochazkova, N. Podolova, I. Safarik, V. Zachleder and T. Branyik, Colloids Surf., B, 2013, 112, 213–218.
12 P. Y. Toh, B. W. Ng, C. H. Chong, A. L. Ahmad, J.-W. Yang, D. J. C. Chan and J. K. Lim, RSC Adv., 2014, 4, 4114–4121.
13 P. Y. Toh, B. W. Ng, A. L. Ahmad, C. J. C. Derek and J. K. Lim, Process Saf. Environ., 2014, DOI: 10.1016/j.psep.2014.03.010.
14 J. K. Lim, C. J. C. Derek, S. A. Jalak, P. Y. Toh, N. H. M. Yasin, B. W. Ng and A. L. Ahmad, Small, 2012, 8, 1683–1692.
15 S. P. Yeap, A. L. Ahmad, B. S. Ooi and J. K. Lim, Langmuir, 2012, 28, 14878–14891.
16 A. K. Lee, D. M. Lewis and P. J. Ashman, J. Appl. Phycol., 2009, 21, 559–567.
17 M. W. Tenney, W. F. Echelberger, R. G. Schuessler Jr. and J. L. Pavoni, Appl. Microbiol., 1969, 18, 965–971.
18 M. Sirmerova, G. Prochazkova, L. Siristova, Z. Kolska and T. Branyik, J. Appl. Phycol., 2013, 25, 1687–1695.
19 C. Park, Z. Ounaies, K. A. Watson, R. E. Crooks, J. Smith Jr., S. E. Lowther, J. W. Connell, E. J. Siochi, J. S. Harrison and T. L. St. Clair, Chem. Phys. Lett., 2002, 364, 303–308.
20 P. B. Dengis, L. R. Nelissen and P. G. Rouxhet, Appl. Environ. Microbiol., 1995, 61, 718–728.
21 J. Norris, R. F. Giese, C. J. van Oss and P. M. Costanzo, Clays Clay Miner., 1992, 40, 327–334.
22 Y. R. Hunter and J. S. Kuwabara, Bull. Environ. Contam. Toxicol., 1994, 52, 311–318.
23 R. Bos, H. C. van der Mei and H. J. Busscher, FEMS Microbiol. Rev., 1999, 23, 179–230.
24 C. J. Van Oss, M. K. Chaudhury and R. J. Good, Chem. Rev., 1988, 88, 927–941.
25 C. J. Van Oss, Mol. Immunol., 1995, 32, 199–211.
26 P. K. Sharma and K. H. Rao, Colloids Surf., B, 2003, 29, 21–38.
27 C. J. Van Oss, Colloids Surf., B, 1995, 5, 91–110.
28 P. C. Hiemenz and R. Rajagopalan, Principles of colloid and surface chemistry, Marcel Dekker, Inc., New York, 3rd edn, revised and expanded, 1997.
29 H. C. Hamaker, Physica, 1937, 4, 1058–1072.
30 C. J. Van Oss, Polar or Lewis acid–base interaction, in Interfacial forces in aqueous media, Marcel Dekker, Inc., New York, 1994, pp. 18–44.
31 C. J. Van Oss, J. Mol. Recognit., 2003, 16, 177–190.
32 M. C. M. Van Loosdrecht, J. Lyklema, W. Norde and A. J. B. Zehnder, Microb. Ecol., 1989, 17, 1–15.
33 M. E. Q. Pilson, An introduction to the chemistry of the sea, University of Rhade Island, Prentice Hall, Pearson Education Inc, UK, 1st edn, 1998, ch. 4.

34 I. F. Hakem and J. Lal, *Europhys. Lett.*, 2013, 64, 204–210.

35 Y. Zhang, M. Tirrell and J. W. Mays, *Macromolecules*, 1996, 29, 7299–7301.

36 D. Surendhiran and M. Vijay, *ISRN Chem. Eng.*, 2014, 1–9.

37 R. Udhaya, L. B. Bruno and S. Sandhya, *Int. J. Environ. Sci.*, 2014, 4, 899–905.

38 D. H. Napper, *Polymeric Stabilization of Colloidal Dispersions*, Academic Press, New York, 1983.

PAPER

Magnetophoretic separation of microalgae: the role of nanoparticles and polymer binder in harvesting biofuel†

Pey Yi Toh,[a] Bee Wah Ng,[ab] Chi Han Chong,[c] Abdul Latif Ahmad,[a] Ji-Won Yang,[d] Chan Juinn Chieh Derek*[a] and JitKang Lim*[ae]

Magnetophoretic separation of Chlorella sp. microalgal biomass is proven to be a feasible downstream processing technology for biofuel production. Kinetic study of cells separation in real time reveals the major steps involved for each stage of low gradient magnetic separation (LGMS) with field gradient (∇B) less than 80 T m^{-1}. Transmission and scanning electron microscopy (TEM & SEM) together with Fourier transforms infrared (FTIR) spectra analysis are employed to confirm the full attachment of surface functionalized iron oxide nanoparticles (SF-IONPs) onto microalgal cells and how the particles distributed on the cell's surfaces. From the cross section TEM images of cells, IONPs shown the tendency to be internalized into Chlorella sp. cells but not affect the biofuel quality.

Introduction

Recently, magnetophoretic separation of microalgae has been widely investigated from different perspectives.[1–8] This idea was first introduced in the mid 1970s.[9,10] Initially, it was presented as an effective water treatment technology, in which removing microalgae blooms from water resources is crucial to avoid eutrophication. With the pressing need to find alternate options to replace fossil fuel, microalgae has gained popularity as potential new generation biofuel resource to combat the energy crisis.[11] Microalgae is widely accepted as the only non-edible feedstock that is capable of delivering high oil yield up to 14 641 gallons acre^{-1} to cope with energy demand and at the same time fulfill the sustainability requirement.[12,13] In prediction, biofuel production technology based on microalgae could reach maturity stage within another 10 to 15 years.[14]

Magnetophoretic separation is one of the most promising approaches for harvesting microalgae since the utilization of iron oxide nanoparticles (IONPs) are both technically[15] and economically[1] competent to remove the suspended cells from surrounding media. For this separation technique to work effectively, the IONPs are first attached to microalgal cell mainly through polymeric binders. Later, an externally applied magnetic field, either operated at high gradient ($\nabla B > 1000$ T m^{-1}) or low gradient ($\nabla B < 100$ T m^{-1}), is introduced to induce further separation. This method is scalable, less energy intensive, highly selective with separation efficiency up to 99% but requires only small land area.[2,16]

Multiple options are available to tag biological compounds with naked-IONPs,[17] and the most popular and straight forward way is the use of cationic polyelectrolyte as binding agent. Common tagging strategies involved polyelectrolyte can be implemented either through (1) attached-to or (2) immobilized-on methods.[2,17] For the attached-to approach, the cells are first coated by polymer binder followed with the attachment of naked-IONPs. For the immobilized-on approach, the naked-IONPs are surface functionalized with polyelectrolyte binder first and then attached on cell surface. In a formal approach, main problem arises as the naked-IONPs could not achieve good dispersibility and tend to aggregate into large particle clusters induced by Van der Waals and magnetostatic attraction.[18,19] Large aggregate of naked-IONPs which bind to the cell surface can be easily detached due to the high shear stress created during magnetophoretic migration.[20] In addition, rapid aggregation of IONPs prior to their attachment onto microalgae cells would significantly lower the particles-to-cells ratio and

[a]School of Chemical Engineering, Universiti Sains Malaysia, Nibong Tebal, Penang 14300, Malaysia. E-mail: chjitkangl@eng.usm.my; ch_derekchan@eng.usm.my

[b]School of Biological Sciences, Universiti Sains Malaysia, Minden, Penang 11800, Malaysia

[c]Department of Physics, Imperial College London, South Kensington Campus, London SW7 2AZ, UK

[d]Department of Chemical & Biomolecular Engineering, Korean Advanced Institute of Science and Technology, Daejon 305-701, Republic of Korea

[e]Department of Physics, Carnegie Mellon University, Pittsburgh, PA 15213, USA

† Electronic supplementary information (ESI) available: Table showing the cell separation efficiency of Chlorella sp., electrophoretic mobility of Chlorella sp., naked-IONPs, and SF-IONPs followed with the charge neutralization by different dosage of chitosan and figures showing the arrangement of LDR sensing system with magnet, kinetic separation of Chlorella sp. in different concentration of SF-IONPs, Fourier transforms infrared (FTIR) spectra of Chlorella sp. and SF-IONPs, and the growth curve of Chlorella sp. pure culture and after its exposure to 50 mg L^{-1} of naked-IONPs and SF-IONPs together with the cell growth inhibition effect. See DOI: 10.1039/c3ra46298f

greatly suppressed the separation efficiency. On the other hand, the immobilized-on approach is preferred as the polymer coating on the particle's surface will form an electrosteric barrier to enhance its colloidal stability prior to it attachment onto the microalgae cells.[21,22] In addition, the electrosteric hindrance layer formed also guarantees the well distribution of the nanoparticles tagged on cell's surface, which eventually promotes better cells separation efficiency.

In order to fully realize the application of magnetophoretic separation for biofuel production, further study on impacts of nanomaterials toward the quality of biofuel produced is necessary. Nanoparticle with size less than 100 nm is unique with its large surface to volume ratio and the availability of abundant active sites.[23,24] Surface property of the nanoparticles, such as charges carried and chemical reactivity,[25] governs the surface interaction and mobility, which could lead to health and environmental hazards.[26] A stable colloidal suspension of nanoparticles resulting in high occurrence rate of interaction between individual nanoparticle with microalgae, may lead to uptake by the microalgae cells or cause toxic effects.[27] However, certain microalgal strains like *Scenedesmus* sp. and *Chlorella* sp. suffered from growth inhibitory when the microalgae cultures are exposed to aluminum oxide nanoparticles ($d < 50$ nm) for 72 hours. This condition is mainly caused by the shading effect of nanoparticles that accumulate on cell surface and inhibit the photosynthesis activity.[27] From the existing literatures, the cytotoxicity of single-walled carbon nanotube[28] and fullerene[29] nanoparticles can be minimized significantly through surface functionalization, where the cytotoxic response decreased down to seven orders of magnitude for the case of fullerene (~60 nm). However, the side effect(s) arises from the interaction of IONPs with microalgae cells still remains unknown. Two key questions need to be addressed here: (1) do the IONPs used as tagging agent only attached onto the microalgal cell's surface with or without internalization, and, (2) do the addition of IONPs during the biomass collection influence the quality of oil collected? The answer for the first question provides a guideline to design surface functionalization strategy which is crucial in determining the success or failure of the magnetic separation of microalgae. Whereas, the answer to the second question is directly related to the engineering practicability of magnetic separation in harvesting algal oil.

There are several illustrations, on both low gradient magnetic separation (LGMS) and high gradient magnetic separation (HGMS) under different operational condition, which provide various ways to harvest magnetic colloid from the suspensions.[1,30-35] In this study, LGMS is chosen based upon the simple fact that as long as we could impart magnetic properties to the none-magnetic microalgal cells, such as illustrated in Fig. 1, the subsequent introduction of magnetic field would induce cells separation. The application of LGMS for microalgae separation, sharing the exact analogy as in Fig. 1, has been extensively studied recently.[1,5,6,8] Nevertheless, cost involved is the main deciding factor in the selection of magnetic separation scheme for microalgae harvesting.[1] Other important considerations such as high separation efficiency, minimum environmental impacts, ease of operation, high through-put and capable to handle large
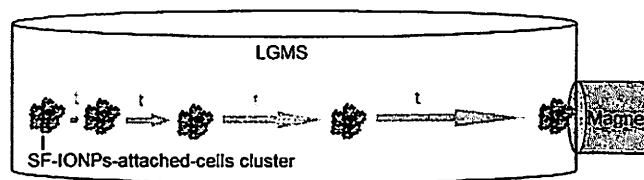

Fig. 1 Schematic diagram shows the movement of SF-IONPs-attached-cells cluster toward the magnet with respect to the distance from the permanent magnet during LGMS.

quantity of feed solution are all vital in designing magnetic separation system for large scale biofuel production.

In this work, we studied the real-time kinetic behavior of magnetophoretic separation of *Chlorella* sp. and the bio-interaction between the *Chlorella* sp. and SF-IONPs under LGMS. Transmission electron microscope (TEM), scanning electron microscope (SEM) and Fourier transforms infrared (FTIR) spectra analysis are employed to probe the attachment of SF-IONPs onto microalgal cells. Moreover, the impact of naked-IONPs/SF-IONPs on the quality of extracted oil is verified by gas chromatography mass spectrometry study (GCMS). A custom-built optical sensing system (also see Fig. S1†) was employed to probe the separation kinetic of the magnetic colloid and measure the overall separation efficiency, while the UV-vis spectrometer was employed to measure the specific cell separation efficiency.

Experimental

Materials

Iron oxide nanoparticles (IONPs) were obtained from Nano-structured & Amorphous Materials, Inc. Low molecular weight chitosan powder (75–85% deacetylated) was supplied by Sigma-Aldrich Chemistry. Hydrochloric acid was purchased from PC Laboratory Reagent. Chloroform and *n*-hexane were obtained from Merck KGaA, Germany, while the methanol was obtained from Fisher Scientific UK Limited. Deionised water was obtained by reverse osmosis and further treated by the Milli-Q Plus system (Lillipore) to 18 MΩ cm resistivity.

Culture and characterization of *Chlorella* sp.

The *Chlorella* sp. strain was obtained from School of Biological Sciences, USM. The cells were cultivated in 500 mL conical flask that contained 250 mL Bold's Basal Medium (BBM) under continuous illumination at 2000 lux and 25 °C. The medium and flask were sterilized at temperature of 121 °C for 15 minutes before cell cultivation. Continuous aeration was provided for the culture medium throughout the cultivation period. The cell counting was conducted by haemocytometer and the desired cell density was achieved with appropriate dilution using the supernatant of centrifuged medium.

Preparation and characterization of surface functionalized iron oxide nanoparticles (SF-IONPs)

In this work, attached-to approach was employed to form attachment between the IONPs and cells.[2] The naked-IONPs used are spherical in shape with dimension of 20–30 nm in

•diameter (Fig. 2a). The chitosan solution was prepared by dispersing 0.02 g of the dry chitosan powder into 10 mL of acetic acid solution with concentration of 1 wt% in DI. The solution was left for one day to achieve complete dissolution. Then a total of 2 mL naked-IONPs dispersion at concentration of 1 g L^{-1} was added into the chitosan solution and then sonicated with using low power bath sonicator (40 kHz) to avoid degradation of polymer molecular weight. The solution was then left on the end-to-end rotating mixer at 40 rpm overnight. After successful surface functionalization of IONPs, a permanent magnet was used to collect the SF-IONPs. The supernatant with freely suspended chitosan was discarded while the SF-IONPs were again dispersed in 2 mL deionized water. This washing step was repeated for three times to ensure full removal of free chitosan molecules. Electrophoretic mobility and the hydrodynamic diameter of SF-IONPs were measured (Malvern Instruments Nanosizer) before and after the surface functionalization with difference chitosan polymer concentration. For every separation study, 2 mL of SF-IONPs was added into 8 mL cell medium to form 10 mL suspension, which followed with hand shaking for 30 seconds to ensure uniform mixing between the particles and cells. The mixture was then left for another 30 seconds before being used for magnetophoretic separation study. These two steps contribute to the total incubation time of one minute.

Attachment of SF-IONPs to *Chlorella* sp.

The linkage between *Chlorella* sp. and SF-IONPs was promoted through simple mixing. The physical attachment of particles onto cell's surface was identified through transmission electron microscope (TEM). Scanning electron microscope (SEM), Fourier transforms infrared (FTIR) spectra analysis were performed after the sample was freeze dried. Scanning Transmission Electron Microscope together with Energy-dispersive X-ray spectroscopy (STEM-EDX Mapping) mapping was employed to determine the iron (Fe) element distribution within the cell.

Magnetic separation of SF-IONPs-attached-cells

Magnetophoretic separation of *Chlorella* sp. was carried under low gradient magnetic separation (LGMS) with a NdFeB permanent magnet in inhomogeneous magnetic field where ∇B < 80 T m^{-1} (see Fig. S1a†). The custom made cuvette used in this study with the dimension of 2 cm × 2 cm (width × depth) was selected to ensure the LGMS process happened within the effective magnetic field range of the NdFeB magnet. The cell separation performance was recorded at 6 minutes separation. The absorbance of the sample was measured spectrophotometrically by UVmini-1240 Shimadzu at the wavelength of 660 nm (measured by Agilent Technologies Carry 60 UV-vis). The cell separation efficiency was determined as

$$\text{Cell separation efficiency}(\%) = \frac{I_0 - I(t)}{I_0 - I_{\text{centrifuged}}} \times 100\% \quad (1)$$

where I_0, $I(t)$ and $I_{\text{centrifuged}}$ are the absorbance intensity of microalgal suspension initially, during magnetophoretic separation at time t and the clear centrifuged sample respectively.
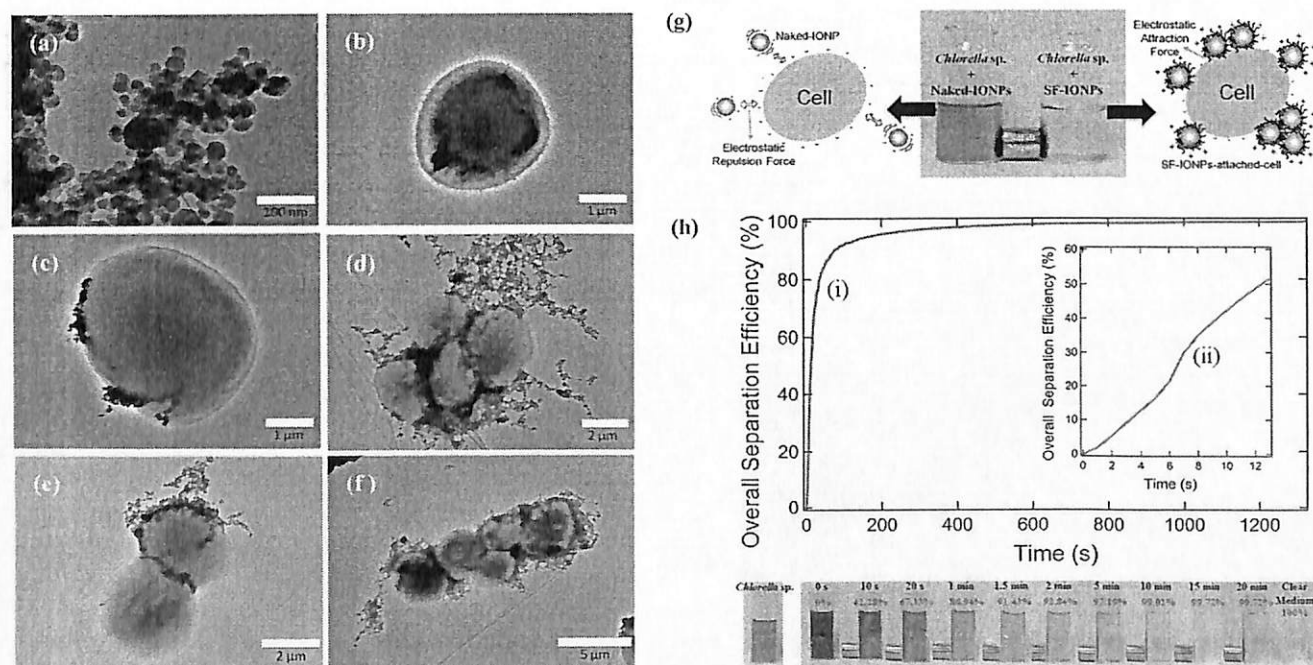

Fig. 2 Transmission Electron Microscopy (TEM) images of (a) naked-IONPs, (b) *Chlorella* sp. cell when mixed with naked-IONPs, (c) SF-IONPs-attached-cells, and the flocculation of SF-IONPs-attached-cells (d) and (e) without and (f) with magnet is introduced. (g) Observation of magnetophoretic separation performance of *Chlorella* sp. cells after the introduction of naked-IONPs and SF-IONPs into each sample respectively. (h) Quantitative curve for the kinetic separation of *Chlorella* sp. (3 × 10^7 cells mL^{-1}) after added with 300 mg L^{-1} SF-IONPs in real time through LGMS for 20 minutes. Curve (ii) shows the lag stage of the magnetophoretic separation that occurred in first few second. Image observation of the real time magnetophoretic separation of *Chlorella* sp. after added with 300 mg L^{-1} SF-IONPs is attached.

However, the kinetic of overall separation in real time and overall separation efficiency were quantified through the self-developed optical light intensity sensing system (LDR setup). The LDR setup (see Fig. S1b†) was connected to a data recorder for automatic data recording purpose. The overall separation efficiency was determined as

$$\text{Overall separation efficiency(\%)} = \frac{V_0 - V(t)}{V_0 - V_{\text{centrifuged}}} \times 100\% \quad (2)$$

where V_0, $V(t)$ and $V_{\text{centrifuged}}$ are the voltage recorded of microalgal suspension initially, during magnetophoretic separation at time t and the clear centrifuged sample respectively.

Oil extraction from *Chlorella* sp.

Oil extraction was carried in two steps, lipid extraction and transesterification. Lipid extraction was performed by adding 5.5 mL of distilled water to the freeze dried biomass inside a tube and sonicated for 5 minutes. Chloroform and methanol at ratio of 5.5 : 6 : 6 (distilled water–chloroform–methanol) were then added into it together with a stirring magnet. The tube was capped and maintained at 60 °C water bath and stirred at 500 rpm for 24 hours. The extracted solution was centrifuged at 3000 rpm for 2 minutes to form two separate layers. The bottom layer that contained lipid and chloroform was collected and then evaporated to dryness under nitrogen.

Transesterification was carried out to obtain the fatty acid profile analysis. The dried lipid was dissolved with 5 mL hexane solvent and transfer into a tube. Methanol and hydrochloric acid (HCl) were then added into the solution at ratio of 5 : 4.25 : 0.215 (hexane–methanol–HCl). The tube was capped and maintained at 85 °C in a water bath follow by constant stirring at 500 rpm for 2 hours. The reacted mixture was centrifuged at 3000 rpm for 2 minutes to form two separate layers. The top layer was collected. The fatty acid profile was measured by using gas chromatography mass spectrometer (GCMS) equipped with OmegawaxTM 250 fused silica capillary column with 30 m × 0.25 mm × 0.25 μm film thickness and helium gas as the carrier at a flow rate of 1 mL min⁻¹. The GCMS was operated at initial temperature of 80 °C with initial time of 1 minute. The temperature was elevated at rate of 8 °C min⁻¹ to final temperature of 230 °C on 25 minutes. The injection temperature was 250 °C and detector temperature was 260 °C. The oil profiles of *Chlorella* sp. under different condition were compared.

Results and discussion

Magnetophoretic separation of *Chlorella* sp.

Magnetophoretic separation of *Chlorella* sp. was achieved by an externally applied low gradient magnetic field ($\nabla B < 80$ T m⁻¹) from a cylindrical NdFeB magnet (also see Fig. S1a†).[2] According to Fig. 2g, microalgal cells registered low separation efficiency, at about 6.20 ± 0.60% (also see Table S1†) if naked-IONPs was used without the presence of binding agents. However, with the introduction of SF-IONPs, the previously greenish microalgal sample became crystal clear at the end of

the separation, with total separation efficiency at 95.61 ± 0.63%. This observation has proven the critical role of binding agent to ease the attachment of SF-IONPs onto the non-magnetic *Chlorella* sp. microalgae and promoted rapid separation. Hypothetically, the attachment of SF-IONPs, with electrophoretic mobility at 3.533 ± 0.333 μm cm V⁻¹ s⁻¹, on negatively charged *Chlorella* sp. (electrophoretic mobility at −2.353 ± 0.562 μm cm V⁻¹ s⁻¹) (Table S2†) is mainly through the electrostatic interaction. The failure of IONPs (−2.041 ± 0.476 μm cm V⁻¹ s⁻¹) to bind with cells is caused by the electrostatic repulsion experienced by two negatively charged species. As shown in Fig. 2b, there is no obvious attachment of naked-IONPs onto *Chlorella* sp., even with the extension of mixing period for 2 hours. Under this scenario the recorded cell separation efficiency is only at 7.96 ± 0.2%. While in Fig. 2c, it is clearly showed that SF-IONPs are attached onto the cell surface. Rapid aggregation of the SF-IONPs-attached-cells can be observed to occur right after the successful SF-IONPs attachment. This process is mainly driven by two aggregation mechanisms: (i) microalgal cells which are decorated by limited number of SF-IONPs formed small cell-particles clusters due to inter-particles Van der Waals and magnetostatic interaction.[17] This cell-particles clusters then (ii) further aggregated into larger group through bridging flocculation between the extended chitosan polymer binder, as showed in Fig. 2d.[36,37] When SF-IONPs-attached-cells are formed, this overall structure may reach net charge neutralization as the combining effect of charged group from both SF-IONPs and microalgal cells (Table S2†). Net charge neutralization effect is proportional to the increment of chitosan dosage coated on the surface of SF-IONPs (Table S3†). Under this condition, electrosteric repulsion between SF-IONPs-attached-cells is far more weaker than those between the SF-IONPs, in which the electrosteric layer of chitosan guarantees the dispersibility of SF-IONPs. Hence the van der Waals and magnetostatic interactions would overcome the weakened electrosteric repulsion between the cell-particles clusters, and at the minimal separation distance bridging flocculation occurred.[37] However, it should also be noted that the electrostatic interaction can also occur on the SF-IONPs-attached-cells with another free cell (Fig. 2e), where the binding agent on the surface of SF-IONPs-attached-cells is experiencing extended conformation.[19]

Binding agent, such as chitosan, not only determine the success or failure of the magnetic separation of microalgal cells, but also dictating the rate at which the SF-IONPs-attached-cells can be separated out from culture broth. For this purpose, the kinetic of microalgae magnetophoretic separation in real time under LGMS was investigated by a light dependent resistor (LDR) based sensing system (a cartoon of complete setup can be found in Fig. S1†).[18] Fig. 2h showed the temporal evolution of microalgal separation throughout a time course of 20 minutes. There was a lag phase with very short time duration (<7 seconds) at the beginning of separation right after the inhomogeneous magnetic field was introduced (Fig. 2h(ii)). This time lag was mainly due to the way NdFeB magnet is being introduced, with association to the point where we started our LDR sensor, for signal recording. The extended time lag as suggested by

Benelmekki and coworkers in which the SF-IONPs have gone through certain degree of flocculation either during or after the attachment onto microalgal cells were not observed on the separation kinetic graph.[38] It is very likely that most of the SF-IONPs have already aggregated on the surface of microalgal cell during the incubation period before the introduction of magnetic field. The presence of these aggregated SF-IONPs-attached-cell clusters further enhance the magnetophoretic collectability of the microalgal cells and contribute to the rapid collection right after the magnetic source is introduced. The suspension turned transparent progressively and became crystal clear at the end of the experiment. Consistent with our separation efficiency measurement (Fig. 2h), rapid collection of SF-IONPs-attached-cell happened in the first two minutes with the previously dark brown suspension becomes almost color free. By varying the concentration of SF-IONPs employed from 25 mg L^{-1} to 800 mg L^{-1} (see Fig. S2†), we found out that working concentration at 300 mg L^{-1} gives the best separation efficiency in relatively shorter timescale. This concentration translated to particle-to-cell mass ratio of 1.58 g g^{-1}.

Under LGMS with homogeneous magnetic field, aggregation process is specifically known as "field-induced-aggregation".[30] This observation can also be generalized to LGMS taken place in inhomogeneous magnetic fielnd.[18] Fig. 2f showed the TEM image of the SF-IONPs-attached-cells cluster formed by field-induced-aggregation, where the SF-IONPs-attached-cells were clumped together to form unidirectional linked structure.[2] We anticipated that this structure is formed during their migration toward the magnetic field source as they aligned with the magnetic field line.[39] The rapid separation achieved in our study is very likely caused by (1) enhanced magnetoshape anisotropy of this structure (Fig. 2f),[2] and also, (2) low viscous drag experienced by this structure during magnetophoresis when compared with more compact, spherical aggregate structure as shown in Fig. 2d.[40] The number of freely suspended magnetic colloids was reduced with time as they continuously attached onto the microalgal cells and caught-up in the sweeping flow of SF-IONPs-attached-cells along their magnetophoresis pathway. Since large particles-cell aggregates are much more magnetophoretically responsive, hence, they tend to be collected first. Under this condition, the size distribution of SF-IONPs-attached-cells aggregate is narrowing down with time in acceleration phase with the remaining of small aggregates left in suspension. This phenomenon provides reason for the decrement of cell separation rate over time and also the prolonged collection time during the stationary phase. The collection time could be decreased by increase the concentration of SF-IONPs (also see Fig. S2†).

Chlorella sp. cell surface examination

Hypothetically, the cationic chitosan polymer was needed to promote the attachment of negatively charged IONPs onto the Chlorella sp. cell through the electrostatic interaction. From the FTIR spectra analysis (also see Fig. S3†), Chlorella sp. cell contained -COO$^-$, -COOH, and -OH functional groups and C=O and N–H bonds while the SF-IONPs contained -NH$_4^+$, -OH

functional groups and -NH bonds. The main interactions contributed to form SF-IONPs-attached-cells are electrostatic interaction between different charge active sites, protonated amino functional groups on SF-IONPs and deprotonated carboxylic functional groups on Chlorella sp. cells. Besides, we hypothesized that hydrogen bonding between the hydrogen bond donors (-OH, -NH) and acceptors (C=O) that are available on both surface of Chlorella sp. cells and SF-IONPs can also be important to promote the linkages between the SF-IONPs and microalgal cell.

The typical SEM micrographs for the collection of Chlorella sp. cells prepared under different conditions, as illustrated in Fig. 3, have provided some insights and supporting fact for this hypothesis. After centrifugation (Sample A), cells were closely packed. If only chitosan was introduced into cell medium, the centrifuged biomass composed of cells which were linked together (Sample B) with the formation of highly porous arrangement.[6,41] This feature of chitosan making it one of the most widely used flocculant for water treatment application.[42,43] Sample C showed the cells surface is free from the attachment of naked-IONPs. From Sample D, after the magnetic separation under low field gradient, SF-IONPs were still well distributed and attached on almost every cells surface but not as ordered as the centrifuged cells. The gaps available between the SF-IONPs-attached-cells are partially filled with particles-polymer matrix, forming a three dimensional structure.[37] In short, the chitosan play important roles (i) as stabilizing agent to ensure the colloidal stability of SF-IONPs prior to attachment, (ii) as binding agent to promote the adhesion of SF-IONPs onto cells surface, and also, (iii) as bridging agent to enhance flocculation of SF-IONPs-attached-cells in order to achieve rapid magnetophoretic separation under low magnetic field gradient. In most likelihood, this loosely bound porous structure as shown in Sample D might formed through magnetic field induced aggregation and is the main reason for rapid cooperative magnetophoresis as observed in Fig. 2h.

Chlorella sp. cell interior examination

Cells interior examination is essential to study the bio-distribution of IONPs inside the cells which eventually might influence the biofuel quality produced. The cross-sectional TEM micrographs of Chlorella sp. (Sample A in Fig. 3) shows it has a pretty simple cell structure. After cells were exposed to naked-IONPs for 2 hours (Sample C), the naked-IONPs had the tendency to enter the cells. After surface functionalization, the internalization of SF-IONPs (TEM micrographs of Sample D in Fig. 3) is majorly promoted by the aid of surface interaction with the cell surface. The internalization of naked-IONPs (Sample C) and SF-IONPs (Sample D) was further confirmed through the element mapping of Fe by STEM-EDX as shown in Fig. 3. The internalization of IONPs may be through a passive uptake or adhesive interaction. Even though the entire internalization process is not fully understood, however, it would be very likely initiated by collision of nanoparticles with cell surface and also the direct electrostatic attraction of SF-IONPs on cells.[44,45]

SEM Micrographs
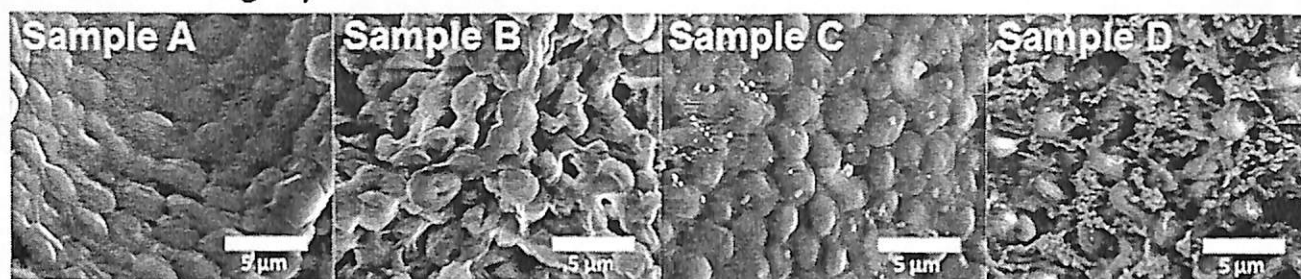
TEM Micrographs (Cell cross-sectional view)
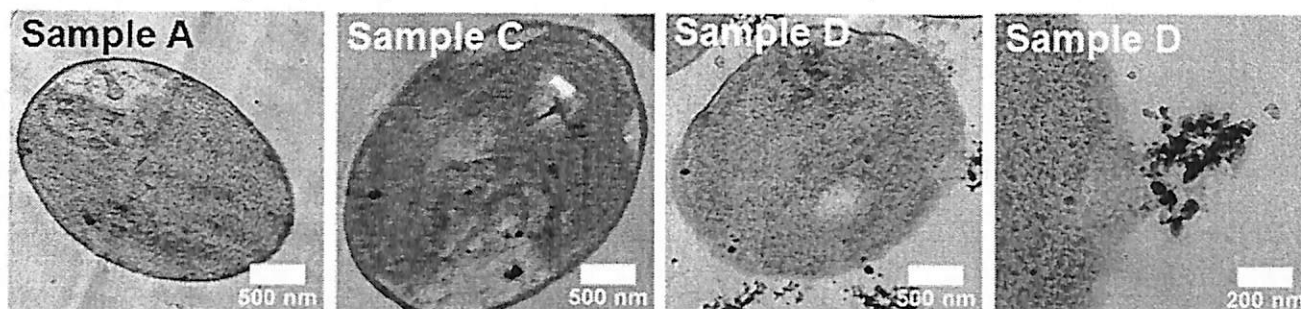
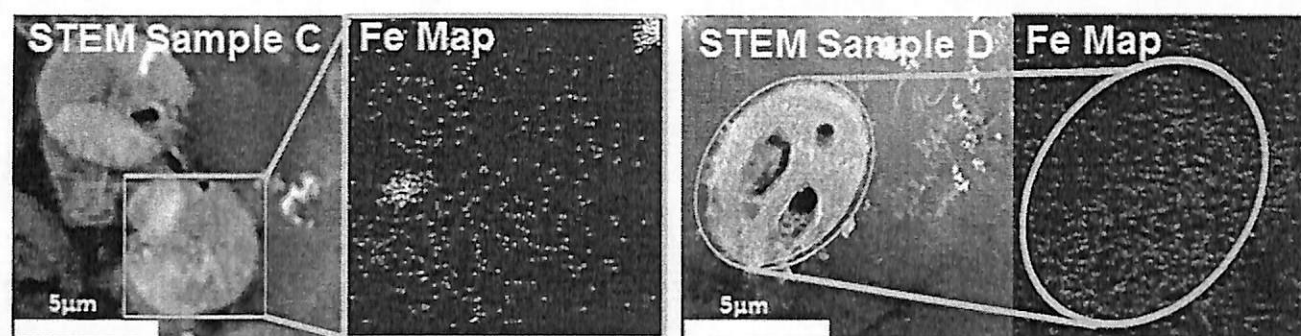## STEM-EDX Mapping for Fe element (Cell cross-sectional view)

Fig. 3 Scanning electron microscope (SEM) of *Chlorella* sp. cells from different collection method (Sample A) *Chlorella* sp. cells obtained from centrifugation, (Sample B) *Chlorella* sp. cells obtained after exposure to chitosan polymer (Sample C) *Chlorella* sp. cells obtained after exposure to naked-IONPs collected *via* centrifugation and (Sample D) *Chlorella* sp. cells with SF-IONPs collected from LGMS. Transmission electron microscopy (TEM) is employed to capture the images of the cross-sectional view of (Sample A) *Chlorella* sp. cells, (Sample C) *Chlorella* sp. cells after exposure to naked-IONPs, and (Sample D) *Chlorella* sp. cells with SF-IONPs collected from LGMS. Element mapping of Fe by Energy-Dispersive X-ray spectroscopy (EDX) is employed to confirm the internalization of Fe into the cells.

Most of the commonly found nanomaterials, such as carbon nanotube,[46] Al_2O_3,[27] CuO, ZnO and TiO_2 (ref. 47) nanoparticles are potentially toxic to microalgae. The inhibition of microalgae growth with the presence of nanomaterials has been reported elsewhere,[47] and the potential toxic mechanism can be due to oxidative stress, agglomeration and physical interactions, sequestration of nutrient elements, and/or shading effects. From our experiment, approximately 50 mg L^{-1} of naked-IONPs/SF-IONPs is sufficient to suppress the growth of *Chlorella* sp. (Fig. S4a†). The supporting result in Fig. S4b† showed that for the case of naked-IONPs the growth inhibition (see ESI† for detail description) of cells always maintained at less than 40% without further increment. While for the case of SF-IONPs, the growth inhibition has dropped to about 10% only. In both cases, the cell culture only suffered from slower growth kinetic without obvious reduction of cell density. This observation has in turn proven that the major inhibition effect is due to light shading rather than permanent damage onto cell membrane and DNA (which would kill the cells permanently and wipe up the entire microalgal colony).[44] In magnetophoretic separation, SF-IONPs are only being introduced into the microalgal medium during the harvesting day (at day 10th). The adverse effect of IONPs toward the oil yield of microalgal is negligible since the algal oil has been produced during the cells growth before the magnetic separation and harvesting were carried out. The fatty acid profile analysis were carried out to confirm our hypothesis with regards to this matter and the results were tabulated in Table 1. Several different types of fatty acid were found to be present in the *Chlorella* sp. cells ranging from C12 to C22.[48] However our study concentrated on the 3 major fatty

Table 1 Fatty acid methyl ester (FAME) content of the oil extracted from (Sample A) *Chlorella* sp., (Sample B) *Chlorella* sp. exposed to 300 mg L^{-1} chitosan, (Sample C) *Chlorella* sp. exposed to 300 mg L^{-1} naked-IONPs, and (Sample D) SF-IONPs-attached-cells collected from LGMS. The value after plus-minus sign is the standard error of 3 replicates[a]

Fatty acid	Percentage (% of total fatty acid)			
	A	B	C	D
$\sum$C16	37.1 ± 5.8	39.9 ± 0.8	33.0 ± 5.7	36.4 ± 5.5
$\sum$C18	37.3 ± 4.3	31.9 ± 2.3	30.8 ± 7.1	35.0 ± 3.4
$\sum$C20	11.7 ± 1.1	8.1 ± 3.8	8.7 ± 3.9	6.9 ± 3.3
$\sum$Saturated (SFA)	16.0 ± 7.3	30.4 ± 8.1	24.7 ± 2.2	27.2 ± 0.4
$\sum$Mono-unsaturated (MUFA)	9.0 ± 0.8	10.2 ± 0.5	9.2 ± 1.5	11.0 ± 0.3
$\sum$Di-unsaturated (DUFA)	47.8 ± 4.8	35.4 ± 6.3	36.7 ± 3.1	37.4 ± 3.3
$\sum$Poly-unsaturated (PUFA)	27.2 ± 3.4	24.1 ± 1.5	29.4 ± 3.7	24.4 ± 3.3

[a] ANOVA analysis verified the homogeneity of variances on the total fatty acid content (value reported in the same row) within each group of fatty acid.

acid present in the cells which are the C16, C18 and C20. The $\sum$C16 and $\sum$C18 fatty acids were found to make up to about 74.4%, which was approximately three quarter of the total fatty acid accumulated in the cells. The third highest fatty acid, $\sum$C20, was about 11.7 ± 1.1% in the control group (Sample A). The results of fatty acid profile were compared with *Chlorella* sp. cells exposed to 300 mg L^{-1} chitosan (Sample B), 300 mg L^{-1} naked-IONPs (Sample C) and SF-IONPs-attached-cells collected from LGMS (Sample D). The analysis of variance (ANOVA) carried out among the tested samples indicated that there is no significant difference in the fatty acid content in the *Chlorella* sp. cells subjected to different treatments. The percentage ratio of $\sum$C16 and $\sum$C18 remains unchanged at around 1 : 1. The exposure of the *Chlorella* sp. cells to chitosan, naked-IONPs and as well as SF-IONPs were also statistically found not to affect the saturation of the fatty acids accumulated in the cells. The $\sum$unsaturated fatty acids (UFA) comprising of the mono-unsaturated (MUFA), di-unsaturated (DUFA) and poly-unsaturated (PUFA), were naturally the highest amounting to about 84.0 ± 7.3% as compared to the $\sum$saturated fatty acid which are around 16.0 ± 7.3%.[49] Moreover, the oxidation of UFA may happen with the presence of transition metal/metal oxide catalysts.[50] Oxidation will occur at carbon–carbon double bond of unsaturated fatty acid and hence result in partial/complete cleavage of the double bond to form mono/dicarboxylic acid. The exposure towards chitosan and even with nanoparticles internalization (with and without surface functionalization) does not seem to affect the quality of fatty acid extracted from the *Chlorella* sp. cells before and after exposure to the polymer/naked-IONPs/SF-IONPs. This indirectly proved the reliability of magnetophoretic separation as an effective tool in microalgal biomass harvesting as the feedstock for biofuel.

Conclusions

Our experimental findings on the bio-interaction and the bio-distribution of the IONPs toward the microalgal cells have sketched the real picture about the interaction between the magnetic nanoparticles and the tagged cell. Kinetic study in real time has explained the transient behavior of SF-IONPs tagged cell in response to low gradient magnetic field. In particles attachment study, the electrostatic interaction plays a major role to bind the IONPs with *Chlorella* sp. together by using polymer binder. Although internalization of the SF-IONPs was witnessed, this scenario did not cause any adverse effects toward the quality and quantity of extracted lipid. These encouraging outcomes prove the reliability of magnetophoretic separation for microalgal biomass collection and can be implemented as an effective downstream process for biofuel production.

References

1 P. Y. Toh, S. P. Yeap, L. P. Kong, B. W. Ng, D. J. C. Chan, A. L. Ahmad and J. K. Lim, *Chem. Eng. J.*, 2012, 22, 211–212.
2 J. K. Lim, C. J. C. Derek, S. A. Jalak, P. Y. Toh, N. H. M. Yasin, B. W. Ng and A. L. Ahmad, *Small*, 2012, 8, 1683.
3 M. Cerff, M. Morweiser, R. Dillschneider, A. Michel, K. Menzel and C. Posten, *Bioresour. Technol.*, 2012, 118, 289.
4 A. Merino-Martos, J. de Vicente, L. Cruz-Pizarro and I. de Vicente, *J. Hazard. Mater.*, 2011, 186, 2068.

5 L. Xu, C. Guo, F. Wang, S. Zheng and C. Z. Liu, *Bioresour. Technol.*, 2011, 102, 10047.

6 D. Liu, F. Li and B. Zhang, *Water Sci. Technol.*, 2009, 1085.

7 G. Prochazkova, I. Safarik and T. Branyik, *Bioresour. Technol.*, 2012, 130, 472.

8 Y. R. Hu, F. Wang, S. K. Wang, C. Z. Liu and C. Guo, *Bioresour. Technol.*, 2012, 138, 387.

9 R. Yadida, A. Abeliovich and G. Belfort, *Environ. Sci. Technol.*, 1977, 11, 913.

10 G. Bitton, J. L. Fox and H. G. Strickland, *Appl. Microbiol.*, 1975, 30, 905.

11 E. Stephens, I. L. Ross, Z. King, J. H. Mussgnug, O. Kruse, C. Posten, M. B. Borowitzka and B. Hankamer, *Nat. Biotechnol.*, 2010, 28, 126.

12 M. B. Johnson, *Microalgal Biodiesel Production through a Novel Attached Culture System and Conversion Parameters: Biological Systems Engineering*, Blacksburg, Virginia, 2009.

13 L. E. de-Bashan and Y. Bashan, *Bioresour. Technol.*, 2009, 101, 1611.

14 R. H. Wijffels and M. J. Barbosa, *Science*, 2010, 329, 796.

15 Z. R. Ulberg and L. G. Marochko, *Colloids Surf., A*, 1999, 159, 513.

16 S. Bucak, S. Sharpe, S. Kuhn and T. A. Hatton, *Biotechnol. Prog.*, 2011, 27, 744.

17 I. Safarik and M. Safarikova, *J. Chromatogr. B: Biomed. Sci. Appl.*, 1999, 722, 33.

18 S. P. Yeap, P. Y. Toh, A. L. Ahmad, S. C. Low, S. A. Majetich and J. K. Lim, *J. Phys. Chem. C*, 2012, 116, 22561.

19 Y. Zhou, Y. Gan, E. J. Wanless, G. J. Jameson and G. V. Franks, *Langmuir*, 2008, 24, 10920.

20 M. H. A. Michels, A. J. van der Goot, N.-H. Norsker and R. H. Wijffels, *Bioprocess Biosyst. Eng.*, 2010, 33, 921.

21 G.-Y. Li, Y.-R. Jiang, K.-L. Huang, P. Ding and L.-L. Yao, *Colloids Surf., A*, 2008, 320, 11.

22 S. P. Yeap, A. L. Ahmad, B. S. Ooi and J. K. Lim, *Langmuir*, 2012, 28, 14878.

23 E. Navarro, A. Baun, R. Behra, N. B. Hartmann, J. Filser, A. J. Miao, A. Quigg, P. H. Santschi and L. Sigg, *Ecotoxicology*, 2008, 17, 372.

24 W. Wu, Q. He and C. Z. Jiang, *Nanoscale Res. Lett.*, 2008, 3, 397.

25 M. N. Moore, *Environ. Int.*, 2006, 32, 967.

26 A. D. Maynard, R. J. Aitken, T. Butz, V. Colvin, K. Donaldson, G. Oberdorster, M. A. Philbert, J. Ryan, A. Seaton, V. Stone, S. S. Tinkle, L. Tran, N. J. Walker and D. B. Warheit, *Nature*, 2006, 444, 267.

27 I. M. Sadiq, S. Parkrashi, N. Chandrasefaran and A. Mukherjee, *J. Nanopart. Res.*, 2011, 13, 3287.

28 C. M. Sayes, F. Liang, J. L. Hudson, J. Mendeza, W. Guo, J. M. Beach, V. C. Moore, C. D. Doyle, J. L. West,

W. E. Billups, K. D. Ausmanb and V. L. Colvin, *Toxicol. Lett.*, 2006, 161, 135.

29 C. M. Sayes, J. D. Fortner, W. Guo, D. Lyon, A. M. Boyd, K. D. Ausman, Y. J. Tao, B. Sitharaman, L. J. Wilson, J. B. Hughes, J. L. West and V. L. Colvin, *Nano Lett.*, 2004, 4, 1881.

30 G. D. L. Cuevas, J. Faraudo and J. Camacho, *J. Phys. Chem. C*, 2008, 112, 945.

31 G. D. Moeser, K. A. Roach, W. H. Green and T. A. Hatton, *AIChE J.*, 2004, 50, 2835.

32 J. A. Oberteuffer, *IEEE Trans. Magn.*, 1973, 9, 303.

33 G. Iacob, A. D. Ciochina and O. Bredetean, *Eur. Cells Mater.*, 2002, 3, 167.

34 M. Benelmekki, LI. M. Martinez, J. S. Andreu, J. Camacho and J. Faraudo, *Soft Matter*, 2012, 8, 6039.

35 M. Zborowski and J. Chalmers, *Magnetic cell separation*, Elsevier, Oxford, UK, 2008, vol. 32.

36 Y. Zhou and G. V. Franks, *Langmuir*, 2006, 22, 6775.

37 M. W. Tenney, W. F. Echelberger Jr, R. G. Schuessler and J. L. Pavoni, *Appl. Microbiol.*, 1969, 18, 965.

38 M. Benelmekki, C. Caparros, A. Montras, R. Goncalves, S. Lanceros-Mendez and L. M. Martinez, *J. Nanopart. Res.*, 2011, 13, 3199.

39 P. Kopcansky, N. Tomasovicova, M. Koneracka, M. Tomko, V. Zavisova and L. Tomco, *Acta Electrotechnica et Informatica*, 2010, 10, 10.

40 J. K. Lim, D. X. Tan, F. Lanni, R. D. Tilton and S. A. Majetich, *J. Magn. Magn. Mater.*, 2009, 321, 1557.

41 A. L. Ahmad, N. H. M. Yasin, C. J. C. Derek and J. K. Lim, *Chem. Eng. J.*, 2011, 173, 879.

42 B. Bina, M. H. Mehdinejad, M. Nikaeen and H. M. Attar, *J. Environ. Health Sci. Eng.*, 2009, 6, 247.

43 J. Roussy, M. V. Vooren, B. A. Dempsey and E. Guibal, *Water Res.*, 2005, 39, 3247.

44 Z. Wang, J. Li, J. Zhao and B. Xing, *Environ. Sci. Technol.*, 2011, 45, 6032.

45 C. Buzea, I. I. Pacheco Blandino and K. Robbie, *Biointerphases*, 2007, 2, MR17.

46 Z. Long, J. Ji, K. Yang, D. Lin and F. Wu, *Environ. Sci. Technol.*, 2012, 46, 8458.

47 V. Aruoja, H.-C. Dubourguier, K. Kasemets and A. Kahru, *Sci. Total Environ.*, 2009, 407, 1461.

48 P. I. Leonardi, C. A. Popovich and M. C. Damiani, *Economic Effects of Biofuel Production*, 2011, 318.

49 L. Gouveia and A. C. Oliveira, *J. Ind. Microbiol. Biotechnol.*, 2009, 36, 269.

50 H. Noureddini and M. Kanabur, *Papers in Biomaterials*, 1999, 76, 305–312.

CrossMark

Magnetophoresis of iron oxide nanoparticles at low field gradient: The role of shape anisotropy

JitKang Lim [a,b,*], Swee Pin Yeap [a], Chee Hoe Leow [a,1], Pey Yi Toh [a,1], Siew Chun Low [a]

[a] School of Chemical Engineering, Universiti Sains Malaysia, Nibong Tebal 14300, Penang, Malaysia
[b] Department of Physics, Carnegie Mellon University, Pittsburgh, PA 15213, USA

ARTICLE INFO

ABSTRACT

Magnetophoresis of iron oxide magnetic nanoparticle (IOMNP) under low magnetic field gradient (<100 T/m) is significantly enhanced by particle shape anisotropy. This unique feature of magnetophoresis is influenced by the particle concentration and applied magnetic field gradient. By comparing the nanosphere and nanorod magnetophoresis at different concentration, we revealed the ability for these two species of particles to achieve the same separation rate by adjusting the field gradient. Under cooperative magnetophoresis, the nanorods would first go through self- and magnetic field induced aggregation followed by the alignment of the particle clusters formed with magnetic field. Time scale associated to these two processes is investigated to understand the kinetic behavior of nanorod separation under low field gradient. Surface functionalization of nanoparticles can be employed as an effective strategy to vary the temporal evolution of these two aggregation processes which subsequently influence the magnetophoretic separation time and rate.

© 2014 Elsevier Inc. All rights reserved.

1. Introduction

Iron oxide magnetic nanoparticles (IOMNPs) have been used extensively in processes ranging from biomedical [1–3] to environmental waste and pollutant removal [4–6]. There are several advantages exhibited by IOMNP which make them a unique nano-agent for aforementioned applications, such as high specific surface area [7], catalytically active [8], magnetically responsive [9], optically tunable [10], and can be easily synthesized by a large selection of chemical and physical methods [2,6]. Out from all these features of IOMNP, the ability of this particle to response to an externally applied magnetic field is crucial for its application in separation processes [11,12]. Here, IOMNPs are typically being employed to imparting a paramagnetic dipole moment to the targeted non-magnetic compounds. These IOMNPs tagged compounds become magnetically susceptible and can be separated out from solution through magnetophoretic collection.

Under the influence of a magnetic field, the IOMNPs would migrate toward the region where the field gradient is the highest [13]. This motion of particles relative to their surrounding fluid is known as magnetophoresis. The ability to capture the IOMNPs from suspension media sets the foundation for various magnetic separation technologies and its core working principles under high gradient ($\nabla B > 1000$ T/m) [14] and low gradient ($\nabla B < 100$ T/m) [15] magnetic field have been actively studied. Traditionally, the removal of magnetic nanoparticles (plus all the magnetically tagged compounds) in solution is carried out through high gradient magnetic separation (HGMS). This HGMS technology has been successfully employed for various applications and is capable to capture particles with sizes from microns to tens of nanometers [16]. However, two major drawbacks of HGMS are (1) high initial investment cost to setup automated separator [17], and (2) inhomogeneous magnetic field associated to the operational of HGMS make it difficult to develop numerical and/or analytical solutions to aid the design of a separation process used for specific applications [18].

On the other hand, low gradient magnetic separation (LGMS) does not involve the use of loading matrix. A nice review article on this topic is recently published by Faraudo and coworkers with detail descriptions on fundamental physics involved [19]. In short, under LGMS the separation of magnetic nanoparticles is first driven by aggregation of particles by an externally applied magnetic field, and later the particle clusters formed can be easily collected through cooperative magnetophoresis [15,20,21]. Since LGMS of IOMNPs is relying on the formation of particle clusters, hence, this

---

* Corresponding author at: School of Chemical Engineering, Engineering Campus, Universiti Sains Malaysia, Seri Ampangan, 14300 Nibong Tebal, Penang, Malaysia. Fax: +60 4 594 1013.
E-mail address: chjitkang1@eng.usm.my (J. Lim).
[1] These authors contributed equally.

process is highly concentration dependent [20]. It is anticipated that the increment of particles concentration will lead to higher collision frequency between the particles, and eventually, higher change for the formation of particle clusters. Furthermore, the chaining of particles due to magnetic dipole–dipole and hydrodynamic interactions also play a significant role in LGMS as enhancement factors to accelerate the collection of IOMNPs [21]. Besides, our group has recently demonstrated the important of surface modification in dictating the magnetophoretic separation rate [22]. From our experimental results, the more colloidal stable the IOMNP is, the harder it is to be magnetophoretically collected. This observation can also be generalized to HGMS process [23].

In previous research on magnetic separation of IOMNPs, by using either HGMS or LGMS, almost all the efforts were dedicated to the understanding of magnetophoretic behavior of spherical particles. Even though rod-like magnetic nanoparticles have been used for various interesting applications [24,25], there are very limited works have been done on the magnetophoresis of nanorod that exhibit magneto-shape anisotropy [26]. Despite its interesting and added benefits in rapid magnetic separation [12], numbers of uncertainties and issues remain unexplored related to the use of magnetic nanorod for separation process. In addition, it is also equally unclear about the contributing factors that would influence the performance of magnetic nanorod in magnetophoretic separation. It is our interest in this paper to show the comparison of cooperative magnetophoresis for spherical and rod-like IOMNPs under low gradient magnetic separation. By monitoring the migration of iron oxide nanorod with respect to an externally applied magnetic field in two and three dimensional space, we investigate the underlying mechanisms and time scale involved within each stage of nanorod magnetophoresis. In addition, we also evaluate the effects of particle concentration and magnetic field gradient on the separation kinetics of nanorod. All these studies are important to establish design rule for LGMS by using rod-like particles as a magnetic tagging agent.

2. Experimental section

2.1. Materials

Iron oxide nanosphere, Fe_3O_4 (APS, 98 + % purity) (Fig. 1a), was purchased from Nanostructured & Amorphous Materials, Inc. Iron oxide nanorods (Fig. 1b) employed in this work were generously supply by TODA American, Inc. (refer to Fig. SI of supporting information for size distribution of these particles). The saturation magnetization M_s for these two species of IOMNPs was measured

previously with value at $\sim$90 emu/g and 74.61 emu/g for nanorod and nanosphere, respectively [12]. Water soluble cationic polyelectrolyte poly(diallyldimethylamonium chloride) (PDDA) with average molecular weight $\sim$100,000–200,000 Da (20 wt.% in H_2O) was supplied by Sigma–Aldrich. Sodium chloride, NaCl used in zeta potential measurement was purchased from Merck Sdn.Bhd. Cylindrical shaped N50-graded Neodymium Boron Ferrite (NdBFe) and Aluminium Nickel Cobalt (Alnico) permanent magnet with 14 mm in diameter and 15 mm in length were purchased from Ningbo YuXiang E&M Int'l Co., Ltd. The remanence B_r for these two magnets is 1.20 Tesla and 1.45 Tesla for Alnico and NdFeB, respectively. All the chemicals were used as received without further modification or purification.

2.2. Preparation of PDDA-coated IOMNPs

Suspension of IOMNPs at 1000 mg/L in deionized water was prepared by ultrasonication to disperse the black powder obtained commercially. At the same time, PDDA solution with concentration at $\sim$0.005 g/mL was prepared by addition of 1.25 mL of as accepted PDDA solution into 48.75 mL of deionized water. This mixture was immediately subjected to intermittent ultrasonication for at least 30 min to promote their dissolution and left overnight on an end-to-end rotator with mixing rate of 40 rpm. This concentration of PDDA is chosen to ensure the available PDDA molecules are at least 500 times more than the estimated amount needed to form monolayer on the particles surface [23]. Before mixing, the IOMNPs solution was subjected to intense sonication for 2 min. Drop wise addition of IOMNPs suspension into PDDA solution was carried under intense sonacfication within a sonicator bath. Successful attachment of PDDA onto IOMNPs was verified by monitoring the electrophoretic mobility changes before and after the PDDA adsorption with Malvern Instruments Nanosizer ZS. By using the same analytical equipment, the particles size distribution before and after the PDDA attachment was measured through dynamic light scattering method (see Fig. SI in supporting information).

2.3. Monitoring magnetophoresis of IOMNPs

A custom built optical sensing system was employed to obtain the kinetic profile of IOMNPs under magnetophoresis [22]. Depends on the extent of light transmitted through the IOMNP suspension, by using a light dependent resistor (LDR), we monitored the voltage changes associate to the changes in intensity of detected light from a light-emitting diode (LED). The wavelength of the LED employed is at around 620 nm and the suspension
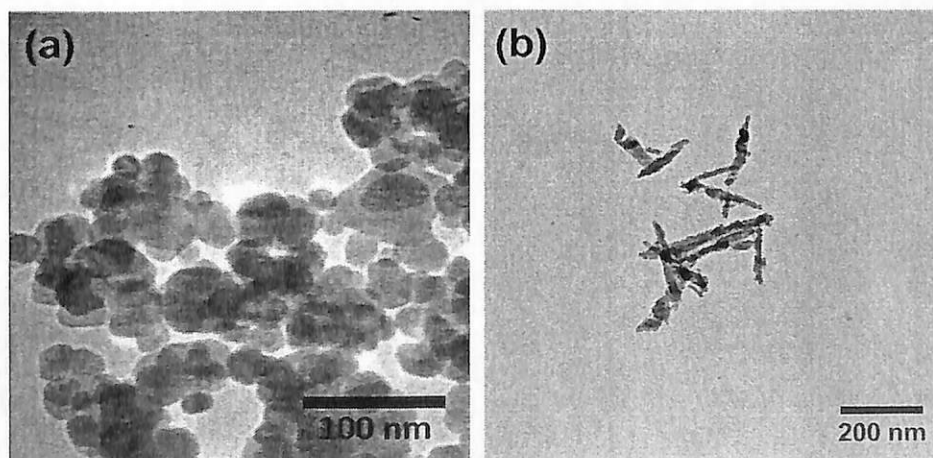

Fig. 1. Transmission electron micrographs of iron oxide (a) nanosphere and (b) nanorod used in this work.

was confined within a standard rectangular 3.5 mL cuvette. These measurements can then be translated into normalized opacity $\theta(t)$ at time t by following equation [15]:

$$\theta(t) = \frac{V(t) - V_{min}}{V(0)}, \tag{1}$$

where $V(0)$ is the initial voltage readout at time zero, V_{min} is the lowest voltage registered and $V(t)$ is the voltage output at time t. At $\theta(t)$ equal to one, the transmitted light is fully blocked correspond to the full dispersion of the particles. Whereas, at $\theta(t)$ equal to zero indicates full transmission of light due to the complete magnetophoretic collection of the IOMNPs.

For optical microscopy monitoring is concerned, we used Olympus BX53 microscope to record the magnetophoresis of IOMNPs. CellSens Dimension imaging software was employed to capture the brightfield images and the magnetophoretic pathway of particles was analyzed by using ImageJ software. In all microscopy observation, NdFeB magnet was used to introduce magnetic field into our system and was positioned at the upper left hand side of the images (front left corner of the microscope) with separation distance of less than 1 cm.

3. Results and discussions

3.1. Magnetophoresis of nanorod and nanosphere

Magnetophoresis of spherical (magnetic core diameter ~50 nm) and rod-like IOMNPs (20 × 300 nm) induced by a cylindrical NdFeB permanent magnet showed remarkably different kinetic behaviors (Fig. 2). In general, nanorod takes significantly less time than nanosphere to be fully separated. This nanorod suspension turned crystal clear at around 90 s after exposure to a permanent magnet. Whereas, the light brown color of a nanosphere suspension can still be observed after 180 s subjected to magnetophoretic separation. The experimental evidence that nanorods could be magnetophoretically collected much rapidly than nanosphere is generally true for both species of particle with or without surface coating. This scenario is mainly due to the fact that the magnetophoresis is favored in anisometric particles [27]. For low Reynolds number (Re ≪ 1) magnetophoresis in a Newtonian fluid, by taking into consideration of drag force, magnetophoretic force and shape factor, the rod geometry gives almost 200 times higher magnetophoretic velocity compared to spherical structure with equivalent volume [28]. In addition, the induced magnetic dipole
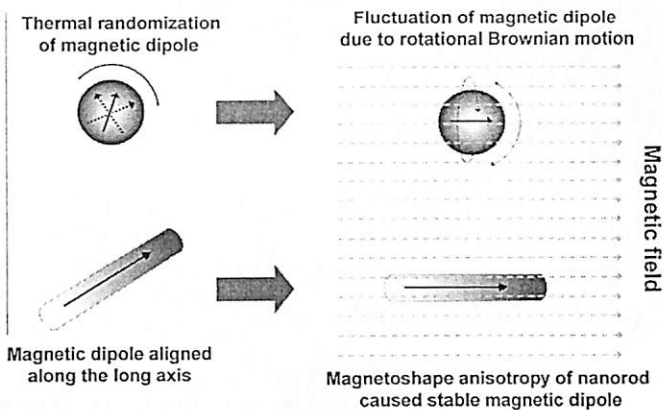

Fig. 3. Alignment of magnetic dipole parallels to the external applied magnetic field. For the case of spherical IOMNP, thermal randomization not only disrupts the magnetophoretic pathway of the particles but also disorients its magnetic dipole orientation within the magnetic field.

aligned along the long axis of nanorod (see Fig. 3) is more stable [29], and hence, less susceptible to the thermal disruption [26,30].

For a spherical IOMNP, its steady state magnetophoretic velocity can be calculated as

$$u_{mag} = \frac{F_{mag}}{6\pi\eta R} \tag{2}$$

where η is the viscosity of the suspension and R is the radius of the IOMNP. F_{mag} is the magnetophoretic force experienced by the IOMNP and can be defined as

$$F_{mag} = (MV_{mag} \cdot \nabla)B \tag{3}$$

where M is the field dependent magnetization, V_{mag} is the magnetic particle volume, and B is the magnetic induction. By taking a 30 nm nanosphere exposed to magnetic field gradient ($\nabla B = 100$ T/m) from a NdFeB magnet like the one showed in Fig. 2, with the assumption of its reached saturation magnetization, the calculated magnetophoretic velocity u_{mag} for none interacting particle is at around 3.26 μm/s [30]. Even by overestimating the field gradient involved, this calculated velocity is still too low to achieve separation kinetic as observed in Fig. 2. With a total travelling distance of 25.4 mm (the diameter of the glass vial in Fig. 2), it will take approximately 130 min for the non-interacting particle on the other side of the vial to be magnetophoretically collected. So in most
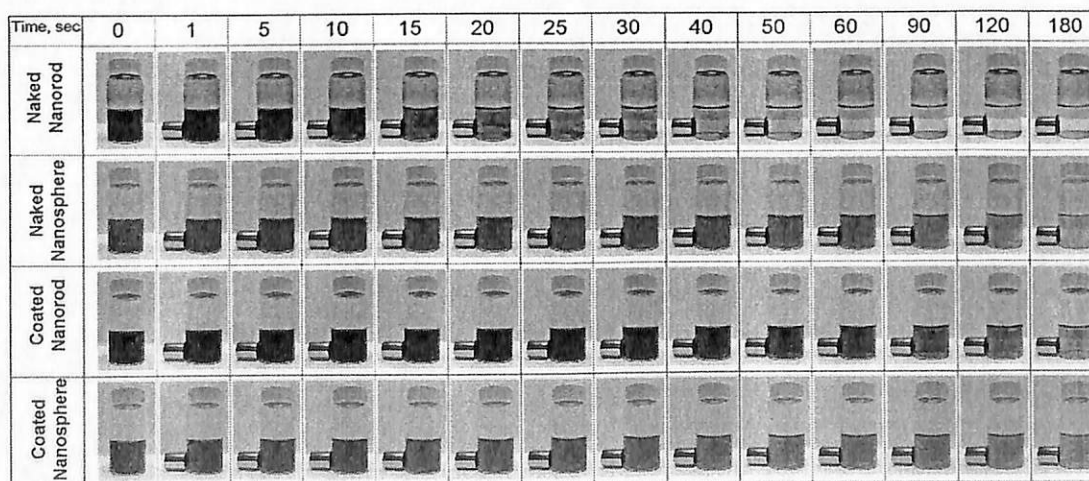

Fig. 2. Temporal evolution of suspension opacity for spherical and rod-like IOMNPs before and after surface functionalization by PDDA under the influence of a NdFeB cylindrical magnet. All particle concentration is at 50 mg/L.

likelihood, the IOMNPs have to undergo certain level of interactions, forming large magnetic clusters and migrate cooperatively towards the permanent magnet [15,21]. This hypothesis can be further confirmed with the magnetophoresis experiment as depicted in Fig. 2. According to the magnetophoresis experiments shown in Fig. 2, the major difference between surface modified and none surface modified particles is in the previous case the magnetophoretic collection time increased quite drastically for both nanorod and nanosphere. At the end of the experiment, the coloring of suspension remained for surface functionalized particles whilst naked IOMNP suspension, both nanorod and nanosphere, turned almost colorless. The adsorbed PDDA layer used to promote colloidal stability has also mitigated the attractive interaction between the IOMNPs, and hence, suppressed aggregation of the particles which is the pre-requirement for rapid cooperative magnetophoresis [22,23]. This unique feature of magnetophoresis, where the kinetic of the particle's motion under low field gradient is dependent on the surface functionalization, is crucial from engineering perspective. It allows the fine tuning of magnetophoretic separation time by changing the surface coating of the magnetic nanoparticles with same size, shape and composition.

3.2. Kinetic behavior of cooperative magnetophoresis

In order to have a more quantitative and better understanding on the cooperative behavior of IOMNP magnetophoresis under low field gradient, we monitored the opacity changes of the particle suspension (Fig. 4) over the time course of 500 s after its exposure to a NdFeB. Here we assumed that light transmitted

through the suspension can be directly related to the remained particles concentration after magnetophoresis by protocol developed by Schaller and coworkers [21]. This assumption might not be necessary true as spatial distribution of the magnetic field strength causes variation in the magnetophoretic velocity of IOMNPs, and hence, non-uniform blocking of light. Nevertheless, the magnetophoretic collection rate can be crudely estimated by linear fit to the first half of the graph where rapid decay of opacity occurred [31].

By referring to Fig. 4a and b, both the magnetophoretic collection rate and time are dependent on the suspension concentration. As the initial concentration of the IOMNPs increased, for both nanorod and nanosphere, the collection time has been shorten with the increment of collection rate. This observation is in accordance to the cooperative magnetophoresis model discussed earlier [15,18]. At concentration below 100 mg/L, the overall decay rate of suspension opacity for nanorod is steeper than nanosphere at same particle concentration indicating that the rapid magnetophoresis of rod-like particle. With the increment of particle concentration from 25 mg/L to 100 mg/L, the collection rate has also been increased from 0.0030 a.u./s to 0.0124 a.u./s for nanosphere and 0.0043 a.u./s to 0.0122 a.u./s for nanorod. At this stage, the influence of magneto-shape anisotropy on the magnetophoretic collection rate becomes irrelevant as the particle concentration increased. Transition of magnetophoretic curve from two independent lines as shown in Fig. 4c collapsed onto a single curve in Fig. 4d implied that not only the collection rate has become particle-shape independent at 100 mg/L but also the separation time. Coincidentally, the magnetophoresis becomes size independent
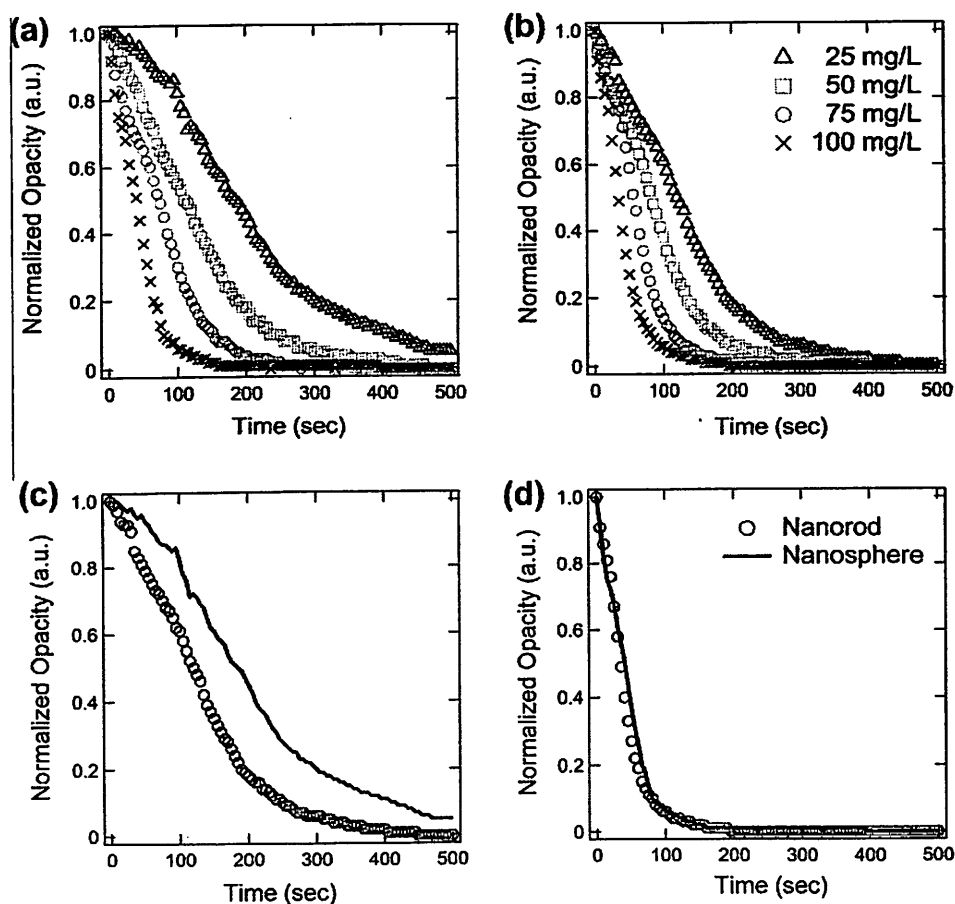

Fig. 4. Concentration dependency of PDDA coated (a) nanosphere and (b) nanorod under low magnetic field gradient magnetophoresis and comparison of magnetophoretic collection of nanorod and nanosphere suspension at (c) 25 mg/L and (d) 100 mg/L. Noted that figures (c) and (d) are redrawn from the same data sets as presented in (a) and (b).

as the particle concentration go beyond 100 mg/L [21], even though the F_{mag} is proportional to the volume of the particles. Since the collision frequency between the single particles depends directly on the particle concentration [32], as concentration increased there is a better chance for aggregation to occur which leading to rapid magnetophoresis. Thus from these results we can concluded that at high concentration the particle's shape will influence the magnetophoresis of an individual particle but not the cooperative magnetophoresis of a particle cluster.

Since the magnetophoretic force is influenced by both the magnetic field strength and gradient (see Eq. (3)), we repeated the magnetophoresis measurement of both PDDA decorated nanosphere and nanorod at the concentration of 50 mg/L to evaluate the influence of these parameters on the separation kinetic (Fig. 5). This working concentration was chosen to ensure higher probability for the distinctive contribution of magneto-shape anisotropy be detected for the ease of comparison. By replacing NdFeB cylindrical magnet with Alnico magnet of same dimension with much lower field gradient at (and also field strength as shown in Fig. 5a), one of the most obvious consequences is the prolonged collection time for both nanorod and nanosphere. By taking linear interpolation on the portion of the magnetophoresis curve that undergo rapid decay (Fig. 5b), we found out that the collection rate of nanorod under the influence of Alnico magnet at 0.0041 a.u./s is approaching the collection rate of nanosphere at 0.0045 a.u./s by NdFeB magnet. For any engineering related application, this unique feature of LGMS allows the optimization of particle shape and/or profile of magnetic field (both strength and gradient) selectively in order to achieve comparable collection rate. This has otherwise provides extra degree of freedom for the design of separation process driven by low magnetic field gradient. It should be noted that our observation in Fig. 5 have directly proven the complex influence of magnetic field gradient in cooperative magnetophoresis which is still an pending issue for further research.

It should also be noted that the initial time lag as observed in Alnico magnet induced magnetophoresis is mainly due to its weak magnetic field strength to cause particles aggregation. In addition, the enhanced colloidal stability introduced by adsorbed layer of PDDA might also play an important role to further aggravate the problem of slow collection time [22].

3.3. Nanorod magnetophoresis in microscopic scale

For cooperative magnetophoretic motion of nanorod, the migration process involved three phases, namely aggregation, alignment

and movement. Typical rod-like nanoparticles would spontaneously assemble into small isotropic structure in order to minimize their surface energy [33]. For magnetic nanorods, the extensive aggregation is most likely caused by the magnetic dipole–dipole and van der Waals interactions [34,35]. Even though the nanorod has been electrosterically stabilized by PDDA through physisorption, the formation of submicron particle clusters is almost inevitable [23,36]. In addition to this high tendency for self-aggregation which leading to the formation of large particle cluster, magnetic alignment of nanorod under the influences of an externally applied magnetic field [37], as depicted in Fig. 3, contributes to the rapid magnetophoretic behavior of rod-like IOMNPs. The stable alignment of nanorod with respect to the magnetic field lines due to its magneto-shape anisotropy making the particles less susceptible to the thermal randomization displacement during magnetophoresis [30].

Besides self aggregation, a colloidally stable suspension composed of iron oxide nanocluster will also undergo aggressive magnetically induced aggregation within few seconds after exposed to magnetic field [22]. This process is almost instantaneous and for magnetic nanoparticles with 100 nm in radius and magnetic Bjerrum length of 2 μm the time taken is ~0.06 s [38]. Here, the Bjerrum length is defined as the distance between particles with parallel dipoles at which the attractive magnetic energy that favor aggregation is equal to the thermal energy. Nevertheless, it should also be noted that for well dispersed individual IOMNPs (not clusters), this aggregation phase under magnetic field gradient of 60 T/m can be further prolonged to 300 s by using citric acid treated spherical superparamagnetic nanoparticles [20].

During the alignment phase, inertial forces play a minor role in nanorod dynamics [39]. Governing equation describing the nanorod rotation can then be obtained by balancing the magnetic torque with the viscous torque, and hence, leading to the relevant drag coefficient γ around the short axes of the rod [40]:

$$\gamma = \frac{\eta\pi}{3}\frac{l^3}{\ln(P) + C_r} \tag{4}$$

$$C_r = -0.662 + \frac{0.917}{P} - \frac{0.05}{P^2} \tag{5}$$

where l is the nanorod length and P is the length to diameter ratio of the nanorod. At such the time t for rotation of a nanorod toward its equilibrium orientation is only depends on the its initial
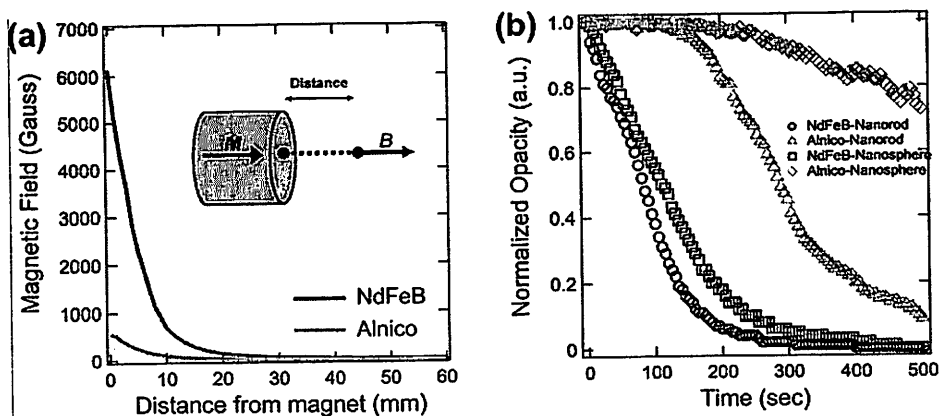

Fig. 5. (a) Magnetic field strength extended out perpendicularly from the surface of a cylindrical magnet (data for NdFeB magnet is extracted from the supporting document of ref 12. By linearized the slope of the graph within first 10 mm from the magnet (equivalent to our working range for magnetophoretic measurement by using a standard cuvette) gives the field gradient ∇B at 53.65 Tesla/m and 4.86 Tesla/m for NdFeB and Alnico magnet, respectively. These approximated values for ∇B have also indirectly proven that all our experiments were carried out under LGMS condition. (b) Magnetophoresis curves of PDDA coated iron oxide nanosphere and nanorod with respect to magnetic field from NdFeB and Alnico permanent magnet. All the IOMNP concentration is at 50 mg/L.

orientation and is directly proportional to β ($t \propto 1/\beta$), which is defined as [37]:

$$\beta = \frac{mB}{\gamma} \tag{6}$$

where m is the magnetic moment of the nanorod. By consider the nanorod has a magnetization very close to saturation throughout the entire duration of magnetophoresis process, which is not necessary true but this estimation serves as the upper bound of our analysis, the magnetic moment can therefore be estimated as $m \approx M_s V_{pt} \rho_{pt}$ [38]. Here M_s is the saturation magnetization per unit mass of the particle (know through magnetometry measurement at 90 emu/g), V_{pt} and ρ_{pt} is the volume and density of the particle, respectively.

The magnetic alignment time needed for a Ni nanorod with 5 µm in length and less than 200 nm in diameter ($\beta = 12.1 \text{ s}^{-1}$) is around 0.7 s [37]. For the iron oxide nanorod employed in this work, with dimension at around 300 nm × 20 nm (see Fig. 1) [26], the estimated β by using Eq. (5) is approximately $1.98 \times 10^6 \text{ s}^{-1}$. Since the alignment time is linearly dependent on $1/\beta$, so by having β which is almost five orders of magnitude larger than the aforementioned Ni nanorod would lead to drastic reduction in alignment time. However, as illustrated in Fig. 6, it takes roughly 0.75 s for the iron oxide nanorods to achieve full alignment. At such, it is very likely that the alignment of nanorod as observed in Fig. 6 is also a cooperative phenomenon in which the collective rotation of the entire clusters with respect to the magnetic field has been heavily suppressed. Besides the large nanoclusters size in micrometer range (larger drag coefficient than

individual nanorod) and hydrodynamic interactions [41], interparticle interactions should also play an important role in determining the associated time scale for the transition of randomly oriented nanorod clusters (Fig. 6a) to partially aligned clusters (Fig. 6b and c), and subsequently leading to fully aligned clusters (Fig. 6d).

Continuous exposure of a fully aligned nanorod cluster to an external magnetic field would lead to its magnetophoresis (Fig. 7). By inspecting magnetophoretic pathway of ten nanorod clusters, it was found that the averaged magnetophoretic velocity is at around 16 µm/s (Table 1). Within the viewable area of our microscopy study, all the clusters investigated are travelling at terminal velocity with no sign of acceleration. It is very likely that the observed clusters have not travelled into the 'capture' zone where the field gradient is the steepest [30]. Even though this measured 2D magnetophoretic velocity is one order of magnitude higher than the calculated nanosphere velocity based upon non-interacting particle assumption discussed earlier, but, it is still insufficient to explain the rapid magnetophoretic collection as demonstrated in Fig. 2. Within our experimental condition, the nanorod suspension is sandwiched within a thin layer of fluid, with thickness at around 136 µm by using adhesive tape as spacer, between a microscope slide and cover slip. Clearly, this confined movement of nanorod clusters (in Fig. 7) is affected by the friction forces, such as viscous drag or friction with the slide surface [42]. More notably, some of the clusters are non-mobile while others migrated toward the magnetic field source suggesting their adhesion to the slide surface. Besides, fattening of the clusters was witnessed if the magnetophoresis experiments were carried in prolonged period >1 min (see Fig. SII in supporting information). Here, two possible results
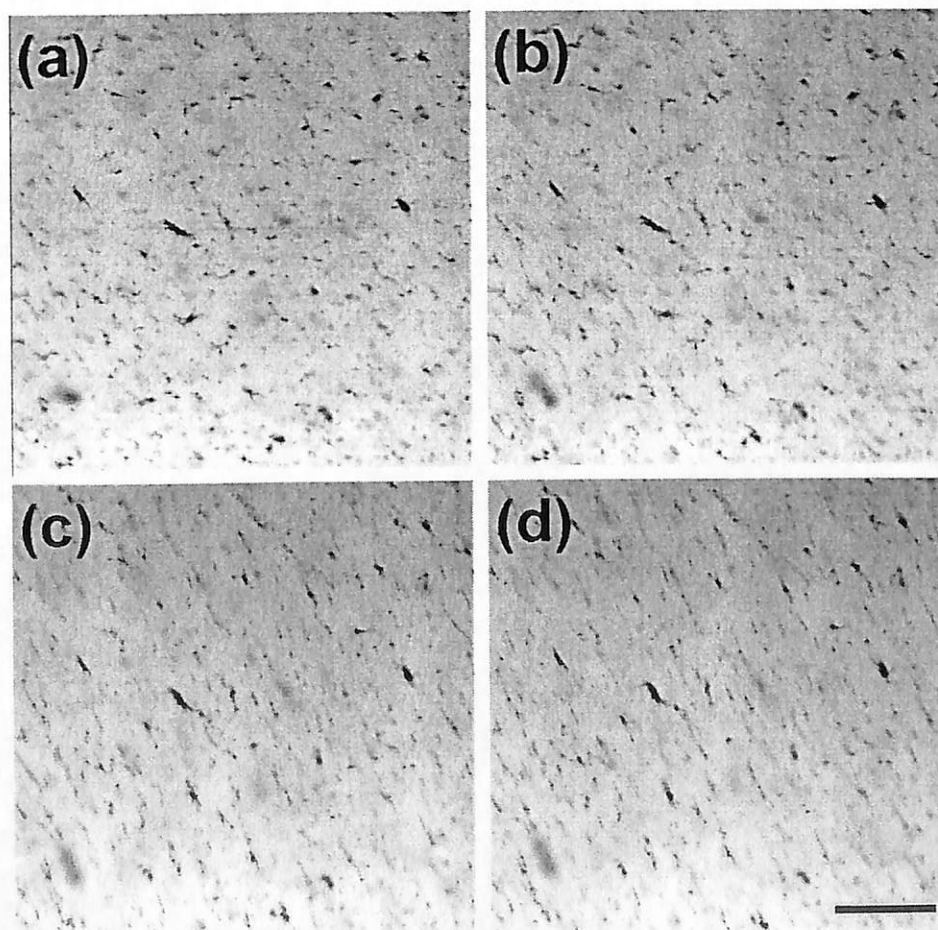

Fig. 6. Transient behavior of nanorod clusters undergoing magnetic alignment from (a) random orientation to (b and c) partial alignment and finally (d) full alignment. The scale bar is 100 µm and time interval between each image is 0.25 s.
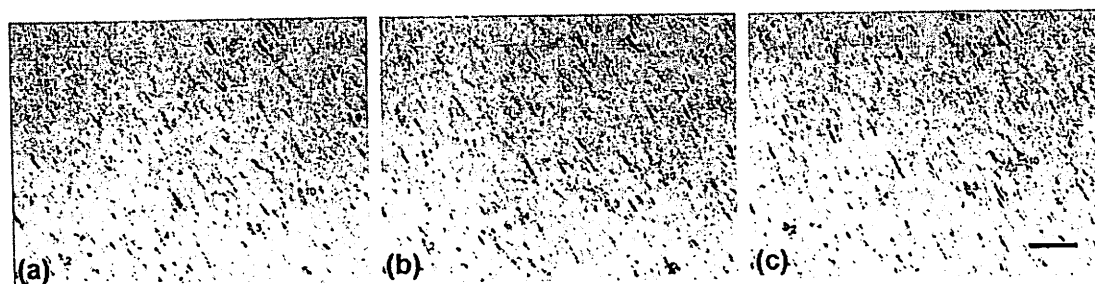
Fig. 7. Time lapse images showing rapid magnetophoresis of nanorod clusters after their alignment with an externally applied magnetic field. All ten groups of nanoclusters are moving toward the left hand corner of the micrograph where the magnet is located and the magnetic field gradient is the steepest. The scale bar is 100 μm and time interval between each image is 2 s.

Table 1
Summarized magnetophoresis results for ten groups of nanorod cluster shown in Fig. 7.

Cluster label	Cluster length (μm)	Travelling distance (μm)	Average velocity (μm/s)
1	27.74	57.36	14.34
2	35.23	52.02	13.01
3	28.95	83.99	21.00
4	45.31	79.09	19.77
5	27.01	53.78	13.45
6	35.70	80.52	20.13
7	34.54	57.81	14.45
8	29.52	38.73	9.68
9	28.89	67.98	17.00
10	43.89	70.18	17.55

of aggregation could still happened as the clusters collided to each other: (1) the formation of longer cluster chain due to tip-to-tip aggregation, or (2) the formation of thicker cluster chain due to lateral aggregation [38]. Our results in which the thicker aggregates is favored over longer chain in collision during magnetophoresis is consistent with their observation and might be the reason for the speedy magnetophoretic collection of nanorods as observed in Fig. 2.

4. Conclusions

We have clearly shown that at low particle concentration the contribution of shape anisotropy is crucial in speeding up the collection rate and shortening the collection time of IOMNPs at low field gradient magnetophoresis. This dependency, however, is highly related to particle concentration. At high particle concentration of 100 mg/L, both the magnetophoretic collection rate and time achieved by nanosphere and nanorod are comparable. In addition, it is possible for nanosphere to match the magnetophoretic collection rate of nanorod, even at low particle concentration of 50 mg/L, by changing the magnetic field gradient. Simultaneous tuning of particle shape and field gradient provides new option for the design of separation strategy which is workable at low field gradient. Combined with the cooperative magneophoresis data in macroscale, our optical microscopy experiments suggested that the entire cooperative magnetophoretic process of nanorod involved three phases, namely aggregation, alignment and movement. The first two phases typically happened in less than a second unless a very weak magnetic field source is used, such as Alnico magnet. These two processes are very likely driven by the cooperative nature of particle interactions. For rapid magnetophoresis is concerned, the measured 2D magnetophoretic velocity at ~16 μm/s is still an underestimated value mainly due to frictional forces arise from the confined motion of the IOMNPs. We anticipated that further collision between the nanorod clusters

during the cooperative magnetophoresis process, which leading to the formation of larger aggregate, is the key factor that contributes to their rapid separation.

Author contributions

The manuscript was written through contributions of all authors. All authors have given approval to the final version of the manuscript.

Appendix A. Supplementary material

Supplementary data associated with this article can be found, in the online version, at http://dx.doi.org/10.1016/J.JCIS.2014.01.044.

References

[1] A.K. Gupta, M. Gupta, Biomaterials 25 (2005) 3995–4021.
[2] J. Gao, H. Gu, B. Xu, Acc. Chem. Res. 42 (2009) 1097–1107.
[3] N.L. Adolphi, D.L. Huber, H.C. Bryant, T.C. Monson, D.L. Fegan, J.K. Lim, J.E. Trujillo, T.E. Tessier, D.M. Lovato, K.S. Butler, P.P. Provencio, H.J. Hathaway, S.A. Majetich, R.S. Larson, E.R. Flynn. Phys. Med. Biol. 55 (2010) 5985–6003.
[4] J. Hu, I.M.C. Lo, G. Chen, Sep. Purif. Technol. 56 (2007) 249–256.
[5] P. Xu, G.M. Zeng, D.L. Huang, C.L. Feng, S. Hu, M.H. Zhao, C. Lai, Z. Wei, C. Huang, G.X. Xie, Z.F. Liu. Sci. Total Environ. 242 (2012) 1–10.
[6] J.S. Hu, L.S. Zhong, W.G. Song, L.J. Wan, Adv. Mater. 20 (2008) 2977–2982.
[7] M. Uota, H. Arakawa, N. Kitamura, T. Yoshimura, J. Tanaka, T. Kijima, Langmuir 21 (2005) 4724–4728.
[8] M. Hermanek, R. Zboril, I. Medrik, J. Pechousek, C. Gregor, J. Am. Chem. Soc. 129 (2007) 10929–10936.
[9] K. Woo, J. Hong, S. Choi, H.W. Lee, J.P. Ahn, C.S. Kim, S.W. Lee, Chem. Mater. 16 (2004) 2814–2818.
[10] V. Mahendran, J. Philip, Langmuir 29 (2013) 4252–4258.
[11] M. Zborowski, G.R. Ostera, L.R. Moore, S. Milliron, J.J. Chalmers, A.N. Schechtery. Biophys. J. 84 (2003) 2264–2638.
[12] J.K. Lim, C.J.C. Derek, S.A. Jalak, P.Y. Toh, N.H. Mat Yasin, B.W. Ng, A.L. Ahmad, Small 8 (2012) 1683–1692.
[13] M. Zborowski, J.J. Chalmers, Magnetic Cell Separation, vol. 32, Elsevier, Oxford, UK. 2008.
[14] G.D. Moeser, K.A. Roach, W.H. Green, T.A. Hatton, P.E. Laibinis, AIChE J. 50 (2004) 2835–2848.
[15] L.G. Cuevas, J. Faraudo, J. Camacho, J. Phys. Chem. C 112 (2008) 945–950.
[16] J. Svoboda, Magnetic Techniques for the Treatment of Material, Kluwer Academic, Dordecht, 2004.
[17] P.Y. Toh, S.P. Yeap, L.P. Kong, B.W. Ng, D.J.C. Chan, A.L. Ahmad, J.K. Lim, Chem. Eng. J. 211–212 (2012) 22–30.
[18] J.S. Andreu, J. Camacho, J. Faraudo, M. Benelmekki, C. Rebollo, Phys. Rev. E 84 (2011) 021402.

[19] J. Faraudo, J.S. Andreu, J. Camacho, Theory Simul. Soft Matter. 9 (2013) 6654–6664.

[20] M. Benelmekki, C. Caparros, A. Montras, R. Gonçalves, S. Lanceros-Mendez, L.M. Martinez, J. Nanopart. Res. 13 (2011) 3199–3206.

[21] V. Schaller, U. Kräling, C. Rusu, K. Petersson, J. Wipenmyr, A. Kozer, G. Wahnström, A. Sanz-Velasco, P. Enoksson, C. Johansson, J. Appl. Phys. 104 (2008) 093918.

[22] S.P. Yeap, P.Y. Toh, A.L. Ahmad, S.C. Low, S.A. Majetich, J.K. Lim, J. Phys. Chem. C 116 (2012) 22561–22569.

[23] S.P. Yeap, A.L. Ahmad, B.S. Ooi, J.K. Lim, Langmuir 28 (2012) 14878–14891.

[24] K.B. Lee, S. Park, C.A. Mirkin, Angew. Chem. Int. Ed. 116 (2004) 3110–3112.

[25] M.K. Gupta, D.D. Kulkarni, R. Geryak, S. Naik, V.V. Tsukruk, Nano Lett. 13 (2013) 36–42.

[26] J.K. Lim, D.X. Tan, F. Lanni, R.D. Tilton, S.A. Majetich, J. Magn. Magn. Mater. 321 (2009) 1557–1562.

[27] A.G. Roca, R. Costo, A.F. Rebolledo, S. Veintemillas-Verdaguer, P. Tartaj, T. González-Carreño, M.P. Morales, C.J. Serna, J. Phys. D: Appl. Phys. 42 (2009) 224002.

[28] J.A. Cribb, T.D. Meehan, S.M. Shah, K. Skinner, R. Superfine, Ann. Biomed. Eng. 38 (2010) 3311–3322.

[29] V.F. Puntes, K.M. Krishnan, A.P. Alivisatos, Science 291 (2001) 2115–2117.

[30] J.K. Lim, C. Lanni, E.R. Evarts, F. Lanni, R.D. Tilton, S.A. Majetich, ACS Nano 5 (2011) 217–226.

[31] L.E. Helseth, T. Skodvin, Meas. Sci. Technol. 20 (2009) 095202.

[32] M. Elimelech, J. Gregory, X. Jia, R.A. Williams, Particle Deposition and Aggregation: Measurement, Modelling and Simulation, Butterworth-Heinemann, Woburn, MA, 1995.

[33] F. Kim, S. Kwan, J. Akana, P. Yang, J. Am. Chem. Soc. 123 (2001) 4360–4361.

[34] P. Evans, W.R. Hendren, R. Atkinson, G.A. Wurtz, W. Dickson, A.V. Zayats, R.J. Pollard, Nanotechnology 17 (2006) 5746–5753.

[35] C.T. Lo, W.T. Lin, J. Phys. Chem. B 117 (2013) 5261–5270.

[36] A. Ditsch, P.E. Laibinis, D.I.C. Wang, A. Hatton, Langmuir 21 (2005) 6006–6018.

[37] Y. Gu, R. Burtovyy, J. Townsend, J.R. Owens, I. Luzinov, K.G. Kornev, Soft Matter. 9 (2013) 8532–8539.

[38] J. Faraudo, J. Camacho, Colloid Polym. Sci. 288 (2010) 207–215.

[39] A. Tokarev, I. Luzinov, J.R. Owens, K.G. Kornev, Langmuir 28 (2012) 10064–10071.

[40] A. Ortega, J.G. de la Torre, J. Chem. Phys. 119 (2003) 9914–9919.

[41] A. Ghosh, P. Mandal, S. Karmakar, A. Ghosh, Phys. Chem. Chem. Phys. 15 (2013) 10817–10823.

[42] K. Ommering, J.H. Nieuwenhuis, Appl. Phys. Lett. 89 (2006) 142511.

Contents lists available at ScienceDirect

Process Safety and Environmental Protection

IChemE

Magnetophoretic separation of Chlorella sp.: Role of cationic polymer binder

CrossMark

Pey Yi Toh[a], Bee Wah Ng[a,b], Abdul Latif Ahmad[a],
Derek Chan Juinn Chieh[a,**], JitKang Lim[a,c,*]

[a] School of Chemical Engineering, Universiti Sains Malaysia, Nibong Tebal, Penang 14300, Malaysia
[b] School of Biological Sciences, Universiti Sains Malaysia, Minden, Penang 11800, Malaysia
[c] Department of Physics, Carnegie Mellon University, Pittsburgh, PA 15213, USA

ABSTRACT

Cationic polyelectrolyte promoted effective attachment of iron oxide nanoparticles (IONPs) onto microalgal cells through electrostatic attraction. Poly(diallyldimethylammonium chloride) (PDDA) and chitosan (ChiL), both are cationic polymer, are feasible to act as binding agent to promote rapid magnetophoretic separation of Chlorella sp. through low gradient magnetic separation (LGMS) with field gradient ∇B less than 80 T/m in real time. Cell separation efficiency up to 98% for the case of PDDA and 99% for the case of ChiL can be achieved in 6 min when 3×10^7 cells/mL Chlorella sp. are exposed to 300 mg/L surface functionalized-IONPs (SF-IONPs). Different polyelectrolytes do not give significant effect on cell separation efficiency as long as the particle attachment occurred. However, the PDDA is more preferable as the binder for all type of microalgae medium than the chitosan (ChiL) since it is not pH dependent. SF-IONPs coated with PDDA guarantee the cell separation performance for all pH range of cell medium, with $98.21 \pm 0.40\%$ at pH 8.84. On the other hand, the ChiL performance will be affected by the cell medium pH, with only $22.93 \pm 31.03\%$ biomass recovery at pH 9.25.

© 2014 The Institution of Chemical Engineers. Published by Elsevier B.V. All rights reserved.

Keywords: Microalgae; Renewable fuel source; Magnetophoretic separation; Polymer binder; Electrostatic interaction; Sustainable

1. Introduction

The energy crisis has ignited the search of an alternative replacement for fossil fuel which can be more environmental friendly and sustainable. Since the microalgae biomass is capable of producing high oil yield on gallons per acre basis up to two orders of magnitude higher than the other oil producer crops (Johnson, 2009), it makes microalgae an attractive option. The renewable fuel source from microalgae is limitless as its energy source is from the sun itself via photosynthesis (Demirbas, 2010). However, the main restriction in preventing the realization for large-scale third generation microalgal oil production is the high harvesting cost of microalgae biomass. The cost associated to downstream separation processes could reach up to 20–30% of the total production cost of biomass (Grima et al., 2003). On the other hand, magnetophoretic separation of microalgae was introduced since 1970s with the main focus targeted on environmental related problem (Bitton et al., 1975; Yadida et al., 1977). This method is currently revisited and applied on the purpose to harvest the microalgal biomass for biofuel production. It is feasible to achieve cell separation efficiency up to 99% for biofuel production purpose (Lim et al., 2012; Toh et al., 2014). The harvesting cost is estimated at about $180/ton dry biomass through the low gradient magnetic separation (LGMS) (Toh et al., 2012).

Currently there is an active pursue, from research groups all around the globe, on both the fundamental and engineering

aspects of microalgae separation by magnetophoresis (Xu et al., 2011; Lim et al., 2012; Toh et al., 2012; Cerff et al., 2012; Liu et al., 2009; Hu et al., 2013; Prochazkova et al., 2012; Wang et al., 2014). There are two mechanism utilized to impart the magnetic property on the microalgal cells: electrostatic-mediated-attachment (Xu et al., 2011; Lim et al., 2012; Toh et al., 2012; Liu et al., 2009; Prochazkova et al., 2012) and adsorption-based-attachment (Cerff et al., 2012; Hu et al., 2013). Previous study on the magnetophoretic separation of freshwater Chlorella sp. showed that the attachment of magnetic nanoparticles on cell surface do not mediated by the adsorption-based-attachment even though this mechanism has been reported feasible in others study (Toh et al., 2014). The cell separation efficiency can only be achieved at 8% even after extended incubation period up to 2 h (Toh et al., 2014). With the introduction of cationic polymer binder, the cell separation of Chlorella sp. is effective (Lim et al., 2012) where it is hypothesized that the attachment is induced by the electrostatic-mediated-attachment. Xu et al. (2011) and Prochazkova et al. (2012), respectively, have further verified this point through a series of pH adjustment by using bare magnetic particles as tagging agent without the use of polyelectrolyte binder. Nevertheless, there is still lacking of experimental data to verify this finding if the cationic polymer binder is employed. Therefore, in this study we demonstrated the feasibility of microalgae separation with the aids of cationic polymer binder to bind together the negatively charged Chlorella sp. cells with the anionic iron oxide nanoparticles (IONPs) in culture medium without any pH adjustment. The mechanism associated to this attachment process promoted by the polymer binder is studied in detail. Furthermore, we also identified the extra benefit of polymer binder for the use in this cell separation method.

2. Materials and methods

2.1. Materials

Iron oxide magnetic nanoparticles (IONPs), Fe_3O_4 (98 + % purity, 20–30 nm) was obtained from Nanostructured & Amorphous Materials, Inc. The very low molecular weight poly(diallyldimethylammonium chloride) (PDDA) in water (35 wt% with Molecular weight, $M_w < 100,000$ g/mol) and the low molecular weight chitosan powder (ChiL) (75–85% deacetylated) were obtained from Sigma–Aldrich, Inc. Deionized water used was obtained by reverse osmosis and further treated by the Milli-Q Plus system (Millipore) to 18 MΩ cm resistivity.

2.2. Cultivation of microalgae

The Chlorella sp. strain was obtained from School of Biological Sciences, USM. It was cultivated in 500 mL conical flask that contained 250 mL Bold's Basal Medium (BBM) under continuous illumination (2000 lux) at 25 °C. The medium and flask were autoclaved at temperature 121 °C for 15 min before cell cultivation. Continuous aeration of the culture medium was provided throughout the cultivation period. A cell density of 3×10^7 cells/mL was used for every single test. The cells were determined by using the hemocytometer and the desired cell density were achieved by appropriate dilution of the cell. The pH of cell medium was adjusted by using hydrochloric acid

(HCl) and sodium hydroxide (NaOH) and measured by Eutech CyberScan pH 1500.

2.3. Preparation of surface functionalized iron oxide magnetic nanoparticles (SF-IONPs)

In this work, the IONPs used were in spherical shape with dimension of 20–30 nm in diameter. A total amount of 0.02 g of IONPs was dispersed into 20 mL deionized water followed with sonication until a uniform dispersion in concentration of 0.001 g/mL was achieved. For PDDA solution preparation, 786.4 μL of as received polyelectrolyte was added into 18 mL of deionized water (18 mL). The ChiL was prepared by dispersing 30 mg of dry powder into 1% acetic acid solution (15 mL). This dispersion was stirred (500 rpm) for one day to achieve complete dissolution. A total of 3 mL of IONPs dispersion (0.001 g/mL) was added into the polymer solution and then sonicated by low power bath sonicator (40 KHz). This solution was then left on an end-to-end rotating mixer at mixing speed of 40 rpm overnight. Later, a permanent magnet, cylindrical shaped N50-graded neodymium boron ferrite (NdFeB) with surface magnetic field of ~6000 G, was used to collect the SF-IONPs and the remaining supernatant containing excess polymer was discarded. The SF-IONPs collected were further dispersed in 2 mL deionized water. During the microalgae separation experiments, 2 mL of SF-IONPs was added into 8 mL of cell medium sample to achieve particle concentration of 300 mg/L and then followed with simple mixing for 30 s to ensure uniform dispersion. The mixture was further left for another 30 s before the introduction of NdFeB permanent magnet. Particle concentration of 300 mg/L is chosen as it is the optimum concentration for SF-IONPs-attached-cells to achieve complete collection by the permanent magnet in real time (Toh et al., 2012). The electrophoretic mobility and hydrodynamic diameter of samples were measured by Malvern Instruments Nanosizer.

2.4. Magnetophoretic separation of Chlorella sp. by using IONPs or SF-IONPs

The magnetic separation of Chlorella sp. cell was carried under LGMS by using an NdFeB permanent magnet with field gradient $\nabla B < 80$ T/m (Toh et al., 2012). The cell separation performance was recorded for 6 min. The absorbance of the sample was measured spectrophotometrically by UVmini-1240 Shimadzu at the wavelength of 660 nm (measured by Agilent Technologies Carry 60 UV-Vis). The cell separation efficiency was determined as

$$\text{Cell separation efficiency (\%)} = \frac{I_0 - I(t)}{I_0 - I_{centrifuged}} \times 100 \qquad (1)$$

where the I_0 represents initial absorbance intensity of microalgae suspension after diluted with 2 mL deionized water, $I(t)$ represents the absorbance intensity of microalgae suspension during magnetophoretic separation at time t, and the $I_{centrifuged}$ represents the clear centrifuged sample subjected to same dilution factor.

(a)

(b)

(c)
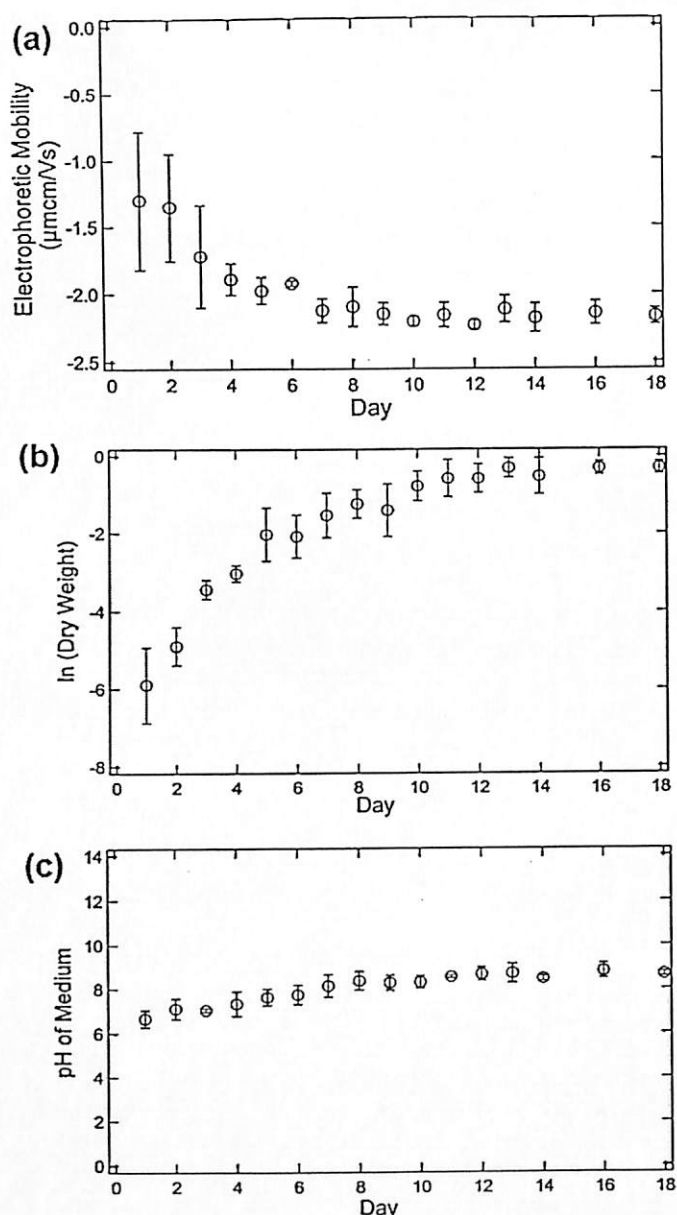
Fig. 1 – (a) Electrophoretic mobility of the *Chlorella* sp. cells in different day of cultivation. (b) Growth curve of *Chlorella* sp. The 250 mL of *Chlorella* sp. (initial cell density of 1.9×10^5 cells/mL) is cultured in a 500 mL conical flask with continuous bubbling under light. (c) The observed pH change of the cell culture medium with respect to cultivation day.

3. Results and discussion

3.1. Characteristic of *Chlorella* sp.

Freshwater *Chlorella* sp. microalgae used in this study carry a net negative charge on its surface (Mclaughlin and Poo, 1981). The surface charge is originated from the functional groups that can be found on the lipid, protein and carbohydrate that made up the cell membrane. The surface charge of cells depends on the stage of life cycle (Henderson et al., 2008). Fig. 1a showed the electrophoretic mobility (which is directly proportional to zeta potential of the microalgae) of the *Chlorella* sp. is increasing with the day of cultivation. It reaches optimum charge and then maintained at the day 7th and onward. This gradual change of electrophoretic mobility is very likely
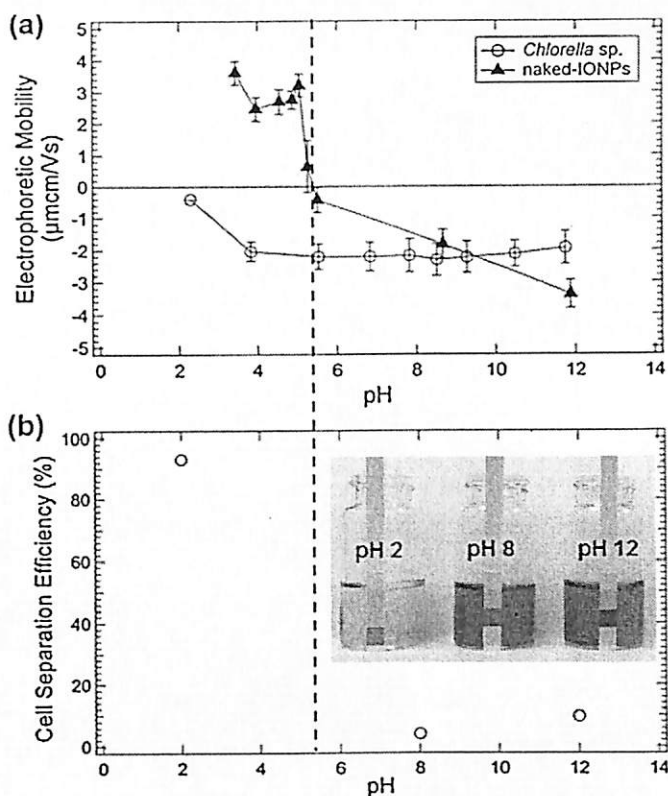

Fig. 2 – (a) Electrophoretic mobility of *Chlorella* sp. and IONPs varation at different pH. (b) Cell separation efficiency of 3×10^7 cells/mL *Chlorella* sp. when mixed with 300 mg/L IONPs through LGMS for 6 min of separation. Image is attached.

due to the induction of microalgal cells to synthesize new surface components stimulated by changing the environmental circumstances during their growth phase (Manly, 1970). The direct consequence of having such changes is the microalgal cells displayed a different overall surface charge. When referring to the growth curve of *Chlorella* sp. as showed in Fig. 1b, the cell growth entered the stationary phase after day 10th of cultivation. Both results showed that the surface charge of a cell is dependent on the cell maturity. So, day 10th has been chosen to harvest the microalgae with optimum biomass and carry optimum surface charge which may benefit the performance of cells separation through magnetophoresis.

3.2. Naked iron oxide nanoparticles (naked-IONPs) attachment to *Chlorella* sp.

Magnetophoretic separation can be performed by imparting magnetic property onto the microalgal cell. In this study, the naked iron oxide nanoparticles (naked-IONPs) with size in range 20–30 nm in diameter is tagged onto the surface of cell with an average diameter of $3.45 \pm 0.42 \, \mu m$. Direct mixing of naked-IONPs, without the presence of binding agent, into the cell medium does not promote any level of particles attachment onto the microalgae cell. This scenario caused extremely low cell separation efficiency at only 4.1% (Fig. 2b). Fig. 2a showed that the naked-IONPs used in this study has an isoelectric point at pH 5.4. The iron oxide (IO) will be protonated and form $IO-OH_2^+$ at pH < 5.4; while at pH above the isoelectric point (pH > 5.4), $IO-O^-$ will be formed through deprotonation (Lucas et al., 2007; Xu et al., 2006). However, the *Chlorella* sp. medium is in range of pH 8–9 at the harvest day 10th and onward. Under this condition the particles are also
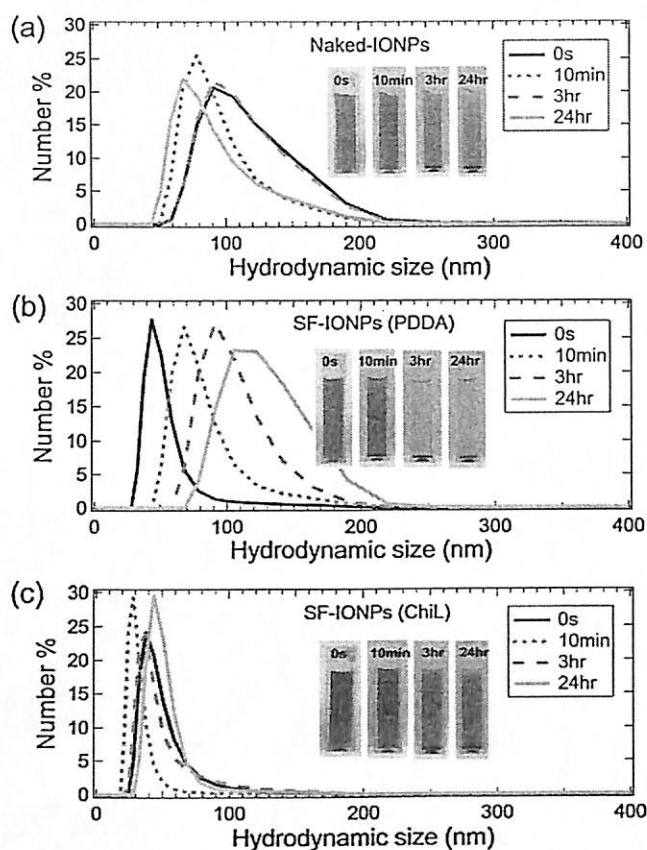
Fig. 3 – The hydrodynamic diameter of the (a) naked-IONPs and the SF-IONPs coated with (b) PDDA and (c) ChiL at 0 s, 10 min, 3 h and 24 h. The nanoparticles dispersions are sonicated at 0 s while the dispersions are re-suspended before each hydrodynamic size measurement by using the Malvern Zetasizer. Rapid settlement of PDDA coated IONPs can be due to the bridging flocculation.

negatively charged. Both these species experienced electrostatic repulsion with very minimum particle attachment can be successfully taken place. Even though nano-size particles have high surface energy, which may induce strong affinity to attach to other surface to minimize the surface energy (Wu et al., 2008), the strong electrostatic repulsion discussed earlier is significant enough to overwhelm this attractive interaction. The recorded low cell separation efficiency at 4.1%, when naked-IONPs mixed with the cell medium at day 10th without any pH adjustment has further confirmed our hypothesis. Moreover, the wide hydrodynamic size distribution of the naked-IONPs (Fig. 3a) has showed the naked-IONPs have higher tendency to flocculate through the van der Waals attraction and tend to form micron sized cluster to minimize their high surface energy. The flocculation of the superparamagnetic naked-IONPs is further promoted by the magnetic dipole–dipole attraction between the particles after the introduction of magnetic field (Yeap et al., 2012a; Li et al., 2008).

3.3. Naked-IONPs attachment to Chlorella sp. mediated by electrostatic interaction

For further validate the contribution of electrostatic interaction on the effectiveness of the nanoparticles-cells attachment, the pH of cell medium was being adjusted to pH2. This pH condition maintains the negative charge on Chlorella sp. but has converted the charge of naked-IONPs to positive as showed in Fig. 2a. Theoretically, opposite charge would induce

attraction between these two entities. According to the result showed in Fig. 2b, the electrostatic-mediated-attachment is effective to attach the naked-IONPs on the cell surface. Magnetophoretic separation has achieved high cell separation efficiency at 93.1% after 6 min of cell collection through low gradient magnetic separation (LGMS). Again, the result has confirmed that the cell separation is quite effective when the attachment of naked-IONPs on cell surfaces is mediated by the electrostatic attraction.

However, the pH adjustment of cell medium to acidic range is impractical for engineering applications since highly acidity media will caused serious environmental issue and also causing unnecessary lysis of microalgal cells An alternative way may be needed to modify the surface charge of naked-IONPs in order to make this separation method feasible for engineering application without the need of pH adjustment.

3.4. Role of cationic polymer binder

Electrostatic-mediated-attachment could drive the adhesion of naked-IONPs on cells in natural cell medium through surface charge reversal of naked-IONPs to positive. To achieve this purpose, two different cationic macromolecule binders were coated on the surface of naked-IONPs respectively to form surface functionalized iron oxide nanoparticles (SF-IONPs). The polymer will coat on the particle surface through adsorption as sketched in Fig. 4 (Kleshchanok and Lang, 2007). This adsorbed layer of macromolecule provides steric hindrance that further stabilized the naked-IONPs against flocculation. Hence, the particles are in colloidally stable form. Hydrodynamic size distribution shown in Fig. 3 has demonstrated that the SF-IONPs experienced higher resistance to particle flocculation compared to the naked-IONPs. In Fig. 3a, the wide hydrodynamic size distribution curve of naked-IONPs showed the naked-IONPs (with mean hydrodynamic diameter of 80–120 nm within 24 h) tend to flocculate to large range of size up to 220 nm even after intensive sonication. However, Fig. 3b showed that the SF-IONPs coated with poly(diallydimethylammonia chloride) (PDDA) experienced faster sedimentation rate than the naked-IONPs and the size distribution curve showed the SF-IONPs (PDDA) tend to flocculate to become three times larger (124 nm) than the initial size (51 nm). Even though the dispersion of SF-IONPs (PDDA) cannot stand stable for long time but PDDA still able promote effective steric stabilization for a short duration (<3 h). The mean hydrodynamic diameter of SF-IONPs (PDDA) is 51 nm right after sonication with a sharp peak showed on the size distribution curve. For the case of SF-IONPs coated with chitosan (ChiL), the dispersion is quite stable even after 24 h as shown in the photos (see Fig. 3c). Their hydrodynamic size distribution did not change too much within the first 24 h and stayed within the mean size of 30–50 nm with upper bound at 100 nm. The steric layer has successfully suppressed the flocculation of particles within the dispersion, especially within the first 3 h after preparation. Besides that, the electrostatic repulsion force generated between the equally charge of SF-IONPs also play role to cause the nanoparticles repelling. The combination of both particle stabilization effects is known as electrosteric stabilization (Fritz et al., 2002) and is suffice to maintain the colloidal stability of magnetic nanomaterials in biological media (Yeap et al., 2012b)

Fig. 5a showed the positive charge of PDDA polyelectrolyte is promoted by the $^+N(CH_3)_2$= active site on each monomers (Kokufuta and Takahashi, 1986). However for the case of
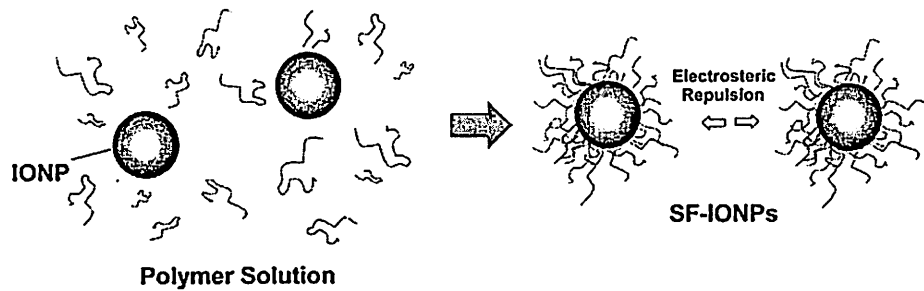
Polymer Solution

Fig. 4 – Surface functionalization scheme involved for PDDA and Chitosan attachment. The surface charge after the functionalization is mainly due to the property of the macromolecules included. Nevertheless, the particle still retained its magnetic property after the surface modification as they are still very responsive toward the externally applied magnetic field.

chitosan, it has no specific charged active site to attach on particle surface (Li et al., 2008). It will only be charged after dissolved in acidic solution (1 wt% of acetic acid solution in this study) through protonation. Under this condition, the amine group will be protonated to form positively charged —$^+$NH$_3$ active site on each monomers (see also Fig. 5b). After the surface functionalization, Fig. 6a showed that the SF-IONPs (PDDA) is in positive charge for range of pH employed while the SF-IONPs (ChiL) has reached an isoelectric point at pH ~9.2. After the protonated chitosan has coated on particle surface, then only the surface property of SF-IONPs (ChiL) would affected by the ChiL layer. When pH less than pH 9.2, the SF-IONPs (ChiL) is positively charged that promoted by the —$^+$NH$_3$ active sites on the extended segment of ChiL. When pH is above 9.2, the ChiL will be deprotonated and loss its charged site on the extended segment of ChiL from the particle surface. So, the SF-IONPs (ChiL) become anionic at pH > 9.2 which is mainly due to the surface property of naked-IONPs. Above discussion proved that the cationic polymer binder would govern the surface property of the SF-IONPs after coated on it.

Result in Fig. 6b showed that the 300 mg/L of SF-IONPs (PDDA) guarantee the highest cell separation efficiency in all range of pH value, which is 98.21±0.40% at pH 8.84. While the SF-IONPs (ChiL) achieved low cell separation efficiency at pH > 9.2, which is only 22.9±31.0% and 11.0±1.9% at pH 9.25 and pH 11.56 respectively. The photo sequences shown in Fig. 7

give a clear idea about the extent of separation can be achieved by going through pH adjustment. For high removal efficiency, greenish microalgal samples turned crystal clear at the end of the separation process. This observation has otherwise indicated the complete removal of the targeted microalgal cells. When in the condition of natural Chlorella sp. cell medium (in pH range from 8 to 9), the SF-IONPs (PDDA) is preferred rather the SF-IONPs (ChiL) because the surface charge of SF-IONPs (ChiL) is not consistence at pH 8–9. Hence, magnetophoretic separation of Chlorella sp. is proved feasible in real condition by the aid of cationic polymer binder, PDDA, without pH adjustment. Besides that, the available of the polymer binder on the surface of SF-IONPs has successfully modified the surface property of naked-IONPs in term of surface charge too. Nevertheless, the parallel result depicted in Fig. 6a and b provide direct evidence that the electrostatic-mediated-attachment of SF-IONPs on cell surface is effective to promote subsequent magnetophoretic separation of microalgae.
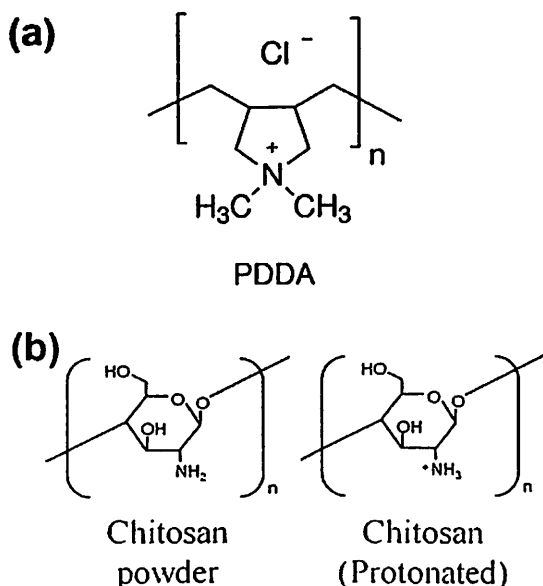

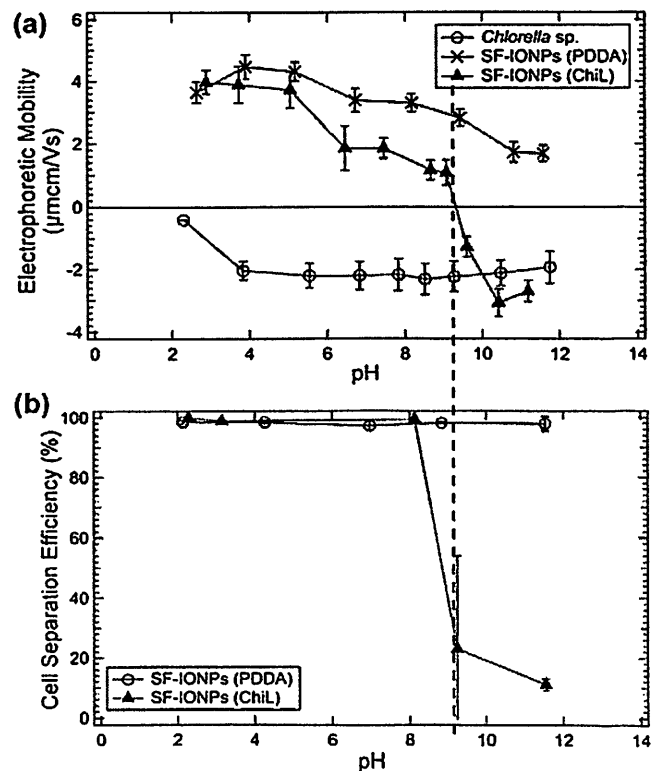Fig. 6 – (a) Electrophoretic mobility of Chlorella sp. and IONPs after surface-functionalized by PDDA and chitosan. (b) Cell separation efficiency of 3 x 10^7 cells/mL of Chlorella sp. cells in function of pH when mixed with 300 mg/L SF-IONPs.
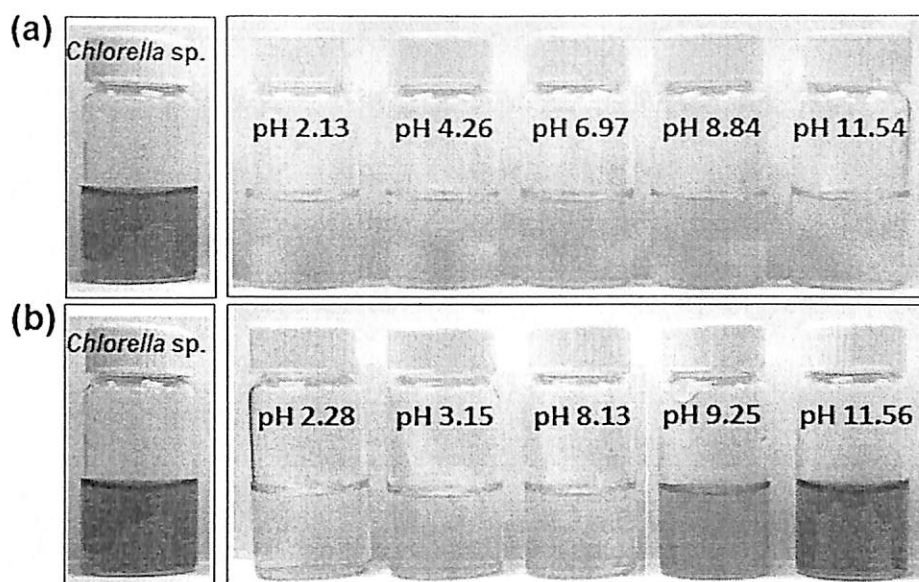

(a) PDDA

(b) Chitosan powder   Chitosan (Protonated)

Fig. 5 – Chemical structure of (a) PDDA and (b) the chitosan powder and after the protonation in 1 wt% acetic acid solution.

Fig. 7 – Images of the *Chlorella* sp. sample (3×10^7 cells/mL) and samples after LGMS separation by using 300 mg/l of SF-IONPs coated by (a) PDDA and (b) ChiL at different pH.

4.   Conclusions

We have verified the feasibility of the microalgae separation from the cell medium through LGMS by the aid of cationic polymer binder. Electrostatic repulsion inhibited the negatively charged naked-IONPs to attach onto the *Chlorella* sp. cell surface in the medium with pH 8–9 on the harvest day 10th. The electrostatic-mediated-attachment of naked-IONPs/SF-IONPs on cell surface is effective to encourage eventual cell separation through magnetophoresis. In pH 2, the positively charged naked-IONPs enabled 93% of cell separation efficiency. While for the positively charged SF-IONPs (PDDA), high cell separation can be achieved in all range of pH value. This study has proved the cationic polymer played an important role as the binding agent to attach the magnetic nanoparticles on cell surface as long as the electrostatic interaction occurred. From practical point of view, PDDA is more preferable as the binder than the ChiL because the attachment mechanism involved is pH independent. Besides as a binder, the polymer has also modified the surface property of the magnetic nanoparticles after coated onto it. The surface charge of SF-IONPs will follows the property of the polymer coated on it but maintains its magnetic property in core. In addition, the polymer layer has formed a steric layer to promote colloidal stability of SF-IONPs suspension. Further study on the effectiveness of electrostatic-mediated-attachment of SF-IONPs on cell surface in different ionic strength condition, especially the seawater, is important since the high ionic strength may suppressed the Debye screening length on the polymer layer and weaken the electrostatic effect.

Acknowledgements

References

Bitton, G., Fox, J.L., Strickland, H.G., 1975. Removal of algae from Florida lakes by magnetic filtration. Appl. Microbiol. 30, 905–908.

Cerff, M., Morweiser, M., Dillschneider, R., Michel, A., Menzel, K., Posten, C., 2012. Harvesting fresh water and marine algae by magnetic separation: screening of separation parameters and high gradient magnetic filtration. Bioresour. Technol. 118, 289–295.

Demirbas, A., 2010. Use of algae as biofuel sources. Energy Convers. Manage. 51, 2738–2749.

Fritz, G., Schadler, V., Willenbacher, N., Wagner, N.J., 2002. Electrostatic stabilization of colloidal dispersions. Langmuir 18, 6381–6390.

Grima, E.M., Belarbi, E.H., Fernandez, F.G.A., Medina, A.R., Chisti, Y., 2003. Recovery of microalgal biomass and metabolites: process options and economics. Biotech. Adv. 20, 491–515.

Henderson, R., Parsons, S.A., Jefferson, B., 2008. The impact of algal properties and pre-oxidation on solid–liquid separation of algae. Water Res. 42, 1827–1845.

Hu, Y.R., Wang, F., Wang, S.K., Liu, C.Z., Guo, C., 2013. Efficient harvesting of marine microalgae nannochloropsis maritime using magnetic nanoparticles. Bioresour. Technol. 138, 387–390.

Johnson, M.B., 2009. Microalgal Biodiesel Production Through a Novel Attached Culture System and Conversion Parameters. Biological Systems Engineering, Blacksburg, Virginia.

Kleshchanok, D., Lang, P.R., 2007. Steric repulsion by adsorbed polymer layers studied with total internal reflection microscopy. Langmuir 23, 4332–4339.

Kokufuta, E., Takahashi, K., 1986. Adsorption of poly(diallyldimethylammonium chloride) on colloid silica from water and salt solution. Macromolecules 19, 351–354.

Li, G.-Y., Huang, K.-L., Jiang, Y.-R., Ding, P., Yang, D.-L., 2008. Preparation and characterization of carboxyl functionalization of chitosan derivative magnetic nanoparticles. Biochem. Eng. J. 40, 408–414.

Lim, J.K., Derek, C.J.C., Jalak, S.A., Toh, P.Y., Yasin, N.H.M., Ng, B.W., Ahmad, A.L., 2012. Rapid magnetophoretic separation of microalgae. Small. 8, 1683–1692.

Liu, D., Li, F., Zhang, B., 2009. Removal of algal blooms in freshwater using magnetic polymer. Water Sci. Technol., 1085–1091.

Lucas, I.T., Durand-Vidal, S., Dubois, E., Chevalet, J., Turq, P., 2007. Surface charge density of maghemite nanoparticles: role of electrostatics in the proton exchange. J. Phys. Chem. C 111, 18568–18576.

Manly, R.S., 1970. Adhesion in Biological Systems. Academic Press, Inc., London.

Mclaughlin, S., Poo, M.-M., 1981. The role of electro-osmosis in the electric-field-induced movement of charged macromolecules on the surfaces of cells. Biophys. J. 34, 85–93.

Prochazkova, G., Safarik, I., Branyik, T., 2012. Harvesting microalgae with microwave synthesized magnetic microparticles. Bioresour. Technol. 130, 472–477.

Toh, P.Y., Pin, S.W., Kong, L.P., Ng, B.W., Chan, D.J.C., Ahmad, A.L., Lim, J.K., 2012. Magnetophoretic removal of microalgae from fishpond water: feasibility of high gradient and low gradient magnetic separation. Chem. Eng. J. 211–212, 22–30.

Toh, P.Y., Ng, B.W., Chong, C.H., Ahmad, L.A., Yang, J.-W., Chan, D.J.C., Lim, J.K., 2014. Magnetophoretic separation of microalgae: the role of nanoparticles and polymer binder in harvesting biofuel. RSC Adv. 4, 4114–4121.

Wang, S.-K., Wang, F., Hu, Y.-R., Stiles, A.R., Guo, C., Liu, C.-Z., 2014. Magnetic flocculant for high efficiency harvesting of microalgal cells. Appl. Mater. Interfaces 6, 109–115.

Wu, W., He, Q., Jiang, C., 2008. Magnetic iron oxide nanoparticles: synthesis and surface functionalization strategies. Nanoscale Res. Lett. 3, 397–415.

Xu, X.Q., Shen, H., Xu, J.R., Xie, M.D., Li, X.J., 2006. The colloidal stability and core-shell structure of magnetite nanoparticles coated with alginate. Appl. Surf. Sci. 253, 2158–2164.

Xu, L., Guo, C., Wang, F., Zheng, S., Liu, C.Z., 2011. A simple and rapid harvesting method for microalgae by in situ magnetic separation. Bioresour. Technol. 102, 10047–10051.

Yadida, R., Abeliovich, A., Belfort, G., 1977. Algae removal by high gradient magnetic filtration. Environ. Sci. Technol. 11, 913–916.

Yeap, S.P., Ahmad, A.L., Ooi, B.S., Lim, J.K., 2012a. Electrosteric stabilization and its role in cooperative magnetophoresis of colloidal magnetic nanoparticles. Langmuir 28, 14878–14891.

Yeap, S.P., Toh, P.Y., Ahmad, A.L., Low, S.C., Majetich, S.A., Lim, J.K., 2012b. Colloidal stability and magnetophoresis of gold-coated iron oxide nanorods in biological media. J. Phys. Chem. C 116, 22561–22569.

Effects of dissolved organic matter and suspended solids on the magnetophoretic separation of microalgal cells from an aqueous environment

Chuan Chun Chai [a], Zhi Hern Lee [a], Pey Yi Toh [a], Derek Chan Juinn Chieh [a], Abdul Latif Ahmad [a], Jit Kang Lim [a,b,*]

[a] School of Chemical Engineering, Universiti Sains Malaysia, Nibong Tebal, Penang 14300, Malaysia
[b] Department of Physics, Carnegie Mellon University, Pittsburgh, PA 15213, USA

HIGHLIGHTS

- Magnetophoretic separation of microalgal cells from fishpond water is feasible.
- Surface functionalization of IONPs with PDDA enables successful seeding of IONPs onto microalgal cells.
- Magnetophoretic separation of microalgae is affected by suspended solids and natural organic matter.
- The concentration of surface functionalized IONPs affects the removal efficiency and collection rate of microalgal cells.

GRAPHICAL ABSTRACT
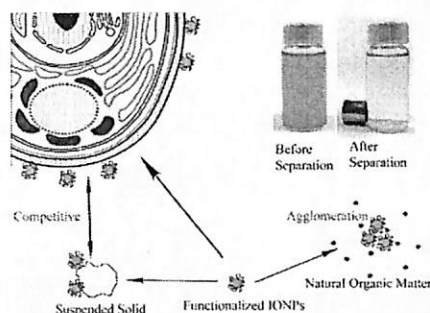
ARTICLE INFO

ABSTRACT

Magnetic seeding of microalgal cells is required prior to the successful implementation of magnetophoretic separation to harvest microalgae from an aqueous environment. Here, poly(diallyldimethylammonium chloride) (PDDA) forms with four different molecular weights were used to surface functionalize iron oxide nanoparticles (IONPs) to promote their attachment onto the cells by electrostatic interaction. We also investigated the effect of suspended solids and natural organic matter (NOM), which are normally found in fish farm water, on the magnetic seeding process. Dynamic light scattering (DLS) and electrophoretic mobility measurement were used to confirm the successful IONP functionalization by PDDA. For particle imaging, both electron and optical microscopes were used to monitor the IONP attachment on microalgal cells. For low particle-to-cell ratios of 10,000:1 or below, the effects of NOM and suspended solids on magnetophoretic separation of microalgae were obvious, with a cell separation efficiency that rarely exceeded 20%. For a particle-to-cell ratio in the intermediate range, the formation of large clusters composed of IONPs-suspended solids/NOM-microalgal cells (which were responsive to the magnetic field) instead of the independent formation of IONPs-suspended solids and/or IONPs-NOM entities is the main reason for minimum interference of suspended solids and NOM on the magnetophoretic separation. For a particle-to-cell ratio of 20,000 or higher (equivalent to 100 mg/L of IONPs), it was possible to achieve 98% separation efficiency even under the strong effects of suspended solids and NOM.

© 2015 Elsevier B.V. All rights reserved.

1. Introduction

Microalgae has been widely accepted as a third-generation biofuel because of its potential to provide renewable energy as biodiesel [1], but it also has negative impacts on freshwater fish farming [2]. In general, algae have a photosynthetic mechanism that produces oxygen as one of the by-products of photosynthesis. From this perspective, microalgae growth in fish ponds appears to help by providing oxygen to the pond, but this conjecture is only partially true during the day time. When the cell density of microalgae increases, microalgae start to compete with one another for sunlight and nutrients. The algae that receive limited sunlight cannot undergo photosynthesis and start to consume oxygen from the water; this scenario typically occurs during the night time, which results in oxygen depletion [3]. Under most circumstances, fish can survive in water with an oxygen level of approximately 5 mg/L. At oxygen levels below 3 mg/L, most fish will start showing signs of distress, and no fish will survive when the dissolved-oxygen level drops below 2 mg/L [4]. Annihilation of the entire fish population can occur overnight when excess microalgae consume most of the dissolved oxygen. This circumstance, which is known as eutrophication, has become the primary water quality issue for most fresh-water and marine ecosystems in the world [5].

To prevent this disaster from occurring, microalgae must be maintained at a desired concentration to preserve the oxygen supply [6]. Numerous methods have been proposed in last few decades to overcome and/or mitigate this problem [7–11]. Several methods are readily available as effective options for fish farmers to employ on their farms. Table S1 shows some conventional methods that have been practiced for algae treatment and their advantages and disadvantages. Among all available methods, the use of herbicides is one of the fastest and easiest methods to overcome microalgae blooming problems [12–16]. In addition, the growth of aquatic plants, the presence of barley straw and side culture of oyster and grass carp are some natural methods that are practiced to control algae blooming [17–20]. More conventional treatment methods involve the use of commonly found operational units or strategies such as nutrient removal, sediment pumping, hypolimnion oxygenation, and alum treatments, which are sometime performed to control eutrophication [21]. Processes such as filtration, centrifugation, flocculation, flotation and settling are also actively pursued as other options [9]. These separation processes are feasible to achieve high microalgae removal efficiencies; however, because of some serious drawbacks such as fouling, intensive energy usage, large time investment and high initial and/or operational cost, their implementation remains notably limited. In this context, magnetic separation has been introduced as an interesting alternative approach to harvesting microalgal cells [22,23].

Magnetic separation has been investigated for microalgae removal by numerous groups of researchers mainly because of the advancement of the chemical route in synthesizing magnetic nanoparticles as the tagging agent and the possible use of magnetic separators, which are operated under low magnetic field gradient [24–27]. At the initial phase of development in the 1970s [22,23], high-gradient magnetic separation of microalgae was performed with submicron magnetic colloidal particles as the tagging agent [28]. This method is attractive because of its high throughput and separation efficiency but suffers from high initial investment and operating costs [3]. Magnetic separation of microalgae is performed to impart magnetic properties to a non-magnetic targeted compound, microalgal cells in this case, by attaching a magnetic particle [29]. Subsequently, an externally applied magnetic field is introduced to induce the final separation of the targeted cells [25,30]. Hence, the ability for the nanoparticles to attach onto the microalgal cell becomes critical for the successful application of this separation process [24].

The attachment of magnetic nanoparticles onto the surface of microalgae notably depends on the surface charge of the nanoparticles [27]. To attach the magnetic nanoparticles onto the microalgae, the nanoparticles must be surface functionalized prior to their introduction to the culture medium [31,32]. This layer of macromolecules, which are mostly cationic polyelectrolyte [27,33], serves as a binding agent to promote the particle attachment onto the targeted microalgal cells, enhances their colloidal stability and maintains their unique property of a high surface-to-volume ratio [34]. Because the major driving factor for the attachment of these surface-functionalized magnetic nanoparticles in freshwater is electrostatic interactions [29], the influence of other charged species such as suspended solids and natural organic matter (NOM) on the effective implementation of magnetic separation must be studied.

Suspended solids, which are mostly made up of silica-based particulate matter, and natural organic matter (NOM) are charged species that are abundantly present in most fish ponds [35,36]. Because both species are negatively charged in fish farm water as are microalgal cells, their presence may cause a serious retardation effect on the magnetic seeding process, where they compete with microalgae for magnetic nanoparticles. Two phenomena can cause this competition: (1) electrostatic attraction between the anionic silica-based suspended solids and the cationic polyelectrolyte-modified magnetic nanoparticles [37] and the (2) electrostatic-induced bridging flocculation by natural organic matter, which rapidly reduces the particle-to-cell ratio [38]. Thus, the effects of these two species on the implementation of magnetic separation technology to control microalgal bloom in fish ponds must be accordingly investigated and is the subject of the present study.

2. Materials and methods

2.1. Materials

Iron oxide magnetic nanospheres (iron(II, III) oxide, nanopowder, cas 1317-61-9) were obtained from Sigma–Aldrich, Inc (please refer to supporting information for the TEM (Fig. S1) and DLS analysis (Fig. S2) of these particles). These particles composed of mixed iron oxide phases of magnetite (Fe_3O_4) and maghemite (γ-Fe_2O_3) with saturation magnetization at 70.4 emu/g [39]. In DLS analysis, naked IONPs (Fig. S2(a)) have bigger hydrodynamic size when compare with functionalized IONPs (Fig. S2(b)). This is due to naked IONPs tend to agglomerate, however they have greater stability after the functionalization. PDDA with a very low molecular weight (vl-PDDA, Mw < 100,000 g/mol), PDDA with a low molecular weight (l-PDDA, Mw = 100,000–200,000 g/mol), PDDA with a medium molecular weight (m-PDDA, Mw = 200,000–350,000 g/mol) and PDDA with a high molecular weight (h-PDDA, Mw = 400,000–500,000 g/mol) and humic acid were obtained from Sigma–Aldrich, Inc. Deionized water was obtained using reverse osmosis and subsequently treated using the Milli-Q Plus system (Millipore) to 18 MΩ cm resistivity. Ethanol and 25% ammonia, which were obtained from Merck, and 98% tetraethylorthosilicate, which obtained from Acros Organics, were used in the preparation process.

2.2. Microalgae culture

A sample of fishpond water (Fig. 1a) was collected from Aik Lee Fishery, which is located at Sungai Bakau, Parit Buntar, Perak. To isolate the microalgae, the collected fish farm water was filled into a 1 L measuring cylinder. The measuring cylinder with fish farm water was left for 1 h to allow the suspended solids to settle. Then, a small amount of fish farm water (0.1 mL) was obtained from the top surface of the measuring cylinder and cultivated in
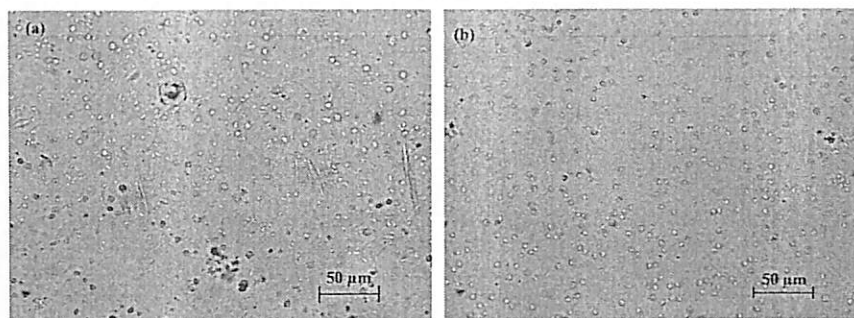
Fig. 1. Optical micrograph of microalgal cells (a) originally from fish farm water and (b) after culturing in the lab. The images were captured using an Olympus CX41RF microscope at 40× with Image Pro Express as the image-processing software.

a Bold Basal medium under aeration. Throughout the entire time course of our culturing period, the culture was subjected to continuous illumination by fluorescent light at 2000 lux. Before the magnetophoretic removal experiments, the cultivation was performed until a concentration of approximately 1.4×10^7 cells/mL was achieved. This step was to ensure that the correct particle-to-cell ratio in subsequent experiments could be maintained by only adjusting the IONP concentration. The pre-cultivation of microalgae was a crucial step to simultaneously standardize our experimental target and avoid all unnecessary interference of the existing suspended solids and/or dissolved organic compounds in our study. The Bold Basal medium was prepared using freshly processed fish pond water (after removing the suspended solids and NOM through centrifugation and filtration) as the background media to ensure that our sample had the same ionic strength as the fish farm water. Microalgae were cultivated for 2 weeks under continuous aeration. This sample was monitored under an Olympus CX41RF microscope, which was equipped with Image Pro Express imaging software, and the result is shown in Fig. 1b. It is clearly illustrated in this figure that after 14 days of cultivation, only one dominating species remained, with an average cell diameter of 6.6 ± 3.8 μm. The microalgal-cell concentration was adjusted based on the cell density, which was fixed at 1.4×10^7 cells/mL for all experiments.

2.3. Functionalization of magnetic nanoparticles

Iron oxide nanoparticles were surface functionalized using PDDA polyelectrolytes with different molecular weights. The main role of the PDDA cationic polyelectrolyte was to serve as a binder to promote the attachment of iron oxide nanoparticles onto microalgal cells [27]. First, iron oxide nanoparticles with a concentration of 1000 mg/L were sonicated for 1 h in an FB15050 FIsherbrand Ultrasonic Analog SRH Baths (2.75 L) to form a nicely dispersed particle suspension in deionized water. Simultaneously, 5 mL of PDDA solution was added into 30 mL of deionized water and left on an end-to-end rotating mixer at 40 rpm for 1 h to promote the complete dissolution of the PDDA polymer. Then, 10 mL of iron oxide nanoparticles with a concentration of 1000 mg/L

was added drop by drop into the PDDA solution, and the mixture was left on an end-to-end rotating mixer at a mixing speed of 40 rpm for two additional hours to achieve complete surface coating of the iron oxide nanoparticles with PDDA polyelectrolyte. These surface-functionalized IONPs were collected using a permanent magnet, and the supernatant, which composed of excess PDDA polyelectrolyte, was discarded. Then, the particles that were collected as retentate were redispersed into 30 mL of deionized water by sonication. The washing steps were repeated for at least 4 times to make sure that all excess PDDA molecules were removed. After the last washing cycle, the collected particles were redispersed in 10 mL of deionized water to form a particle suspension with a concentration of 1000 mg/L. The electrophoretic mobility and hydrodynamic diameter of the nanoparticle before and after the functionalization were measured using a Malvern Instruments Nanosizer to ensure the successful functionalization with PDDA (see Table 1) [27].

2.4. Microalgae separation

Iron oxide nanoparticles that were functionalized using PDDA with different molecular weights were used to test their capability in removing microalgal cells from fish farm water. In addition, the effect of various experimental constraints such as the concentrations of suspended solids and NOM were also tested to assess the robustness of this separation strategy. The concentration of microalgae was measured with a DR 5000 UV–Vis spectrophotometer at a wavelength of 675 nm. In addition, the transient behavior of magnetophoretic separation was also be spectrophotometrically monitored while the separation process was performed with the experimental setup that we previously discussed [40]. In short, the cuvette, which was filled with the mixture of microalgae and surface-functionalized IONPs, was placed into the UV–Vis spectrophotometer with a permanent magnet (NdFeB) so that its direction of magnetization was perpendicular to the light path to continuously monitor (10 min) the progressive changes in cell concentration during magnetic separation. The real-time collection of tagged microalgal cells can be effectively monitored using this arrangement [3]. To further validate the UV–Vis measurement in

Table 1
Hydrodynamic diameter and electrophoretic mobility of IONPs before and after the functionalization with PDDA of different molecular weights. All measurement were conducted within the pH range of 6.3–6.6.

Functionalization	Hydrodynamic size (nm)	Electrophoretic mobility (μm cm/V s)
No functionalization	327.6 ± 20.37	-2.27 ± 0.10
vl-PDDA (Mw < 100,000 g/mol)	195.87 ± 3.97	4.20 ± 0.01
l-PDDA (Mw = 100,000–200,000 g/mol)	202.07 ± 2.83	4.77 ± 0.12
m-PDDA (Mw = 200,000–350,000 g/mol)	250.40 ± 2.80	4.98 ± 0.09
h-PDDA (Mw = 400,000–500,000 g/mol)	317.07 ± 0.53	5.26 ± 0.12

determining the microalgal cell separation efficiency, we visually inspected the cell density of our sample using the optical microscope at different concentrations after the magnetic separation (see Table S2 in the supporting information for detail). We observed a systematic reduction of the absolute microalgal cell number, and the extent of reduction was at the same order of magnitude as recorded by the spectrophotometry measurement.

2.5. Effect of suspended solids and NOM

Suspended solids or NOM was added into the system to test their retardation effect on the separation efficiency of functionalized IONPs. Here, submicron-sized, monodispersed silica nanoparticles were prepared using the Stöber process and taken as the model suspended solids. The experiment was conducted with the presence of either suspended solids or NOM to independently test their individual effect on the magnetic separation at different concentrations. Before the addition of IONPs into the system for separation, the suspended solids or NOM was first added into the system at a controlled concentration. Then, IONPs were mixed into the system and vigorously shaken for 2 min. Subsequently, this mixture was immediately transferred into a cuvette. Using a permanent magnet (NdFeB), this cuvette was inserted into a UV–Vis spectrophotometer to continuously monitor (10 min) the progressive changes in cell concentration during magnetic separation [41].

3. Results and discussion

3.1. Effect of the binding agent molecular weight on cell separation

Table 1 shows that after surface functionalization by PDDA, the IONPs have a smaller hydrodynamic diameter than the bare particles. This PDDA coating layer plays a role in providing electrosteric stabilization to the particle suspension with the formation of an electro-physical barrier around the IONPs. Furthermore, both hydrodynamic diameter and electrophoretic mobility of the PDDA-coated IONPs increase with the molecular weight of PDDA, as shown in Table 1. Hence, it is reasonable to hypothesize that the removal efficiency of the particles will also increase with the molecular weight of PDDA based on two factors. First, the particles with a large hydrodynamic diameter should have a larger capturing/anchoring range because of the thicker anchoring PDDA layer. In addition, because the electrophoretic mobility is directly related to the surface charge of the particles, this feature strongly affects the surface absorption process [42]. Hence, a higher electrophoretic mobility should correspond to a higher surface absorption efficiency [43,44]. A direct consequence of these two basic factors is the improvement in magnetic seeding of IONPs onto microalgal cells, which subsequently boost the magnetophoretic separation efficiency of the targeted cells.

The achieved microalgal removal efficiency using IONPs, which were coated with PDDA of different molecular weights, was tested and compared. IONP concentrations of 50 and 100 mg/L, which corresponded to particle-to-cell ratios of 1.06×10^4 and 2.12×10^4 particles/cell, respectively, were used to perform the experiments. The separation efficiency of each species of PDDA-decorated IONPs is shown in Table 2. Although the results are consistent with our hypothesis, the overall improvement is not notably significant. For example, at a particle-to-cell ratio of 1.06×10^4 particles/cell, the microalgae removal efficiency were marginally improved by approximately 1.26% (from 87.02% to 88.28%) when the PDDA molecular weight increased from very low to high. After doubling the particle-to-cell ratio (Table 2), we continued to observe that the PDDA molecular weight played a negligible role in affecting the microalgal cell separation efficiency at fixed particle-to-cell ratios. It should be noted that this observation contradicts with our previous observation when using PDDA to induce the flocculation of microalgal cells [27]. Nevertheless, our observation indicates the negligible contribution of the binder molecular weight on the IONP-to-cell attachment at high particle concentrations.

In addition to the final microalgae removal efficiency, the real-time overall cell separation behavior of IONP-seeded microalgal cells under low field gradient was also monitored throughout the experiment, as illustrated in Fig. 2. For the first 10 s of separation time, the separation rate for vl-PDDA-, l-PDDA-, m-PDDA- and h-PDDA-coated IONPs were 6.05%/s, 6.35%/s, 6.97%/s, and 6.42%/s, respectively. There was almost no dependency of the separation kinetics on the binder molecular weight. Nevertheless, in this
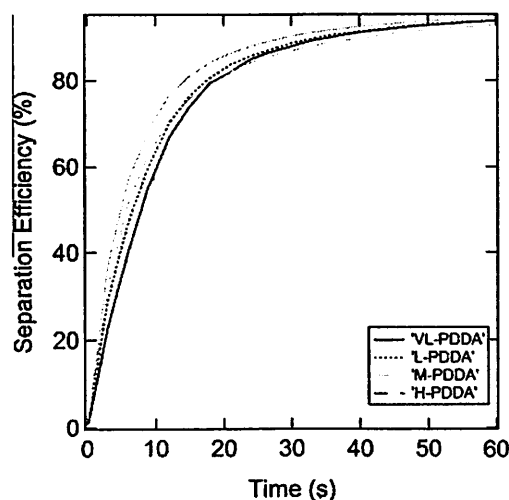

Fig. 2. Real-time overall separation efficiency of magnetically seeded microalgae cells from fish pond water using IONPs, which were functionalized with vl-PDDA, l-PDDA, m-PDDA and h-PDDA.
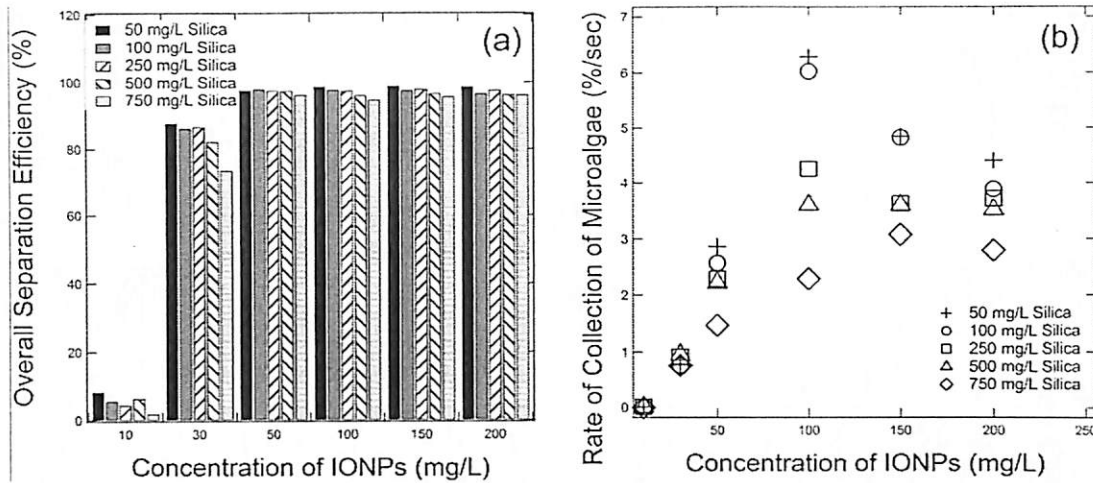
Table 2

Overall microalgae separation efficiency that was achieved after exposure to an externally applied magnetic field for 10 min using vl-PDDA-, l-PDDA-, m-PDDA- and h-PDDA-coated IONPs.

Concentration of iron oxide (mg/L)	Number of nanoparticle per cell	Molecular weight of PDDA	Efficiency (%)
50	10.6×10^3	<100,000 g/mol (vl-PDDA)	87.02
		100,000–200,000 g/mol (l-PDDA)	87.87
		200,000–350,000 g/mol (m-PDDA)	88.05
		400,000–500,000 g/mol (h-PDDA)	88.28
100	21.2×10^3	<100,000 g/mol (vl-PDDA)	97.67
		100,000–200,000 g/mol (l-PDDA)	97.67
		200,000–350,000 g/mol (m-PDDA)	97.94
		400,000–500,000 g/mol (h-PDDA)	97.75

Fig. 3. (a) Overall separation efficiency and (b) initial separation rate of microalgal cells that were seeded with PDDA-functionalized IONPs at different silica colloid concentrations.

study, we selected m-PDDA as the binding agent for subsequent experiments because the m-PDDA-coated IONPs provided a slightly better result in terms of the separation efficiency and the consistent harvesting time for microalgae separation.

3.2. Effect of the suspended solids

In this study, silica colloid was used to simulate the role of suspended solids in the fish farm water. The silica colloid that we used has a hydrodynamic diameter of 427.4 nm and is positively charged with a zeta potential of −41.9 mV (electrophoretic mobility of −3.281 μm cm/V s). Because the removal of microalgal cells with IONPs is strongly dependent on the surface charge [27], the presence of silica colloid with a similar charge to that of microalgal cells (electrophoretic mobility at −1.856 μm cm/V s) imposes a competitive effect to serve as an alternate platform for the attachment of IONPs. In this situation, the performance of the IONPs to remove microalgae from fish farm water can be suppressed; hence, its contribution must be evaluated.

It has been reported that the average concentration of suspended solids for ground water is approximately 200 mg/L and can approach 600 mg/L in some extreme cases [45,46]. Hence, our experiment was performed in the concentration range of 50–750 mg/L of silica colloid to cover the typical and extreme ranges of suspended solids. Fig. 3a shows that only at low IONP concentrations was the effect of silica colloid on the overall microalgae removal substantial. The overall removal efficiency increased to approximately 98% for all concentration ranges of silica colloid in this study and remained constant when the IONP concentration exceeded 100 mg/L. However, magnetic collection of microalgal cell at IONP concentrations below 50 mg/L (1.06×10^4 - particles/cell) was lower than 98% because of the insufficient amount of IONPs attaching onto the surface of the microalgae cells. Because the magnetophoretic force is directly proportional to the magnetic volume, a sufficient amount of IONPs is necessary to initiate the magnetic separation. This experimental finding contradicts with the collision frequency analysis (see the supporting information for the calculation), where the IONPs-silica colloid with a collision frequency on the order of approximately 10^{27} is much higher than the IONPs-microalgae collision in the range of 10^{17}–10^{18} (Table 3). With a collision frequency at almost 10 orders of magnitude higher, the formation of IONPs-silica colloid should be more dominant than IONPs-microalgae, which subsequently prohibits the effective separation of microalgal cells using IONPs. However, as shown in Fig. 3a, the presence of silica colloid even

at a notably high IONP-to-silica ratio of 14.74 particles/colloid, which corresponds to a silica colloid concentration of 750 mg/L and a IONP concentration of 50 mg/L, imposed minimum effects on the overall cell separation efficiency.

By further examining the IONP distribution on the silica colloid and microalgal cells using TEM, we observed that the IONPs were intensively adsorbed on both species (Fig. 4). These adsorbed IONPs further induced the bridging flocculation between the silica colloid and the microalgae, which led to the formation of a silica colloid-IONP-cell cluster. Because of the excessive inclusion of magnetic IONPs in this cluster, the magnetic separation of microalgal cells (in the form of silica colloid-IONP-cell clusters) from its aqueous environment can still be performed without decreasing its overall separation efficiency as illustrated in Fig. 3a. However, an obvious detrimental effect on the magnetic separation of microalgal cells with an excessive amount of silica colloid is the decrease in the separation rate (Fig. 3b).

Throughout the entire range of IONP concentration that we investigated, the separation rate of microalgae decreased when the concentration of silica colloid increased. The most dramatic reduction was observed at the IONP concentration of 100 mg/L (equivalent to an IONP-to-cell ratio of 2.12×10^4), where the initial separation rate decreased from 6%/s to less than 2%/s when the concentration of silica colloid increased from 50 to 750 mg/L. More interestingly, an IONP concentration of 100 mg/L is a turning point for all cases of silica colloid, where the separation rate increased with the IONP concentration up to 100 mg/L and started to decrease with further increases in IONP concentration. The declining separation rate with the increase in IONP concentration is counter-intuitive because the magnetophoretic force is proportional to the magnetic volume; hence, the driving force of magnetic separation should be higher when the IONP concentration increased [3]. By monitoring the size of the silica colloid-IONPs-cell clusters that formed from 100 to 150 mg/L (Table S3 in the supporting information), we observed that the averaged cluster size decreased from approximately 700 μm to approximately 100 μm. The reduction in silica colloid-IONP-cell cluster size, which was accompanied by the decrease in effective magnetic volume that was embedded in this cluster, is the main contributing factor toward the decrease in separation rate when the IONP concentration increases beyond 100 mg/L.

The cluster formation notably depends on the surface charge of the microalgae. In fact, the attachment of functionalized IONPs onto a microalgal cell changes its surface charge (initial electrophoretic mobility at −1.856 μm cm/V s) from negative to

Table 3
Calculated collision frequency of IONPs–microalgae and IONPs–silica colloids at different IONP concentrations. The concentration of silica colloid in this calculation is 750 mg/L, which is almost the upper limit for the suspended solids concentration that was found in surface water.

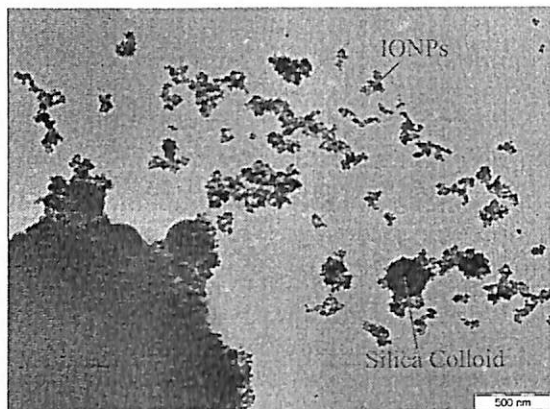|	Collision frequency (collision/s m³) Concentration of IONPs (mg/L)				
	10	50	100	150	200
IONPs–microaglae	4.5×10^{17}	2.2×10^{18}	4.5×10^{18}	6.8×10^{18}	9.0×10^{18}
IONPs–silica colloid	1.5×10^{27}	7.8×10^{27}	1.5×10^{27}	2.3×10^{28}	3.1×10^{28}

Fig. 4. TEM micrograph of the attachment of IONPs onto both microalgal cells (large dark spot at the bottom left corner) and silica colloids.

positive. Microalgal cells that are fully covered with IONPs have positive surface charges, whereas the non-covered portions of the cells are negatively charged. Hence, at low IONP concentrations such as at 100 mg/L, the incomplete surface coverage of microalgal cells and silica colloid makes the inter- and intra-bridging of these two entities to occur more readily. This circumstance leads to the formation of larger particle-cell clusters, which are more magnetophoretically responsive, as observed in Fig. 5. At higher IONP concentrations such as 150 mg/L, we suspect that because of the higher number of presenting IONPs, the surface coverage of microalgal cells with IONP increases until a point at which the particle-stabilized cell/silica colloid remains pseudo-stable. Hence, the silica colloid-IONPs-cell clusters that are formed are relatively smaller, and this situation leads to a lower separation rate.

3.3. Effect of natural organic matter (NOM)

Fig. 5a shows that the removal efficiency of microalgal cells from fish farm water increases as the concentration of functionalized IONPs that is added to the system increases. With the increase in IONP concentration, the absolute magnetic volume that is associated with each cell after seeding also increases. Under the principle of cooperative magnetophoresis, this scenario improves the overall microalgae separation efficiency [27]. In addition to the particle concentration effect in Fig. 5a, the presence of NOM (humic acid) obviously imposes negative effects on the performance of IONPs in microalgae removal.

The adsorption of NOM has been discussed by Sposito, and it involves several mechanisms such as electrostatic interaction, ligand exchange surface complexation, hydrophobic interaction and cation bridging [47]. Because electrostatic interaction is the key driving mechanism for the attachment of surface-functionalized IONPs on microalgal cells in fresh water [27,29], the presence of negatively charged NOM will significantly interfere with this attachment process. Humic acid, which is used to simulate the role of NOM, has a molecular structure containing phenolic and carboxylic compounds as the associated functional group that contributes to its negative surface charge [48]. This characteristic makes NOM easily attracted to the surface-functionalized IONPs with an opposite surface charge via electrostatic interaction, which causes extensive flocculation prior to their attachment onto the microalgal cells. From only this perspective, the flocculation of IONPs likely suppresses the magnetic separation efficiency (see Fig. 5a) because of two reasons: (1) the formation of particle clusters will significantly decrease the absolute number of available particles for the cells and (2) although the formed particle cluster, which has a much larger magnetic volume, can be attached onto the cells, it will eventually experience a much higher magnetophoretic force during the separation process [49]. The resulting stress that is
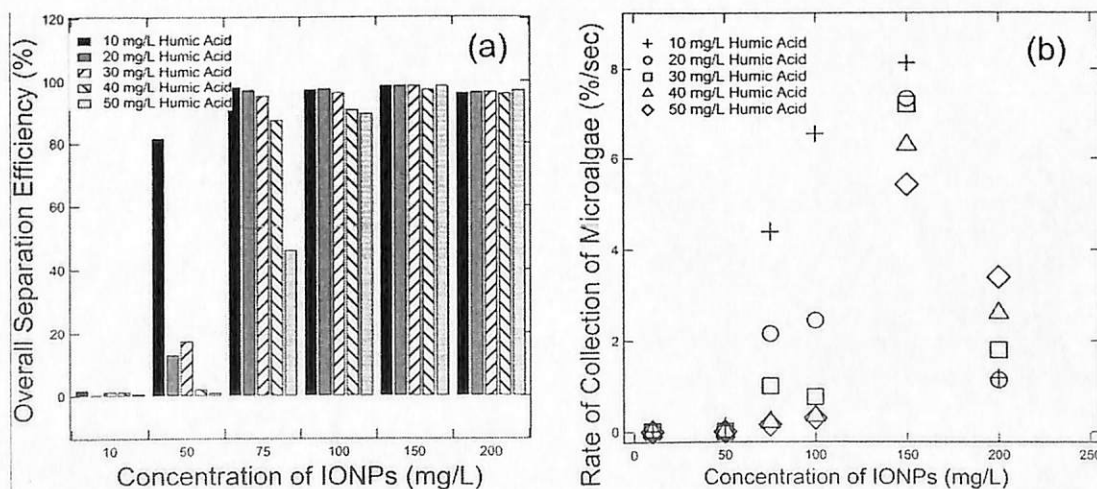

Fig. 5. (a) Overall separation efficiency and (b) separation rate of microalgal cells that were seeded with PDDA-functionalized IONPs at different humic acid concentrations.

imposed onto the binding region between the cluster and the cell may be too high, i.e., up to an extent where the entire cluster can be ripped away from the labeled cell surface during its migration along the field gradient. Fig. 5a shows that the adverse effect of NOM becomes almost negligible when the IONP concentration exceeds 100 mg/L. This observation further supports our hypothesis, where the dependency of the magnetophoretic separation of microalgae on the IONP concentration is a threshold phenomenon: beyond the particle-to-cell ratio of 5.3×10^4 particles/cell, the separation efficiency is independent of the particle concentration.

In addition to the overall separation efficiency, the initial collection rate of IONP-tagged microalgae also strongly depends on the NOM concentration. Fig. 5b illustrates the kinetic profile of the magnetophoretic separation process with IONP concentrations of 10, 50, 75, 100, 150 and 200 mg/L. The initial collection rate profile exhibits a notably similar trend as those in Fig. 3b. Fig. 5b shows that the initial collection rate of microalgae is suppressed by the increase in NOM concentration. At the "optimal" IONP concentration, the sample(s) with lower humic acid concentrations shows higher initial rates of recollection, whereas a lower initial collection rate is observed for those sample(s) with higher humic acid concentrations. The presence of IONPs enables microalgae and IONPs to form larger clusters and consequently experience a larger magnetophoretic force for easy collection [50]. However, humic acid causes bridging flocculation, which may destabilize the IONPs and lead to the formation of larger particle clusters [51]. This particle cluster formation significantly reduces the number of available IONPs, which serve as the magnetic seeding agent. Although a single large cluster of IONPs can experience a higher magnetophoretic force compared to the individual IONPs, it is statistically less effective in promoting the particles–microalgae–humic acid aggregation. With fewer available IONPs to initiate further aggregation of humic acid and microalgal cells, smaller particles–microalgae–humic acid clusters are formed. We conclude that this phenomenon is the main reason for the observed decrease in the rate of microalgae separation in Fig. 5b.

4. Conclusion

Magnetic seeding of microalgal cells with IONPs is a required step prior to successful implementation of magnetophoretic separation. The surface functionalization of IONPs with cationic polyelectrolyte PDDA enables the successful attachment of IONPs onto the surface of microalgal cells using mainly electrostatic interaction, and the recorded cell separation efficiency was as high as 98%. Nevertheless, the molecular weight of polyelectrolyte, which was used to surface functionalize IONPs, has a notably negligible to almost no effect on the total cell separation efficiency. At low particle-to-cell ratios, the presence of suspended solids and NOM strongly suppresses the overall separation efficiency and collection rate of microalgae. All of these negative effects are diminished at high particle-to-cell ratios mainly because both NOM and suspended solids play an important role in inducing IONPs–microalgae aggregation. When more IONPs are trapped within, the formation of large particle–cell clusters with higher magnetic content speeds up the separation process and boosts the overall cell separation efficiency. Our study suggests that the magnetophoretic separation process is almost entirely governed by a threshold phenomenon, where a certain "optimal" particle-to-cell ratio is required to ensure successful magnetic seeding. To successfully adapt the magnetophoretic process to separate microalgae from fish farm water or any aqueous environment with the presence of foreign species, it is imperative to determine the proper particle-to-cell ratio to exclude all external interferences.

Appendix A. Supplementary data

Supplementary data associated with this article can be found, in the online version, at http://dx.doi.org/10.1016/j.cej.2015.06.108.

References

[1] T.M. Mata, A.A. Martins, N.S. Caetano, Microalgae for biodiesel production and other applications: a review, Renew. Sust. Energy Rev. 14 (2010) 217–232.
[2] F.P. Meyer, L.A. Barclay, Field manual for the investigation of fish kills, US Fish and Wildlife Service, 1990.
[3] P.Y. Toh, S.P. Yeap, L.P. Kong, B.W. Ng, C.J.C. Derek, A.L. Ahmad, J. Lim, Magnetophoretic removal of microalgae from fishpond water: feasibility of high gradient and low gradient magnetic separation, Chem. Eng. J. 211–212 (2012) 22–30.
[4] K. Kangur, A. Kangur, P. Kangur, R. Laugaste, Fish kill in Lake Peipsi in summer 2002 as a synergistic effect of cyanobacterial bloom, high temperature and low water level, Proceedings of the Estonian Academy of Sciences. Biology Ecology, 2005, pp. 67–80.
[5] V.H. Smith, D.W. Schindler, Eutrophication science. Where do we go from here?, Trends Ecol Evol. 24 (2009) 201–207.
[6] I. Valiela, J. McClelland, J. Hauxwell, P.J. Behr, D. Hersh, K. Foreman, Macroalgal blooms in shallow estuaries: controls and ecophysiological and ecosystem consequences, Limnol. Oceanogr. 42 (1997) 1105–1118.
[7] S. Wang, F. Wang, Y.-R. Hu, A. Stiles, C. Guo, C.-Z. Liu, Magnetic flocculant for high efficiency harvesting of microalgal cells, ACS Appl. Mater. Interfaces 6 (2013) 109–115.
[8] D. Vandamme, I. Foubert, K. Muylaert, Flocculation as a low-cost method for harvesting microalgae for bulk biomass production, Trends Biotechnol. 31 (2013) 233–239.
[9] G. Prochazkova, I. Safarik, T. Branyik, Harvesting microalgae with microwave synthesized magnetic microparticles, Bioresour. Technol. 130 (2012) 472–477.
[10] Y.-C. Lee, K. Lee, Y.-K. Oh, Recent nanoparticle engineering advances in microalgal cultivation and harvesting processes of biodiesel production: a review, Bioresour. Technol. 184 (2014) 63–72.
[11] G. Prochazkova, N. Podolova, I. Safarik, V. Zachleder, T. Branyik, Physicochemical approach to freshwater microalgae harvesting with magnetic particles, Colloids Surf. B 112 (2013) 213–218.
[12] C.C. Mischke, Aquaculture Pond Fertilization: Impacts of Nutrient Input on Production, John Wiley & Sons, 2012.
[13] M.J. Hanson, H.G. Stefan, Side effects of 58 years of copper sulfate treatment of the Fairmont Lakes, Minnesota, J. Am. Water Resour. Assoc. 20 (1984) 889–900.
[14] W.E. Lynch Jr., Controlling filamentous algae in ponds, Ohio State University Extension Fact Sheet A-3-09, 2009.
[15] K.K. Schrader, M.Q. de Regt, P.D. Tidwell, C.S. Tucker, S.O. Duke, Compounds with selective toxicity towards the off-flavor metabolite-producing cyanobacterium Oscillatoria cf. chalybea, Aquaculture 163 (1998) 85–99.
[16] D. Jancula, B. Maršálek, Critical review of actually available chemical compounds for prevention and management of cyanobacterial blooms, Chemosphere 85 (2011) 1415–1422.
[17] A.S. Ball, M. Williams, D. Vincent, J. Robinson, Algal growth control by a barley straw extract, Bioresour. Technol. 77 (2001) 177–181.
[18] T. Kanabkaew, U. Puetpaiboon, Aquatic plants for domestic wastewater treatment: lotus (Nelumbo nucifera) and hydrilla (Hydrilla verticillata) systems, Aquatic 26 (2004) 750.
[19] R. Gersberg, B. Elkins, S. Lyon, C. Goldman, Role of aquatic plants in wastewater treatment by artificial wetlands, Water Res. 20 (1986) 363–368.
[20] J.-K. Wang, Managing shrimp pond water to reduce discharge problems, Aquacult. Eng. 9 (1990) 61–73.
[21] B. Moss, Engineering and biological approaches to the restoration from eutrophication of shallow lakes in which aquatic plant communities are important components. Biomanipulation Tool for Water Management, Springer, 1990. pp. 367–377.
[22] G. Bitton, J. Fox, H. Strickland, Removal of algae from Florida lakes by magnetic filtration, Appl. Environ. Microbiol. 30 (1975) 905–908.
[23] R. Yadidia, A. Abeliovich, G. Belfort, Algae removal by high gradient magnetic filtration, Environ. Sci. Technol. 11 (1977) 913–916.

[24] Y.-R. Hu, F. Wang, S.-K. Wang, C.-Z. Liu, C. Guo, Efficient harvesting of marine microalgae Nannochloropsis maritima using magnetic nanoparticles, Bioresour. Technol. 138 (2013) 387–390.

[25] K. Lee, S.Y. Lee, J.-G. Na, S.G. Jeon, R. Praveenkumar, D.-M. Kim, W.-S. Chang, Y.-K. Oh, Magnetophoretic harvesting of oleaginous Chlorella sp. by using biocompatible chitosan/magnetic nanoparticle composites, Bioresour. Technol. 149 (2013) 575–578.

[26] Y.-R. Hu, C. Guo, F. Wang, S.-K. Wang, F. Pan, C.-Z. Liu, Improvement of microalgae harvesting by magnetic nanocomposites coated with polyethylenimine, Chem. Eng. J. (2014).

[27] J.K. Lim, D.C.J. Chieh, S.A. Jalak, P.Y. Toh, N.H.M. Yasin, B.W. Ng, A.L. Ahmad, Rapid magnetophoretic separation of microalgae, Small 8 (2012) 1683–1692.

[28] J.B. Miller, E.K. Hobbie, Nanoparticles as macromolecules, J. Polym. Sci. B Polym. Phys. 51 (2013) 1195–1208.

[29] P.Y. Toh, B.W. Ng, A.L. Ahmad, D.C.J. Chieh, J. Lim, The role of particle-to-cell interactions in dictating nanoparticle aided magnetophoretic separation of microalgal cells, Nanoscale 6 (2014) 12838–12848.

[30] Y.-R. Hu, C. Guo, L. Xu, F. Wang, S.-K. Wang, Z. Hu, C.-Z. Liu, A magnetic separator for efficient microalgae harvesting, Bioresour. Technol. 158 (2014) 388–391.

[31] A.J. Hurd, The electrostatic interaction between interfacial colloidal particles, J. Phys. Chem. B 18 (1985) L1055.

[32] N. Lang, S. Holloway, J. Nørskov, Electrostatic adsorbate–adsorbate interactions: the poisoning and promotion of the molecular adsorption reaction, Surf. Sci. 150 (1985) 24–38.

[33] P.Y. Toh, B.W. Ng, C.H. Chong, A.L. Ahmad, J.-W. Yang, J. Lim, Magnetophoretic separation of microalgae: the role of nanoparticles and polymer binder in harvesting biofuel, RSC Adv. 4 (2014) 4114–4121.

[34] J. Jiang, G. Oberdörster, P. Biswas, Characterization of size, surface charge, and agglomeration state of nanoparticle dispersions for toxicological studies, J. Nanopart. Res. 11 (2009) 77–89.

[35] Y. Avnimelech, Feeding with microbial flocs by tilapia in minimal discharge bio-flocs technology ponds, Aquaculture 264 (2007) 140–147.

[36] G. Aiken, Organic matter in ground water, US Geological Survey Artificial Recharge Workshop Proceedings, 2002, pp. 21–23.

[37] N. Saleh, H.-J. Kim, T. Phenrat, K. Matyjaszewski, R.D. Tilton, G.V. Lowry, Ionic strength and composition affect the mobility of surface-modified FeO nanoparticles in water-saturated sand columns, Environ. Sci. Technol. 42 (2008) 3349–3355.

[38] J.A. Nason, S.A. McDowell, T.W. Callahan, Effects of natural organic matter type and concentration on the aggregation of citrate-stabilized gold nanoparticles, J. Environ. Monit. 14 (2012) 1885–1892.

[39] L. Kong, X. Gan, A.L. Bin Ahmad, B.H. Hamed, E.R. Evarts, B. Ooi, J. Lim, Design and synthesis of magnetic nanoparticles augmented microcapsule with catalytic and magnetic bifunctionalities for dye removal, Chem. Eng. J. 197 (2012) 350–358.

[40] S.P. Yeap, P.Y. Toh, A.L. Ahmad, S.C. Low, S.A. Majetich, J. Lim, Colloidal stability and magnetophoresis of gold-coated iron oxide nanorods in biological media, J. Phys. Chem. C 116 (2012) 22561–22569.

[41] S.P. Yeap, S.S. Leong, A.L. Ahmad, B.S. Ooi, J. Lim, On size fractionation of iron oxide nanoclusters by low magnetic field gradient, J. Phys. Chem. C 118 (2014) 24042–24054.

[42] A. Martin-Molina, M. Quesada-Perez, F. Galisteo-González, R. Hidalgo-Alvarez, Electrophoretic mobility and primitive models: surface charge density effect, J. Phys. Chem. B 106 (2002) 6881–6886.

[43] S. Patil, A. Sandberg, E. Heckert, W. Self, S. Seal, Protein adsorption and cellular uptake of cerium oxide nanoparticles as a function of zeta potential, Biomaterials 28 (2007) 4600–4607.

[44] L. Xu, C. Guo, F. Wang, S. Zheng, C.-Z. Liu, A simple and rapid harvesting method for microalgae by in situ magnetic separation, Bioresour. Technol. 102 (2011) 10047–10051.

[45] G. Cary, J. McMahon, W. Kuc, The effect of suspended solids and naturally occurring dissolved organics in reducing the acute toxicities of cationic polyelectrolytes to aquatic organisms, Environ. Toxicol. Chem. 6 (1987) 469–474.

[46] A. Imeson, J. Verstraten, Suspended solids concentrations and river water chemistry, Earth Surf. Process. 6 (1981) 251–263.

[47] G. Sposito, The Surface Chemistry of Soils, Oxford University Press, 1984.

[48] E. Illés, E. Tombácz, The role of variable surface charge and surface complexation in the adsorption of humic acid on magnetite, Colloids Surf. A 230 (2003) 99–109.

[49] K.E. McCloskey, J.J. Chalmers, M. Zborowski, Magnetic cell separation: characterization of magnetophoretic mobility, Anal. Chem. 75 (2003) 6868–6874.

[50] J. Lim, S.P. Yeap, H.X. Che, S.C. Low, Characterization of magnetic nanoparticle by dynamic light scattering, Nanoscale Res. Lett. 8 (2013) 1–14.

[51] E. Illés, E. Tombácz, The effect of humic acid adsorption on pH-dependent surface charging and aggregation of magnetite nanoparticles, J. Colloid Interface Sci. 295 (2006) 115–123.

NANO REVIEW   **Open Access**

Characterization of magnetic nanoparticle by dynamic light scattering

JitKang Lim[1,2*], Swee Pin Yeap[1], Hui Xin Che[1] and Siew Chun Low[1]

Abstract

Here we provide a complete review on the use of dynamic light scattering (DLS) to study the size distribution and colloidal stability of magnetic nanoparticles (MNPs). The mathematical analysis involved in obtaining size information from the correlation function and the calculation of Z-average are introduced. Contributions from various variables, such as surface coating, size differences, and concentration of particles, are elaborated within the context of measurement data. Comparison with other sizing techniques, such as transmission electron microscopy and dark-field microscopy, revealed both the advantages and disadvantages of DLS in measuring the size of magnetic nanoparticles. The self-assembly process of MNP with anisotropic structure can also be monitored effectively by DLS.

Keywords: Dynamic light scattering; Magnetic nanoparticles; Colloidal stability; Surface functionalization; Review

Review

Introduction

Magnetic nanoparticles (MNPs) with a diameter between 1 to 100 nm have found uses in many applications [1,2]. This nanoscale magnetic material has several advantages that provide many exciting opportunities or even a solution to various biomedically [3-5] and environmentally [6-8] related problems. Firstly, it is possible to synthesize a wide range of MNPs with well-defined structures and size which can be easily matched with the interest of targeted applications. Secondly, the MNP itself can be manipulated by an externally applied magnetic force. The capability to control the spatial evolution of MNPs within a confined space provides great benefits for the development of sensing and diagnostic system/techniques [9,10]. Moreover MNPs, such as Fe^0 and Fe_3O_4, that exhibit a strong catalytic function can be employed as an effective nanoagent to remove a number of persistent pollutants from water resources [11,12]. In addition to all the aforementioned advantages, the recent development of various techniques and procedures for producing highly monodispersed and size-controllable MNPs [13,14] has played a pivotal role in promoting the active explorations and research of MNPs.

In all of the applications involving the use of MNPs, the particle size remained as the most important parameter as many of the chemical and physical properties associated to MNPs are strongly dependent upon the nanoparticle diameter. In particular, one of the unique features of a MNP is its high-surface-to-volume ratio, and this property is inversely proportional to the diameter of the MNP. The smaller the MNP is, the larger its surface area and, hence, the more loading sites are available for applications such as drug delivery and heavy metal removal. Furthermore, nanoparticle size also determines the magnetophoretic forces (F_{mag}) experienced by a MNP since F_{mag} is directly proportional to the volume of the particles [15]. In this regard, having size information is crucial as at nanoregime, the MNP is extremely susceptible to Stoke's drag [16] and thermal randomization energy [17]. The successful manipulation of MNP can only be achieved if the F_{mag} introduced is sufficient to overcome both thermal and viscous hindrances [18]. In addition, evidences on the (eco)toxicological impacts of nanomaterials have recently surfaced [19]. The contributing factors of nanotoxicity are still a subject of debate; however, it is very likely due to either (1) the characteristic small dimensional effects of nanomaterials that are not shared by their bulk counterparts with the same chemical composition [20] or (2) biophysicochemical interactions at the nano-bio interface dictated by colloidal forces [21]. For either reason, the MNP's size is one of the determining factors.

* Correspondence: chjitkangl@eng.usm.my
[1]School of Chemical Engineering, Universiti Sains Malaysia, Nibong Tebal, Penang 14300, Malaysia
[2]Department of Physics, Carnegie Mellon University, Pittsburgh, PA 15213, USA

The technique of dynamic light scattering (DLS) has been widely employed for sizing MNPs in liquid phase [22,23]. However, the precision of the determined particle size is not completely understood due to a number of unevaluated effects, such as concentration of particle suspension, scattering angle, and shape anisotropy of nanoparticles [24]. In this review, the underlying working principle of DLS is first provided to familiarize the readers with the mathematical analysis involved for correct interpretation of DLS data. Later, the contribution from various factors, such as suspension concentration, particle shape, colloidal stability, and surface coating of MNPs, in dictating the sizing of MNPs by DLS is discussed in detail. It is the intention of this review to summarize some of the important considerations in using DLS as an analytical tool for the characterization of MNPs.

Overview of sizing techniques for MNPs

There are numerous analytical techniques, such as DLS [25], transmission electron miscroscopy (TEM) [26], thermomagnetic measurement [27], dark-field microscopy [17,18], atomic force microscopy (AFM) [28], and acoustic spectrometry measurement [29], that have been employed to measure the size/size distribution of MNPs (Table 1). TEM is one of the most powerful analytical tools available which can give direct structural and size information of the MNP. Through the use of the short wavelengths achievable with highly accelerated electrons, it is capable to investigate the structure of a MNP down to the atomic level of detail, whereas by performing image analysis on the TEM micrograph obtained, it is possible to give quantitative results on the size distribution of the MNP. This technique, however, suffered from the small sampling size involved. A typical MNP suspension composed of 10^{10} to 10^{15} particles/mL and the size analysis by measuring thousands or even tens of thousands of particles still give a relatively small sample pool to draw statistically conclusive remarks.

Thermomagnetic measurement extracts the size distribution of an ensemble of superparamagnetic nanoparticles from zero-field cooling (ZFC) magnetic moment, m_{ZFC} (T), data based on the Néel model [27]. This method is an indirect measurement of particle size and relies on the

underlying assumption of the mathematical model used to calculate the size distribution. In addition, another limitation of this analytical method includes the magnetic field applied for ZFC measurements which must be small compared to the anisotropy field of the MNPs [30], and it also neglects particle-particle dipolar interactions which increase the apparent blocking temperature [31]. This technique, however, could give a very reliable magnetic size of the nanoparticle analyzed.

Dark-field microscopy relies on direct visual inspection of the optical signal emitted from the MNP while it undergoes Brownian motion. After the trajectories of each MNP over time t are recorded, the two-dimensional mean-squared displacement $<r^2> = 4Dt$ is used to calculate the diffusion coefficient D for each particle. Later on, the hydrodynamic diameters can be estimated via the Stokes-Einstein equation for the diffusion coefficients calculated for individual particles, averaging over multiple time steps [18]. Successful implementation of this technique depends on the ability to trace the particle optically by coating the MNP with a noble metal that exhibits surface Plasmon resonance within a visible wavelength. This extra synthesis step has significantly restricted the use of this technique as a standard route for sizing MNPs. The size of an MNP obtained through dark-field microscopy is normally larger than the TEM and DLS results [17]. It should be noted that dark-field microscopy can also be employed for direct visualization of a particle flocculation event [32]. As for AFM, besides the usual topographic analysis, magnetic imaging of a submicron-sized MNP grown on GaAs substrate has been performed with magnetic force microscopy equipment [33]. Despite all the recent breakthroughs, sample preparation and artifact observation are still the limiting aspect for the wider use of this technology for sizing MNPs [34].

The particle size and size distribution can also be measured with an acoustic spectrometer which utilizes the sound pulses transmitted through a particle suspension to extract the size-related information [29]. Based on the combined effect of absorption and scattering of acoustic energy, an acoustic sensor measures attenuation frequency spectra in the sample. This attenuation spectrum is used to calculate the particle size distribution. This technique has advantages over the light scattering method in studying samples with high polydispersity as the raw data for calculating particle size depend on only the third power of the particle size. This scenario makes contribution of the small (nano) and larger particles more even and the method potentially more sensitive to the nanoparticle content even in the very broad size distributions [35].

DLS, also known as photon correlation spectroscopy, is one of the most popular methods used to determine the size of MNPs. During the DLS measurement, the

Table 1 Common analytical techniques and the associated range scale involved for nanoparticle sizing

Techniques	Approximated working size range
Dynamic light scattering	1 nm to approximately 5 μm
Transmission electron microscopy	0.5 nm to approximately 1 μm
Atomic force microscopy	1 nm to approximately 1 μm
Dark-field microscopy	5 to 200 nm
Thermomagnetic measurement	10 to approximately 50 nm

MNP suspension is exposed to a light beam (electromagnetic wave), and as the incident light impinges on the MNP, the direction and intensity of the light beam are both altered due to a process known as scattering [36]. Since the MNPs are in constant random motion due to their kinetic energy, the variation of the intensity with time, therefore, contains information on that random motion and can be used to measure the diffusion coefficient of the particles [37]. Depending on the shape of the MNP, for spherical particles, the hydrodynamic radius of the particle R_H can be calculated from its diffusion coefficient by the Stokes-Einstein equation $D_f = k_B T / 6\pi\eta R_H$, where k_B is the Boltzmann constant, T is the temperature of the suspension, and η is the viscosity of the surrounding media. Image analysis on the TEM micrographs gives the 'true radius' of the particles (though determined on a statistically small sample), and DLS provides the hydrodynamic radius on an ensemble average [38]. The hydrodynamic radius is the radius of a sphere that has the same diffusion coefficient within the same viscous environment of the particles being measured. It is directly related to the diffusive motion of the particles.

DLS has several advantages for sizing MNPs and has been widely used to determine the hydrodynamic size of various MNPs as shown in Table 2. First of all, the measuring time for DLS is short, and it is almost all automated, so the entire process is less labor intensive and an extensive experience is not required for routine measurement. Furthermore, this technique is non-invasive, and the sample can be employed for other purposes after the measurement. This feature is especially important for the recycle use of MNP with an expensive surface functional group, such as an enzyme or molecular ligands. In addition, since the scattering intensity is directly proportional to the sixth power of the particle radius, this technique is extremely sensitive towards the presence of small aggregates. Hence, erroneous measurement can be prevented quite effectively even with the occurrences of limited aggregation events. This unique feature makes DLS one of the very powerful techniques in monitoring the colloidal stability of MNP suspension.

Table 2 Hydrodynamic diameter of different MNPs determined by DLS

Type of MNPs	Surface coating	Hydrodynamic diameter by DLS (nm)	Reference
Fe^0	Carboxymethyl cellulose	15-19	[39]
	Guar gum	350-700	[40]
	Poly(methacrylic acid)-poly(methyl methacrylate)-poly (styrenesulfonate) triblock copolymer	100-600	[41]
	Poly(styrene sulfonate)	30-90	[22]
γ-Fe_2O_3	Oleylamine or oleic acid	5-20	[42]
	Poly(N,N-dimethylacrylamide)	55-614	[43]
	Poly(ethylene oxide)-block-poly(glutamic acid)	42-68	[44]
	Poly(ethylene imine)	20-75	[45]
	Poly(ε-caprolactone)	193 ± 7	[46]
Fe_3O_4	Phospholipid-PEG	14.7 ± 1.4	[47]
	Polydimethylsiloxane	41.2 ± 0.4	[48]
	Oleic acid-pluronic	50-600	[49]
	Polyethylenimine (PEI)	50-150	[23,50]
	Polythylene glycol	10-100	[51]
	Triethylene glycol	16.5 ± 3.5	[52]
	Poly(N-isopropylacrylamide)	15-60	[53]
	Pluronic F127	36	[54]
	Poly(sodium 4-styrene sulfonate)	~200	[55]
	Poly(diallyldimethylammonium chloride)	107.4 ± 53.7	[56]
FePt	Poly(diallyldimethylammonium chloride)	30-100	[57]
NiO	Cetyltrimethyl ammonium bromide	10-80	[58]
	Fetal bovine serum	39.05	[59]
	Not specified	750 ± 30	[60]
CoO, Co_2O_3	Poly(methyl methacrylate)	59-85	[61]
CoFe	Hydroxamic and phosphonic acids	6.5-458.7	[62]

The underlying principle of DLS

The interaction of very small particles with light defined the most fundamental observations such as why is the sky blue. From a technological perspective, this interaction also formed the underlying working principle of DLS. It is the purpose of this section to describe the mathematical analysis involved to extract size-related information from light scattering experiments.

The correlation function

DLS measures the scattered intensity over a range of scattering angles θ_{dls} for a given time t_k in time steps Δt. The time-dependent intensity $I(q, t)$ fluctuates around the average intensity $I(q)$ due to the Brownian motion of the particles [38]:

$$[I(q)] = \lim_{t_k \to \infty} 1/_{t_k} \int_0^{t_k} I(q,t) \cdot dt \approx \lim_{k \to \infty} \frac{1}{k} \Sigma_{i=1}^k I(q, i \cdot \Delta t) \qquad (1)$$

where $[I(q)]$ represents the time average of $I(q)$. Here, it is assumed that t_k, the total duration of the time step measurements, is sufficiently large such that $I(q)$ represents average of the MNP system. In a scattering experiment, normally, θ_{dls} (see Figure 1) is expressed as the magnitude of the scattering wave vector q as

$$q = (4\pi n/\lambda) \sin(\theta_{dls}/2) \qquad (2)$$

where n is the refractive index of the solution and λ is the wavelength in vacuum of the incident light. Figure 2a illustrates typical intensity fluctuation arising from a dispersion of large particles and a dispersion of small particles. As the small particles are more susceptible to random forces, the small particles cause the intensity to fluctuate more rapidly than the large ones.

The time-dependent intensity fluctuation of the scattered light at a particular angle can then be cha-

racterized with the introduction of the autocorrelation function as

$$c(q, \tau) = \lim_{t_k \to \infty} 1/_{t_k} \int_0^{t_k} I(q,t) \cdot I(q, t + \tau) \cdot dt \qquad (3)$$

$$\approx \lim_{k \to \infty} \frac{1}{k} \Sigma_{j=0}^k I(q, i \cdot \Delta t) \cdot I(q, (i+j) \cdot \Delta t)$$

where $\tau = i \, \Delta t$ is the delay time, which represents the time delay between two signals $I(q, i \, \Delta t)$ and $I(q, (i + j) \Delta t)$. The function $C(q, \tau)$ is obtained for a series of τ and represents the correlation between the intensity at t_1 ($I(q, t_1)$) and the intensity after a time delay of τ ($I(q, t_1 + \tau)$). The last part of the equation shows how the autocorrelation function is calculated experimentally when the intensity is measured in discrete time steps [37]. As for nanoparticle dispersion, the autocorrelation function decays more rapidly for small particles than for the large particles as depicted in Figure 2b. The autocorrelation function has its highest value of $[I(q,0)]^2$ at $\tau = 0$. As τ becomes sufficiently large at long time scales, the fluctuations becomes uncorrelated and $C(q, \tau)$ decreases to $[I(q)]^2$. For non-periodic $I(q,t)$, a monotonic decay of $C(q, \tau)$ is observed as τ increases from zero to infinity and

$$C(q, \tau)/_{[I(q)]^2} = g^{(2)}(q, \tau) = 1 + \xi \left| g^{(1)}(q, \tau) \right|^2 \qquad (4)$$

where ξ is an instrument constant approximately equal to unity and $g^{(1)}(q, \tau)$ is the normalized electric field correlation function [63]. Equation 4 is known as the Siegert relation and is valid except in the case of scattering volume with a very small number of scatterers or when the motion of the scatterers is limited. For monodisperse, spherical particles, $g^{(1)}(\tau)$ is given by
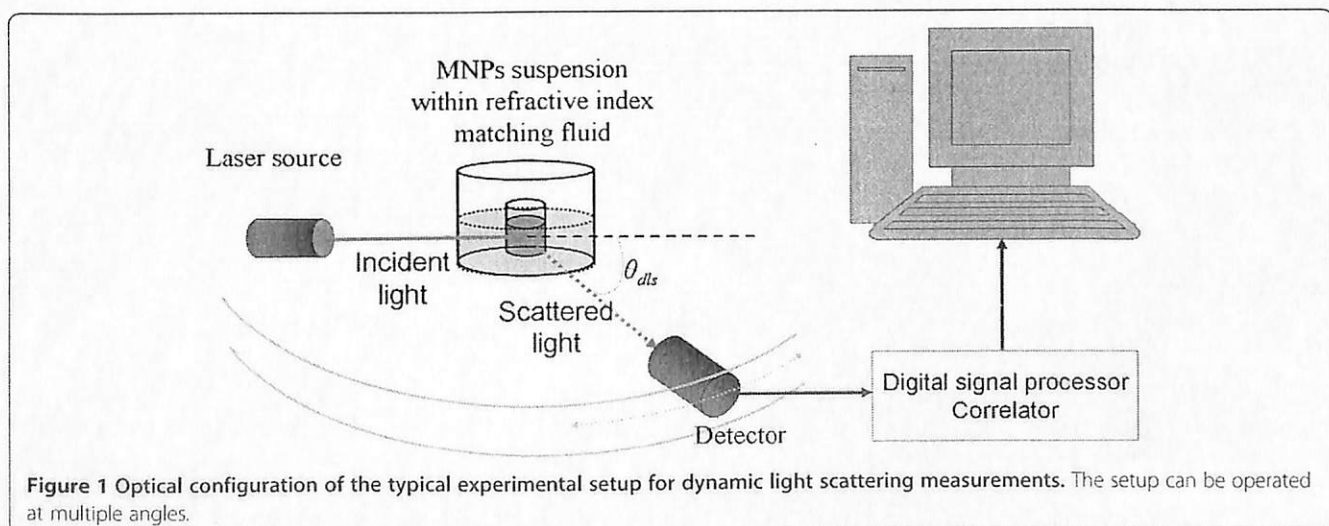

Figure 1 Optical configuration of the typical experimental setup for dynamic light scattering measurements. The setup can be operated at multiple angles.
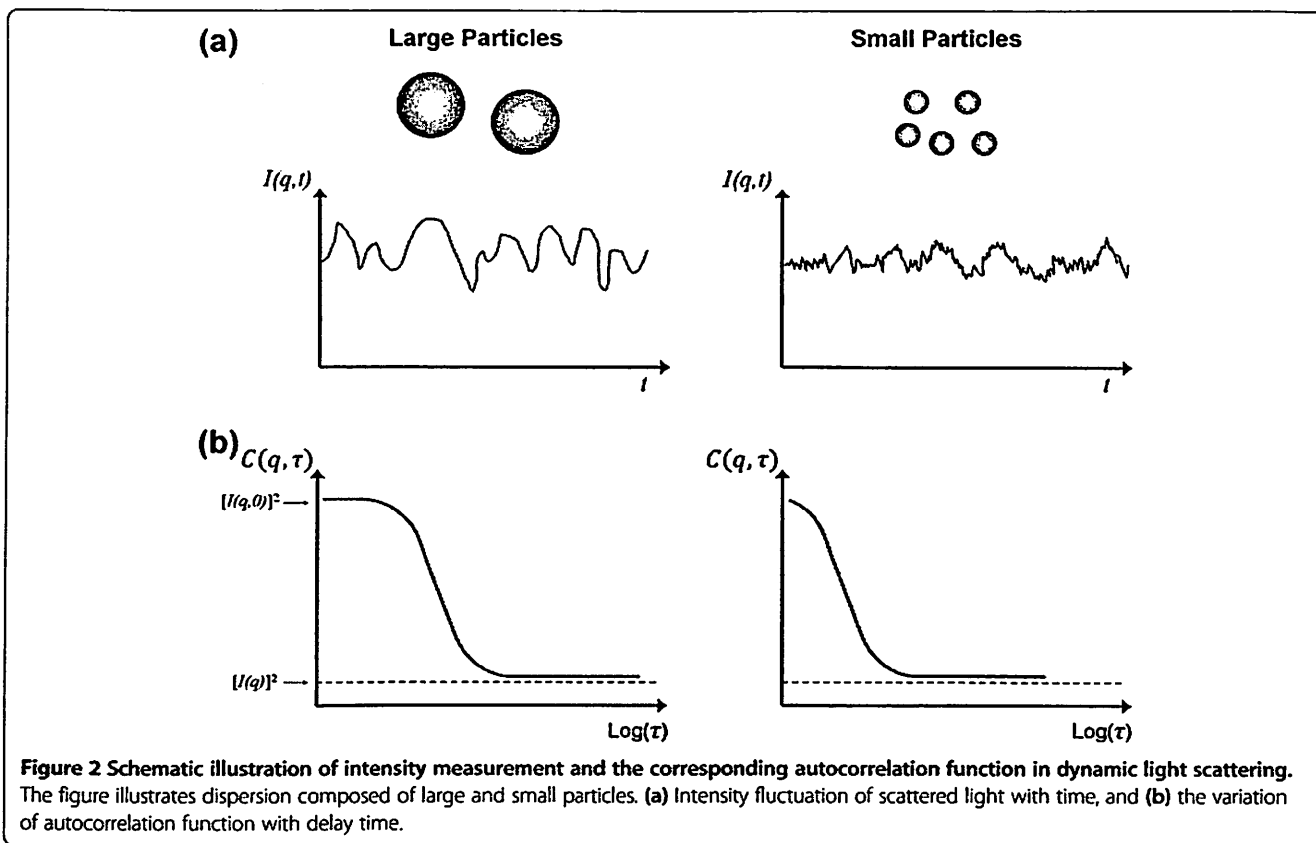
Figure 2 Schematic illustration of intensity measurement and the corresponding autocorrelation function in dynamic light scattering.
The figure illustrates dispersion composed of large and small particles. (a) Intensity fluctuation of scattered light with time, and (b) the variation
of autocorrelation function with delay time.

$$g^{(1)}(q, \tau) = \exp\left(-D_f q^2 \tau\right).$$

Once the value of D_f is obtained, the hydrodynamic diameter of a perfectly monodisperse dispersion composed of spherical particles can be inferred from the Stokes-Einstein equation. Practically, the correlation function observed is not a single exponential decay but can be expressed as

$$g^{(1)}(q, \tau) = \int_0^\infty G(\Gamma) e^{-\Gamma \tau} d\Gamma \tag{6}$$

where $G(\Gamma)$ is the distribution of decay rates Γ. For a narrowly distributed decay rate, cumulant method can be used to analyze the correlation function. A properly normalized correlation function can be expressed as

$$\ln\left(g^{(1)}(q, \tau)\right) = -\langle \Gamma \rangle \tau + \frac{\mu_2}{2} \tau^2 \tag{7}$$

where $\langle \Gamma \rangle$ is the average decay rate and can be defined as

$$\langle \Gamma \rangle = \int_0^\infty G(\Gamma) \Gamma d\Gamma \tag{8}$$

and $\mu_2 = \langle \Gamma \rangle^2 - \langle \Gamma \rangle^2$ is the variance of the decay rate distribution. Then, the polydispersity index (PI) is defined as PI $= \mu_2/\langle \Gamma \rangle^2$. The average hydrodynamic radius is obtained from the average decay rate $\langle \Gamma \rangle$ using the relation

$$R_H = \frac{k_B T}{6\pi\eta\langle \Gamma \rangle} q^2 \tag{9}$$

Z-average

In most cases, the DLS results are often expressed in terms of the Z-average. Since the Z-average arises when DLS data are analyzed through the use of the cumulant technique [64], it is also known as the "cumulant mean." Under Rayleigh scattering, the amount of light scattered by a single particle is proportional to the sixth power of its radius (volume squared). This scenario causes the averaged hydrodynamic radius determined by DLS to be also weighted by volume squared. Such an averaged property is called the Z-average. For particle suspension with discrete size distribution, the Z-average of some arbitrary property y would be calculated as

$$\langle y \rangle = \frac{\Sigma_i n_i R_{H,i}^6 y_i}{\Sigma_i n_i R_{H,i}^6} \tag{10}$$

where n_i is the number of particles of type i having a hydrodynamic radius of $R_{H,i}$ and property y. If we assume that this particle dispersion consists of exactly two sizes of particles 1 and 2, then Equation 10 yields

$$\langle y \rangle = \frac{n_1 R_{H,1}^6 y_1 + n_2 R_{H,2}^6 y_2}{n_1 R_{H,1}^6 + n_2 R_{H,2}^6} \tag{11}$$

where $R_{H,i}$ and y_i are the volume and arbitrary property for particle 1 ($i = 1$) and particle 2 ($i = 2$). Suppose that two particles 1 combined to form one particle 2 and assume that we start with n_0 total of particle 1, some of which combined to form n_2 number of particle 2. With this assumption, we have $n_1 = n_0 - n_2$ number of particle 1. Moreover, under this assumption $R_{H,2} = 2\ R_{H,1}$. Substitute these relations into Equation 11; then, the Z-average of property y becomes

$$\frac{\langle y \rangle}{y_1} = \frac{1 + \left(2\left(\frac{y_2}{y_1}\right)-1\right)2\left(\frac{n_2}{n_0}\right)}{1 + 2\left(\frac{n_2}{n_0}\right)} \tag{12}$$

where $2n_2/n_0$ is the fraction of total particle 1 existing as particle 2. Solving this fraction, we obtained

$$\frac{2n_2}{n_0} = \frac{\frac{\langle y \rangle}{y_1}-1}{\frac{2y_2}{y_1}-\frac{\langle y \rangle}{y_1}-1} \tag{13}$$

However, it should be noted that Z-average should only be employed to provide the characteristic size of the particles if the suspension is monomodal (only one peak), spherical, and monodisperse. As shown in Figure 3, for a mixture of particles with obvious size difference (bimodal distribution), the calculated Z-average carries irrelevant size information.

DLS measurement of MNPs

The underlying challenges of measuring the size of MNPs by DLS lay in the facts that (1) for engineering applications, these particles are typically coated with macromolecules to enhance their colloidal stability (see Figure 4) and (2) there present dipole-dipole magnetic interactions between the none superparamagnetic nanoparticles. Adsorbing macromolecules onto the surface of particles tends to increase the apparent R_H of particles. This increase in R_H is a convenient measure of the thickness of the adsorbed macromolecules [65]. This section is dedicated to the scrutiny of these two phenomena and also suspension concentration effect in dictating the DLS measurement of MNPs. All DLS measurements were performed with a Malvern Instrument Zetasizer Nano Series (Malvern Instruments, Westborough, MA, USA) equipped with a He-Ne laser (λ = 633 nm, max 5 mW) and operated at a scattering angle of 173°. In all measurements, 1 mL of particle suspensions was employed and placed in a 10 mm × 10 mm quartz cuvette. The iron oxide MNP used in this study was synthesized by a high-temperature decomposition method [17].

Size dependency of MNP in DLS measurement

In order to demonstrate the sizing capability of DLS, measurements were conducted on three species of Fe_3O_4 MNPs produced by high-temperature decomposition method which are surface modified with oleic acid/oleylamine in toluene (Figure 5). The TEM image analyses performed on micrographs shown in Figure 5 (from top to bottom) indicate that the diameter of each particle species is 7.2 ± 0.9 nm, 14.5 ± 1.8 nm, and 20.1 ± 4.3 nm, respectively. The diameters of these particles obtained from TEM and DLS are tabulated in Table 3. It is very likely that the main differences between the measured diameters from these two techniques are due to
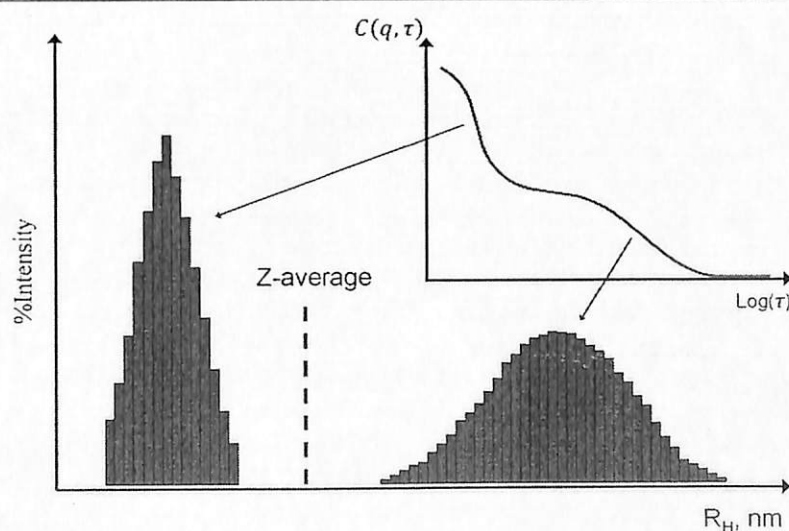

Figure 3 Z-average (cumulant) size for particle suspension with bimodal distribution.
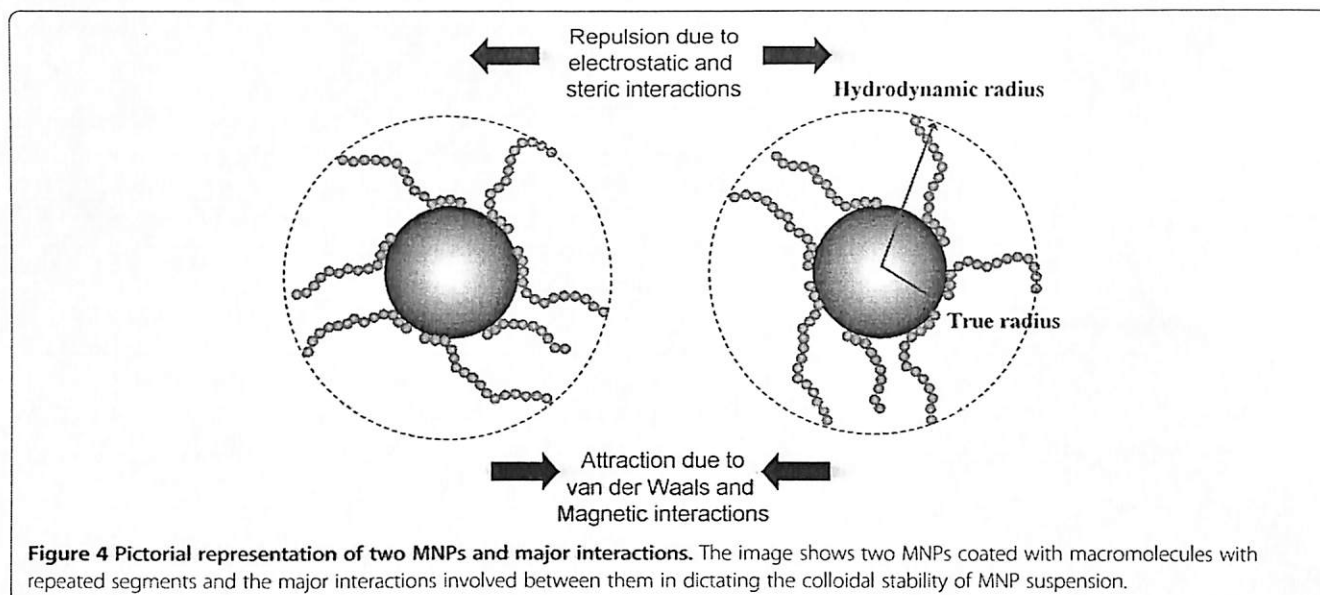
Figure 4 Pictorial representation of two MNPs and major interactions. The image shows two MNPs coated with macromolecules with repeated segments and the major interactions involved between them in dictating the colloidal stability of MNP suspension.

the presence of an adsorbing layer, which is composed of oleic acid (OA) and oleylamine (OY), on the surface of the particle. Small molecular size organic compounds, such as OA and OY, are electron transparent, and therefore, they did not show up in the TEM micrograph (Figure 5). Given that the chain lengths of OA and OY are approximately 2 nm [66,67], the best match of DLS and TEM, in terms of measured diameter, can be observed from middle-sized Fe_3O_4 MNPs.

For small-sized MNPs, the radius of curvature effect is the main contributing factor for the large difference observed on the averaged diameter from DLS and TEM. This observation has at least suggested that for any inference of layer thickness from DLS measurement, the particles with a radius much larger than the layer thickness should be employed. In this measurement, the fractional error in the layer thickness can be much larger than the fractional error in the radius with the measurement standard deviation of only 0.9 nm for TEM but at a relatively high value of 5.2 nm for DLS. At a very large MNP size of around 20 nm (bottom image of Figure 5), the Z-average hydrodynamic diameter is 23 nm larger than the TEM size. Moreover, the standard deviation of the DLS measurement of this particle also increased significantly to 14.9 nm compared to 5.2 and 5.5 nm for small- and middle-sized MNPs, respectively. This trend of increment observed in standard deviation is consistent with TEM measurement. Both the shape irregularity and polydispersity, which are the intrinsic properties that can be found in a MNP with a diameter of 20 nm or above, contribute to this observation. For a particle larger than 100 nm, other factors such as electroviscous and surface roughness effects should be taken into consideration for the interpretation of DLS results [68].

MNP concentration effects

In DLS, the range of sample concentration for optimal measurements is highly dependent on the sample materials and their size. If the sample is too dilute, there may be not enough scattering events to make a proper measurement. On the other hand, if the sample is too concentrated, then multiple scattering can occur. Moreover, at high concentration, the particle might not be freely mobile with its spatial displacement driven solely by Brownian motion but with the strong influences of particle interactions. This scenario is especially true for the case of MNPs with interparticle magnetic dipole-dipole interactions.

Figure 6 illustrates the particle concentration effects on 6- and 18-nm superparamagnetic iron oxide MNPs, with no surface coating, dispersed in deionized water. Both species of MNPs show strong concentration dependency as their hydrodynamic diameter increases with the concentration increment. The hydrodynamic diameter for small particles increases from 7.1 ± 1.9 nm to 13.2 ± 3.3 nm as the MNP concentration increases from 25 to 50 mg/L. On the other hand, the hydrodynamic diameter of large particles remains to be quite constant until around 100 mg/L and then only experiences a rapid jump of the detected size from 29.3 ± 4.6 nm (at 100 mg/L) to 177.3 ± 15.8 nm (at 250 mg/L). Since the concentration of the MNP is prepared in mass basis, the presence of an absolute number of particles in a given volume of solution is almost two orders of magnitude higher in a small-particle suspension. For example, at 100 mg/L, the concentrations for small and larger particles are calculated as 1.7×10^{20} particles (pts)/m^3 and 6.3×10^{18} pts/m^3 by assuming that the composition material is magnetite with a density of 5.3 g/cm^3. This
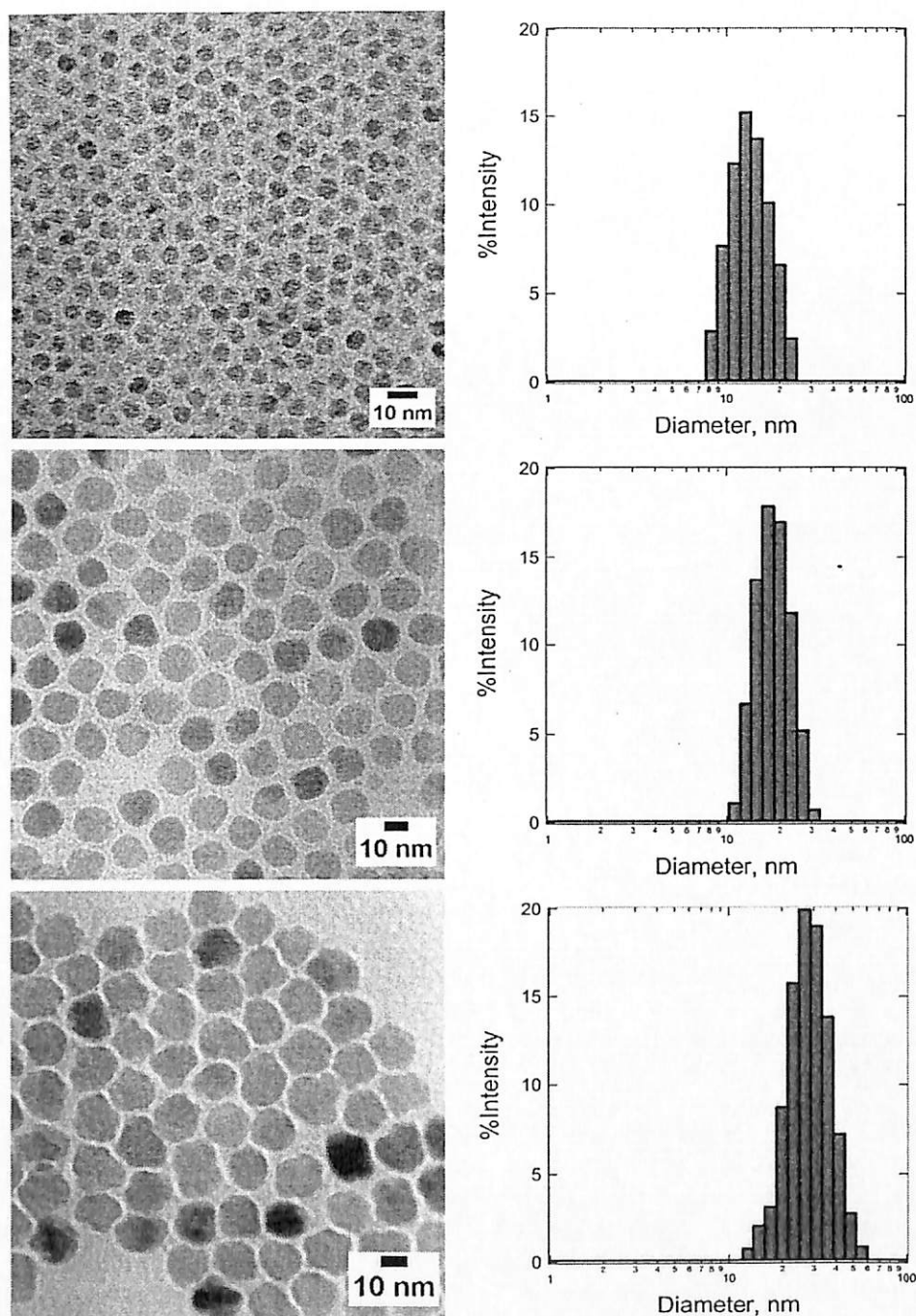
Figure 5 TEM micrographs of Fe$_3$O$_4$ MNPs with their size distribution determined by DLS. The Z-average of MNP calculated from the DLS data is (top) 16.9 ± 5.2 nm, (middle) 21.1 ± 5.5 nm, and (bottom) 43.1 ± 14.9 nm, respectively.

Table 3 Diameter of Fe$_3$O$_4$ MNP determined by TEM and DLS (Z-average)

Particle	TEM (nm)	DLS (nm)	Difference (nm)
Fe$_3$O$_4$	7.2	16.9	9.7
	14.5	21.1	6.6
	20.1	43.1	23.0

concentration translated to a collision frequency of 85,608 s^{-1} and 1,056 s^{-1}. So, at the same mass concentration, it is more likely for small particles to experience the non-self-diffusion motions.

For both species of particles, the upward trends of hydrodynamic diameter, which associates to the decrement of diffusion coefficient, reflect the presence of a strong interaction between the particles as MNP concentration
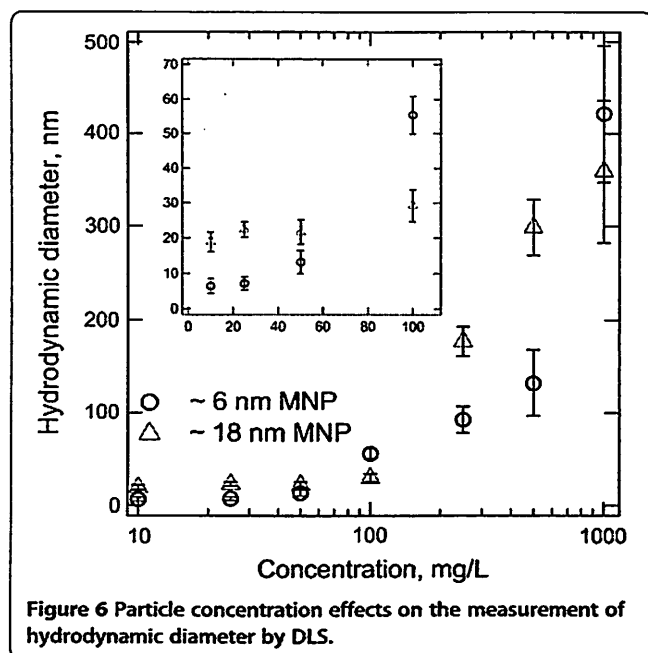
Figure 6 Particle concentration effects on the measurement of hydrodynamic diameter by DLS.

increases. Furthermore, since the aggregation rate has a second-order dependency on particle concentration [69], the sample with high MNP concentration has higher tendency to aggregate, leading to the formation of large particle clusters. Therefore, the initial efforts for MNP characterization by using DLS should focus on the determination of the optimal working concentration.

Colloidal stability of MNPs

Another important use of DLS in the characterization of MNPs is for monitoring the colloidal stability of the particles [70]. An iron oxide MNP coated with a thin layer of gold with a total diameter of around 50 nm is further subjected for surface functionalization by a variety of macromolecules [65]. The colloidal stability of the MNP coated with all these macromolecules suspended in 154 mM ionic strength phosphate buffer solution (PBS) (physiologically relevant environment for biomedical application) is monitored by DLS over the course of 5 days (Figure 7). The uncoated MNP flocculated immediately after their introduction to PBS and is verified with the detection of micron-sized objects by DLS.

As shown in Figure 7, both polyethylene glycol (PEG) 6k and PEG 10k are capable of tentatively stabilizing the MNPs in PBS for the first 24 and 48 h. Aggregation is observed with the detection of particle clusters with a diameter of more than 500 nm. After this period of relative stability, aggregation accelerated to produce micron-sized aggregates by day 3. Actually, the continuous monitoring of MNP size by DLS after this point is less meaningful as the dominating motion is the sedimentation of large aggregates [71]. For PEG 6k and PEG 10k

that have a rather low degree of polymerization, the loss of stability over a day or two could have been due to slow PEG desorption that would not be expected of larger polymers. Nevertheless, PEG 100k-coated MNPs were not as well stabilized as the PEG 6k- or PEG 10k-coated ones, despite the higher degree of polymerization that one might expect to produce greater adsorbed layer thicknesses and therefore longer-ranged steric forces. In addition to the degree of polymerization, as discussed by Golas and coworkers [72], the colloidal stability of polymeric stabilized MNPs is also dependent on other structural differences of the polymer employed, such as the chain architecture and the identity of the charged functional unit. In their work, DLS was used to confirm the nanoparticle suspensions that displayed the least sedimentation which was indeed stable against aggregation.

In addition to the popular use of DLS in sizing individual MNPs, this analytical technique is also being employed to monitor the aggregation behavior of MNPs and the size of final clusters formed [55,73]. The study of particle aggregates is important since the magnetic collection is a cooperative phenomenon [74,75]. Subsequently, it is much easier to harvest submicron-sized MNP clusters than individual particles. Hence, a magnetic nanocluster with loss-packed structure and uniform size and shape has huge potential for various engineering applications in which the real-time separation is the key requirement [76]. Therefore, the use of DLS to monitor the aggregation kinetic of MNPs is important to provide direct feedback about the time scale associated with this process [55,77]. Figure 8 illustrates the aggregation behavior of three species of 40-nm reactive nanoscale iron particles (RNIP), 27.5-nm magnetite (Fe_3O_4) MNP, and 40-nm hematite (α-Fe_2O_3) MNP [73]. Phenrat and coworkers have demonstrated that DLS can be an effective tool to probe the aggregation behavior of MNPs (Figure 8a). The time evolution of the hydrodynamic radius of these particles from monomodal to bimodal distribution revealed the aggregation kinetic of the particles. Together with the in situ optical microscopy observation, the mechanism of aggregation is proposed as the transitions from rapidly moving individual MNPs to the formation of submicron clusters that lead to chain formation and gelation (Figure 8b). By the combination of small-angle neutron scattering and cryo-TEM measurements, DLS can also be used as an effective tool to understand the fractal structure of this aggregate [78].

DLS measurement of non-spherical MNPs

Even though, under most circumstances, a more specialized analytical technique known as depolarized dynamic light scattering is needed to investigate the structural contribution of anisotropic materials [79], it is still possible to extract useful information for rod-like MNPs by
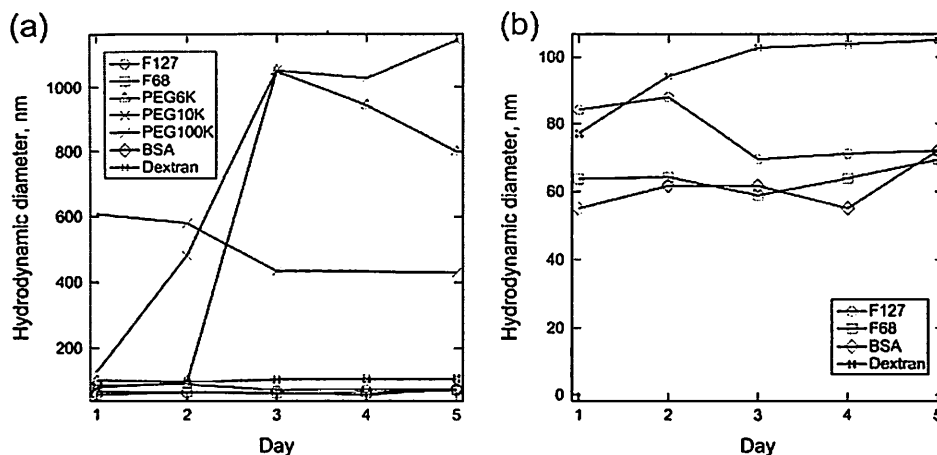
Figure 7 Intensity-weighted average hydrodynamic diameter for core-shell nanoparticles with different adsorbed macromolecules in PBS. (a) Extensive aggregation is evident with PEG 6k, PEG10k, and PEG100k, while **(b)** bovine serum albumin (BSA), dextran, Pluronic F127, and Pluronic F68 provided stable hydrodynamic diameters over the course of 5 days. 'Day 0' corresponds to the start of the overnight adsorption of macromolecules to the MNPs. Copyright 2009 American Chemical Society. Reprinted with permission from [65].
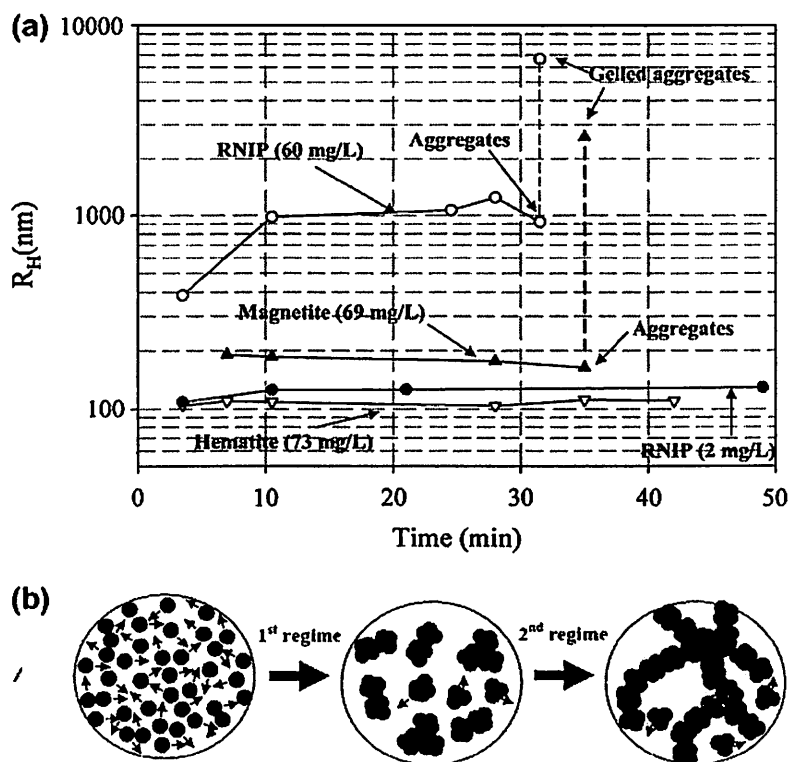
Figure 8 Evolution of hydrodynamic radius and MNP aggregation and gelation. (a) Evolution of the average hydrodynamic radius of dominant size class of MNPs as a function of time for RNIP (Fe^0/Fe$_3$O$_4$), magnetite, and hematite at pH 7.4. The particle size distribution for RNIP and magnetite becomes bimodal at the last measured point due to gelation of aggregates. **(b)** Rapid MNP aggregation and subsequent chain-like gelation: rapid aggregation of MNP to form micron-sized clusters (first regime) and chain-like aggregation and gelation of the micron-sized aggregates (second regime). Copyright 2007 American Chemical Society. Reprinted with permission from [73].

indicating that all the building blocks are self-assembled into the large aggregates within the experiment time frame agrees well with the SEM observation (Figure 10a). This kinetic data time scale is involved in the full assembly of anisotropic nanomaterials from single building blocks to 2-D arrays and, eventually, 3-D micron-sized assemblies.

Conclusion

Dynamic light scattering is employed to monitor the hydrodynamic size and colloidal stability of the magnetic nanoparticles with either spherical or anisotropic structures. This analytical method cannot be employed solely to give feedbacks on the structural information; however, by combining with other electron microscopy techniques, DLS provides statistical representative data about the hydrodynamic size of nanomaterials. In situ, real-time monitoring of MNP suspension by DLS provides useful information regarding the kinetics of the aggregation process and, at the same time, gives quantitative measurement on the size of the particle clusters formed. In addition, DLS can be a powerful technique to probe the layer thickness of the macromolecules adsorbed onto the MNP. However, the interpretation of DLS data involves the interplay of a few parameters, such as the size, concentration, shape, polydispersity, and surface properties of the MNPs involved; hence, careful analysis is needed to extract the right information.

References
1. Lu AH, Salabas EL, Schüth F: Magnetic nanoparticles: synthesis, protection, functionalization, and application. *Angew Chem Int Ed* 2007, 46:1222–1244.
2. Pankhurst QA, Connolly J, Jones SK, Dobson J: Applications of magnetic nanoparticles in biomedicine. *J Phys D Appl Phys* 2003, 36:R167.
3. Adolphi NL, Huber DL, Bryant HC, Monson TC, Fegan DL, Lim JK, Trujillo JE, Tessier TE, Lovato DM, Butler KS, Provencio PP, Hathaway HJ, Majetich SA, Larson RS, Flynn ER: Characterization of single-core magnetite nanoparticles for magnetic imaging by SQUID relaxometry. *Phys Med Biol* 2010, 55:5985–6003.
4. Gupta AK, Gupta M: Synthesis and surface engineering of iron oxide nanoparticles for biomedical applications. *Biomaterials* 2005, 25:3995–4021.
5. Hao R, Xing R, Xu Z, Hou Y, Gao S, Sun S: Sythesis, functionalization and biomedical applications of multifunctional magnetic nanoparticles. *Adv Mater* 2010, 22:2729–2742.
6. Cumbat L, Greenleaf J, Leun D, SenGupta AK: Polymer supported inorganic nanoparticles: characterization and environmental applications. *React Funct Polym* 2003, 54:167–180.
7. Yantasee W, Warner CL, Sangvanich T, Addleman RS, Carter TG, Wiacek RJ, Fryxell GE, Timchalk C, Warner MG: Removal of heavy metals from aqueous systems with thiol functionalized superparamagnetic nanoparticles. *Environ Sci Technol* 2007, 41:5114–5119.
8. Hu J, Lo IMC, Chen G: Comparative study of various magnetic nanoparticles for Cr(VI) removal. *Sep Purif Technol* 2007, 56:249–256.
9. Dobson J: Remote control of cellular behavior with magnetic nanoparticles. *Nat Nanotech* 2008, 3:139–143.
10. Gao J, Zhang W, Huang P, Zhang B, Zhang X, Xu B: Intracellular spatial control of fluorescent magnetic nanoparticles. *J Am Chem Soc* 2008, 130:3710–3711.
11. Fiedor JN, Bostick WD, Jarabek RJ, Farrell J: Understanding the mechanism of uranium removal from groundwater by zero-valent iron using X-ray photoelectron spectroscopy. *Environ Sci Technol* 1998, 32:1466–1473.
12. Feng J, Hu X, Yue PL, Zhu HY, Lu GQ: Degradation of azo-dye orange II by a photoassisted Fenton reaction using a novel composite of iron oxide and silicate nanoparticles as a catalyst. *Ind Eng Chem Res* 2003, 42:2058–2066.
13. Sun S: Recent advances in chemical synthesis, self-assembly, and applications of FePt nanoparticles. *Adv Mater* 2006, 18:393–403.
14. Park J, Joo J, Kwon SG, Jang Y, Hyeon T: Synthesis of monodisperse spherical nanocrystals. *Angew Chem Int Ed* 2007, 46:4630–4660.
15. Zborowski M, Sun L, Moore LR, Williams PS, Chalmers JJ: Continuous cell separation using novel magnetic quadrupole flow sorter. *J Magn Magn Mater* 1999, 194:224–230.
16. Purcell EM: Life at low Reynolds number. *Am J Phys* 1977, 45:3–11.
17. Lim JK, Eggeman A, Lanni F, Tilton RD, Majetich SA: Synthesis and single-particle optical detection of low-polydispersity plasmonic-superparamagnetic nanoparticles. *Adv Mater* 2008, 20:1721–1726.
18. Lim JK, Lanni C, Evarts ER, Lanni F, Tilton RD, Majetich SA: Magnetophoresis of nanoparticles. *ACS Nano* 2011, 5:217–226.
19. Nel A, Xia T, Mädler L, Li N: Toxic potential of materials at the nanolevel. *Science* 2006, 311:622–627.
20. Auffan M, Rose J, Bottero JY, Lowry GV, Jolivet JP, Wiesner MR: Towards a definition of inorganic nanoparticles from an environmental, health and safety perspective. *Nat Nanotech* 2009, 4:634–641.
21. Nel A, Madler T, Velegol D, Xia T, Hoek E, Somasundaran P, Klaessig F, Castranova V, Thompson M: Understanding biophysicochemical interactions at the nano-bio interface. *Nat Mater* 2009, 8:543–557.
22. Phenrat T, Kim HJ, Fagerlund F, Illangasekare T, Tilton RD, Lowry GV: Particle size distribution, concentration, and magnetic attraction affect transport of polymer-modified Fe⁰ nanoparticles in sand columns. *Environ Sci Technol* 2009, 43:5079–5085.
23. Goon IY, Lai LMH, Lim M, Munroe P, Gooding JJ, Amal R: Fabrication and dispersion of gold-shell-protected magnetite nanoparticles: systematic control using polyethyleneimine. *Chem Mater* 2009, 21:673–681.
24. Takahashi K, Kato H, Saito T, Matsuyama S, Kinugasa S: Precise measurement of the size of nanoparticles by dynamic light scattering with uncertainty analysis. *Part Part Syst Charact* 2008, 25:31–38.
25. Goldburg WI: Dynamic light scattering. *Am J Phys* 1999, 67:1152–1160.
26. Chatterjee J, Haik Y, Chen CJ: Size dependent magnetic properties of iron oxide nanoparticles. *J Magn Magn Mater* 2003, 257:113–118.
27. DiPietro RS, Johnson HG, Bennett SP, Nummy TJ, Lewis LH: Determining magnetic nanoparticle size distributions from thermomagnetic measurements. *Appl Phys Lett* 2010, 96:222506.
28. Silva LP, Lacava ZGM, Buske N, Morais PC, Azevedo RB: Atomic force microscopy and transmission electron microscopy of biocompatible magnetic fluids: a comparative analysis. *J Nanopart Res* 2004, 6:209–213.
29. Dukhin AS, Goetz PJ: Acoustic and electroacoustic spectroscopy. *Langmuir* 1996, 12:4336–4344.
30. Chantrell RW, Wohlfarth EP: Rate dependent of the field-cooled magnetisation of a fine particle system. *Phys Status Solidi A* 1985, 91:619–626.

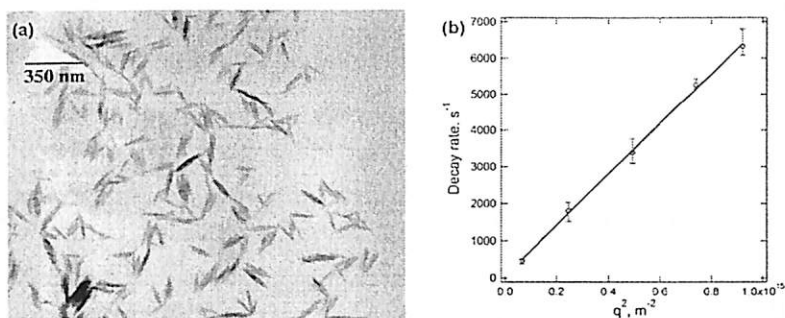**Figure 9 TEM images and graph of decay rate. (a)** TEM images of β-FeOOH nanorods and **(b)** angle-dependent decay rate Γ of the nanorod showing a linear trend. Copyright 2009 Elsevier. Reprinted with permission from [86].

conventional DLS measurement [80,81]. For rod-like particles, the decay rate in Equation 6 can be defined as

$$\Gamma = q^2 D_T + 6 D_R \tag{14}$$

where in a plot of Γ vs q^2, the value of rotational diffusion D_R can be obtained directly by an extrapolation of q to zero and the value of translational diffusion D_T from the slope of the curve [79]. For rigid non-interacting rods at infinite dilution with an aspect ratio (L/d) greater than 5, D_R and D_T can be expressed using Broersma's relations [82,83] or the stick hydrodynamic theory [84]. By performing angle-dependent DLS analysis on rod-like β-FeOOH nanorods as shown in Figure 9a, we found that the decay rate is linearly proportional to q^2 and passes through the origin (Figure 9b), suggesting that the nanorod motion is dominated by translational diffusion [85]. From Figure 9b, the slope of the graph yields the translational diffusion coefficient, $D_T = 7 \times 10^{-12}$ m²/s. This value of D_T corresponds to an equivalent spherical hydrodynamic diameter of 62.33 nm, suggesting that the

DLS results with a single fixed angle of 173° overestimated the true diameter [86]. By taking the length and width of the nanorods as 119.7 and 17.5 nm (approximated from TEM images in Figure 9a), the D_T calculated by the stick hydrodynamic theory and Broersma's relationship is 7.09 × 10⁻¹² m²/s and 6.84 × 10⁻¹² m²/s, respectively, consistent with the DLS results.

Since the β-FeOOH nanorods are self-assembled in a side-by-side fashion to form highly oriented 2-D nanorod arrays and the 2-D nanorod arrays are further stacked in a face-to-face fashion to form the final 3-D layered architectures, DLS can serve as an effective tool to monitor these transient behaviors [87]. Figure 10a depicts the structural changes of self-assembled nanorods over a time course of 7 h. To monitor the in situ real-time behavior of this self-assembly process, DLS was employed to provide the size distribution of the intermediate products that formed in the solution (Figure 10b). The temporal evolution of the detected size from 60 to 70 nm, to dual peaks, to eventually only a single distribution with a peak value of 700 nm
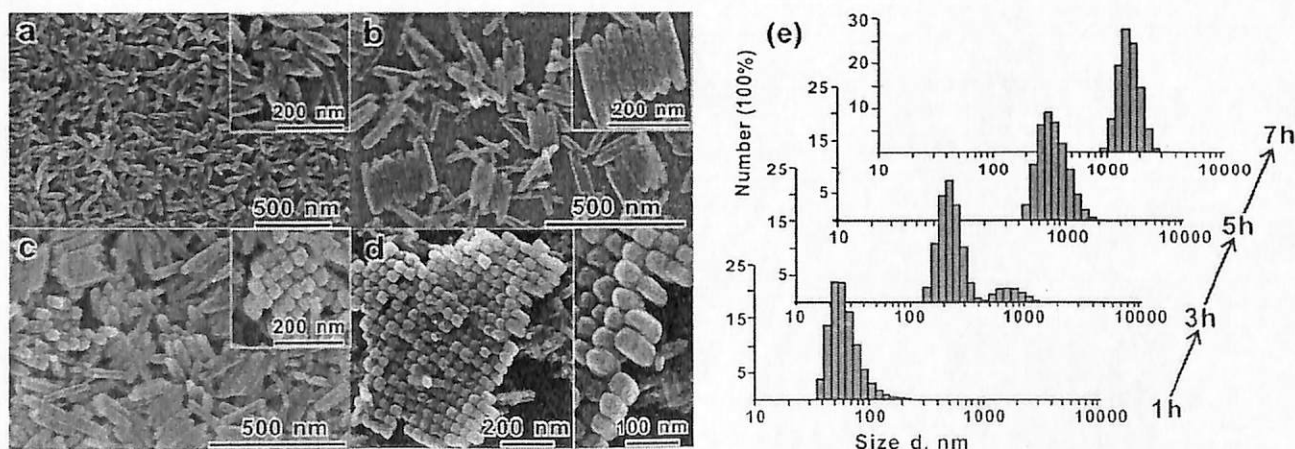

Figure 10 SEM images of the morphological evolution in the time-dependent experiments. (a) 1 h, **(b)** 3 h, **(c)** 5 h, and **(d)** 7 h. **(e)** Size distribution of the products obtained in the time-dependent experiments was monitored by DLS with the number averaged. Copyright 2010 American Chemical Society. Reprinted with permission from [87].

31. El-Hilo M, O'Grady K, Chantrell RW: Susceptibility phenomena in a fine particle system: I. Concentration dependence of peak. *J Magn Magn Mater* 1992, 114:295–306.

32. Jans H, Liu X, Austin L, Maes G, Huo Q: Dynamic light scattering as a powerful tool for gold nanoparticle bioconjugation and biomolecular binding studies. *Anal Chem* 2009, 81:9425–9432.

33. Ando K, Chiba A, Tanoue H: Uniaxial magnetic anisotropy of submicron MnAs ferromagnets in GaAs semiconductors. *Appl Phys Lett* 1998, 73:387.

34. Lacava LM, Lacava BM, Azevedo RB, Lacava ZGM, Buske N, Tronconi AL, Morais PC: Nanoparticles sizing: a comparative study using atomic force microscopy, transmission electron microscopy, and ferromagnetic resonance. *J Magn Magn Mater* 2001, 225:79–83.

35. Dukhin AS, Goetz PJ, Fang X, Somasundaran P: Monitoring nanoparticles in the presence of larger particles in liquids using acoustics and electron microscopy. *J Colloid Interface Sci* 2010, 342:18–25.

36. Van de Hulst HC: *Light Scattering by Small Particles.* New York: Dover Publications; 1981.

37. Hiemenz PC, Rajagopalan R: *Principles of Colloid and Surface Chemistry.* 3rd edition. New York: Marcel Dekker; 1997.

38. Berne BJ, Pecora R: *Dynamic Light Scattering: With Applications to Chemistry, Biology and Physics.* New York: Dover Publications; 2000.

39. He F, Zhao D: Manipulating the size and dispersibility of zerovalent iron nanoparticles by use of carboxymethyl cellulose stabilizers. *Environ Sci Technol* 2007, 41:6216–6221.

40. Tiraferri A, Chen KL, Sethi R, Elimelech M: Reduced aggregation and sedimentation of zero valent iron nanoparticles in the presence of guar gum. *J Colloid Interface Sci* 2008, 324:71–79.

41. Saleh N, Phenrat T, Sirk K, Dufour B, Ok J, Sarbu T, Matyjaszewski K, Tilton RD, Lowry GV: Adsorbed triblock copolymer deliver reactive iron nanoparticles to the oil/water interface. *Nano Lett* 2005, 5:2489–2494.

42. Vidal-Vidal J, Rivas J, López-Quintela MA: Synthesis of monodisperse maghemite nanoparticles by the microemulsion method. *Colloid Suface A: Physiochem Eng Aspects* 2006, 288:44–51.

43. Babič M, Horák D, Jendelová P, Glogarová K, Herynek V, Trchová M, Likavčannová K, Lesny P, Pollert E, Hájek M, Syková E: Poly(N, N-dimethylacrylamide)-coated maghemite nanoparticles for stem cell labelling. *Bioconjugate Chem* 2009, 20:283–294.

44. Kaufner L, Cartier R, Wüstneck R, Fichtner I, Pietschmann S, Bruhn H, Schütt D, Thünemann AF, Pison U: Poly(ethylene oxide)-block-poly(glutamic acid) coated maghemite nanoparticles: in vitro characterization and in vivo behavior. *Nanotechnology* 2007, 18:115710.

45. Thünemann AF, Schütt D, Kaufner L, Pison U, Möhwald H: Maghemite nanoparticles protectively coated with poly(ethyleneimine) and poly (ethylene oxide)-block-poly(glutamic acid). *Langmuir* 2006, 22:2351–2357.

46. Flesch C, Bourgeat-Lami E, Mornet S, Duguet E, Delaite C, Dumas P: Synthesis of colloidal superparamagnetic nanocomposites by grafting poly(ε-caprolactone) from the surface of organosilane-modified maghemite nanoparticles. *J Polym Sci A1* 2005, 43:3221–3231.

47. Nitin N, LaConte LEW, Zurkiya O, Hu X, Bao G: Functionalization and peptide-based delivery of magnetic nanoparticles as an intracellular MRI contrast agent. *J Biol Inorg Chem* 2004, 9:706–712.

48. Thompson Mefford O, Vadala ML, Goff JD, Carroll MRJ, Mejia-Ariza R, Caba BL, St Pierre TG, Woodward RC, Davis RM, Riffle JS: Stability of polydimethysiloxane-magnetite nanoparticle dispersions against flocculation: interpartide interactions of polydisperse materials. *Langmuir* 2008, 24:5060–5069.

49. Jain TK, Morales MA, Sahoo SK, Leslie-Pelecky DL, Labhasetwar V: Iron oxide nanoparticles for sustained delivery of anticancer agents. *Mol Pharmaceutics* 2005, 2:194–205.

50. Arsianti M, Lim M, Lou SN, Goon IY, Marquis CP, Amal R: Bi-functional gold-coated magnetite composites with improved biocompatibility. *J Colloid Interface Sci* 2011, 354:536–545.

51. Xie J, Xu C, Kohler N, Hou Y, Sun S: Controlled PEGylation of monodispersed Fe₃O₄ nanoparticles for reduced non-specific uptake by macrophage cells. *Adv Mater* 2007, 19:3163–3166.

52. Wan J, Cai W, Meng X, Liu E: Monodisperse water-soluble magnetite nanoparticles prepared by polyol process for high-performance magnetic resonance imaging. *Chem Commun* 2007,5004–5006.

53. Narain R, Gonzales M, Hoffman AS, Stayton PS, Krishnan KM: Synthesis of monodisperse biotinylated p(NIPAAm)-coated iron oxide magnetic nanoparticles and their bioconjugation to streptavidin. *Langmuir* 2007, 23:6299–6304.

54. Gonzales M, Krishnan KM: Phase transfer of highly monodisperse iron oxide nanocrystals with Pluronic F127 for biomedical applications. *J Magn Magn Mater* 2007, 311:59–62.

55. Yeap SW, Ahmad AL, Ooi BS, Lim JK: Electrosteric stabilization and its role in cooperative magnetophoresis of colloidal magnetic nanoparticles. *Langmuir* 2012, 28:14878–14891.

56. Lim JK, Derek CJC, Jalak SA, Toh PY: Mat Yasin NH, Ng BW, Ahmad AL: rapid magnetophoretic separation of microalgae. *Small* 2012, 8:1683–1692.

57. Taylor RM, Huber DL, Monson TC, Ali AMS, Bisoffi M, Sillerud LO: Multifunctional iron platinum stealth immunomicelles: targeted detection of human prostate cancer cells using both fluorescence and magnetic resonance imaging. *J Nanopart Res* 2011, 13:4717–4729.

58. Ahmad T, Ramanujachary KV, Lofland SE, Ganguli AK: Magnetic and electrochemical properties of nickel oxide nanoparticles obtained by the reverse-micellar route. *Solid State Sci* 2006, 8:425–430.

59. Horie M, Fukui H, Nishio K, Endoh S, Kato H, Fujita K, Miyauchi A, Nakamura A, Shichiri M, Ishida N, Kinugasa S, Morimoto Y, Niki E, Yoshida Y, Iwahashi H: Evaluation of acute oxidative stress induced by nio nanoparticles in vivo and in vitro. *J Occup Health* 2011, 53:64–74.

60. Zhang Y, Chen Y, Westerhoff P, Hristovski K, Crittenden JC: Stability of commercial metal oxide nanoparticles in water. *Water Res* 2008, 42:2204–2212.

61. King S, Hyunh K, Tannenbaum R: Kinetics of nucleation, growth, and stabilization of cobalt oxide nanoclusters. *J Phys Chem B* 2003, 107:12097–12104.

62. Baldi G, Bonacchi D, Franchini MC, Gentili D, Lorenzi G, Ricci A, Ravagli C: Synthesis and coating of cobalt ferrite nanoparticles: a first step toward the obtainment of new magnetic nanocarriers. *Langmuir* 2007, 23:4026–4028.

63. Min GK, Bevan MA, Prieve DC, Patterson GD: Light scattering characterization of polystyrene latex with and without adsorbed polymer. *Colloids Surf A* 2002, 202:9–21.

64. Koppel DE: Analysis of macromolecular polydispersity in intensity correlation spectroscopy: the method of cumulants. *J Chem Phys* 1972, 57:4814–4820.

65. Lim JK, Majetich SA, Tilton RD: Stabilization of superparamagnetic iron oxide-gold shell nanoparticles in high ionic strength media. *Langmuir* 2009, 25:13384–13393.

66. Zhang L, He R, Gu HC: Oleic acid coating on the monodisperse magnetite nanoparticles. *Appl Surf Sci* 2006, 253:2611–2617.

67. Wang Z, Wen XD, Hoffmann R, Son JS, Li R, Fang CC, Smilgies DM, Hyeon TH: Reconstructing a solid-solid phase transformation pathway in CdSe nanosheets with associated soft ligands. *Proc Natl Acad Sci USA* 2010, 107:17119–17124.

68. Gittings MR, Saville DA: The determination of hydrodynamic size and zeta potential from electrophoretic mobility and light scattering measurements. *Colloid Suface A: Physiochem Eng Aspects* 1998, 141:111–117.

69. Elimelech M, Gregory J, Jia X, Williams RA: *Particle Deposition and Aggregation: Measurement, Modeling and Simulation.* Stoneham: Butterworth-Heinemann; 1998.

70. Wiogo HTR, Lim M, Bulmus V, Yun J, Amal R: Stabilization of magnetic iron oxide nanoparticles in biological media by fetal bovine serum (FBS). *Langmuir* 2011, 27:843–850.

71. Donselaar LN, Philipse AP: Interactions between silica colloids with magnetite cores: diffusion sedimentation and light scattering. *J Colloid Interface Sci* 1999, 212:14–23.

72. Golas PL, Lowry GV, Matyjaszewski K, Tilton RD: Comparative study of polymeric stabilizers for magnetite nanoparticles using ATRP. *Langmuir* 2010, 26:16890–16900.

73. Phenrat T, Saleh N, Sirk K, Tilton RD, Lowry GV: Aggregation and sedimentation of aqueous nanoscale zerovalent iron dispersion. *Environ Sci Technol* 2007, 41:284–290.

74. Cuevas GDL, Faraudo J, Camacho J: Low-gradient magnetophoresis through field-induced reversible aggregation. *J Phys Chem C* 2008, 112:945–950.

75. Andreu JS, Camacho J, Faraudo J: Aggregation of superparamagnetic colloids in magnetic field: the quest for the equilibrium state. *Soft Matter* 2011, 7:2336–2339.

76. Ditsch A, Lindenmann S, Laibinis PE, Wang DIC, Hatton TA: High-gradient magnetic separation of magnetic nanoclusters. *Ind Eng Chem Res* 2005, 44:6824–6836.

77. Yeap SP, Toh PY, Ahmad AL, Low SC, Majetich SA, Lim JK: Colloidal stability and magnetophoresis of gold-coated iron oxide nanorods in biological media. *J Phys Chem C* 2012, 116:22561–22569.
78. Shen L, Stachowiak A, Fateen SEK, Laibinis PE, Hatton TA: Structure of alkanoic acid stabilized magnetic fluids. A small-angle neutron and light scattering analysis. *Langmuir* 2001, 17:288–299.
79. Lehner D, Lindner H, Glatter O: Determination of the translational and rotational diffusion coefficients of rodlike particles using depolarized dynamic light scattering. *Langmuir* 2000, 16:1689–1695.
80. Nath S, Kaittanis C, Ramachandran V, Dalal NS, Perez JM: Synthesis, magnetic characterization, and sensing applications of novel dextran-coated iron oxide nanorods. *Chem Mater* 2009, 21:1761–1767.
81. Lim JK, Tan DX, Lanni F, Tilton RD, Majetich SA: Optical imaging and magnetophoresis of nanorods. *J Magn Magn Mater* 2009, 321:1557–1562.
82. Broersma S: Rotational diffusion constant of a cylindrical particle. *J Chem Phys* 1960, 32:1626.
83. Broersma S: Viscous force and torque constants for a cylinder. *J Chem Phys* 1981, 74:6989.
84. Vasanthi R, Bhattacharyya S, Bagchi B: Anisotropic diffusion of spheroids in liquids: slow orientational relaxation of the oblates. *J Chem Phys* 2002, 116:1092.
85. Phalakornkul JK, Gast AP, Pecora R: Rotational and translational dynamics of rodlike polymers: a combined transient electric birefringence and dynamic light scattering study. *Macromolecules* 1999, 32:3122–3135.
86. Farrell D, Dennis CL, Lim JK, Majetich SA: Optical and electron microscopy studies of Schiller layer formation and structure. *J Colloid Interface Sci* 2009, 331:394–400.
87. Fang XL, Li Y, Chen C, Kuang Q, Gao XZ, Xie ZX, Xie SY, Huang RB, Zheng LS: pH-induced simultaneous synthesis and self-assembly of 3D layered β-FeOOH nanorods. *Langmuir* 2010, 26:2745–2750.